

ADAPTIVE DUPLEXER FOR
SOFTWARE RADIO

Shyama Dilrukshi Kannangara, B. Eng. (Hons)

DOCTOR OF PHILOSOPHY

2006

Adaptive Duplexer for Software Radio



**VICTORIA
UNIVERSITY**

Shyama Dilrukshi Kannangara
B. Eng. (Hons)

THESIS SUBMITTED IN FULFILLMENT OF THE REQUIREMENTS FOR THE
DEGREE OF
DOCTOR OF PHILOSOPHY

Centre for Telecommunications and Micro-Electronics
Faculty of Health, Engineering and Science
Victoria University,
Melbourne, Australia

November 2006

This thesis is dedicated with love and gratitude

to

My dear parents – Malani, Thilak

and

My dear husband – Chanaka

*“Nobody believes in theoretical calculations,
except the one who did it.*

*Everybody believes in experimental results,
except the one who did it.”*

-Albert Einstein

Abstract

Different geographies and localities around the world have adopted various wireless interface standards for mobile communications. As a result roaming users will require multiple handsets with multiple standards and multiple band capabilities. Triple-band hand sets are currently offered for high end users. In the future quad-band handsets including GSM 850 will become common in the market. This trend will continue. The addition of third generation functionality to second generation platforms will be even more difficult and complex. The radio handset should be able to use the same hardware for communications anywhere in the world. Therefore users will require small low cost terminals with multi-mode/multi-band capability. The software radio concept has been developed to address these challenges.

The replacement of fixed frequency components in the front end of the software radio is one of the key architectural changes required. The duplexer is one such component. Since duplexing filters are not normally tuneable, each band requires a separate duplexer in a multi-band system. The duplexers are passive devices (ceramic or SAW) and multiple duplexers lead to a dramatic increase in terminal cost and size.

This thesis proposes a new adaptive duplexer architecture to reduce/eliminate the multiple duplexer problem in software radio. This technique is based on combining a low isolation device with an adaptive double loop cancelling scheme. The proposed double loop cancellation provides the required transmitter leakage and transmitter noise isolation over wideband using a delay element and an adjustable vector attenuator in each cancellation path. This thesis analyses the double loop cancellation technique. The cancellation path delay constraints are derived for coefficients with limited adjustment range in the cancellation paths. A linear relationship between the bandwidth and the achievable cancellation level is obtained. It is shown that the residual signal power is proportional to the square of the duplexing frequency. It is concluded that the delays in the cancellation paths should be chosen to straddle the expected range variation of the delay in the main path, predominantly caused by variations in antenna matching. The new algorithm uses a single cost function to achieve simultaneous cancellation in both the transmit band and the receive band. A direct conversion receiver architecture was chosen for the hardware prototype, since it is more suitable for multi-band systems. Alternate structures are also possible.

A prototype of the adaptive duplexer using a 20dB circulator and a single loop cancelling technique was designed and implemented. It achieved a total Tx leakage cancellation of 69dB at 2GHz with 45MHz duplexing frequency. However it was not possible to simultaneously cancel the transmitter noise in the receiver band. The original prototype was extended to include the second loop. The achieved isolation between the transmit and the receive signals and the achieved reduction of the transmitter noise in the receiver band were 66.8dB and 58dB respectively. These results were obtained over 5MHz bandwidth and using a 190MHz duplexing frequency. The performance is more than adequate for W-CDMA applications. Lowering the duplexing frequency improves the cancellation bandwidth and so the scheme performs better with other standards, such as IS-95 (CDMA), using 45MHz duplexing offset.

Acknowledgements

I take this opportunity to thank and express my sincere gratitude to Victoria University of Technology and the Department of Electrical & Electronic Engineering for providing support to obtain my Bachelor of Engineering with first class honours and carry out this Ph.D. research degree.

I would like to thank my supervisor, Professor Michael Faulkner for giving me the opportunity to conduct research in his group and introducing me to the topic “Adaptive Duplexer for Software Radio”. I would also like to express him my deep appreciation and gratitude for all the given support, essential guidance and valuable time in helping me during my Ph.D. study and through writing of this thesis. The support of my co-supervisor Associate Professor Fu-Chun Zheng is also thankfully acknowledged.

I am grateful to Professor Akhtar Kalam and Professor Jugdutt Singh for their encouragement for me to become a researcher after my undergraduate studies and start a Ph.D. study. Along with them, many thanks go to Professor Aladin Zayegh, all of whom have rendered invaluable support and encouragement during both my undergraduate and research studies in numerous ways.

Special thanks goes to Matthew Williamson who carries out further research on adaptive wideband duplexer, for his assistance at later stages

of this research in obtaining some experimental results. I also thank Melvyn Pierra, Ying Tan, Nghia Truong, & Michael Mewburn for providing me with technical assistance and support in the DSP laboratory.

Also, I wish to thank academic and administrative staff of VUT, Natalie Sciberras in the Research Office and especially Lesley Birch for her support in coordinating with scholarship matters and arranging maternity leave for me.

I would like to acknowledge the financial assistance provided by the Australian Government for this research through Australian Postgraduate Award (APA) scheme and Australian Telecommunications Cooperative Research Centre (ATcrc) through the top-up scholarship.

Gratefully acknowledged are my parents for bringing me into this world and my two sisters for providing me with a warm and loving family. It is with great appreciation, that I thank my parents, June and especially my elder sister Lakmali for looking after my children time to time during my studies. It is with love that I greatly admire the exceptional support and continuous encouragement of my father who also did the proof reading of this thesis.

Thank you also my gorgeous sons Lahiru, Isuru and Riviru; you are the driving force behind everything I do. Especially Lahiru's sacrifices amidst various hardships after the birth of Isuru & Riviru are fondly appreciated during this inevitable difficult times. Surely you have been my solace to keep me going. My deepest gratitude and appreciation are conveyed to my husband for his tremendous support throughout this study, and whose inherent acceptance of belief in my goals has given me strength to complete this work.

In addition, I am indebted to all my relatives and friends who have helped me in numerous ways during this research.

Author's Declaration

I declare that the Ph.D. thesis entitled “Adaptive Duplexer for Software Radio” contains no material that has been submitted previously, in whole or in part, for the award of any other academic degree or diploma. Except where otherwise indicated, this thesis is my own work.

Shyama Kannangara

November 2006

Table of Contents

ABSTRACT.....	III
ACKNOWLEDGEMENTS.....	V
AUTHOR'S DECLARATION.....	VII
TABLE OF CONTENTS.....	VIII
LIST OF FIGURES.....	XII
LIST OF TABLES.....	XIX
LIST OF ABBREVIATIONS.....	XX
LIST OF SYMBOLS.....	XXIV
CHAPTER 1 INTRODUCTION.....	1
1.1 THE INTRODUCTION TO THE THESIS.....	1
1.2 THE OBJECTIVE OF THE THESIS.....	4
1.3 CONTRIBUTION TO KNOWLEDGE.....	4
1.4 SUMMARY OF FINDINGS.....	5
1.5 PUBLICATION SUMMARY.....	6
1.6 ORGANISATION OF THE THESIS.....	8
CHAPTER 2 TECHNOLOGY BACKGROUND.....	10
2.1 INTRODUCTION.....	10
2.2 1 ST GENERATION SYSTEMS.....	11
2.3 2 ND GENERATION SYSTEMS.....	12
2.4 2.5 GENERATION SYSTEMS.....	14
2.5 3 RD GENERATION SYSTEMS.....	15
2.6 4 TH GENERATION SYSTEMS.....	21
2.7 THE SOFTWARE RADIO.....	21

2.8	RECEIVER ARCHITECTURES.....	27
2.8.1	Heterodyne Receivers	27
2.8.2	Homodyne Receivers	29
2.8.2.1	<i>Design Issues</i>	30
2.8.2.1.1	<i>DC Offset</i>	30
2.8.2.1.2	<i>I/Q Mismatch</i>	31
2.8.2.1.3	<i>Even Order Distortion</i>	31
2.8.2.1.4	<i>Flicker Noise</i>	32
2.8.3	Single Conversion Low-IF Receivers	32
2.8.4	Double Conversion Wideband-IF Receivers	33
2.9	CONCLUSION	35
CHAPTER 3 THE DUPLEXER.....		36
3.1	INTRODUCTION.....	36
3.2	TDD SYSTEMS	37
3.3	FDD SYSTEMS.....	38
3.4	INTRODUCTION TO THE DUPLEXER	40
3.5	NEED FOR AN ADAPTIVE DUPLEXER IN MULTI-BAND SYSTEMS	43
3.6	THE EFFECT OF RECEIVER NON-LINEARITY AND THE Tx LEAKAGE SIGNAL.....	45
3.6.1	Receiver Desensitisation	45
3.6.2	Cross Modulation	48
3.6.3	Intermodulation Distortion	51
3.6.3.1	<i>Third Order Intermodulation</i>	52
3.6.3.2	<i>Second Order Intermodulation</i>	54
3.6.4	DC Offset in Direct Conversion Receivers Due to the Tx Leakage Signal.....	56
3.7	DUPLEXER REQUIREMENTS.....	58
3.8	CONCLUSION	61
CHAPTER 4 LITERATURE REVIEW.....		62
4.1	INTRODUCTION.....	62
4.2	TRADITIONAL DUPLEXING FILTERS.....	63
4.2.1	Lumped Element Filters.....	64
4.2.2	Cavity Duplexing Filters	64
4.2.3	Ceramic Duplexing Filters	66
4.2.4	SAW Duplexing Filters.....	68
4.2.5	MEMS Devices	70
4.2.5.1	<i>MEMS Resonators</i>	71
4.2.6	Stripline or Microstrip Line Duplexing Filters	74
4.3	REVIEW OF LITERATURE RELATED TO ACTIVE/MULTI-BAND DUPLEXING STRUCTURES.....	77
4.4	CONCLUSION	85

CHAPTER 5 THE NEW ADAPTIVE DUPLEXER ARCHITECTURE	86
5.1 INTRODUCTION	86
5.2 THE NEW ADAPTIVE DUPLEXER ARCHITECTURE	87
5.3 DESIGN CONSIDERATIONS FOR THE LOW ISOLATION DEVICE	91
5.3.1 Wideband Circulator	91
5.3.2 Directional Coupler	92
5.3.3 Low Selectivity Stripline or Microstrip Filters	92
5.3.4 Separate Antennas	93
5.4 CONCLUSION	94
CHAPTER 6 DESIGN AND IMPLEMENTATION OF THE SINGLE LOOP CANCELLATION SYSTEM	95
6.1 INTRODUCTION	95
6.2 SINGLE LOOP CANCELLATION SYSTEM	96
6.3 EFFECT OF PHASE AND AMPLITUDE MISMATCH ON SIGNAL CANCELLATION	98
6.4 EFFECT OF DELAY MISMATCH ON SIGNAL CANCELLATION	102
6.5 SIMULATION OF THE CANCELLATION UNIT WITH SINGLE LOOP	105
6.5.1 Signal Cancellation	105
6.5.2 Noise Cancellation	108
6.6 DESCRIPTION OF THE SINGLE LOOP CANCELLATION SYSTEM	110
6.7 EXPERIMENTAL RESULTS	112
6.8 DOUBLE NULL USING SINGLE LOOP CANCELLATION	114
6.9 CONCLUSION	117
CHAPTER 7 DESIGN AND IMPLEMENTATION OF THE DOUBLE LOOP CANCELLATION SYSTEM	119
7.1 INTRODUCTION	119
7.2 DOUBLE LOOP CANCELLATION SYSTEM	120
7.3 DELAY EFFECTS	123
7.4 THE RELATIONSHIP BETWEEN THE PATH DELAYS AND THE DUPLEXING FREQUENCY	124
7.4.1 When $0 < \tau_1 < \tau_2$	125
7.4.2 When $\tau_1 < 0$ and $\tau_2 > 0$	128
7.5 DERIVATION OF CONDITIONS FOR $ P_{TX} \leq 1$ AND $ Q_{TX} \leq 1$	130
7.5.1 $\tau_1 > 0$ and $\tau_2 > 0$	130
7.5.2 $\tau_1 < 0$ and $\tau_2 > 0$	133
7.6 THE RELATIONSHIP BETWEEN THE BANDWIDTH AND THE ACHIEVABLE CANCELLATION LEVEL	136
7.6.1 τ_1 Not Equal to τ_2	144
7.6.2 τ_1 (Almost) Equal to τ_2	145

7.7	THE PROPOSED ALGORITHM.....	147
7.8	EXPERIMENTAL SETUP AND RESULTS.....	151
7.9	PERFORMANCE ANALYSIS	153
7.10	CONCLUSION	157
CHAPTER 8 CONCLUSIONS AND SUGGESTIONS FOR FUTURE WORK.....		160
8.1	CONCLUSIONS	160
8.2	PUBLICATIONS RESULTING FROM THIS WORK.....	162
8.3	SUGGESTIONS FOR FUTURE RESEARCH	162
8.3.1	Vector Attenuators	163
8.3.2	Low Isolation Device.....	163
8.3.3	Adaptive Control and Algorithm	163
8.3.4	Integration	164
8.3.5	Four Loop Cancellation.....	164
REFERENCES.....		168
APPENDIX A - Summary of Standards.....		186
APPENDIX B - MEMS Based Front End Receiver Architectures.....		189
APPENDIX C - Four Cases of Delay Constraints		191
APPENDIX D - Delay Effects.....		192
APPENDIX E - Photographs of the Experimental Setup.....		193

List of Figures

Figure 1-1	Conventional duplexer; Hardware structure (left) and frequency response (right).....	3
Figure 1-2	Adaptive duplexer provides two nulls at the transmitter frequency and the desired receiver frequency.....	4
Figure 2-1	Evolution towards third-generation mobile systems in terms of data rate support [18].	20
Figure 2-2	Traditional multi-mode/multi-band receiver.....	22
Figure 2-3	An ideal software radio architecture.....	23
Figure 2-4	Practical wideband software receiver architecture [20].	25
Figure 2-5	Practical wideband software transmitter architecture [20].....	25
Figure 2-6	Simplified block diagram of a heterodyne receiver architecture.....	27
Figure 2-7	Rejection of image vs suppression of interference for (a) high-IF and (b) low-IF [36].	29
Figure 2-8	A simplified block diagram of a homodyne receiver architecture. ...	30
Figure 2-9	Self-mixing in DCR due to LO leakage signal in the LNA/mixer input port.	31

Figure 2-10	A block diagram of a simplified single conversion low-IF receiver architecture.	33
Figure 2-11	Block diagram of a simplified double conversion wideband-IF receiver architecture.	34
Figure 3-1	The principle of operation in TDD systems.....	37
Figure 3-2	The principle of operation in FDD systems.....	39
Figure 3-3	Receiver desensitisation.....	41
Figure 3-4	Transmitter noise.	42
Figure 3-5	The multi-band RF front end (a) using number of duplexers (b) using an adaptive duplexer.....	44
Figure 3-6	Receiver blocking.	47
Figure 3-7	Cross modulation due to the Tx leakage signal and a jammer signal.	49
Figure 3-8	Intermodulation due to LNA non-linearity (two tone test signal). $2\omega_{Tx} - \omega_j$ and $2\omega_j - \omega_{Tx}$ are the third order intermodulation products.....	52
Figure 3-9	The effect of third order intermodulation between the Tx leakage signal and a narrowband jammer.	52
Figure 3-10	Linear and third order intermodulation products vs amplitude. a_3 is normally negative, causing amplifier compression.	53
Figure 3-11	Spectrum of the baseband component due to second order distortion caused by the Tx leakage signal in a W-CDMA terminal.....	54
Figure 3-12	Effect of second order distortion from the LNA feeding through the mixer.....	55
Figure 3-13	Illustration of IIP2. The second order response has a slope of 2...56	
Figure 3-14	Self-mixing in DCR due to theTx leakage signal in LO port.....	57
Figure 4-1	Cut-away views of typical band-pass and band-reject cavities [82].....	65

Figure 4-2	A six-cavity duplexer and the frequency response [81].....	66
Figure 4-3	A base station duplexer for GSM 1800 [83].	66
Figure 4-4	Dual-mode ceramic puck resonator loaded cavity[86].....	67
Figure 4-5	Construction of a ceramic coaxial resonator [87].	68
Figure 4-6	Structure of a conventional SAW filter (wire bonding type) [91]....	69
Figure 4-7	Schematic diagram of a SAW duplexer [92].	70
Figure 4-8	Film bulk acoustic wave resonator – fabricated on a layer of piezoelectric material placed between top and bottom metal electrodes [104].	72
Figure 4-9	Solidly mounted resonator – fabricated on top of multiple reflectors [97].....	72
Figure 4-10	Photography of the Agilent Technologies produced FBAR duplexer and simplified schematic (designed for CDMA PCS 1900 MHz) [97].	73
Figure 4-11	General microstrip line structure.	74
Figure 4-12	General strip line structure.	75
Figure 4-13	Schematics of duplexer structures (a) Two SAW filters (one Tx and one Rx) with microstrip line for matching impedance (b) One chip SAW filters (combined Tx and Rx) with stripline for matching impedance [118].	76
Figure 4-14	Simplified diagram of self-cancelling RF communication system (uses the same spectrum at the same time) [121].	78
Figure 4-15	A schematic diagram of the transmitter interference cancellation arrangement for co-located GPS receiver [127].	80
Figure 4-16	Active cancellation concept of the Tx/Rx feedthrough applying an auxiliary transmitter [127].	81
Figure 4-17	A Tx noise cancellation system configuration [128].	82
Figure 4-18	The block diagram for an adaptive duplexer with improved isolation between Tx and antenna port [132].	83

Figure 4-19	An adaptive duplexer characteristics for dual-path cancellation. Improved duplexing characteristics by achieving double nulls in the receive band of the system.....	84
Figure 5-1	The proposed adaptive duplexer architecture.....	87
Figure 5-2	Obtaining the error signals from a direct conversion receiver.....	90
Figure 5-3	(a) A 3-port circulator (b) A circulator used as an isolation device in a transceiver.....	91
Figure 6-1	The single loop cancellation configuration.	96
Figure 6-2	Vector representation of signal cancellation with phase and gain mismatch.....	98
Figure 6-3	The gain phase mismatch with achievable cancellation levels for single loop cancellation.....	100
Figure 6-4	Achievable cancellation levels with phase mismatch for different values of gain mismatch.....	101
Figure 6-5	The vector representation of signal cancellation with delay mismatch.....	103
Figure 6-6	The delay mismatch with achievable cancellation levels for single loop cancellation.....	104
Figure 6-7	The schematic diagram of the simulated cancellation unit with single loop.....	106
Figure 6-8	Spectrum of the received signals without the single loop cancellation unit. m_1 -transmitter interference signal, m_2 -desired receive signal.	107
Figure 6-9	Received signal spectrum with the cancellation unit. m_1 -transmitter interference signal, m_2 -desired receive signal.....	107
Figure 6-10	The ADS schematic diagram for the noise cancellation.....	109
Figure 6-11	The experimental setup.....	110
Figure 6-12	Spectrum of the received transmitter leakage signal before and after the cancellation.	112

Figure 6-13	The 10kHz received signal before the cancellation (a) and after the cancellation (b). Settings: (a)-20mV/square (b)-50mV/square. .	113
Figure 6-14	Error learning curve.	114
Figure 6-15	Geometric representation of cancellation signals at Tx frequency and Rx frequency using single loop cancellation (a) $\tau_1 \neq 1/f_d$, (b) $\tau_1 = 1/f_d$	115
Figure 6-16	Two nulls using single loop cancellation ($f_d = 190\text{MHz}$ & $f_{TX} = 2\text{GHz}$).	116
Figure 7-1	The double loop cancellation configuration.	120
Figure 7-2	Vector representation of signal components at the double loop summation point (four different delay differences). a) at ω_{TX} b) at ω_{RX} . For perfect cancellation the vectors must sum to 1. Note the possible magnitude relationships.....	122
Figure 7-3	The nulls at Tx and Rx frequencies with double loop cancellation. ($a \Rightarrow \tau_1 = -1\text{ns}$ $\tau_2 = 0.5\text{ns}$ $f_d = 190\text{MHz}$, $b \Rightarrow \tau_1 = -0.5\text{ns}$ $\tau_2 = 0.5\text{ns}$ $f_d = 190\text{MHz}$, $c \Rightarrow \tau_1 = -0.5\text{ns}$ $\tau_2 = 0.5\text{ns}$ $f_d = 45\text{MHz}$).....	124
Figure 7-4	Geometric representation of signal components at the double loop summation point ($\tau_1 > 0$ and $\tau_2 > 0$). The rotation of $Q(P)$ vector is caused by a change in frequency of f_d acting on the delay path $\tau_2(\tau_1)$. Note here in this cancellation $\tau_2 > \tau_1$ because the Q vector undergoes a greater phase shift.	125
Figure 7-5	Geometric representation of signal components at the double loop summation point ($\tau_1 < 0$ and $\tau_2 > 0$). The rotation of $Q(P)$ vector is caused by a change in frequency of f_d acting on the delay path $\tau_2(\tau_1)$	128
Figure 7-6	Cancellation signals when $ P_{TX} \leq 1$ and $ Q_{TX} \leq 1$ and the joining point of the vectors lies in 1 st or 2 nd quadrant (case (1)).	130
Figure 7-7	Cancellation signals when $ P_{TX} \leq 1$ and $ Q_{TX} \leq 1$ and the joining point of the vectors lies in the 3 rd or 4 th quadrant (case (2)).	132
Figure 7-8	Contours of maximum ($ h_1 $ or $ h_2 $) for various delay differences, $\tau_1 f_d$ and $\tau_2 f_d$, in path ₁ and path ₂ (note the normalisation	

	by f_d). The shaded areas show the conditions for coefficient gains less than unity.	135
Figure 7-9	Geometrical illustration of the achievable cancellation when the frequency deviates from the null frequencies.....	137
Figure 7-10	The behaviour of the frequency response. Points E, F, G, H, show the band edges for a cancellation level of $ Ca $	138
Figure 7-11	Effects of (normalised) delays, $\tau_1 f_d$ and $\tau_2 f_d$, on different (normalised) cancellation bandwidths, B/f_d , for a fixed cancellation level of $ Ca ^2 = -40\text{dB}$ (using Eq. 7-43). The curves are undefined when $\tau_1 = \tau_2$	141
Figure 7-12	Bandwidth contours vs τ_1 and τ_2 when $f_d = 190\text{MHz}$ and the cancellation level is $< -40\text{dB}$. The simplified Eq. 7-50 and the original Eq. 7-43 (marked +). Only the first quadrant is shown.	146
Figure 7-13	Spectrum at LNA input (with the cancellation loop inactivated)..	147
Figure 7-14	Obtaining the cost function from the direct conversion receiver. e_1 is the transmitter leakage signal and e_2 a pilot used to measure the noise leakage signal.....	148
Figure 7-15	The learning curve ($\tau_2 = -\tau_1$, $\tau_1 f_d = 0.045$).	149
Figure 7-16	Number of iterations for $E < -60\text{dB}$ vs $\tau_1 f_d$ (top: $\tau_2 = 2\tau_1$; bottom $\tau_2 = -\tau_1$).	150
Figure 7-17	Frequency response of the canceller.....	151
Figure 7-18	The spectrum of the received signal.....	152
Figure 7-19	Simulated frequency response of the cancellation unit. ($a \Rightarrow \tau_1 = -1\text{ns}$ $\tau_2 = 0.2\text{ns}$ $f_d = 190\text{MHz}$; $b \Rightarrow \tau_1 = -\tau_2 = -1\text{ns}$; $f_d = 190\text{MHz}$; $c \Rightarrow \tau_1 = -\tau_2 = -1\text{ns}$ $f_d = 45\text{MHz}$)	153
Figure 7-20	Experiment results for the cancellation unit. ($c \Rightarrow$ without the cancellation unit $a \Rightarrow \tau_1 = -1\text{ns}$ $\tau_2 = 0.2\text{ns}$ $f_d = 190\text{MHz}$, $b \Rightarrow \tau_1 = -1\text{ns}$ $\tau_2 = 1\text{ns}$ $f_d = 190\text{MHz}$)	154

Figure 7-21	Experiment results for the cancellation unit. ($c \Rightarrow$ without the cancellation unit $a \Rightarrow \tau_1 = -\tau_2 = -1\text{ns}$ $f_d = 190\text{MHz}$, $b \Rightarrow \tau_1 = -\tau_2 = -1\text{ns}$ $f_d = 45\text{MHz}$).....	154
Figure 7-22	Adaptive (b) and Manual (c) frequency response for $\tau_1 = -\tau_2 = 1.1\text{ns}$ and $f_d = 45\text{MHz}$ (c) without the cancellation unit.	156
Figure 7-23	Learning curve of adaptive algorithm for $\tau_1 = -\tau_2 = 1.1\text{ns}$ and $f_d = 45\text{MHz}$	156
Figure 8-1	Four loop cancellation	165
Figure 8-2	Four loop adaptive duplexer architecture.....	166
Figure 8-3	Frequency response of the four loop cancellation unit.	167
Figure B-1	Possible front end receiver architecture utilizing a parallel bank of tuneable/switchable micromechanical filters for a first stage of channel selection [111]..	189
Figure B-2	MEMS based receiver employing tuneable front end filter – serves partial channel selection and a wide dynamic range for possible fully integrated radio receiver [112].....	190
Figure B-3	Proposed MEMS based receiver with acoustic resonant IF filter banks – eliminates the requirement of tuning the first local oscillator, but requires very fast switching speed and low phase- noise at very high oscillator frequencies [112].....	190
Figure D-1	Magnitude of h_1 for various delay differences in path ₁ and path ₂	192
Figure D-2	Magnitude of h_2 for various delay differences in path ₁ and path ₂	192
Figure E-1	Photographs of the single loop cancellation system.	193
Figure E-2	Photographs of the double loop cancellation system.	194

List of Tables

Table 2-1	Major analogue cellular system standards [2].....	12
Table 2-2	Second generation digital cellular standards summary [3], [4]	13
Table 2-3	W-CDMA (UMTS) technical summary [13].....	19
Table 2-4	CDMA2000 technical summary [14]	20
Table 3-1	Anticipated performance for W-CDMA duplex arrangement [56].....	43
Table 3-2	Summary of RF receiver requirements for 3G W-CDMA mobile equipments [56].	57
Table 3-3	Duplexing frequency and frequency bandwidth	58
Table 3-4	The maximum output power	59
Table 3-5	The receiver sensitivity level.....	60
Table 6-1	Noise voltages at different nodes.....	109
Table 7-1	n_1 and n_2 for different cases	139
Table 7-2	l_1 , l_2 and l_3 for different cases.....	140
Table A-1	PCS standards overview [3]	186
Table A-2	Digital cordless air interface parameters summary [3].....	186
Table A-3	TD-CDMA technical summary [15].....	187
Table A-4	TD-SCDMA technical summary [16]	188
Table A-5	WCDMA (DoCoMo) technical summary [17].....	188

List of Abbreviations

1G, 2G, 2.5 And 3G 1st 2nd Intermediate and 3rd Generation Systems

3GPP	Third Generation Partnership Project
ADC	Analogue to Digital Conversion
ADS	Advanced Design System
AlN	Aluminium Nitride
AM	Amplitude Modulation
AMPS	Advanced Mobile Phone Service
AMR	Adaptive Multi-Rate
ARIB	Association of Radio Industries and Business
ASIC	Application Specific Integrated Circuit
BAW	Bulk Acoustic Wave
Bi-CMOS	Bi-Polar Complementary Metal-Oxide Semiconductor
BPF	Band-pass Filters
BS	Base Station
CAD	Computer Aided Design
CDMA	Code Division Multiple Access
CMOS	Complementary Metal-Oxide Semiconductor
CRC	Cyclic Redundancy Check
CW	Continuos Wave
DAC	Digital to Analogue Converter
D-AMPS	Digital-Advanced Mobile Phone Services
DC	Direct Current
DCR	Direct Conversion Receiver
DCS 1800	Digital Communication System 1800
DECT	Digital Enhanced Cordless Telecommunications
DL	Down Link

DQPSK	Differential Quadrature Phase Shift Keying
DR	Dynamic Range
DS-CDMA	Direct Sequence-Code Division Multiple Access
DSP	Digital Signal Processing
EDGE	Enhanced Data Rates for Global Evolution
EFR	Enhanced Full Rate
ETACS	Extended Total Access Communication System
ETSI	European Telecommunications Standards Institute
EV-DO	Evolution-Data Optimized
EV-DV	Evolution-Data and Video
FBAR	Film Bulk Acoustic Wave Resonator
FDD	Frequency Division Duplex
FDMA	Frequency Division Multiple Access
FFSK	Fast Frequency Shift Keying
FIR	Finite Impulse Response
FM	Frequency Modulation
FPGA	Field Programmable Gate Arrays
FPLMTS	Future Public Land Mobile Telecommunication Systems
GaAs	Gallium Arsenide
GFLOPS	Giga Floating Point Operations per Second
GMSK	Gaussian Minimum Shift Keying
GPRS	General Purpose Radio Services
GPS	Global Positioning System
GSM	Global System of Mobile Communication
HEM	Dual Hybrid Electromagnetic Modes
HPA	High-Pass Amplifier
HS	High Speed
HSCSD	High Speed Circuit Switched Data
HSPDA	High Speed Packet Downlink Access
HTS	High-Temperature Superconductor
IF	Intermediate Frequency
IIP2	Second Order Input Intercept Point
IIP3	Third Order Input Intercept Point
IM2	Second Order Intermodulation

IMD	Intermodulation Distortion
IMT-2000	International Mobile Telecommunications for the Year 2000
IMT-DS	IMT-Direct Sequence
IMT-FT	IMT-Frequency Time
IMT-MC	IMT-Multi Carrier
IMT-SC	IMT-Single Carrier
IMT-TC	IMT-Time Code
IP2	Second Order Intercept Point
IP3	Third Order Intercept Point
IS-54, IS-95, IS-136	Interim Standard 54, 95, 136
ITU	International Telecommunication Union
JDC	Japan Digital Cellular
LMS	Least-Mean Square
LNA	Low Noise Amplifier
LO	Local Oscillator
LPF	Low-Pass Filter
LTCC	Low-Temperature Co-Fired Ceramic
MEMS	Micro Electro-Mechanical Systems
MIMO	Multiple Input Multiple Output
MMIC	Monolithic Microwave Integrated Circuit
MS	Mobile Station
MSPS	Million Sampling Per Second
NF	Noise Figure
NMT	Nordic Mobile Telephone
NTT DoCoMo	Nippon Telegraph and Telephone Do Communications over the Mobile Network <i>Also DoCoMo Means "Anywhere" In Japanese</i>
OFDM	Orthogonal Frequency Division Multiplexing
OHG	Operators Harmonization Group
OIP3	The Third order Output Intercept Point
PDC	Pacific Digital Cellular
PHS	Personal Handy Phone Systems
PN	Pseudonoise
PSD	Power Spectrum Density
PSK	Phase Shift Keying

PZT	Lead Zirconate Titanate
QCELP	Qualcomm Purevoice
QPSK	Quadrature Phase-Shift Keying
REL _P -LTP	Regular Pulse Excited Linear Prediction-Long Term Prediction
RF	Radio Frequency
RLS	Recursive Least-Squares
RTT	Radio Transmission Technologies
SAW	Surface Acoustic Wave
SID	Sound Interface Device
SiGe	Silicon Germanium
SISO	Single Input Single Output
SMR	Solidly Mounted Resonator
SNR	Signal to Noise Ratio
SVD	Singular Value Decomposition
TACS	Total Access Communication System
TD-CDMA	Time Division CDMA
TDD	Time Division Duplex
TDMA	Time Division Multiple Access
TD-SCDMA	Time Division Synchronous CDMA
TE	Transverse Electric Modes
TIA	Telecommunications Industry Association
TM	Transverse Magnetic Modes
TTA	Telecommunications Technology Association
UL	Up Link
UMTS	Universal Mobile Telecommunications Systems
UTRA	UMTS Terrestrial Radio Access
UWC	Universal Wireless Communication
VLSI	Very Large-Scale Integration
VSELP	Vector Sum Excited Linear Prediction
WARC-92	World Administrative Radio Conference In 1992
W-CDMA	Wideband Code Division Multiple Access
W-LAN	Wireless Local Area Network.
WRC-2000	World Radio Conference In 2000
ZnO	Zinc Oxide

List of Symbols

a_i	i^{th} order non-linearity constant
A_j	amplitude of the jammer signal
A_{Rx}	amplitude of the desired receive signal
A_{Tx}	amplitude of the transmitter interference signal
B	bandwidth of the cancellation signal
C	cancellation signal
c	correction factor
E	cost function of the algorithm
e_1	error signal 1
e_2	error signal 2
f	frequency
$f\delta$	frequency deviation with respect to f_{Tx} or f_{Rx}
f_δ	frequency of the Tx pilot signal
f_c	carrier frequency
f_d	duplexing frequency
f_j	jamming signal
f_{LO}	frequency of the local oscillator
F_r	receiver noise figure
f_{Rx}	receive frequency
F_t	transmitter noise figure
f_{Tx}	transmit frequency
g	attenuation of the main path
G	gain of the amplifier

h_1	<i>complex gain/attenuation of the cancellation path₁</i>
h_2	<i>complex gain/attenuation of the cancellation path₂</i>
k	<i>Boltzmann's constant</i>
m	<i>modulation index</i>
N_{Rx}	<i>receiver noise floor</i>
Out	<i>desired signal</i>
Out_{Rx}	<i>desired signal at Rx frequency</i>
Out_{Tx}	<i>desired signal at Tx frequency</i>
P'_{Tx}	<i>the Tx leakage power at the input of the receiver</i>
P_{cmod}	<i>cross modulation power referred to input of the receiver</i>
P_{ip}	<i>the receiver third order input intercept point power</i>
P_{jam}	<i>the single tone jammer signal at the input of the receiver</i>
P_{Rx}	<i>signal vectors of cancellation path₁ at Rx frequency</i>
P_{Tx}	<i>signal vectors of cancellation path₁ at Tx frequency</i>
P_u	<i>the power of the undesired signal</i>
P_x	<i>signal vector of cancellation path₁</i>
Q_{Rx}	<i>signal vectors of cancellation path₂ at Rx frequency</i>
Q_{Tx}	<i>signal vectors of cancellation path₂ at Tx frequency</i>
Q_x	<i>signal vector of cancellation path₂</i>
R	<i>V_2^2 / V_1^2 in dB</i>
S_{Rx}	<i>desired receive signal</i>
S_x	<i>transmitter interference signals</i>
T	<i>room temperature</i>
T_s	<i>span of the delay variation</i>
V_1	<i>gain of the reference (interference) signal</i>
V_2	<i>gain of the resultant signal</i>
$x(t)$	<i>input to the system</i>
y	<i>cancellation signal</i>
$\%d$	<i>the percentage of modulation on the desired signal due to cross modulation</i>
$\%u$	<i>percentage of modulation on the undesired signal</i>

θ	<i>relative phase error of the cancellation signal</i>
φ_j	<i>phase of the jammer signal</i>
φ_{Rx}	<i>phase of the desired receive signal</i>
φ_{Tx}	<i>phase of the transmitter interference signal</i>
ω_d	<i>angular duplexing frequency</i>
ω_{IF}	<i>angular frequency of the intermediate frequency signal</i>
ω_j	<i>angular frequency of the jammer signal</i>
ω_{LO}	<i>angular frequency of the local oscillator</i>
ω_m	<i>angular frequency of the modulated signal</i>
ω_{RF}	<i>angular frequency of the RF signal</i>
ω_{Rx}	<i>angular frequency of the desired receive signal</i>
ω_{Tx}	<i>angular frequency of the transmitter interference signal</i>
δ	<i>relative gain error of the cancellation signal</i>
δf_d	<i>mismatch of duplexing frequency</i>
β	<i>relative phase of the resultant signal</i>
β_{Rx}	<i>phase difference between the leakage and the cancelling path at Rx frequency</i>
β_{Tx}	<i>phase difference between the leakage and the cancelling path at Tx frequency</i>
α	<i>the amount of cross modulation power that penetrates into the in-band signal (the soaking factor)</i>
τ_1	<i>the delay difference between the main path and the cancellation path₁ (τ_b, τ_a)</i>
τ_2	<i>the delay difference between the main path and the cancellation path₂ (τ_c, τ_a)</i>
τ_a	<i>main path delay</i>
τ_b	<i>cancellation path₁ delay</i>
τ_c	<i>cancellation path₂ delay</i>
ΔV_1	<i>(1 + δ) in dB</i>
$ C ^2$	<i>residual signal power</i>
$\Delta\omega\tau_1$	<i>additional phase error term</i>

CHAPTER 1

Introduction

1.1 The Introduction to the Thesis

Software radio is a multi-mode/multi-band concept that has been developed as a solution for the growing number of incompatible radio air-interface standards. The radio handset should be able to use the same hardware for communications anywhere in the world. This means that the phone should accommodate the GSM (Global System of Mobile Communication) and W-CDMA (Wideband-Code Division Multiple Access) standards in Europe, the PDC (Pacific Digital Cellular) and PHS (Personal Handy Phone System) standards in Asia as well as the IS-54 (Interim Standard 54), IS-95 (Interim Standard 95) and CDMA2000 (Code Division Multiple Access 2000) standards in the United States. Further the phone should be capable of accommodating different functionalities such as cellular UMTS (Universal Mobile Telecommunications Systems), cordless (e.g. DECT (Digital Enhanced Cordless Telecommunications)), satellite UMTS, personal area networks (e.g. Bluetooth) and local area networks (e.g. IEEE 802.11). Over the

next years future fourth generation mobile systems will be added to this list. All schemes are capable of full duplex operation. No single standard covers all areas and all service requirements, so users will require multi-mode/multi-band handsets. To do this in a very small package is a difficult task.

The software radio approach is to replace many of the traditional analogue radio functions, such as channel selection, demodulation and synchronization, with digital signal processing (DSP). Configuring the radio to different standards becomes a software exercise. The remaining radio functions must be made generic (multi-band), the analogue to digital interface must have large dynamic range and the DSP sections must have low power consumption. It is interesting to note that over the past years tremendous progress has been made in reducing the part count of the baseband functions of a wireless mobile. However, little progress has happened in the RF functions. Today third generation mobile communication systems (3G) are at the beginning of their introduction. Through a number of technological advancements the evolution of practical software radio is accelerating. Some of these technologies making significant contributions include wideband RF devices, smart antennas, and integrated circuits.

An important issue in the design of a software radio is the replacement of fixed frequency components. One such component is the duplexing filter required for frequency division duplexing (FDD) systems. A new set of duplexing filters is required for each frequency band and each duplexing offset the radio must handle. In addition, a duplexer is required for each antenna in diversity systems. Normally two band-pass filters (BPF_{TX} and BPF_{RX}) as shown in Figure 1-1, are combined to form a duplexer. The band-pass filter in the transmitter path (BPF_{TX}) stops the transmitter noise artificially increasing the receiver noise figure while the band-pass filter in the receiver path (BPF_{RX}) stops the transmitter signal overloading the receiver (desensitisation). These band-pass filters are designed to isolate the sensitive receiver circuits from the high power transmitter output.

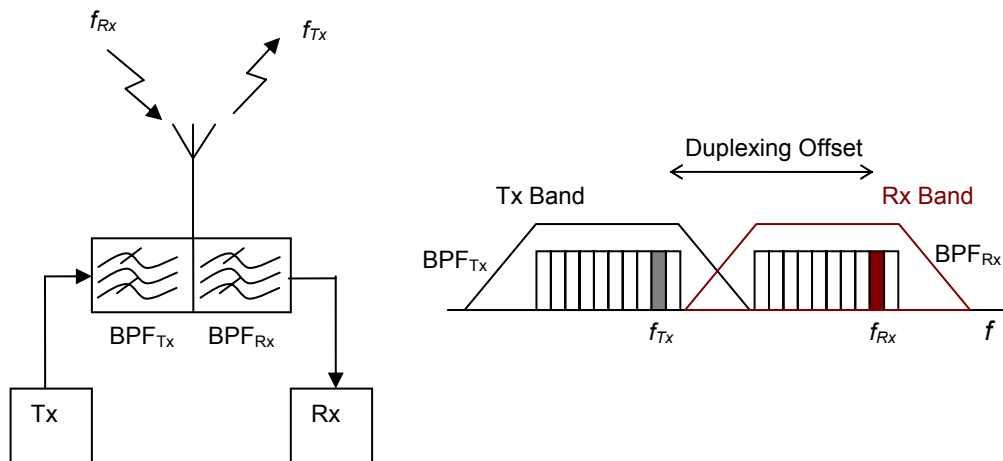


Figure 1-1 Conventional duplexer; Hardware structure (left) and frequency response (right).

A duplexer can be built in many ways using classical resonant circuits (e.g. ceramic or cavity resonators). Recently, duplexers are being built using multilayer technology with the use of slotline or microstrip line coupling structures to improve the level of integration. Other popular techniques include Surface Acoustic Wave (SAW) and Film Bulk Acoustic Wave Resonator (FBAR) devices.

Existing duplexers cannot be implemented in an integrated circuit. Here in this thesis an adaptive/active duplexer architecture that eliminates the need for multiple duplexers or reduces their requirements for software radio implementation is proposed. The adaptive duplexer architecture involves a reduced isolation circuit or device combined with a double loop cancellation process. Using this technique it is possible to obtain two adjustable nulls for cancelling the transmitter leakage signal (at frequency f_{Tx}) and its associated noise components (at frequency f_{Rx}) that fall in the receiver band (Figure 1-2).

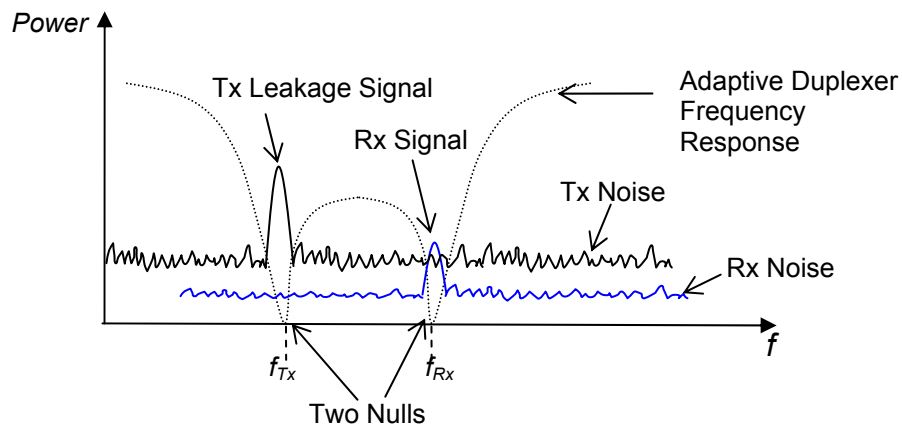


Figure 1-2 Adaptive duplexer provides two nulls at the transmitter frequency and the desired receiver frequency.

1.2 The Objective of the Thesis

The aim of this project is to study the feasibility of replacing or partially replacing the duplexing filter with an active cancellation unit. The unit will bleed a controlled amount of out-of-phase signal into the receiver front end to subtract out the jamming signal.

1.3 Contribution to Knowledge

The pace of change in telecommunications technology is increasing rapidly. In the area of mobile telephone systems, researchers are already exploring new technologies to realize a software radio system that supports multiple mobile telephony standards and multi-mode operation. The adaptive duplexer architecture in this work removes a significant barrier in the successful implementation of the software radio concept thus allowing the users of the mobile telephones to use a single handset to subscribe to all services. A duplexer that can handle multiple bands and which will enable a “future proof” solution by allowing the addition of new bands with different duplexing separations is at present unavailable. Hence,

this work on an adaptive duplexer with these capabilities will be a significant contribution to the realization of the software radio concept.

1.4 Summary of Findings

- A novel adaptive duplexer architecture that eliminates the need for multiple duplexers in a software radio front end is presented. Using this method the required transmitter leakage isolation and required transmitter noise cancellation levels that meet the 2G and 3G mobile wireless standards were achieved. A Tx leakage cancellation level of 66.8dB and a Tx noise cancellation of 58dB were achieved over a 5MHz bandwidth using a 190MHz duplexing frequency. This satisfies the typical requirement for a WCDMA duplexer of 48dB to 60dB.
- Cancellation performance is shown to be affected by delay differences between the main path and the cancellation paths. The tolerable delay variation depends on the dynamic range of the control elements in the cancellation paths. The achievable cancellation also depends on the duplexing frequency and systems with smaller duplexing frequencies achieve higher cancellation levels.
- The behaviour of the double loop cancellation technique is identified for the first time using geometrical analysis. This leads to an in depth knowledge of double loop cancellation theory that helps in determining important design parameters.
- It is shown that the delay difference close to zero in either of the cancellation paths results in a wide bandwidth. The coefficient values of the cancellation paths become very large when the difference of the path delays is close to an integral number of the reciprocal of the duplexing frequency and this condition must be avoided.
- The delay differences in the cancellation paths of the double loop cancellation should be chosen to straddle the expected range variation of the delay in the main path.

- An expression for the achievable cancellation level at a specified bandwidth is derived in terms of the delays and the duplexing frequency. It is shown that the relationship between the cancellation bandwidth and the achievable cancellation level is linear (6dB/octave). It is also shown that the residual signal power ($|C|^2$) is proportional to the bandwidth (B) squared, duplexing frequency (f_d) squared and the time delays (τ_1 , τ_2) squared ($|C|^2 = \pi^4 B^2 (f_d)^2 (\tau_1)^2 (\tau_2)^2$).
- Cancellation in the Tx band and cancellation in the Rx band are shown to be interdependent. Therefore the control algorithm must use a cost function, which when minimised, provides cancellation in both bands. A new algorithm to achieve the required dual band cancellation is described.

1.5 Publication Summary

The following publications have resulted in from this research.

Conference Papers

1. S. Kannangara and M. Faulkner, "Adaptive Duplexer for Software Radio," *2nd ATerc Telecommunications and Networking Conference*, Fremantle, WA, Australia, 16-18 October 2002.
2. S. Kannangara and M. Faulkner, "Simulation of a Cancellation Unit in an Adaptive Duplexer for Software Radio," *Proceedings of the 4th International Conference on Modelling & Simulation MS'02*, Melbourne Australia, 11-13 November 2002, pp. 148-152.
3. S. Kannangara and M. Faulkner, "Adaptive Duplexer for Multiband Transreceiver," *IEEE Proceedings of Radio and Wireless Conference*, Boston, USA, 10-13 August 2003, pp. 381-384.

4. S. Kannangara and M. Faulkner, "Effects of Delay Differences in Double Loop Cancellation on Active Wideband Duplexer," *7th International Symposium on Digital Signal Processing and Communication Systems*, Gold Coast, Australia, 8-11 December 2003.
5. S. Kannangara, M. Williamson and M. Faulkner, "Performance Analysis of the Cancellation Unit in an Adaptive Wideband Duplexer for Software Radio," *3rd ATcrc Telecommunications and Networking Conference*, Melbourne, Australia, 11-12 December 2003.
6. M. Williamson, S. Kannangara, and M. Faulkner, "Performance Analysis of Adaptive Wideband Duplexer," *Australian Telecommunications Networks and Applications Conference*, Melbourne, Australia, 8-10 December 2003.

Journal Articles

7. S. Kannangara and M. Faulkner, "Simulation of a Cancellation Unit in an Adaptive Duplexer for Software Radio," *AMSE Best of book 2002*, AMSE press, pp.63-72, 2003.
8. S. Kannangara, and M. Faulkner, "An Algorithm to Use in Adaptive Wideband Software Radio", *IEICE Transactions on Communications*, vol. E86-B, no. 12, pp. 3452-3455, December 2003.
9. S. Kannangara and M. Faulkner, "Analysis of an Adaptive Wideband Duplexer with Double Loop Cancellation," *accepted (24 July 2006) for IEEE Transactions on Vehicular Technology*.

1.6 Organisation of the Thesis

This thesis is organized in eight chapters. Chapter 1, which corresponds to this introduction, states the objective, provides a contribution to knowledge, summary of findings, publications summary and a thesis overview.

Chapter 2 reviews the technology background. First it summarises the 1st and 2nd generations of mobile cellular systems. Next the 2.5 generation, that extends the 2nd generation platform to provide data rate enhancements and other premium services, is briefly looked at. Then the 3rd generation systems that bring about revolutionary changes are discussed. The convergence of different mobile cellular standards to form a unified 3G standard is also discussed along with a brief introduction to future 4th generation systems. The software radio as a concept to implement multi-band/multi-mode systems is also investigated. The duplexer front end component is recognised as one of the main challenges in realisation of a practical software radio. Finally some receiver architectures which are particularly suitable for integration and multi-band systems are examined.

Chapter 3 gives an introduction to the duplexer. Here the need for an adaptive duplexer for software radio is investigated. When a high transmitter leakage signal is present at the receiver input, a number of non-linear adverse effects can occur that degrade the receiver sensitivity. These include desensitisation, blocking, cross modulation and intermodulation and are discussed in this chapter. The main requirements associated with a duplexer are also specified.

A review of existing duplexing filter technologies along with a review of the literature associated with active duplexing structures are discussed in Chapter 4.

The new adaptive duplexer architecture which is based on a low isolation device and a cancellation unit is proposed and discussed in Chapter 5. Some design considerations for the low isolation device are also discussed.

Chapter 6 concentrates on the single loop cancellation method. This part of the research focussed only on the cancellation of the Tx leakage signal at the receiver. The work includes design and implementation details and also investigates phase and gain mismatches, delay effects and the control algorithm. Finally the experimental results are presented.

The new double loop cancellation system that suppresses both the Tx leakage and the Tx noise signals is presented in Chapter 7. The system is analysed using a geometric method. The influence of various parameters on the cancellation is examined. A new algorithm that controls the cancellation process is offered and the experimental results are presented.

Chapter 8 draws a number of conclusions based on the work completed and suggests some future work including a possible extension to four loop cancellation.

Technology Background

2.1 Introduction

Second generation mobile communication systems were created to address the need for increased capacity over first generation analogue systems. It is expected that at the beginning of 3G operation the second generation systems would coexist. Therefore transceivers should support both 2G and 3G functional requirements. Since the user preference is for a single mobile terminal, the transceiver requires multi-mode/multi-band capabilities. The software radio concept is being developed as a solution to this problem. There are many issues still to be addressed in the realisation of the software radio concept. The duplexer is one of the main problems of the RF front end since it is a fixed frequency component.

This chapter begins with a brief history and a summary of the first and second generation wireless system standards. Then it gives an overview to 3G systems and associated standards. The software radio and RF front end from the receiver

perspective are discussed in the next section. The adaptive duplexer in this research is based on a direct conversion receiver architecture (DCR) which is more suitable for software radio design. The direct conversion receiver is examined with some other receiver architectures in the final section.

2.2 1st Generation Systems

With the invention of microprocessors and the cellular communications concept in the 1970s and 1980s, the first generation (1G) mobile communication systems were born [1]. First generation systems use cellular coverage, where the coverage area is divided into small cell areas. The 1G systems were essentially analogue systems using Frequency Division Multiple Access (FDMA) to communicate and were designed for voice transmission only (no data). NMT (Nordic Mobile Telephone), AMPS (Advanced Mobile Phone Service), TACS (Total Access Communication System), ETACS (Extended Total Access Communication System), JDC (Japan Digital Cellular) etc., were among first generation systems. NMT was the first analogue cellular phone system that started operating in Scandinavia in 1979. In the beginning, it used the 450MHz band and therefore was named NMT 450. Later it used the 900MHz band because of the need for more capacity and was called NMT 900. AMPS was introduced in 1978 by the Bell telephone company in the USA and started operation in 1983 in Chicago. TACS was introduced in UK in 1982. ETACS was the extended version of TACS and was deployed in 1985. The cellular systems called C-450 (operated in the 450 MHz band) and Radicom 2000 (operated in the 200 MHz band) were also introduced in Germany and in France respectively in 1985.

These systems had numerous problems such as capacity limitations of TDMA (Time Division Multiple Access), incompatibilities across geographies (USA, Japan and Europe), only nationwide coverage, no open interfaces except the radio interface, low speech quality and no security in speech transmission. The major first generation analogue cellular radio system standards [2] are compared in Table 2-1. (Please refer to the list of abbreviations for descriptions in the tables.)

Table 2-1 Major analogue cellular system standards [2]

Specification	AMPS	TACS	NMT450	NMT900
Channels	832	1320	180	1000/2000
TX frequency	824-849	872-905	453-457.5 (& other bands)	872-905
Channel separation	30kHz	25kHz	25/30kHz	25kHz/12.5
Frequency stability	± 2.5 PPM	± 2.5 PPM	± 5. PPM	± 5 PPM
Tx power	3 watts	2.8 watts	1.5 watts	3 watts
Voice deviation	12kHz	9.5kHz	4.7kHz	4.7kHz
Data deviation	8kHz	6.4kHz	3.5kHz	3.5kHz
Receiver sensitivity	12dBc @-116dBm	20dBc @-113dBm	20dBc @-113dBm	20dBc @-113dBm
Adjacent channel selectivity	60dB	55dB	70dB	70dB
Spurious rejection	60dB	65/55dB	70dB	70dB
Intermodulation	65dB	65/55dB	67dB	67dB
Signalling method	Manchester	Manchester	FFSK	FFSK
Speed	10kbps	8 kbps	1.2kbps	1.2 kbps
Duplexing method	FDD	FDD	FDD	FDD

2.3 2nd Generation Systems

Second generation systems started to appear across the world in the early 1990s. Advances in integrated circuit technology brought digital transmission to mobile communications. Second generation systems are based on digital technology and offer data speed up to 9.6kb/s and use TDMA or CDMA access methods in combination with FDMA. Second generation systems are capable of providing voice, data, fax transfer as well as other services. 2G systems can be categorised as 2G cellular mobile systems and 2G Personal Communication Systems (PCSs). GSM, US-TDMA (IS-136), cdmaOne (IS-95) and PDC are included in second

generation cellular systems. The four most popular 2G cellular radio standards [3], [4] are listed in Table 2-2.

Table 2-2 Second generation digital cellular standards summary [3], [4]

Specification	GSM	IS-54	PDC	IS-95
Year of introduction	1990	1991	1993	1993
Frequencies	890-915 MHz(R) 935-960 MHz (F)	824-849 MHz (R) 869-894 MHz (F)	810-830 & 1429-1453 MHz (R) 940-960 & 1477-1501 MHz (F)	829-849 & 1850-1910 MHz (R) 940-960 & 1477-1501MHz (F)
Multiple access	TDMA/FDMA/FDD	TDMA/FDMA / FDD	TDMA/FDMA/ FDD	CDMA
Modulation	GMSK ($BT=0.3$)	$\pi/4$ DQPSK	$\pi/4$ DQPSK	QPSK OQPSK
Carrier separation	200kHz	30kHz	25kHz	1.25MHz
Channel data rate	1 270.833kbps	48.6kbps	42kbps	19.2kbps
Number of voice channels	1000	2500	3000	4000
Spectrum efficiency (overall bit rate)	1.35bps/Hz	1.62bps/Hz	1.68bps/Hz	2.58bps/Hz
Speech coding	REL P-LTP @ 13kbps	VSELP @7.95kbps	VSELP @ 6.7kbps	QCELP @ 9.6kbps / @ 14.4kbps
Channel coding	CRC with R=1/2; L=5 Conv.	7 bit CRC with r=112; =6 Conv.	CRC with Cony.	NA
Equalizers	Adaptive	Adaptive	Adaptive	Adaptive
Portable Tx. power max./ avg.	1 W/125mW	600mW/200 mW	125mW	200mW
Duplexing method	TDD/FDD	TDD/FDD	TDD/FDD	FDD

D-AMPS (Digital-Advanced Mobile Phone Services) is a digital version of AMPS. D-AMPS is also known as US-TDMA/IS-136. IS-54 (US Digital Cellular) service is an old version of the IS-136. GSM was originally designed to operate in the 900MHz band but was later adapted to operate in 1800MHz and 1900MHz bands. The GSM 450 (operate at 450MHz band) may start to operate in some

countries to replace old analogue networks. Currently the maximum data rate for GSM is 14.4kbps. IS-95 is based on narrowband spread spectrum technology and uses 1.25MHz channel bandwidth. Therefore it offers increased capacity, wider bandwidth and is very flexible because it uses CDMA access method. IS-95 and IS-136 are capable of operating in the same band as AMPS and specified to be dual-mode systems. 2G systems compared with 1G systems allow more efficient use of the radio spectrum since they can handle more calls than analogue FDMA technology.

PDC is the Japanese 2G standard. It is somewhat similar to IS-54 standard, but uses 4-ary modulation for voice and control channels, making it more like IS-136 in North America [3].

DCS 1800 (Digital Communication System 1800) and PHS are also included in 2G PCSs [3] and are listed in Table A-1 in Appendix A. The major 2G digital cordless air interface standards [3] are also listed in Table A-2 in Appendix A.

2.4 2.5 Generation Systems

2.5 generation systems address the data capacity limitations associated with the 2nd generation systems. Even though the boundary between 2G systems and 2.5G systems is somewhat unclear, 2.5G systems provide clear upgrades to the 2G systems that almost make it possible to provide similar capabilities as 3G systems. A number of technologies are commonly used to provide these capabilities such as High Speed Circuit Switched Data (HSCSD), Enhanced Data rates for Global Evolution (EDGE) and General Purpose Radio Services (GPRS).

HSCSD is the easiest upgrade to achieve higher data rates. It improves the maximum user data rate of the air interface by using more than one time slot for data connections. Implementations that use up to four time slots for data connections are commercially available. This is an innovative and inexpensive

way to upgrade the current wireless platform as the changes involve only upgrading the software used in the network.

Using GPRS, data rates up to 115kbps with error correction are possible using approximately eight time slots. This technology is based on packet switching and thus makes efficient use of the available bandwidth using variable bit rates. It is also suitable for services that use bursty data due to its ability to dynamically allocate resources.

EDGE is an improvement over GSM which increases the traditional GSM data rates over 300%. It uses eight phase shift keying (8 PSK) method for modulation. This is an attractive solution for existing GSM networks as the change required is only a software upgrade. Due to its ability to co-exist with the Gaussian minimum shift keying modulation, it allows users to continue using their current handsets. IS-136 also can be upgraded using EDGE.

In addition to these methods, NTT DoCoMo (Nippon Telegraph and Telephone DoCoMo) from Japan has developed their own proprietary packet based technology called i-mode which provides users an efficient mechanism for wireless internet browsing and email access.

2.5 3rd Generation Systems

Third generation systems opened the way for a completely new era of wireless services that enabled access across multiple geographies. 3G systems provide a platform that is common for multiple wireless standards and technologies. They are aimed to carry data up to 2Mb/s, about 200 times faster than the 2G systems in indoor environment and a minimum of 144kb/s in other environments [5]. Because of the high-speed data rate, 3G systems will be able to support services such as audio, video, multimedia, internet, data and speech.

The key objectives of 3G development are to provide [6]:

- multi-standard user terminals that operate effectively for all types of services, in all radio environments
- service quality that is comparable to the current fixed public network
- flexible new capabilities and services such as WWW, high bit-rate data and multimedia
- network to air interface flexibility
- compatibility with second generation e.g. GSM/DCS
- “Future proof” systems to easily accommodate added capabilities

The main requirements that apply to third generation systems are [7]:

- support for high data rates up to at least 144kbits/s (384kbits/s for full area coverage) in all radio environments and up to 2Mbits/s in low mobility and indoor environments
- support for symmetrical and asymmetrical data transmission
- support for packet-switched and circuit switched services, such as Internet (IP) traffic and real-time video
- support for good voice quality (compatible with wireline quality)
- support for greater capacity and improved spectrum efficiency compared with existing second-generation wireless systems
- support for several simultaneous services to end-users and terminals – that is, for multimedia service capabilities
- support for coexistence and interconnection with mobile satellite services
- support for roaming, including international roaming, between different IMT-2000 (International Mobile Telecommunications for the year 2000) operators
- support for scale-of economy and an open global standard to meet mass-market needs

The goal of 3G technologies is to create a single global standard that allows for global roaming. The International Telecommunication Union (ITU) and the United Nations organisation responsible for global telecommunications began its

studies on global personal telecommunications in 1986. The ITU World Administrative Radio Conference in 1992 (WARC-92) identified 230MHz, in the 2GHz band, on a world wide basis for the satellite and terrestrial components of Future Public Land Mobile Telecommunication Systems (FPLMTS) [8]. Later it was renamed as IMT-2000. WRC-2000 (World Radio Conference in 2000) identified three additional bands i.e. 806-960MHz, 1710-1885MHz and 2500-2690MHz for terrestrial IMT-2000.

The European Telecommunications Standards Institute (ETSI) regards 3G systems as UMTS. In 1998 the first decision in the standardisation process of UMTS was made by ETSI. ETSI chose the W-CDMA concept to be adopted in the spectrum (for uplink one band of spectrum and for down link another band of spectrum, - FDD duplex mode) of UMTS. It also chose the TD-CDMA (Time Division-CDMA) concept to be adopted in unpaired band (a single monolithic block of spectrum – TDD duplex mode) of UMTS. UMTS will consist of both satellite and terrestrial components as in IMT-2000 and will support both circuit-switched and packet-switched services. The Telecommunications Technology Association (TTA) in South Korea and Association of Radio Industries and Business (ARIB) in Japan have developed standards based on W-CDMA. The Telecommunications Industry Association (TIA) in United States proposed CDMA2000. The major difference between W-CDMA and CDMA2000 is that W-CDMA is backward compatible with GSM networks and CDMA2000 is backward compatible with IS-95 networks [9]. Due to the different technologies used in different regions in the world, a family of compatible standards were adopted under IMT-2000 umbrella.

The five standards included in IMT-2000 terrestrial radio interfaces are shown below [10], [11].

1. IMT-DS (Direct Sequence CDMA - FDD duplex type) - This is known as UTRA FDD (UMTS Terrestrial Radio Access FDD) or W-CDMA and adopted in Europe and Japan. This has been specified by 3GPP (Third Generation Partnership Project) and operates in the IMT-2000 paired bands

- at a chip rate of 3.84Mcps, spread over approximately 5MHz. This mode of operation will be used in the UMTS macro and micro-cellular environment.
2. IMT-MC (Multi-Carrier CDMA - FDD duplex type) - This is known as CDMA2000. This has been specified by 3GPP2 and operates on the downlink at a basic chip rate of 1.288Mcps, occupying 1.25MHz of bandwidth.
 3. IMT-TC (Time Code CDMA - TDD duplex type) - This is known as TD-CDMA. It is a combination of the UTRA TD D and the TD-SCDMA. This operates in unpaired spectral bands at a chip rate of 3.84Mcps, spread over approximately 5MHz.
 4. IMT-SC (Single Carrier - FDD duplex type) - This is known as UWC-136 and proposed by the Universal Wireless Communication (UWC) Consortium and Telecommunication Industry Association (TIA). It represents convergence between the TDMA-136, GSM and EDGE standards. UWC-136 will adopt the GPRS packet data network architecture, while enhancing the TDMA-136 radio interface to include GSM/EDGE compatibility and a high data rate indoor solution. The UWC-136 solution provides backward compatibility with the AMPS, IS-54, IS-136 and GSM networks.
 5. IMT-FT (Frequency Time - TDD duplex type) - This is known as DECT.

In May 1999, the Operators Harmonization Group (OHG) concluded the harmonization discussion at a meeting in Toronto, Canada, which resulted in a single 3G CDMA standard with three modes; i.e. a direct sequence mode based on W-CDMA, a multi-carrier mode based on CDMA2000 and a TDD mode based on UTRA TDD [12]. Combined time division and code division multiple access scheme is used in UTRA TDD.

W-CDMA (UTRA FDD) technical summary [13] is shown in Table 2-3 and CDMA2000 technical summary [14] is shown in Table 2-4. TD-CDMA [15], TD-SCDMA [16] and W-CDMA (DoCoMo) [17] technical summaries are shown in Table A-3, Table A-4, and Table A-5 in Appendix A.

Table 2-3 W-CDMA (UMTS) technical summary [13]

Frequency band	1920MHz -1980MHz and 2110MHz - 2170MHz (Frequency Division Duplex) UL and DL
Minimum frequency band required	~ 2x5MHz
Frequency re-use	1
Carrier spacing	4.4MHz - 5.2MHz
Maximum number of (voice) channels on 2x5MHz	~196 (spreading factor 256 UL, AMR 7.95kbps) / ~98 (spreading factor 128 UL, AMR 12.2kbps)
Voice coding	AMR codecs (4.75kHz - 12.2kHz, GSM EFR=12.2kHz) and SID (1.8kHz)
Channel coding	Convolutional coding, Turbo code for high rate data Duplexer needed (190kHz separation), Asymmetric connection supported
Tx/Rx isolation	MS: 55dB, BS: 80dB
Receiver	Rake
Receiver sensitivity	Node B: -121dBm, Mobile -117dBm at BER of 10^{-3}
Data type	Packet and circuit switch
Modulation	QPSK
Pulse shaping	Root raised cosine, roll-off = 0.22
Chip rate	3.84Mcps
Channel raster	200kHz
Maximum user data rate (physical channel)	~ 2.3Mbps (spreading factor 4, parallel codes (3 DL / 6 UL), 1/2 rate coding), but interference limited.
Maximum user data rate (offered)	384 kbps (year 2002), higher rates (~ 2 Mbps) in the near future. HSPDA will offer data speeds up to 8-10 Mbps (and 20 Mbps for MIMO systems)
Channel bit rate	5.76Mbps
Frame length	10ms (38400 chips)
Number of slots / frame	15
Number of chips / slot	2560 chips
Power control period	Time slot = 1500Hz rate
Power control step size	0.5, 1, 1.5 and 2dB (Variable)
Power control range	UL 80dB, DL 30dB
Mobile peak power	Power class 1: +33 dBm (+1dB/-3dB) = 2W; class 2 +27 dBm, class 3 +24 dBm, class 4 +21 dBm
Number of unique base station identification codes	512 / frequency

Table 2-4 CDMA2000 technical summary [14]

Frequency band	Any existing band. (Frequency Division Duplexing)
Minimum frequency band required	1x: 2x1.25MHz, 3x: 2x3.75
Chip rate	1x: 1.2288, 3x: 3.6864Mcps
Maximum user data rate	1x: 144 kbps now, 307kbps in the future 1xEV-DO: max 384 kbps - 2.4 Mbps, 1xEV-DV: 4.8Mbps.
Frame length	5ms, 10ms or 20ms
Power control rate	800Hz
Spreading factors	4 ... 256 UL

The evolution of the third-generation mobile telecommunication system IMT-2000, in terms of data rate support [18] is shown in Figure 2-1. The capability targets for the 3G have been defined as 384 kbit/s for full area coverage and 2Mbit/s for local area coverage.

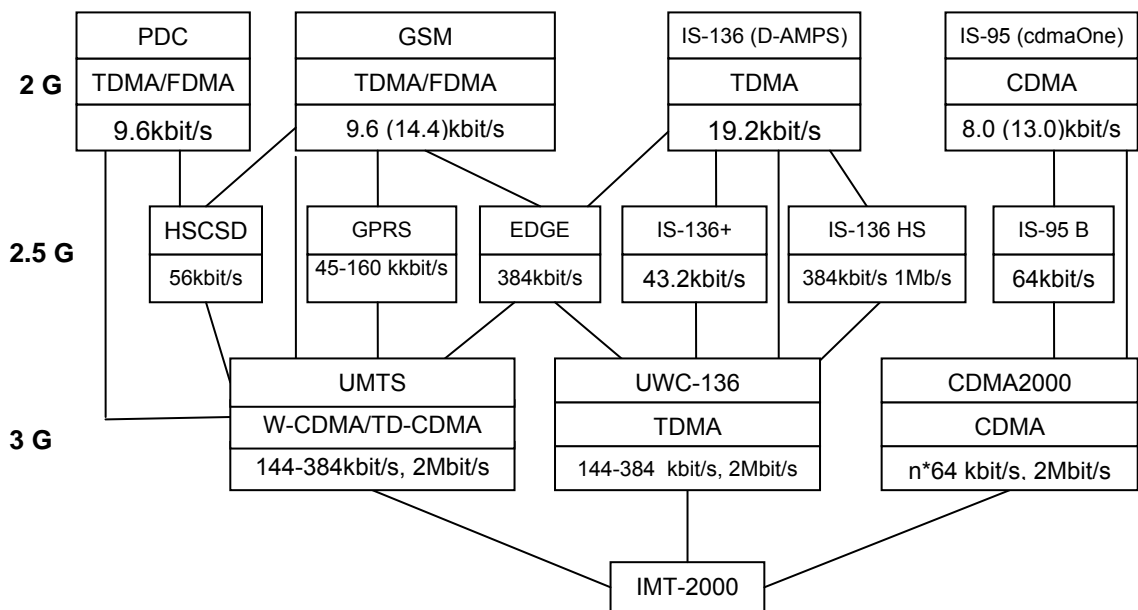


Figure 2-1 Evolution towards third generation mobile systems in terms of data rate support [18].

W-CDMA is capable of providing more capacity as it uses a 4 times wider channel allocation compared to narrow band CDMA. It is based on the radio

access technique proposed by the ETSI Alpha group and the specifications were finalised in 1999 [13].

The AMPS, GSM, IS-95 (CDMA) and UMTS FDD (W-CDMA) standards are of particular interest to this thesis as they all specify FDD operation and therefore require a duplexing filter.

2.6 4th Generation Systems

As envisaged currently, the 4th generation systems will involve providing IP connectivity over the wireless interface. It will encompass all 2nd and 3rd generation wireless mobile technologies and will provide a standard that ensures the interoperability between satellite and terrestrial wireless mobile technologies and W-LANs (Wireless Local Area Networks). Interoperability of network technologies is going to be a major challenge in 4G systems. It is projected that the 4G systems will provide at least 100 Mbps peak data rates in full-mobility wide area coverage and 1 Gbps in low-mobility local area coverage [19]. OFDM (Orthogonal Frequency Division Multiplexing) modulation, multiple antenna technology and CDMA are being considered as elements for 4G systems.

2.7 The Software Radio

The software radio is a highly flexible radio base station or subscriber terminal platform, incorporating many advanced features and technologies, which enables it to provide flexibility and programmability well beyond conventional analogue or digital radios[20]. A software radio is a radio in which the channel modulation waveforms are defined in software [21]. It is a new radio architecture concept that is being researched to overcome a number of drawbacks associated with the traditional narrow band radio architecture. In a traditional narrowband receiver most of the functions such as filtering, amplification, down converting and demodulation are performed using analogue techniques before the signal is

digitised. In software radio the emphasis is given to replace most of the traditional RF functions by digital signal processing techniques. So that the user can have one single transceiver that can tune to different channels of different wireless systems. Software radio will allow the terminals to connect to multiple networks that use different air interface standards. Switching between different wireless standards becomes only a software upgrade without a need to change or upgrade hardware. An excellent overview and discussion on the software radio concept/architecture is presented in [22], [23].

A simple realization concept of a multi-mode receiver that consists of switched multiple traditional receiver chains is shown in Figure 2-2. The required channel is selected by using a fixed channel select filter at an intermediate frequency and channel bandwidth set by the parameters of the particular standard.

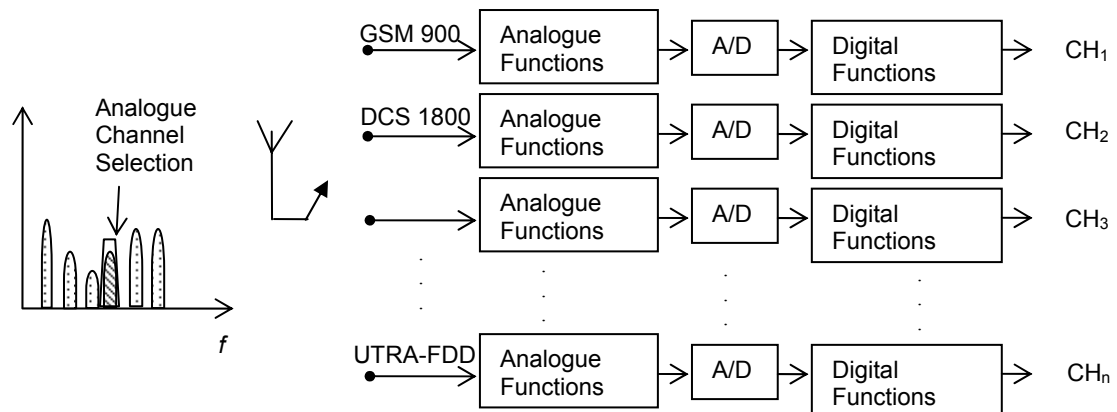


Figure 2-2 Traditional multi-mode/multi-band receiver.

The ideal software radio architecture is shown in Figure 2-3. In this concept the analogue to digital conversion is carried out directly at the front end. Here, the entire band under consideration, which consists of number of channels, will be digitised so that all functions of the radio can be performed using programmable Digital Signal Processing (DSP) microprocessors or Field Programmable Gate Arrays (FPGAs) or some dedicated Application Specific Integrated Circuits

(ASICs). Hence the ideal receiver architecture can be reconfigured to suit any RF band, modulation or data format. This makes it capable of operating within any communications network and would have significant benefits such as reduction of size, cost and power consumption of radio systems.

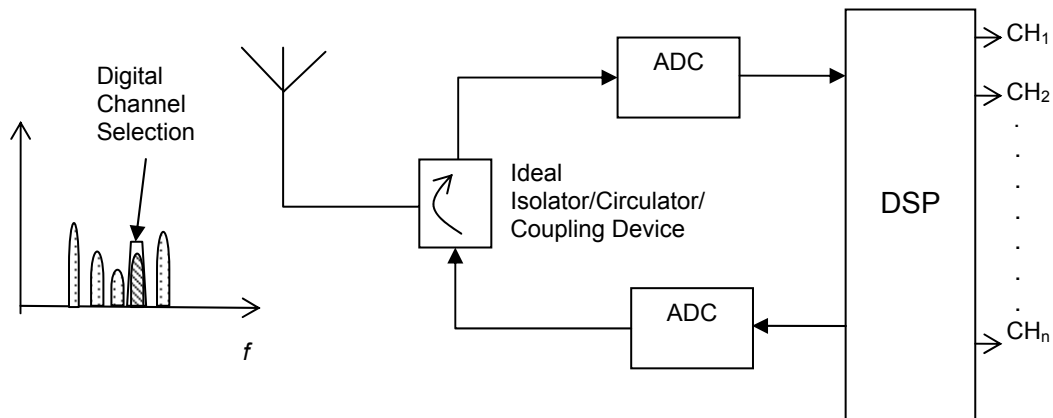


Figure 2-3 An ideal software radio architecture.

If the radio functions are performed using DSP, the new features and upgrades could be done using software upgrades, which become only a reprogramming task. The other significant advantage of using software radio is its ability to support multiple standards. With software radio the receiver could be programmed to receive incompatible technologies such as TDMA (Time Division Multiple Access), GSM and CDMA in the same receiver.

However there are a number of challenges that lie ahead in achieving this concept, mainly in the speed of current Analogue to Digital Conversion (ADC) and DSP capabilities. The total digital processing requirements in such a radio may add up to more than 10GFLOPS (Giga Floating Point Operations per Second) [22]. By January 2005 Texas Instruments have accelerated their fastest DSP to 1500MFLOPS (Mega Floating Point Operations per Second) [24]. Still this is not sufficient for processing the entire radio functionality required by software radio. Since the band of interest could be many megahertz wide (3G mobile's spectrum is 200MHz) and is in the microwave frequency range, it requires very high speed

ADCs to sample the signal. The ADCs must satisfy the Nyquist criterion for sampling so that the original signal can be digitised without the risk of losing information. Up to 500MSPS (Million Sampling per second) of sample rate will be required by 3G mobile with 200MHz bandwidth. Even if the ADCs capability of performing the required conversion rates were available, the power requirements associated with these devices would prevent these ADCs being used in mobile handsets. Kenington's [25] work shows for 20bits (121.76 dB dynamic range) resolution, the theoretical minimum power consumption would be 600mW when operating at 48MSPS. This makes it highly unlikely that the ADC technology in current form would ever be appropriate for pure software radio implementation without a revolutionary change in the ADC architectures [26].

Therefore, radio frequency digitization as in ideal software radio architecture is currently not feasible even though it is an ultimate goal of technology developers. Therefore the receiver configuration should have a pre-selection filter and a low noise amplifier between the antenna and the ADC (and a reconstruction filter and a power amplifier between the DAC (Digital to Analogue Converter) and antenna in the Tx chain). Even then it is debatable whether an ADC exists which could perform well enough at reasonable cost to make a system economically viable [27]

A practical wideband software receiver architecture [20] is illustrated in Figure 2-4. Here, all the channel processing systems will share the wideband front end. The entire band or sub band is digitized by the ADC and the RF front end remains the same as in the traditional design.

A wideband software radio transmitter architecture [20], is shown in Figure 2-5. Here, channels are digitally combined and up-converted after baseband processing, using the counterparts of the wideband receive process.

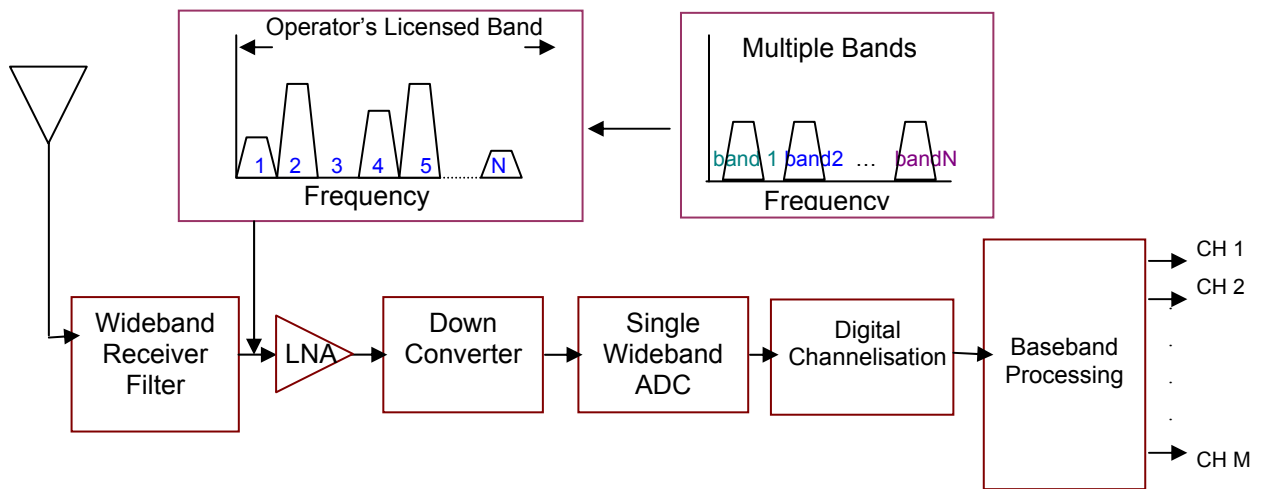


Figure 2-4 Practical wideband software receiver architecture [20].

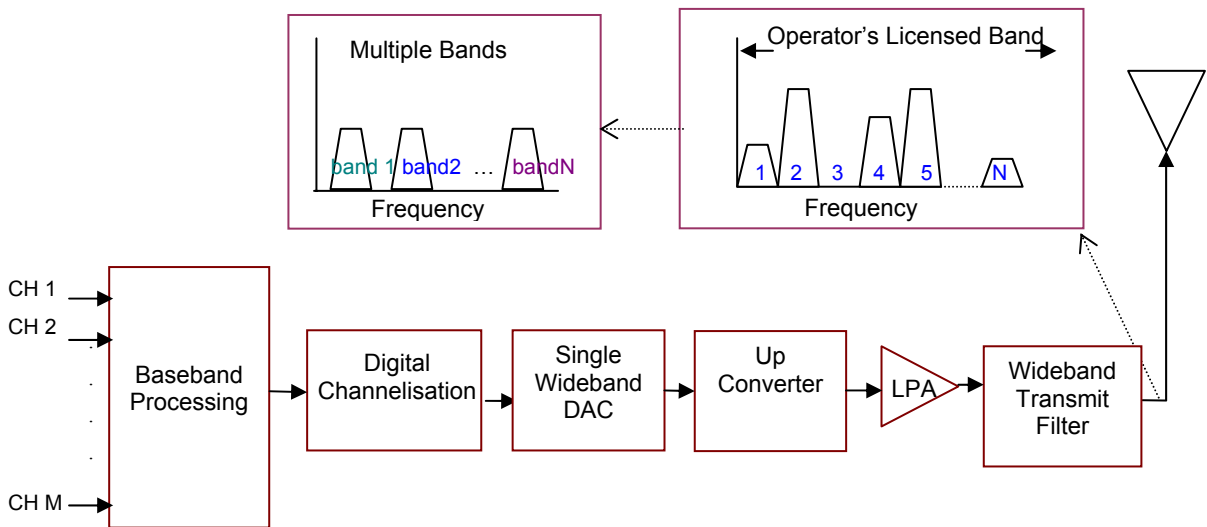


Figure 2-5 Practical wideband software transmitter architecture [20].

Various software radio architectures and design considerations are described in [28], [29], [30], [31] and [32]. In the implementation of software radio architecture in a mobile handset, one of the main challenges lies in the design of a suitable RF front end. The latest sub micron CMOS (Complementary Metal-Oxide Semiconductor) VLSI (Very Large-Scale Integration) techniques available

today have not been a great benefit to RF performance because the dynamic range is reduced by the lower supply voltage. Most of the miniaturisation of RF circuits has been accomplished through a reduction in the packaging size of passive components. Currently, Si bipolar and GaAs are used in most high performance analogue RF front-ends. CMOS is often used for low cost and lower performance front ends as used in W-LANs.

The other main hardware challenges in the RF front end are:

- The Antenna – consumer demand is for mobile communication devices which are lightweight and small in size. In such devices, transmission and receiving must be made by a common antenna [33]. Nearly all cellular phones use a single antenna. The antenna should be able to cover the whole radio spectrum (over 200MHz for 3G). Using a multi-band antenna, software radio can cover both the 2G and 3G spectrum. For example, the AN-40 super wideband antenna which is from US company “Adams-Russel” can cover over 300MHz of spectrum [34] in the 2GHz band.
- The Duplexer – to prevent the receiver from desensitising due to high interference signals, it requires a duplexer in the front end. Currently available duplexing filters are not capable of tuning to the entire required band. Therefore some sort of adaptive duplexing is required. This is discussed in chapter 3.
- The RF power Amplifier - wideband systems require amplifiers with very high dynamic range. Since a non-linear amplifier has dynamic range limitations, a highly linear wideband power amplifier is required.

A review of technical challenges of software radio can be found in [35]. Interoperability between incompatible wireless communication systems can be achieved using a fully programmable software radio. Clear benefits and flexibility lie when the reprogramming of the handset is done using the over-the-air interface. Further, reprogramming and software upgrades can be done using smartcards, over the internet and at kiosks etc. Software difficulties or requirements are not discussed in this section as it is out of the scope of this work.

2.8 Receiver Architectures

At present receiver architectures such as heterodyne, homodyne, image-reject digital intermediate frequency and sub-sampling exist. Super heterodyne receivers have been used widely for radio systems since this architecture has a number of significant benefits including image rejection and adjacent channel selectivity. There is a resurgence of interest in research into homodyne, low-IF and wideband-IF receiver architectures due to the high level of integration requirements for software radio. This section gives an overview of these receiver architectures. The research of the adaptive duplexer presented in this thesis is based on the homodyne receiver architecture. It can be adapted to other receiver architectures as well.

2.8.1 Heterodyne Receivers

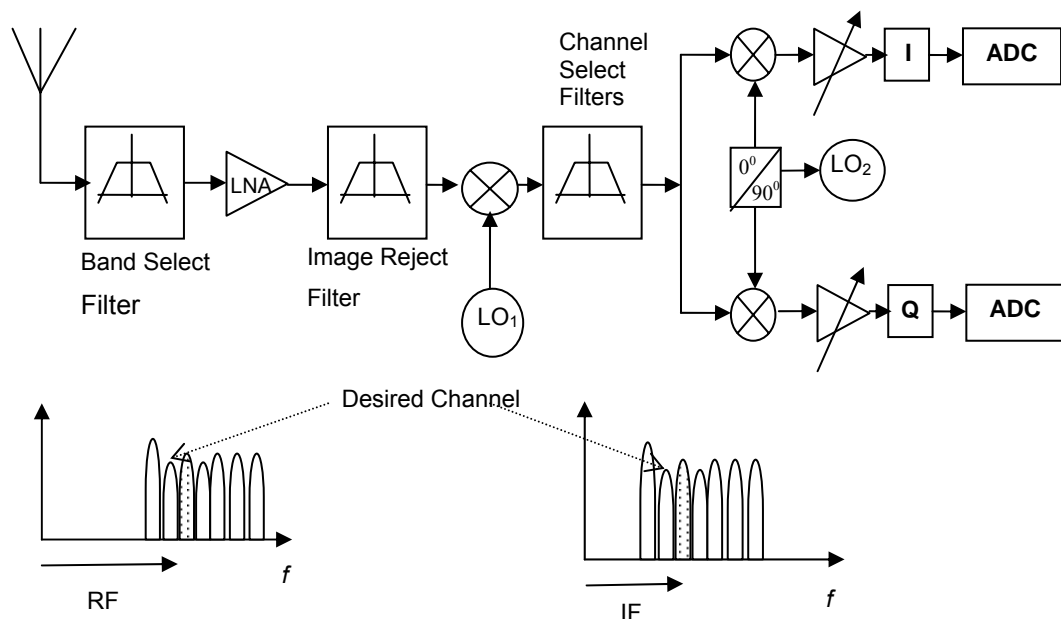


Figure 2-6 Simplified block diagram of a heterodyne receiver architecture.

A simplified block diagram of a heterodyne receiver is shown in Figure 2-6. The received RF signal from the antenna is filtered to remove out-of-band signals using a band select filter. It is then amplified by a Low Noise Amplifier (LNA) to amplify the signal without strengthening the noise component. The channel select filter down the receiver chain (which is used to filter the desired channel) requires high Q's. In order to relax this requirement, the RF signal after the LNA is down converted to an Intermediate Frequency (IF), that is much lower than the received RF signal. The channel select filter then performs channel selection at IF. The selection of the IF is a major consideration in heterodyne receiver architectures. The frequency translation process generates an unwanted signal which may interfere with the desired signal. If the LO (Local Oscillator) frequency is $\omega_{LO} (= \omega_{RF} + \omega_{IF})$, then the desired receiver band centred at ω_{RF} is translated to ω_{IF} . In addition to this, $\omega_{RF} + 2\omega_{IF}$ is also translated to ω_{IF} . This unwanted signal is known as the image signal. The image problem is a critical one since image signal power can be much higher than that of the desired signal [36]. Therefore to remove the image signal, the output of the LNA signal is filtered by an image reject filter before the down conversion.

As shown in Figure 2-7 when the IF is high, the image rejection filter can have high attenuation in the image band [36]. If the IF is low, then the image band attenuation is low but the channel selection filter can produce higher attenuation to the adjacent channel interference signals. Therefore a significant trade-off between sensitivity and selectivity must be done in the design of heterodyne receivers. The channel selection filters in the first IF stage are normally made with SAW filters since highly selective transfer functions are impractical in current IC technology [37]. The centre frequencies and bandwidth of these filters are not flexible and not wide enough to support a multi-band receiver. Further, separate IF selection is required for each mode due to the fixed receive bandwidth of the heterodyne receiver architecture [38]. Therefore it is difficult to manufacture broadband terminals with heterodyne architecture. Another important drawback of this architecture is that the LNA must drive a 50Ω load because the image reject filter is placed off-chip [39].

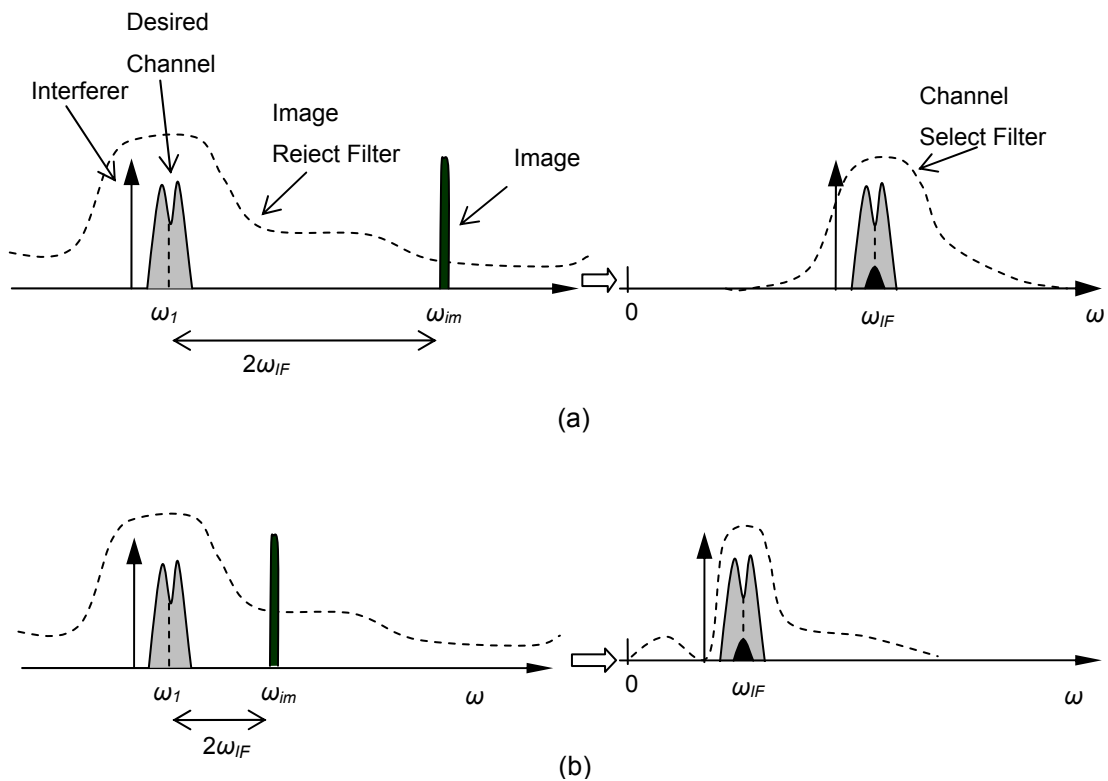


Figure 2-7 Rejection of image vs suppression of interference for (a) high-IF and (b) low-IF [36].

2.8.2 Homodyne Receivers

The homodyne receiver architecture eliminates many discrete components in the receiver chain. In a direct conversion receiver (homodyne, zero-IF), the incoming RF signal is amplified by an LNA and then the desired receiver band is directly translated to zero frequency using a single mixer stage (Figure 2-8). Here LO frequency is equal to the desired carrier frequency. Channel selection of the I and Q signals is done by low-pass filters. Quadrature I and Q channels are necessary in typical phase and frequency modulated signals because the two side bands of the RF spectrum contain different information and results in irreversible corruption if they overlap each other without being separated into the two phases [39]. The advantages over the heterodyne architecture are, it has a simple design,

no image reject filter is required and therefore the LNA need not drive a 50Ω load simplifying the LNA design.

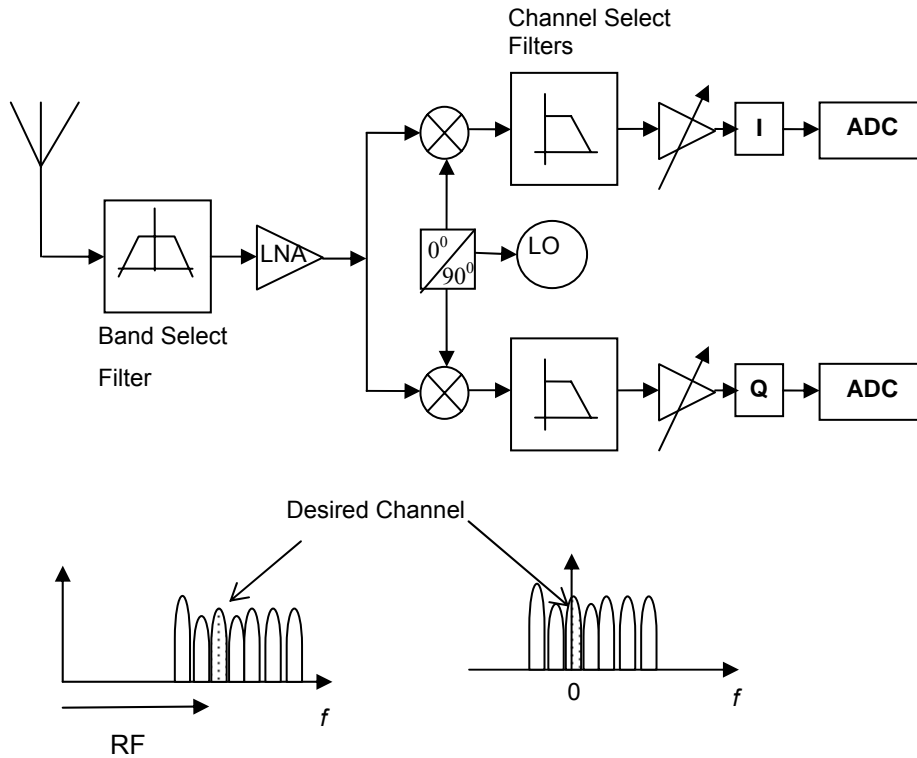


Figure 2-8 A simplified block diagram of a homodyne receiver architecture.

2.8.2.1 Design Issues

There are well known design issues compared to the heterodyne architecture which are discussed in this section.

2.8.2.1.1 DC Offset

Since the receive signal is down converted to zero frequency, DC offset voltages can corrupt the receive signal and can saturate the following stages. There are three types of DC offsets. One is caused when a large interferer leaks from the output of the LNA to the LO port and mixes with the signal itself (self-mixing). This interferer can be the Tx leakage signal in the receiver as discussed in Section

3.6.4. The second is caused by the LO leakage signal mixing with the LO signal. The LO leakage signal can appear at the input of the LNA or the input of the mixer as shown in Figure 2-9. The third occurs when the LO leaks into the antenna and is radiated; it is subsequently reflected from moving objects back to the antenna to generate a time varying DC offset.

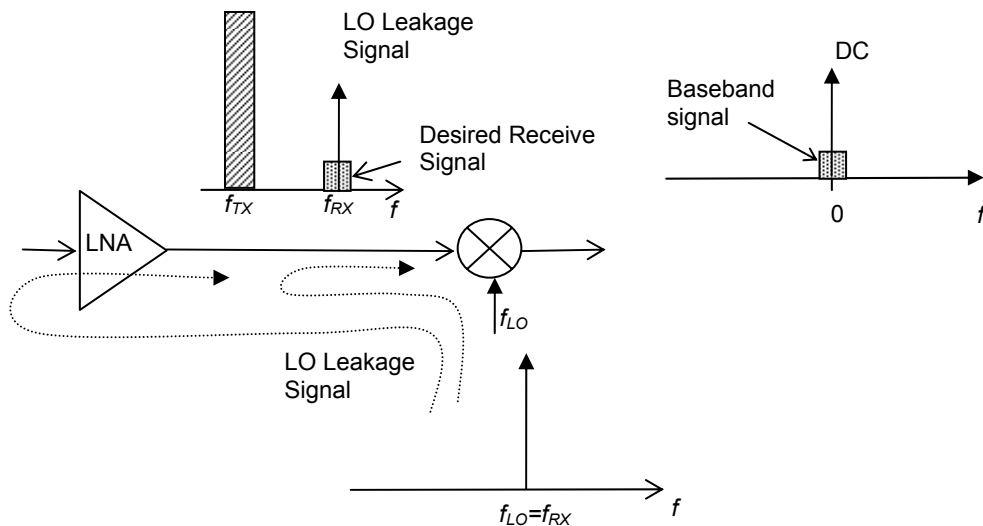


Figure 2-9 Self-mixing in DCR due to LO leakage signal in the LNA/mixer input port.

2.8.2.1.2 I/Q Mismatch

The errors in the nominally 90° phase shifter and mismatches between the amplitudes of the I and Q paths, contribute to gain and phase errors [39] that cause unwanted side bands and distortions in the desired signal. Fortunately, pilot symbol assisted channel estimation is done in W-CDMA systems and this estimation leads to a correction of the I/Q phase and amplitude mismatches [38].

2.8.2.1.3 Even Order Distortion

If two strong interferers close to each other are present at the input to the LNA, a second order non-linearity produces a low frequency beat signal. This phenomenon is discussed in Section 3.6.3.2. In addition a second order distortion

creates a time variant DC offset when amplitude modulated signals are present at the input of the I/Q mixers [38].

2.8.2.1.4 Flicker Noise

Flicker noise is an intrinsic noise source found in semiconductor devices and has a spectral density that is inversely proportional to frequency (so named as $1/f$). Since in direct conversion receivers the down converted spectrum is located around zero frequency, the $1/f$ noise of devices can corrupt the signals. An analysis of $1/f$ noise in direct conversion receivers can be found in [40].

The major design issue out of all the above, is the DC offset component. It must be removed to prevent the large DC component from desensitising the baseband demodulator. For UMTS however, the problem is not so serious, because of the spread spectrum nature of the air-interface. With such a wide bandwidth, it is possible to use AC coupling in the receiver to filter out the DC offsets and some of the other 2nd order products without significantly degrading the sensitivity [41]. These design issues put higher requirements on RF gain, LO-to-RF isolation, IIP3 (third order input intercept point), IIP2 (second order input intercept point) and noise performance. Despite these disadvantages, the direct conversion receiver architecture offers a higher degree of integration than the conventional heterodyne architecture and is more suitable for broadband terminals. The channel select filters (LPFs) and RF to baseband section, can be easily integrated into one chip using Bi-CMOS (especially with SiGe) technology. Recently published direct conversion receiver architectures for multi-band applications can be found in [42], [43], [44], [45], [46] and [47].

2.8.3 Single Conversion Low-IF Receivers

In the single conversion low-IF receiver architecture [48], [49], [50] which is similar to zero-IF receiver architecture, all of the desired channels are down converted to a low intermediate frequency, as shown in Figure 2-10. This low-IF is of the order of one or two channel bandwidths. The main advantages over

zero-IF receiver are that there is no DC offset, flicker noise and LO self-mixing problems because the desired channel is not at DC; in fact it is offset from DC. Since this low-IF architecture avoids the use of discrete components such as image reject filters, it allows a higher level of integration. As the desired carrier is down converted to low-IF, image rejection must be performed by an on-chip image rejection mixer. The image-rejection is limited by matching considerations to about 40dB [50].

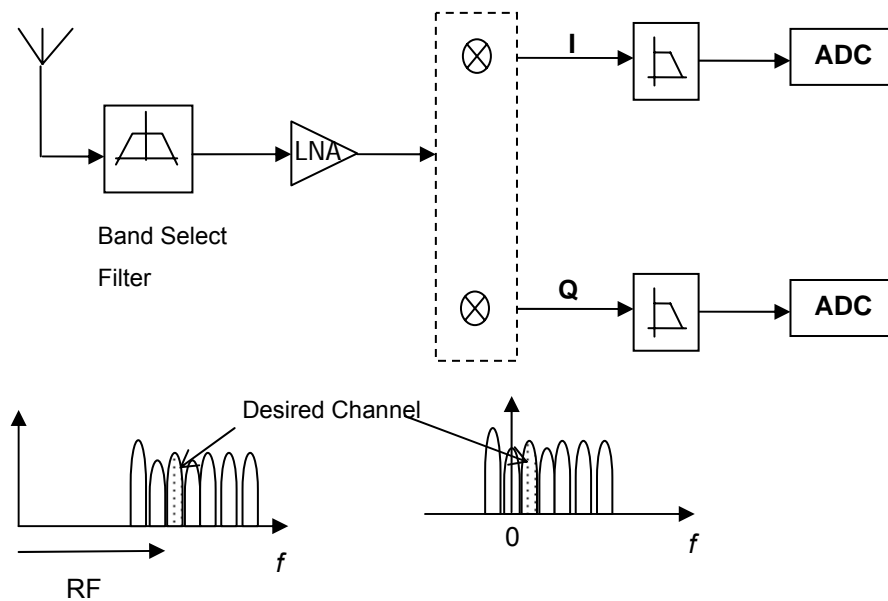


Figure 2-10 A block diagram of a simplified single conversion low-IF receiver architecture.

2.8.4 Double Conversion Wideband-IF Receivers

The double conversion wideband-IF architecture [50], translates all of the receive signal channels to IF frequency using a mixer with a fixed frequency LO (LO_1), thus maintaining a larger bandwidth. Then the up-converted frequency components are removed using a simple low-pass filter. All the received channels after the LPF (Low-Pass filter) are then down converted to baseband using a tuneable channel select low frequency synthesiser (LO_2). Since the desired receive

channel is selected firstly in the first-IF and secondly in the lower second-IF, relaxed Q filters can be used. Here also digitally programmable baseband filters are used and multi-standard capability can be achieved as in the zero-IF receiver architecture. Although the LO_2 is at the same frequency as the IF desired carrier in the wideband-IF system, the offset at baseband which results from self-mixing is relatively constant and is easily cancelled [50].

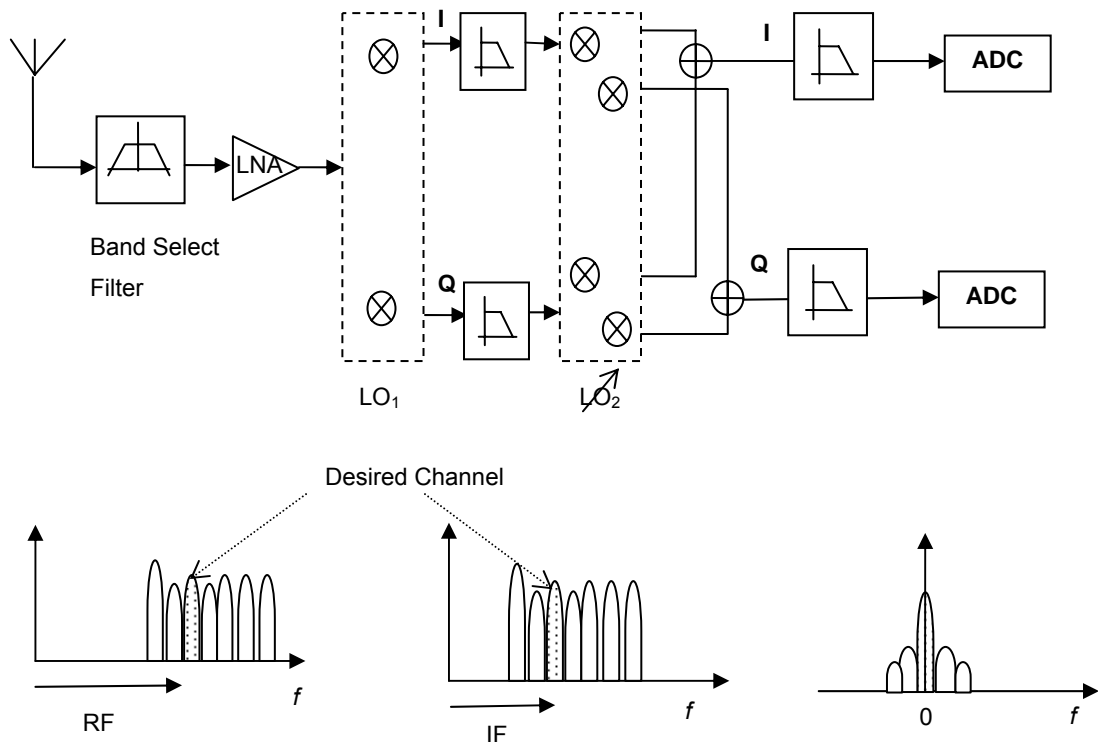


Figure 2-11 Block diagram of a simplified double conversion wideband-IF receiver architecture.

The image rejection filter and channel select filter in heterodyne receiver are normally implemented off-chip. For different standards different image reject filters and different channel select filters have to be used, making it difficult to achieve a highly integrated low cost receiver for multi-band applications. In the DCR architecture no image rejection filter is needed and low-pass filters can be integrated with low power consumption. Although low-IF receiver architectures allow a similar level of integration as zero-IF architectures, they are less suitable

for multi-standard applications [50]. The wideband-IF architecture is also suitable for multi-band applications since the second LO (LO_2) is programmable.

The direct conversion receiver is chosen among the above receiver architectures to test the proposed duplexer architecture in this thesis, since it is more suitable for multi-band applications.

2.9 Conclusion

Mobile devices have evolved significantly and the need for unified standards has become even more important. It is rather unlikely that the whole world would adopt one wireless standard soon. Therefore for the end user the flexibility of having one handset that is tuneable to multiple modes and bands is quite important. Software radio attempts to address this need and one of the key requirements is to implement a low cost multi-band/multi-mode RF front end.

Since the significance of the duplexer in RF front end is primarily in FDD operation, this research focuses on implementing a solution for standards which use FDD operations. Some of the standards that require duplexing filters are AMPS, GSM (base stations), CDMA2000 and W-CDMA.

Near future wireless communication systems with multi-band capability require highly integrated programmable receiver architectures. Therefore the direct conversion receiver has become a more suitable choice due to significantly reduced component count and that has led to significant size, cost and power reductions. The adaptive duplexer architecture in this thesis is based on a direct conversion receiver architecture.

The next chapter introduces the duplexer, TDD operation, FDD operation and discusses the need for an adaptive duplexer.

The Duplexer

3.1 Introduction

Full duplex systems allow simultaneous radio transmission and reception between a subscriber and a base station, by providing two simultaneous but separate channels (frequency division duplex or FDD) or adjacent time slots on a single radio channel (time division duplex or TDD). These are the two duplex modes proposed in the 3rd Generation Partnership Project (3GPP). These two popular ways of achieving full duplex transmission and reception are explained at the beginning of this chapter. Then an introduction to the duplexing for FDD systems is presented. The duplexing requirement for multi-band systems is then looked at with an emphasis on its application to software radio. The effects of non-linearities in the receiver due to any Tx leakage signal are also examined.

3.2 TDD Systems

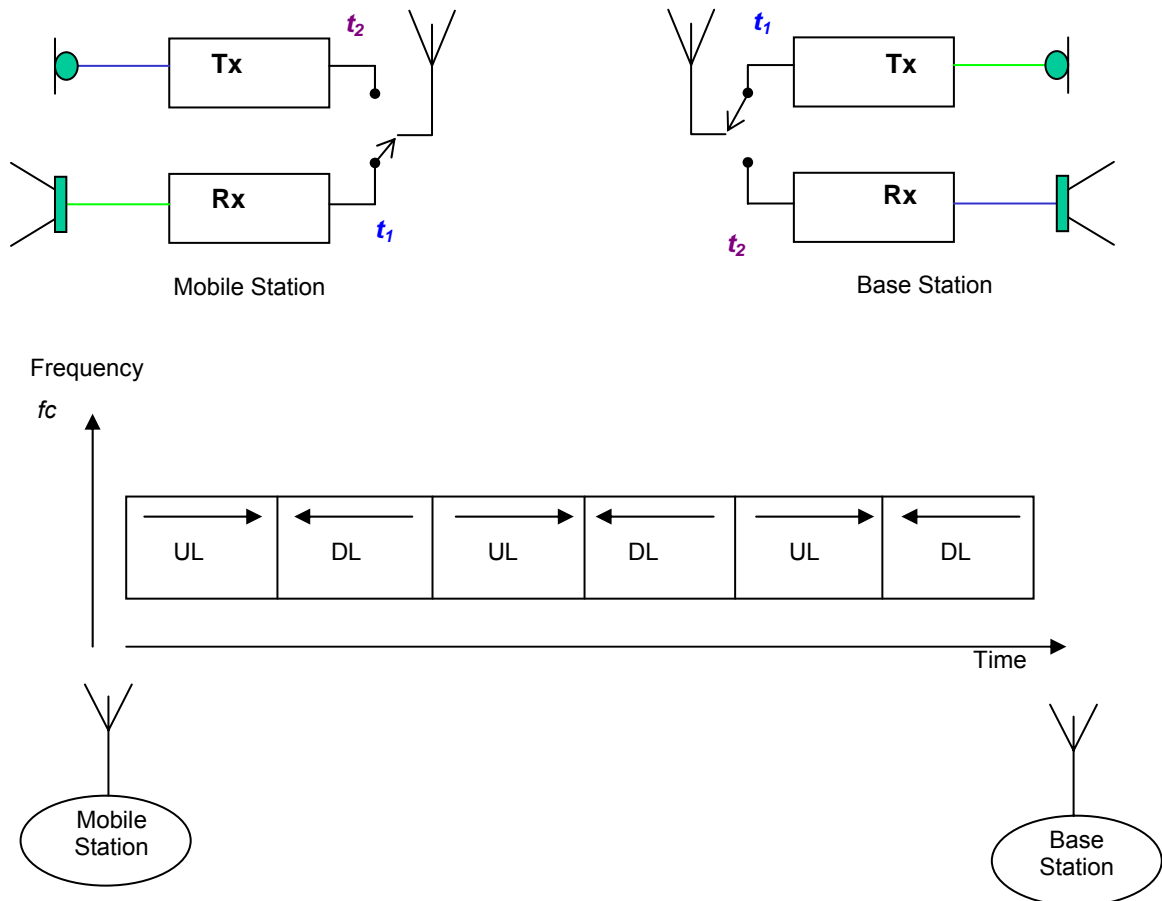


Figure 3-1 The principle of operation in TDD systems.

The principle of operation of a TDD system is shown in Figure 3-1. Here the radio communication system alternately transmits and receives a signal having the same frequency. There is no simultaneous transmission in both directions at a given instant of time. However, due to the fact that the data transmission rate is very much higher than the user's data rate, it is possible to provide the appearance of a full duplex operation to the end user [51]. TDD is only possible with digital transmission formats and digital modulation, and is very sensitive to timing. It is for this reason that TDD has only recently been used, and only for indoor or small

area wireless applications where the physical coverage distances (and thus the radio propagation time delay) are much smaller than the many kilometres used in conventional cellular telephone systems [3]. Compared with FDD, TDD is advantageous in that there is no problem in allocating a frequency to each of the transmitting and receiving signals, and that the transmitting and receiving efficiencies (propagation losses) can be made substantially equal [51].

TDD systems use a switch inside the subscriber unit to switch between transmitter and receiver time slots, thus eliminating the need for a duplexer. This reduces the cost associated with duplexer component. Further this system reuses the filters, mixers, frequency sources and synthesizers, thereby eliminating cost and complexity.

3.3 FDD Systems

In frequency division duplexing (FDD), the subscriber and the base station use simultaneous radio transmission channels, so that they both may constantly transmit while simultaneously receiving signals from each other. The principle of operation in FDD systems is shown in Figure 3-2. Here, a pair of simplex channels (f_1 , f_2) with a fixed and known frequency separation (called as the duplexing frequency, duplexing offset or f_d) is used to define a specific radio channel in the system. The channel used to convey traffic to the mobile user from a base station is called the forward channel, while the channel used to carry traffic from the mobile user to a base station is called the reverse channel. Separate transmit and receive antennas can be used in the base station to accommodate the two separate channels. At the subscriber unit a single antenna is used for both transmission and reception from the base station, and a duplexer is used inside the subscriber unit to enable the same antenna to be used for simultaneous transmission and reception.

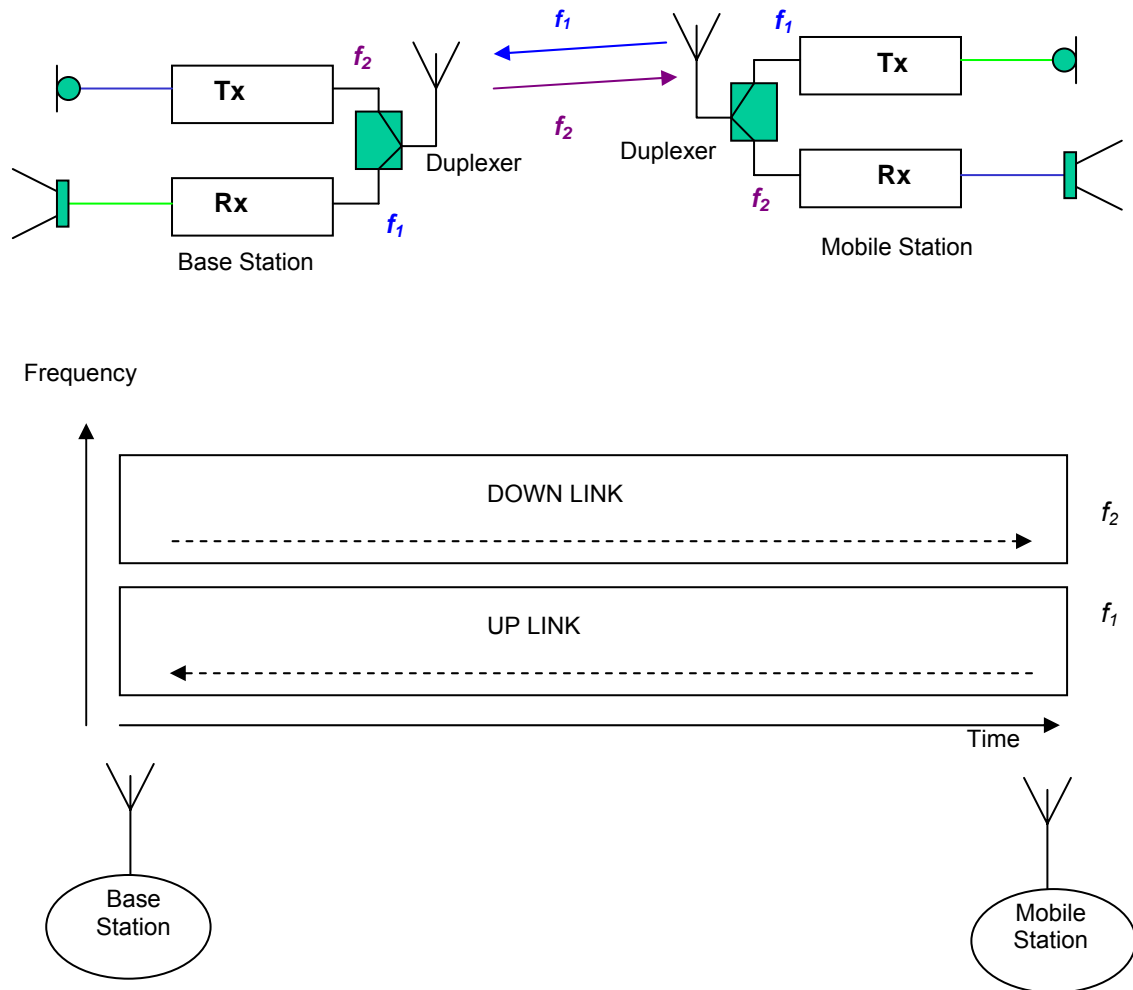


Figure 3-2 The principle of operation in FDD systems.

The basic problem in FDD radio design is transmitter to receiver isolation. Sufficient isolation is required to prevent the transmitter from desensitising and/or damaging the receiver. A frequency duplexing circuit is typically used to provide the required isolation. Alternatively two separate antennas could be used for sending and receiving signals in FDD systems.

To facilitate FDD, it is necessary to separate transmit and receive frequencies by about 5% of the nominal RF frequency, so that the duplexer can provide sufficient isolation while being inexpensively manufactured. In the United States' (U.S.)

AMPS standard, the reverse channel has a frequency that is exactly 45MHz lower than that of the forward channel. In the UMTS W-CDMA standard, the duplexing frequency is 190MHz.

3.4 Introduction to the Duplexer

The duplexer is a device that isolates the receiver from the transmitter while permitting them to share a common antenna. The duplexer is often the key component that allows two way radios to operate in a full duplex manner. An ideal duplexer provides perfect isolation with no insertion loss, to and from the antenna.

A conventional duplexer is a three-port device and normally consists of two band-pass filters and an impedance transforming circuit to allow both filters to connect to a common antenna port (see Figure 1-1).

The band-pass filter in the receiving path (BPF_{RX} in Figure 1-1) stops the transmitter signal from jamming the receiver (receiver blocking or receiver desensitisation), by attenuating the transmit energy incident at the antenna port as shown in Figure 3-3. Receiver desensitisation, commonly called ‘receiver desense’, is caused when high RF signal levels enter a receiver’s antenna input. When desense occurs, the usual symptom is as though the desired signal was reduced; the signal becomes noisy or even fades out completely [52]. There could be a considerable difference between the frequency of the desensitising signal and the frequency of the desired signal. This interfering signal can be wideband noise and/or spurious emissions from the associated transmitter or other nearby transmitters [52].

The front-end of a radio receiver always consists of a low noise amplifier. The LNA’s main function is to amplify extremely low signals without adding noise and to amplify large signals without introducing any distortions [53]. The LNA provides sufficient gain to the smallest possible signal at its input. It is well

known that the gain of an amplifier starts to decrease, when the input power increases beyond a certain value (beyond its dynamic range). In FDD systems, a strong transmitter signal can leak into the receiver and bias the input of the receiver beyond this value. This desensitising phenomenon is mathematically analysed in Section 3.6.1.

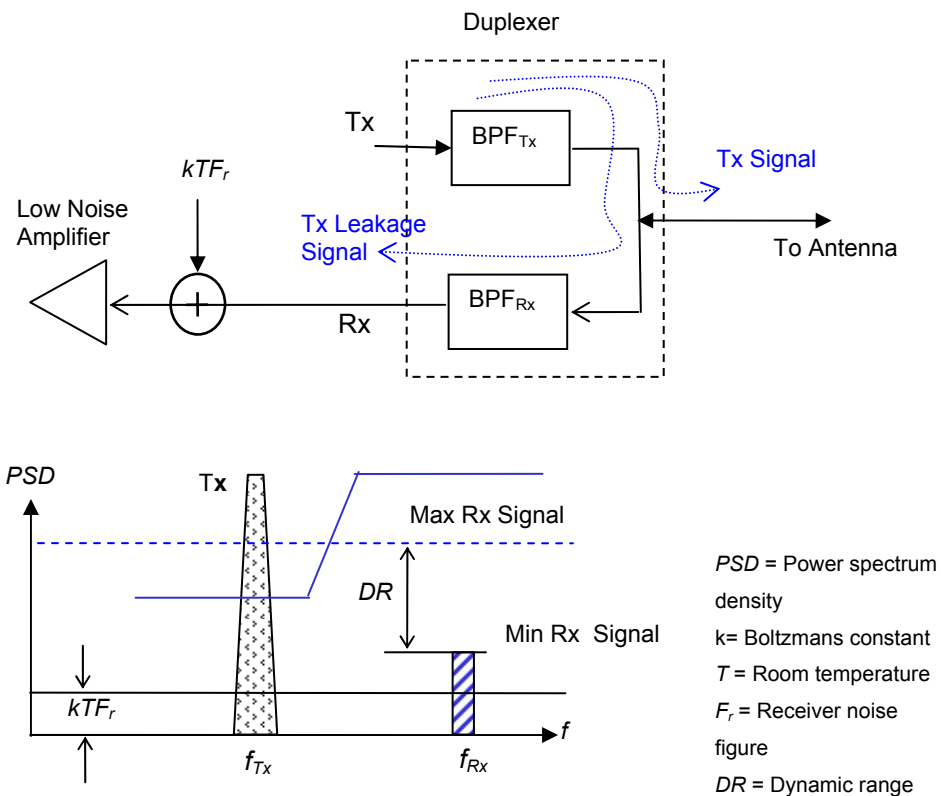


Figure 3-3 Receiver desensitisation.

Every transmitter emits signals other than those on the desired frequency. The function of the transmitter is to supply a modulated RF carrier at the required frequency and power level to the aerial system, with spurious components including harmonics below a required level [54]. The power amplifier is capable of increasing the power level of the Tx signal but at the same time it increases the noise floor across the whole amplifier bandwidth. The band-pass filter in the transmitting path (BPF_{Tx} in Figure 3-4) stops this transmitter noise leaking into the

receiver by attenuating the energy at the receive frequency present on the transmit carrier as shown in Figure 3-4.

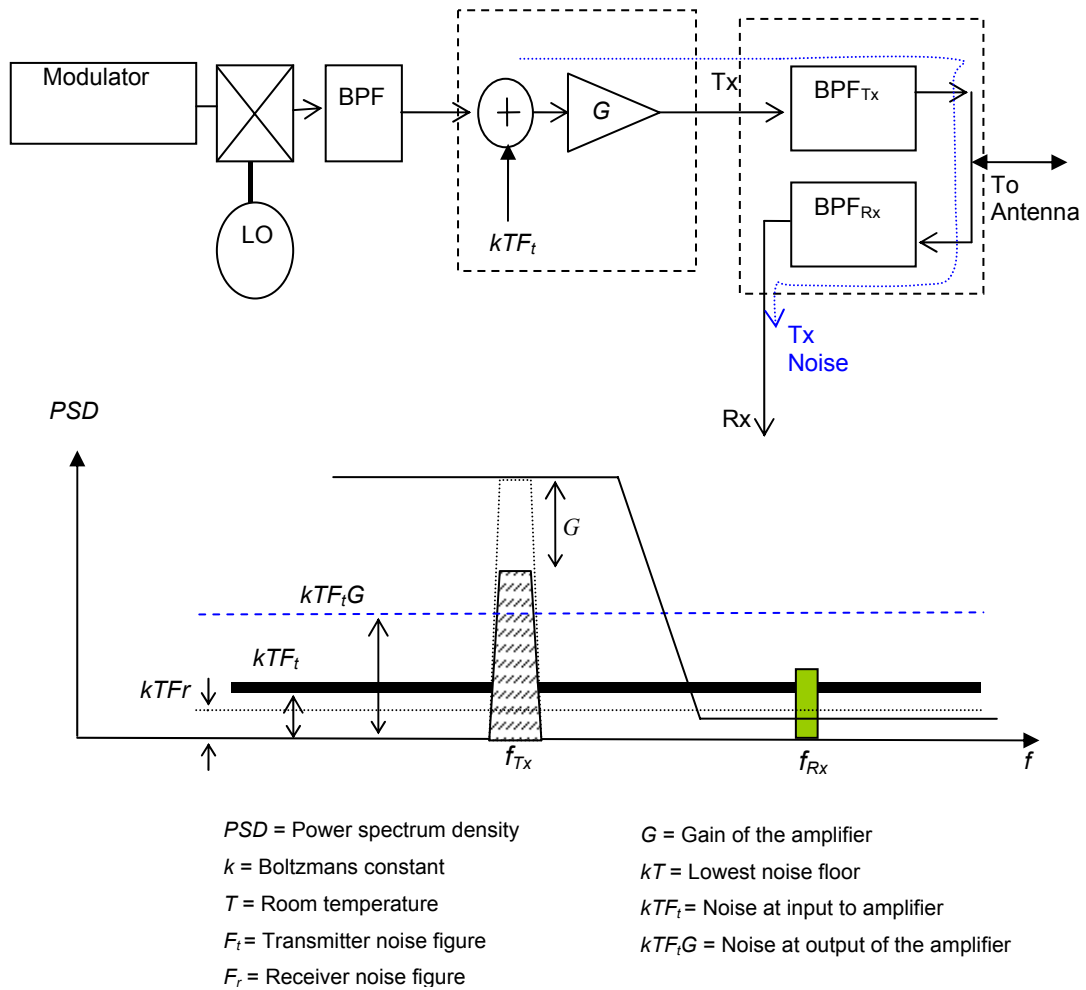


Figure 3-4 Transmitter noise.

The duplexing filters can also provide suppression of out-of-band spurious and image signals [55]. The duplexer can be the most expensive component in the mobile subscriber unit. Duplexers can be implemented in many ways. Some of the common implementations are based on hybrid ring, cavity notch and band-pass/band-reject designs.

A duplexer is normally characterised by Tx and Rx insertion loss and Tx-Rx isolation. As an example, if the Tx and Rx insertion loss is 3dB, then the Tx power should be increased by 3dB to compensate the loss in the Tx signal and Rx

noise figure is increased by 3dB. This means an increase in the insertion loss degrades the receiver noise figure, and hence the receiver sensitivity, but increases the Tx-Rx isolation. Therefore a good duplexer design should make accurate trade offs among the Tx insertion loss, Rx insertion loss and Tx-Rx isolation.

An estimate of duplex circuit performance for W-CDMA [56] is listed in Table 3-1.

Table 3-1 Anticipated performance for W-CDMA duplex arrangement [56]

Duplexer Parameter	Anticipated Performance
Duplex filter Tx loss (dB)	<1.5
Duplex filter Rx loss	<3.0
Loss of system select switch and antenna feed (dB)	<1.0
Combined Tx loss(dB)	<2.5
Combined Rx loss(dB)	2.0 to 4.0
Duplex filter Tx-Rx isolation in Tx band (dB)	>60
Transmitter power classes (hand-held and fixed mounted units) (dBm)	33/27/24/21

3.5 Need for an Adaptive Duplexer in Multi-Band Systems

The filters in FDD duplexers are generally not tuneable. It may not be possible to implement duplexing filters with tuneable centre frequencies and tuneable bandwidths for both 2G and 3G systems in the near future. Recent advances in passive duplexer design have led to smaller, cheaper, and simpler designs [57],

[58], [59], [60]. Tuneable passive duplexers that are tuneable over a limited frequency range are described in [61] and [62]. The first duplexer is designed for a dual-mode AMPS/CDMA cellular system and tunes the response of the Tx filter using voltage variable capacitors. The latter is designed for GSM1800/1900 and tunes the filters using voltage controlled varactor diodes. However these duplexer designs still do not cover multi-band requirements. Therefore the software radio that covers a number of bands will require more than one duplexer. This is shown in Figure 3-5 (a), where two duplexers are connected to the transmitter and receiver using a switch to enable operation on two bands. For multiple bands, the circuit becomes more of a problem. Having more than one duplexer is bulky and is not a viable solution for the mobile handset that has very strict space requirements. The same functionality can be implemented using an adaptive duplexer as shown in Figure 3-5 (b). The proposed adaptive duplexer architecture is explained in detail in Chapter 5.

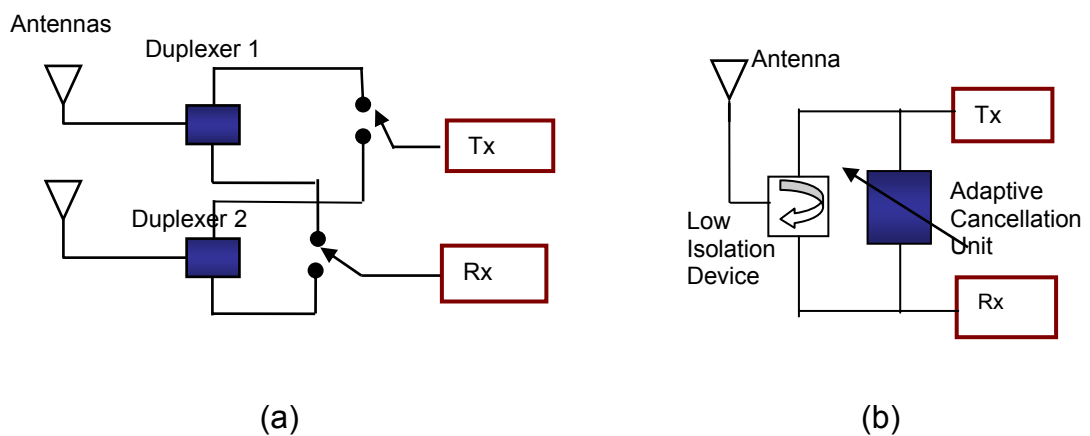


Figure 3-5 The multi-band RF front end (a) using number of duplexers (b) using an adaptive duplexer.

3.6 The Effect of Receiver Non-linearity and the Tx Leakage Signal

Usually the Tx leakage power through the duplexer is significantly higher than any other RF input signal, including jamming signals and the desired signal. Tx leakage becomes the predominant factor that activates non-linearities in the receiver chain since this signal can interact with any other interference signal (in band, out of band or adjacent channel) or the desired signal itself to produce interference products in the receiver band. When the distortions are in band, they can no longer be filtered away. Therefore non-linearity effects need to be considered when determining the duplexer isolation.

An LNA is typically constructed from active devices that operate in the linear range, but the output is never quite linear. Non-linearities in the active devices (transistors) distort the amplified output signal. When there is a high transmitter leakage present at the input, a number of adverse effects including, desensitisation, blocking, cross modulation and intermodulation that degrade the receiver sensitivity can occur. In this section of the thesis, the effects of non-linearities are analysed.

3.6.1 Receiver Desensitisation

The desensitisation determines the receiver's ability to operate successfully under strong interferers. As shown below, when the input power increases to a value that is high enough, the gain of the amplifier starts to decrease. This value is commonly characterised by a compression point measured at the input (*icp*) or at the output (*ocp*) of the amplifier. Hence when there is a high interfering signal, such as the Tx leakage, the gain of the desired signal is reduced causing the signal-to-noise ratio at the detector input to drop. This desensitisation effect can be mathematically analysed as follows.

According to Taylor's series, the output of a nonlinear memory-less amplifier can be expressed as

$$y(t) = a_1x(t) + a_2x^2(t) + a_3x^3(t) + \dots + a_ix^i(t) + \dots \quad \text{Eq. 3-1}$$

where $x(t)$ is the input to the system and a_i is the i^{th} order non-linearity constant.

In general, amplifiers have memory, i.e. the output signals are dependent on the previous instantaneous values of the input signals. If the reciprocal of the bandwidth of the input signal is much larger than the memory of the amplifier, the amplifier can be modelled as memory-less. For very wideband signals memory of the amplifier becomes a significant fraction of the reciprocal of bandwidth of the input signal. This results in a frequency dependent transfer function. The Volterra series approach should be used in such cases. Here, we use the power series approach because even W-CDMA, with 5MHz bandwidth, can be considered narrowband in terms of memory effects in the LNA.

When a desired signal ($A_{Rx}, \omega_{Rx}, \varphi_{Rx}$) and a Tx interference signal ($A_{Tx}, \omega_{Tx}, \varphi_{Tx}$) (this can be any interference signal) are present at the LNA input, i.e.

$$x(t) = A_{Rx} \cos(\omega_{Rx}t + \varphi_{Rx}) + A_{Tx} \cos(\omega_{Tx}t + \varphi_{Tx}) \quad \text{Eq. 3-2}$$

the output can be expressed as

$$\begin{aligned} y(t) = & \left(\frac{a_2 A_{Rx}^2}{2} + \frac{a_2 A_{Tx}^2}{2} \right) + \left(a_1 A_{Rx} + \frac{3a_3 A_{Rx}^3}{4} + \frac{3a_3 A_{Rx} A_{Tx}^2}{2} \right) \cos(\omega_{Rx}t + \varphi_{Rx}) + \\ & \frac{a_2 A_{Rx}^2}{2} \cos 2(\omega_{Rx}t + \varphi_{Rx}) + \frac{a_3 A_{Rx}^3}{4} \cos 3(\omega_{Rx}t + \varphi_{Rx}) + \left(a_1 A_{Tx} + \frac{3a_3 A_{Tx}^3}{4} + \frac{3a_3 A_{Rx}^2 A_{Tx}}{2} \right) \cos(\omega_{Tx}t + \varphi_{Tx}) + \\ & + \frac{a_2 A_{Tx}^2}{2} \cos 2(\omega_{Tx}t + \varphi_{Tx}) + \frac{a_3 A_{Tx}^3}{4} \cos 3(\omega_{Tx}t + \varphi_{Tx}) + \dots \end{aligned}$$

Eq. 3-3

The second term represents the fundamental component of the desired signal. Some of its components are modified by the term a_3 and cause distortion. The receiver front end LNA causes compression in which case $a_3 < 0$. When the interference signal (f_{Tx}) is very large and the desired signal (f_{Rx}) is weak ($A_{Rx} \ll A_{Tx}$), the gain of the desired signal reduces to $[a_1 A_{Rx} + (3a_3 A_{Rx} A_{Tx}^2)/2]$, which is a function of A_{Tx} . This is called desensitisation. When the interference is large enough, so that $A_{Tx}^2 = (2|a_1|/3|a_3|)$, the gain of the desired signal drops to zero. Then the signal is blocked. The difference in dB between the blocking signal level and the sensitivity level is known as the receiver blocking ratio and is shown in Figure 3-6.

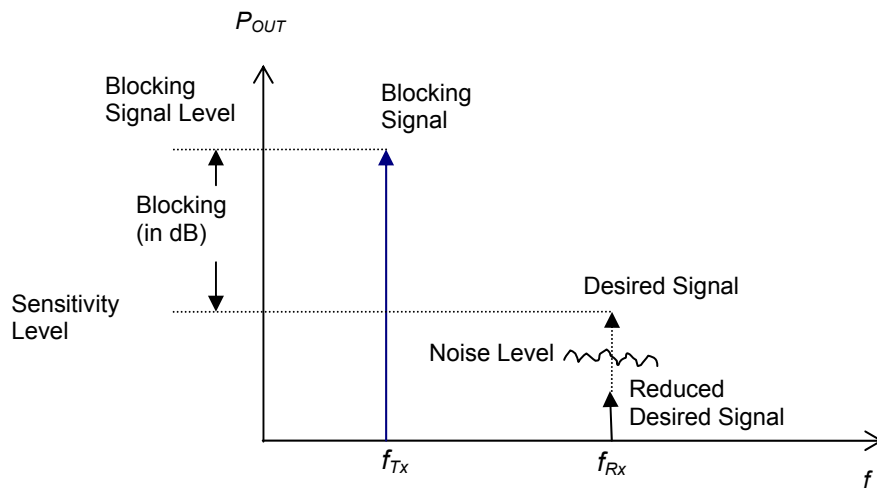


Figure 3-6 Receiver blocking.

The largest signal that can be received by a receiver establishes an upper power level limit of what can be handled by the system while preserving voice or data quality [63]. The dynamic range of the LNA (or the dynamic range of the receiver) which is the difference between the maximum receivable signal and the minimum receivable signal defines the quality of the receiver chain. According to the IS-98A/95B standard, the required minimum receiver sensitivity of a CDMA mobile station is -104dBm , while the maximum received signal power is -25dBm , giving a dynamic range of 79dB .

3.6.2 Cross Modulation

Cross modulation causes a transfer of the amplitude information of the Tx leakage signal to the desired receive signal or the adjacent channel. W-CDMA and CDMA systems exhibit an effective amplitude modulation (AM) of the Tx signal and one effect of interest is the Crest Factor [64]. There are two types of cross modulation.

Type 1: This type of cross modulation can occur when the modulation (or noise) on the amplitude of the Tx leakage signal transfers to the amplitude of the desired signal. This phenomenon is described in [36]. If the amplitude of the Tx leakage signal is modulated by $(1 + m \cos \omega_m t)$, where m is the modulation index ($m < 1$), then the modulated leakage signal becomes $A_{Tx}(1 + m \cos \omega_m t) \cos(\omega_{Tx} t + \phi_{Tx})$. By substituting into the fundamental component of the Eq. 3-3 ($A_{Rx} \ll A_{Tx}$ and $a_3 < 0$) the output becomes

$$y(t) = \left[a_1 A_{Rx} + \frac{3}{2} a_3 A_{Rx} A_{Tx}^2 \left(1 + \frac{m^2}{2} + \frac{m^2}{2} \cos 2\omega_m t + 2m \cos \omega_m t \right) \right] \cos(\omega_{Rx} t + \phi_{Rx}) + \dots$$

Eq. 3-4

Therefore the desired signal at the output of an LNA contains amplitude modulation at ω_m and $2\omega_m$.

Cross modulation specifies the amount of AM which is transferred from an undesired signal to a desired signal. The percentage of modulation on the desired signal due to cross modulation can be expressed as [65]

$$\%d = \frac{\%u(4P_u)}{(P_{ip} + 2P_u)}$$

Eq. 3-5

where,

$\%d$ = the percentage of modulation on the desired signal due to cross modulation

$\%u$ = the percentage of modulation on the undesired signal

P_u = the power of the undesired signal

P_{ip} = the receiver third order input intercept point power

Type 2: This type of cross modulation can occur when there is an amplitude modulated Tx leakage signal ($A_{Tx}(1 + m \cos \omega_m t)\cos(\omega_{Tx}t + \phi_{Tx})$) and another interference signal (single tone jammer – A_j, ω_j, ϕ_j), which is close to the desired signal (adjacent channel). This can cause spectral contamination of the desired signal (Figure 3-7) by transferring the AM onto the adjacent channel, effectively increasing its bandwidth into the neighbouring channels. The ω_j term of the output of the LNA becomes

$$y(t) = \left[a_1 A_j + \frac{3a_3 A_j^3}{4} + \frac{3}{2} a_3 A_j A_{Tx}^2 \left(1 + \frac{m^2}{2} + \frac{m^2}{2} \cos 2\omega_m t + 2m \cos \omega_m t \right) \right] \cos(\omega_j t + \phi_j) + \dots$$

Eq. 3-6

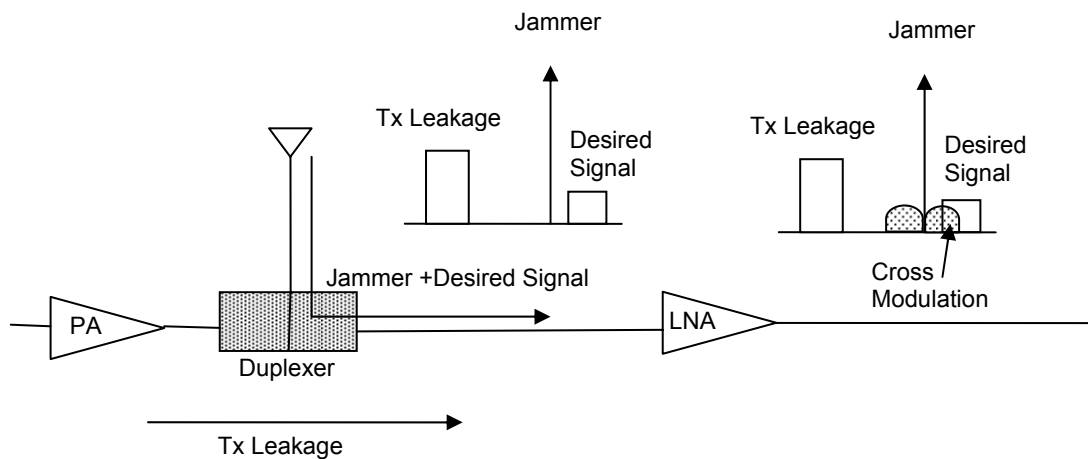


Figure 3-7 Cross modulation due to the Tx leakage signal and a jammer signal.

Aparin [66] analysed the jammer cross modulation from a Tx CDMA leakage signal in a common emitter circuit using the Volterra series and statistical theory. He showed that the cross modulation power depends on the circuit impedances not only at the jammer and Tx leakage centre frequencies, but also at the Tx baseband and at the sum and differences of the Tx leakage and jammer frequencies. In [67], Ko quantitatively dealt with cross modulation in CDMA

receivers and showed that duplexer isolation and LNA IIP3 are responsible for the cross modulation. He also showed that the required LNA IIP3 is about 4-5dBm with a duplexer isolation of 50dB.

The generated cross modulation power in CDMA can be expressed as [67]

$$P_{c\text{mod}} = 2P'_{Tx} + P_{jam} - 2IIP3_{LNA} + 20\log m(\text{dB}) + 12(\text{dB}) + \alpha(\text{dB}) \quad \text{Eq. 3-7}$$

Where

$P_{c\text{mod}}$ = cross modulation power referred to input of the receiver expressed in dBm/1.23MHz

P'_{Tx} = the Tx CDMA signal leakage power at the input of the receiver expressed in dBm/1.23MHz

P_{jam} = the single tone jammer signal at the input of the receiver

m = the modulation index

α = the amount of cross modulation power that penetrates into the in- band signal (the soaking factor)

The authors in [67] have also noted that $P_{c\text{mod}}$ increases by 2dB as the Tx leakage power increases by 1dB, while $P_{c\text{mod}}$ increases by 1dB as the single tone jammer power increases by 1dB.

The generated cross modulation power in W-CDMA can be expressed as [64]

$$P_{c\text{mod}}(\text{dBm}) = (2P'_{Tx} + P_{jam}) - 2IP3 + c \quad \text{Eq. 3-8}$$

where c = the correction factor

It is often the cross modulation that determines the required IIP3 of the LNA in mobile W-CDMA receiver [68]. Here the single tone jammer is replaced by an adjacent W-CDMA channel, although not narrow band, the effect of the spectral spreading due to the cross modulation is still the same. The adjacent channel signal can be as high as -52dBm [64] and the transmit leakage signal can go as high as -20dBm, depending on the transmit power. Desensitisation occurs when

the resulting cross modulated interfering spectrum approaches the receiver sensitivity limit of -92.7dBm .

3.6.3 Intermodulation Distortion

When two sufficiently strong interfering signals are present at the input of the non-linear system, they will mix and create spurious signals at the output known as intermodulation products. One of these interfering signals can be the Tx leakage signal. These intermodulation products can be obtained as shown below.

When the Tx leakage signal $(A_{Tx}, \omega_{Tx}, \varphi_{Tx})$ and jamming signal $(A_j, \omega_j, \varphi_j)$ are present at the input, i.e.

$$x(t) = A_{Tx} \cos(\omega_{Tx}t + \varphi_{Tx}) + A_j \cos(\omega_j t + \varphi_j) \quad \text{Eq. 3-9}$$

Substituting into Eq 3-1 gives the following expression for the output

$$y(t) = a_1(A_{Tx} \cos(\omega_{Tx}t + \varphi_{Tx}) + A_j \cos(\omega_j t + \varphi_j)) + a_2(A_{Tx} \cos(\omega_{Tx}t + \varphi_{Tx}) + A_j \cos(\omega_j t + \varphi_j))^2 + a_3(A_{Tx} \cos(\omega_{Tx}t + \varphi_{Tx}) + A_j \cos(\omega_j t + \varphi_j))^3 + \dots \quad \text{Eq. 3-10}$$

The frequencies, at which the intermodulation distortion (*IMD*) products are generated, is illustrated in Figure 3-8, and can be expressed as

$$IMD = \pm p\omega_{Tx} \mp q\omega_j \quad \text{Eq. 3-11}$$

p and q are positive integers

The second and third order intermodulation products are very common and are difficult to control. We limit our discussion in this section to these distortions only.

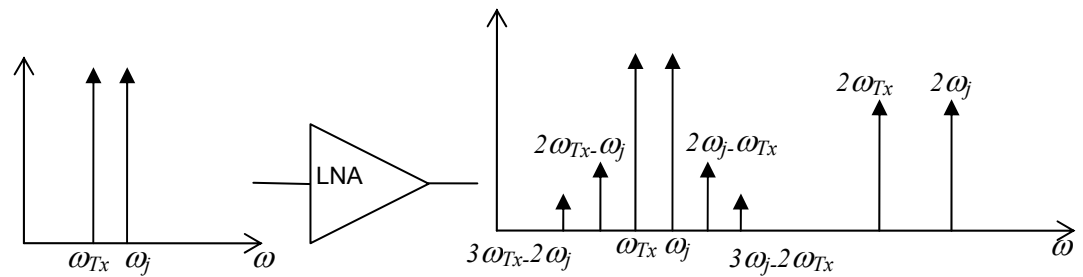


Figure 3-8 Intermodulation due to LNA non-linearity (two tone test signal). $2\omega_{Tx} - \omega_j$ and $2\omega_j - \omega_{Tx}$ are the third order intermodulation products.

3.6.3.1 Third Order Intermodulation

Third order intermodulation products occur at $2\omega_{Tx} \pm \omega_j$ and $2\omega_j \pm \omega_{Tx}$ by mixing the second harmonic of ω_{Tx} with the fundamental ω_j , and by mixing the second harmonic of ω_j with the fundamental ω_{Tx} . Since these distortion products come from the cubic term in the non-linearity, they cause a broadening of the spectrum to approximately three times its original bandwidth, thus leaking into both lower and upper adjacent channels [68]. When the weak desired Rx signal is accompanied by a strong Tx leakage signal (f_{Tx}) and a jamming signal (f_j), third order IMD is generated. One of the products can fall in the receiver band corrupting the desired signal. This can occur particularly, when the difference between f_{Tx} and f_j is small. This effect is shown in Figure 3-9.

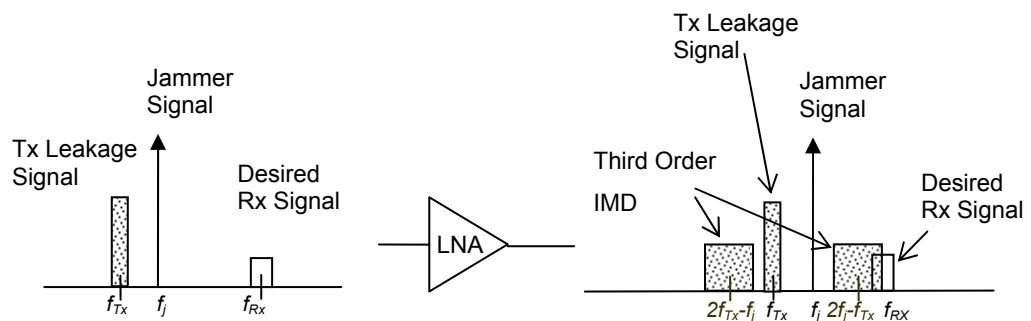


Figure 3-9 The effect of third order intermodulation between the Tx leakage signal and a narrowband jammer.

The third order intercept point (IP3) is used to compare the linearity of different circuits. The IP3 is the theoretical point at which the desired signal and the third order distortion products are equal in amplitudes. This parameter is measured by a two tone test ($A_{Tx} = A_j = A$) in which A is chosen to be sufficiently small so that higher order nonlinear terms are negligible and the gain is relatively constant and equal to a_1 [36]. Then the third order inter modulation products are

$$2\omega_{Tx} \pm \omega_j : \frac{3a_3A^3}{4} \cos((2\omega_{Tx} + \omega_j)t + (2\phi_{Tx} + \phi_j)) + \frac{3a_3A^3}{4} \cos((2\omega_{Tx} - \omega_j)t + (2\phi_{Tx} - \phi_j))$$

Eq. 3-12

$$2\omega_j \pm \omega_{Tx} : \frac{3a_3A^3}{4} \cos((2\omega_j + \omega_{Tx})t + (2\phi_j + \phi_{Tx})) + \frac{3a_3A^3}{4} \cos((2\omega_j - \omega_{Tx})t + (2\phi_j - \phi_{Tx}))$$

Eq. 3-13

From the above two equations we can see that the third order intrmodulation products increase in proportion to A^3 as is shown in Figure 3-10. IIP3 is called the third order input intercept point and OIP3 is called the third order output intercept point. When there is a higher intercept point, the amplifier can handle higher level signals before it starts generating intermodulation products.

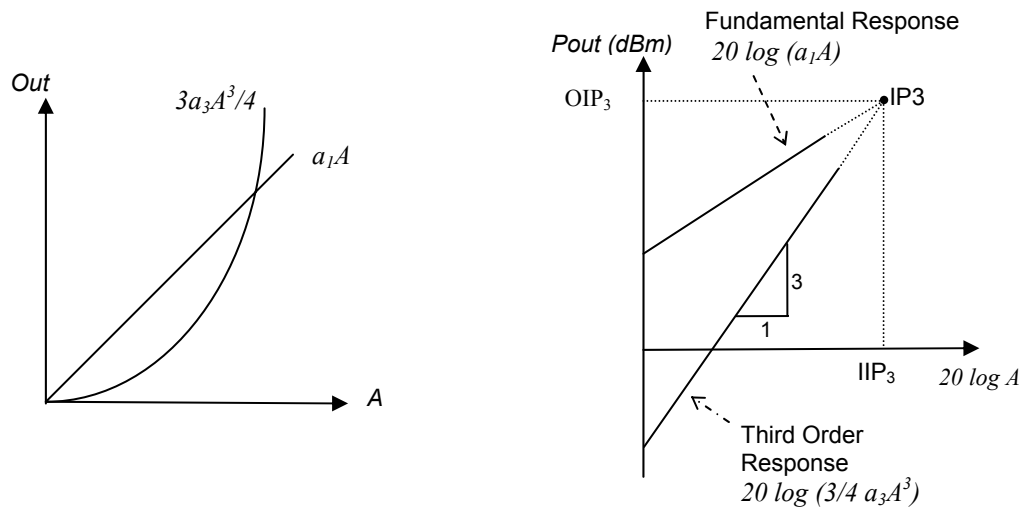


Figure 3-10 Linear and third order intermodulation products vs amplitude. a_3 is normally negative, causing amplifier compression.

3.6.3.2 Second Order Intermodulation

The even terms of the non-linear system characteristics cause second order intermodulation. When a strong modulated signal with time-varying envelope, experiences a second order intermodulation distortion, it produces a spurious baseband signal. This strong modulated signal can be the Tx leakage signal. The spurious baseband signal is proportional to the squared envelope and has twice the bandwidth of the interference signal. It can corrupt the desired baseband signal, and cannot be removed by filtering. This can be mathematically analysed as follows:

If the modulated Tx leakage signal is $(A_{Tx}(1 + m \cos \omega_m t) \cos(\omega_{Tx} t + \varphi_{Tx}))$, the second order term in the output becomes

$$a_2 x^2(t) = \frac{a_2 A_{Tx}^2 (1 + m \cos \omega_m t)^2}{2} + \frac{a_2 A_{Tx}^2 (1 + m \cos \omega_m t)^2}{2} \cos 2(\omega_{Tx} t + \varphi_{Tx}) \quad \text{Eq. 3-14}$$

This baseband output component (the first term) can be expanded to show a DC component and other components including a high frequency component with twice the bandwidth $(2\omega_m)$ of the Tx leakage signal. This DC component can be large compared to the desired receive signal. Therefore direct conversion receivers are very vulnerable to second order distortions. Figure 3-11 shows the second order distortion expected from a W-CDMA signal.

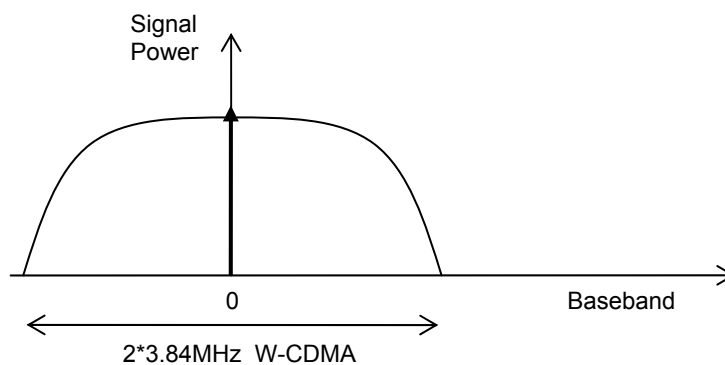


Figure 3-11 Spectrum of the baseband component due to second order distortion caused by the Tx leakage signal in a W-CDMA terminal.

Another example of even order distortion can be presented as follows. Consider Eq. 3-11, with $p = q = 1$, The IMD products become

$$\omega_{Tx} \pm \omega_j : a_2 A_{Tx} A_j \cos((\omega_{Tx} + \omega_j)t + \varphi_{Tx} + \varphi_j) + a_2 A_{Tx} A_j \cos((\omega_{Tx} - \omega_j)t + \varphi_{Tx} - \varphi_j)$$

Eq. 3-15

Therefore when a Tx leakage signal and another jamming signal are present at the input of the LNA and especially when the difference between these two interferers are very small, the output generates a low frequency beat. This becomes awkward in direct conversion receivers because this low frequency beat can leak through the mixer and corrupt the down converted desired signal. This effect is shown in Figure 3-12.

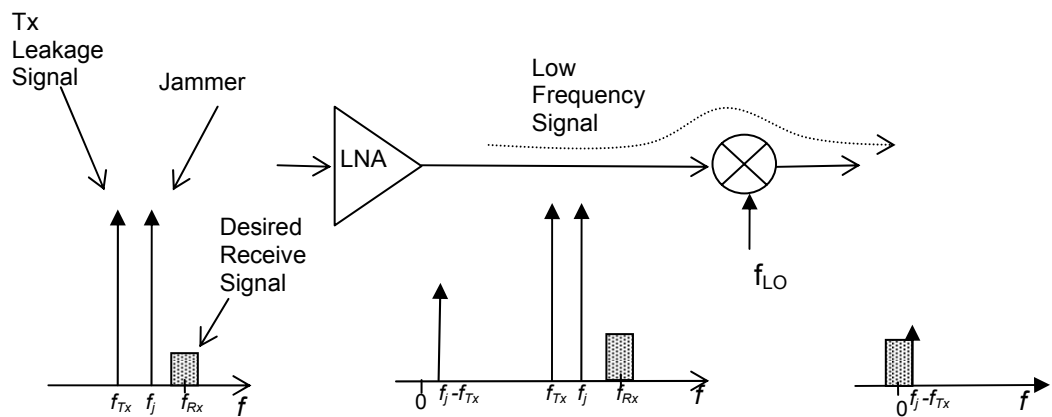


Figure 3-12 Effect of second order distortion from the LNA feeding through the mixer.

Second order distortion can be characterised using a second order intercept point, IP2 (Figure 3-13). This can be measured using a two-tone test, similar to IP3.

In [56], the required receiver IIP2, was shown to be about 47dBm for W-CDMA terminal with transmitter leakage of -50dB. This was based on the assumption that the second order product should be suppressed at least 10dB below the noise level. A multi-band receiver may require the use of a wide-band LNA to cater for the different RF bands. Wide-band input matching is necessary and this increases the frequency range over which interference signals can be present. A higher

second order input intercept point is required to lower the effect of interference originating from these other bands [69].

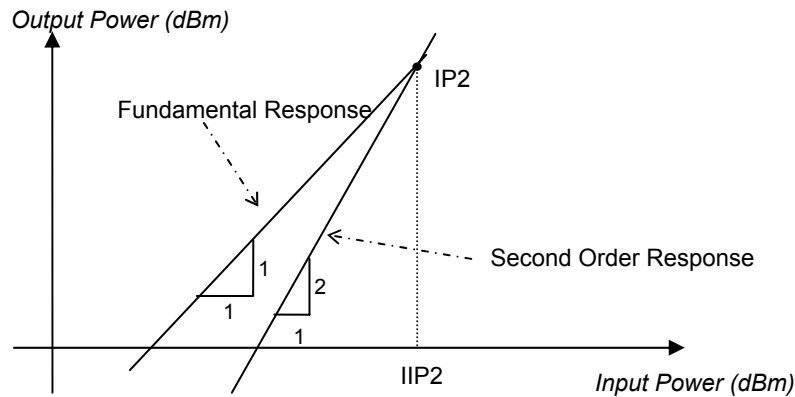


Figure 3-13 Illustration of IIP2. The second order response has a slope of 2.

3.6.4 DC Offset in Direct Conversion Receivers Due to the Tx Leakage Signal

In most receiver architectures, such as the superheterodyne receivers, an additional filter is introduced after the LNA to suppress the residual transmitter leakage signal. This protects other components down the receiver chain from being influenced by the transmitter leakage. For the direct conversion receiver architecture this is not necessarily effective. The Tx leakage can still be high at the input to the mixer, even if it is not high enough to activate the mixer nonlinearities. When some Tx leakage signal leaks from the LNA circuit (avoiding the filter after the LNA) or from the mixer input to the local oscillator port, it produces (by self-mixing) another source of second order intermodulation distortion. This results in a DC component in the baseband. This DC component varies with the square of the Tx leakage signal's amplitude and has twice the bandwidth of that signal since the squaring (self-mixing) action makes the IM2 (second order intermodulation) signal bandwidth dependent on the amplitude modulation of the Tx leakage signal [70]. The effect of self-mixing in DCR due to Tx leakage signal is shown in Figure 3-14. The cure for this type of IM2 signal is to reduce leakage into the LO port, not to reduce distortion in the mixer itself.

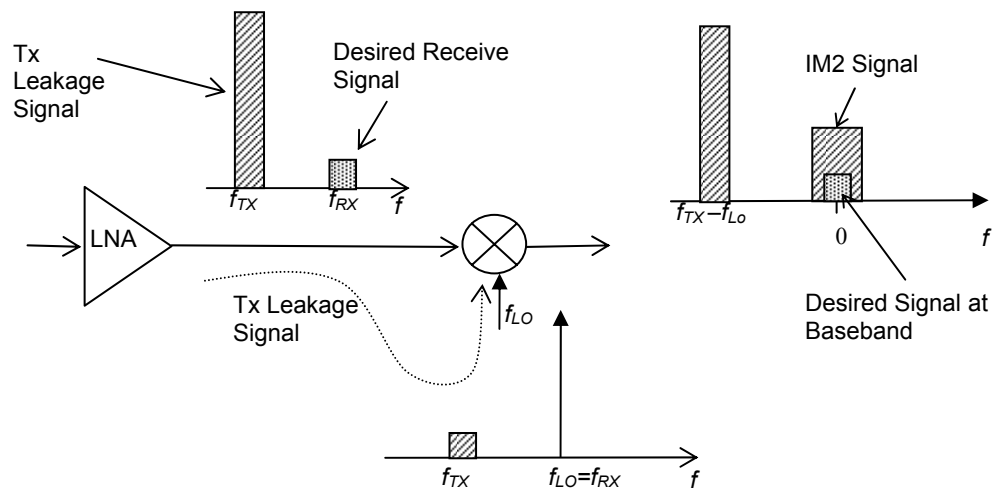


Figure 3-14 Self-mixing in DCR due to the Tx leakage signal in LO port.

A summary of receiver requirements for W-CDMA for the entire receiver and the part of the receiver [56] that follows the duplex circuits is listed in Table 3-2.

Table 3-2 Summary of RF receiver requirements for 3G W-CDMA mobile equipments [56].

Requirement	Entire Receiver	After Duplex
Noise figure	≤ 9	≤ 5
In-band selectivity (dB)		
First adjacent channel (5MHz)	≥ 33	≥ 33
CW interferer (10MHz)	≥ 58	≥ 58
Third adjacent channel (15MHz)	≥ 58	≥ 58
Modulation blocker (>15MHz)	≥ 58	≥ 58
Intercept points (dBm)		
IIP2 (10MHz)	≥ - 16	≥ - 18
IIP2 (15MHz)	≥ 8	≥ 6
IIP2 (Tx)		≥ 47
IIP3 (10/20MHz)	≥ -17	≥ -19
IIP3 (67.4/134.8MHz)		≥ -8
Image rejection (>85MHz) (dB)	≥ 84	n/a
Oscillator noise sidebands at >8MHz offset (dBc/Hz)	≤ -129	

3.7 Duplexer Requirements

There are five main requirements a duplexer should satisfy when considering multi-band applications:

- 1) The duplexer should be able to handle the frequency specifications of the different standards. Since the software radio has to work with the standards of second and third generation, the frequency region should be between 800-2200 MHz. The signal frequency bandwidths are from 25KHz (PDC) to 5MHz (UMTS) [66]. Table 3-3 lists the duplexing frequency and frequency bandwidth for the most common air interface standards. The last three entries have no TDD component and so require duplexing filters.

Table 3-3 Duplexing frequency and frequency bandwidth

Air Interface Standard	[Downlink]/ [Uplink] (MHz)	Duplexing Frequency (MHz)	Channel Spacing
PDC	[940-956]/[810-826]	130	25kHz
GSM 900	[890-915] / [935-960]	45	200kHz
DCS 1800	[1710-1785] / [1805-1880]	95	200kHz
PCS 1900	[1850-1910] / [1930-1990]	80	200kHz
IS-95	[824-849]/[869-894]	45	1.25MHz
UMTS FDD (CDMA2000)	[1850-1910] / [1930-1990]	80	1.25MHz
UMTS FDD (Europe)	[1920-1980] / [2110-2170]	190	5 MHz

- 2) The duplexer must be able to handle the maximum output power of the transmitter. The transmitter power levels depend on the standards and the terminal classes or levels. FDD maximum output powers are shown in Table 3-4.

Table 3-4 The maximum output power

Air-Interface Standard	Maximum Tx Output Power(dBm)
GSM 900	Terminal class 2: 39 3: 37 4: 33 5: 29
DCS 1800	Terminal class 1: 30 2: 24 3: 36
PCS 1900	Terminal level 1: 30 2: 24 3: 33
IS-95	3 : 30
UMTS FDD (Europe)	Terminal level 1: 33 2: 27 3: 24 4: 21

- 3) The duplexer must be able to provide sufficient isolation to prevent receiver desensitisation. As previously described, when there is a high interfering signal, the gain of the desired signal is reduced, becomes noisy or even fades out completely (see Figure 3-3). In a conventional duplexer the duplexing filter in the receiver path, prevents the receiver desensitisation. A typical value for the acceptable maximum spurious Tx signal at the receiver input is -27dBm . The duplexer isolation requirement for W-CDMA would therefore be between 48dB to 60dB depending on the power class (see Table 3-4).

- 4) The duplexer must be able to provide adequate rejection of the transmitter noise at the desired receive frequency. The noise level of a system sets the minimum signal strength that can be detected. Receiver sensitivity levels for most common FDD air interface standards are shown in Table 3-5. If the requirement for the Tx noise is not to decrease the receiver sensitivity, then the Tx noise at the receiver input should be below the Rx noise floor ($-174+N_{\text{Rx}}$ dBm/Hz). According to the noise figure calculations in [56],

the noise figure requirement for W-CDMA entire receiver is $N_{Rx} \leq 9$. This noise figure must be met in the presence of the Tx leakage signal. Even if the Tx chain has a relatively low noise, the duplexer requires an attenuation of about 40dB [4].

Table 3-5 The receiver sensitivity level

Air Interface Standard		Reference Sensitivity Level (dBm)
GSM 900	Small MS Other MS	-102 -104
DCS 1800	Class 1 or Class 2 Class 3	-100/ -102 -102
PCS 1900	Normal Other	-102 -104
UMTS (FDD)	12.2kbps 64kbps 144kbps 384kbps	-92 -99.2 -102.7 -107

- 5) The duplexer should add a minimum of additional insertion loss to the Tx and Rx paths. Insertion loss occurs in both the Tx and Rx paths of a duplexer. The greater the insertion loss, the lower the output level, the higher the noise figure and the greater the power dissipation and temperature rise in the filters. In a conventional duplexer, a high Tx insertion loss may reduce its maximum power handling capability. As shown in Table 3-1, for W-CDMA a 3dB duplex filter Rx loss is common and this will increase the Rx noise figure by a similar amount. Due to the small physical size requirements of the duplexer, this increase is unavoidable. However in the adaptive duplexer architecture (Section 5.2), careful consideration has been given to select components that minimize Rx insertion loss.

3.8 Conclusion

The duplexer in FDD system is used to provide simultaneous transmission and reception. The continuous presence of the Tx leakage signal in FDD systems create problems such as receiver desensitisation, cross modulation, intermodulation distortion and DC offset in direct conversion receivers due to non-linearities and leakage in the RF front end. These problems highlight the need for high performance duplexers.

Multi-band radios require multiple switched high isolation duplexers. This is difficult due to the stringent space constraints of multi-band software radio handsets because existing duplexers cannot be implemented in an integrated circuit. Further, multiple duplexers consume significant cost. Therefore an integratable adaptive/active duplexer with the same functionality is needed. An adaptive duplexer with a low isolation device and an active cancellation unit is proposed in this thesis. Adaptive duplexing eliminates many external components in a multi-band transceiver front end. The adaptive duplexer architecture is described and analysed in the following chapters.

There are five main requirements for an active duplexer in multi-band applications. The duplexer should be able to handle multi-bands (800-2200MHz), handle the maximum output power of the Tx (33dBm for UMTS FDD), provide sufficient Tx-Rx isolation (60dB), provide adequate rejection of Tx noise at the desired Rx frequency (40dB) and give minimum insertion loss to the Tx path and Rx path (1.5dB-Tx, 3dB-Rx). A literature survey of duplexing methods is presented in the next chapter.

Literature Review

4.1 Introduction

Passive filters in conventional transceivers often take the form of ceramic, cavity or SAW structures. These filters demonstrate very linear, low noise characteristics. Since these devices have a fixed centre frequency and bandwidth they are not tuneable. This imposes a design constraint for multi-band systems. Today filter technologies are dominated by ceramics (dielectric) and SAWs in wireless mobile communications such as GSM, CDMA and W-CDMA. Ceramic filters/duplexers are relatively large in size. SAW filters have a size advantage over ceramic filters but suffer from a low power handling capability and poor sensitivity. Recent research in BAW (Bulk Acoustic Wave) technology potentially indicates superior performance to SAW technology. BAW devices exhibit better power handling capability and size reduction. BAW filters are very attractive candidates for integration with ICs (RF CMOS & RF MEMS (Micro Electro-Mechanical Systems)) as they can be grown directly on silicon to provide the high

Q resonant components needed in radio multi-chip modules for front-end filtering [71]. However, BAW devices have the disadvantage of being fixed frequency.

This chapter begins with an introduction to traditional duplexing filters (passive filters), followed by a review of the literature related to adaptive duplexing that can be extended for multi-band systems. Numerous architectural options with their relative merits and tradeoffs are also discussed.

4.2 Traditional Duplexing Filters

Duplexers can be constructed in several ways. FDD systems use two singly terminated filters known as diplexers or duplexing filters. The two duplexing filters are connected at the terminating port to form a three-terminal network.

There are many ways to combine filters to perform duplex operation such as band-pass duplexers, band-reject or notch duplexers or vari-notch type duplexers. Specifically [52]:

- Band-pass filters that have a specific centre frequency and pass-band with losses that increase as the frequency deviation from the pass-band edge increases.
- Reject or Notch filters which operate opposite to a band-pass filter. These are designed to cause high losses at the centre frequency and lesser losses as the frequencies increase from the centre frequency.
- Specialized filters such as Tx Rx Systems vari-notch filter, which has characteristics of both a band-pass and notch filter in one device.

There are several types of filters such as lumped element (LC) filters, cavity, ceramic, SAW etc.

4.2.1 Lumped Element Filters

Usually, lumped element filters are constructed using parallel-plate chip capacitors and air-wound inductors soldered into a small housing [72]. Typical lumped element filters are designed for low frequency ranges from 25 to 1000MHz [73]. High Q capacitors and coils with associated parasitic are used to implement these filters. Due to the large size of the lumped element duplexers these are used in base stations and half-duplex transceivers (where strong transmitter leakage is not present, thus lower out of band attenuation can be considered).

Lumped element filters are now at microwave frequencies up to about 18GHz [74]. Low Q is still a significant issue in passive LC filters implemented on-chip so far. There has been significant improvement in the conventional lumped element filters with the development of miniaturised components that have high Q at high frequencies and also due to the employment of CAD (Computer Aided Design) techniques in the design process. This type of filter has tremendous design flexibility and practically no lower frequency limit or upper bandwidth limit [75]. However these filters demonstrate poor Q at high frequencies. Tuneable LC band-pass filters can be found in [76] and [77]. A design and results of quasi-lumped element LTCC (Low-Temperature Co-fired Ceramic) filters suitable for using in a duplexer for wireless communication systems is presented in [78]. LTCC is a low loss, high precision substrate that allows higher number of passive components to be integrated in a smaller area.

4.2.2 Cavity Duplexing Filters

A cavity is a single resonator, usually in the form of an electrical quarter wavelength [79]. A resonant cavity filter is typically a two port device and the response characteristic depends on the filter type (band-pass, band-reject, notch or vari-notch). Most resonant cavity filters are made of seamless aluminium and finished with a passivated alodined finish [80]. Cavity resonator filters are usually implemented with helical, coaxial, or waveguide resonators. Coaxial filters are

available in frequencies from 30MHz to over 10GHz and helical filters from below 10MHz to 2GHz [75].

A number of cavities is cascaded to form a duplexer. Duplexer isolation can be adjusted by changing the number and size of the cavities. These duplexers have very high Q factors, and their resonant frequencies are determined by mechanical components, especially by the tuning rod. The rod is usually made of a material which has a limited thermal expansion coefficient (such as Invar) [81]. Cavity filters are mostly used in base stations and repeaters. Cut-away views of typical band-pass and band-reject cavities [82] are shown in Figure 4-1.

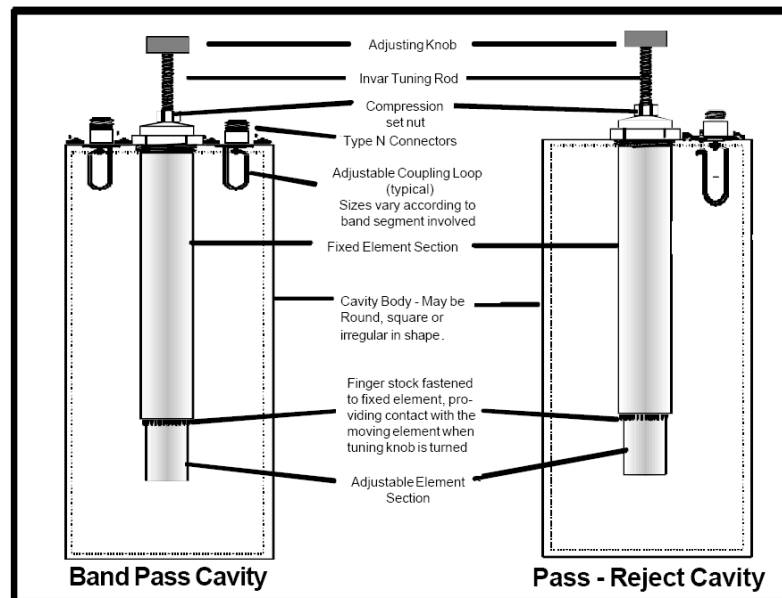


Figure 4-1 Cut-away views of typical band-pass and band-reject cavities [82].

A six-cavity duplexer [81] for use with a 144MHz repeater and the frequency response of the duplexer is shown in Figure 4-2 (a) and (b). The Rx filter (3 cavities) is tuned to pass 146.34MHz and notch 146.94MHz. The Tx filter is tuned vice versa. For mechanical stability, the cavities are fastened to a plywood base. The duplexer isolation is about 100dB.

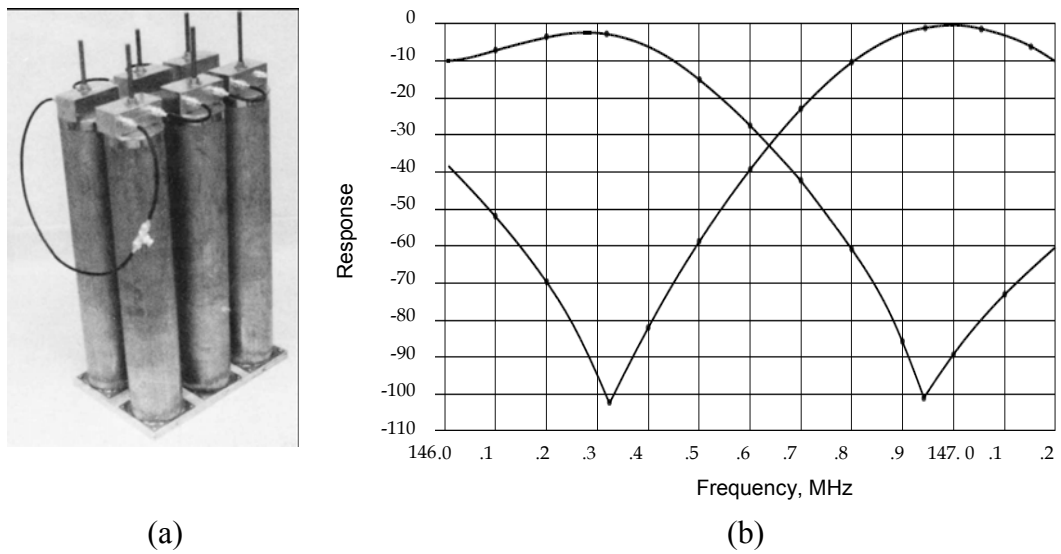


Figure 4-2 A six-cavity duplexer and the frequency response [81].

Recent developments have realised low weight low volume cavity duplexers for high frequencies. One such design, a GSM 1800 base station duplexer (FD183005-1) [83] is shown in Figure 4-3. In this duplexer design, the air cavity filters provide a high level of isolation between the uplink and downlink bands while keeping the insertion loss at a very low level. In order to keep the passive intermodulation levels low, the filter body is made in one piece.



Figure 4-3 A base station duplexer for GSM 1800 [83].

4.2.3 Ceramic Duplexing Filters

Ceramic filters are sometimes referred to as dielectric filters. The ceramic filters are dielectric loaded filters where the resonators are formed by metallized holes inside a plated monoblock of high-permittivity ceramic [84]. The typical resonator consists of a shorted $\lambda/4$ line section. There are several operating modes for

dielectric resonator filters. Some of them are single transverse electric (TE) modes, single transverse magnetic (TM) modes, dual hybrid electromagnetic (HEM) modes, triple TM modes and triple TE modes [85] etc. The unloaded Q, size and spurious performance of these filters are dependent on these modes.

The two main type of ceramic resonator filters are

- ceramic puck filters
- ceramic coaxial filters

In a ceramic puck construction, dielectric constant pucks are enclosed within a metal cavity. The puck can be cylindrical, spherical, or cubic. A dual-mode ceramic puck resonator [86] is shown in Figure 4-4.

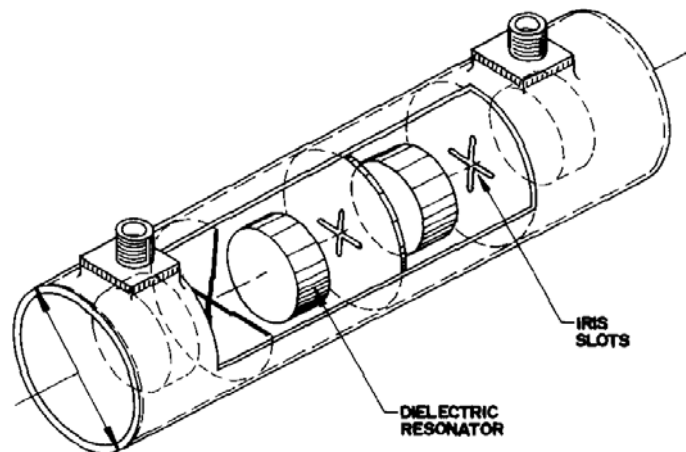


Figure 4-4 Dual-mode ceramic puck resonator loaded cavity [86].

Figure 4-5 shows the typical construction of a commercially available ceramic coaxial resonator [87] with an approximately square cross-section outer conductor and a round (cylindrical) centre conductor.

Typically, a ceramic coaxial element can be obtained in a specified length, with one end plated to “short-circuit” the centre conductor to the outer conductor [87].

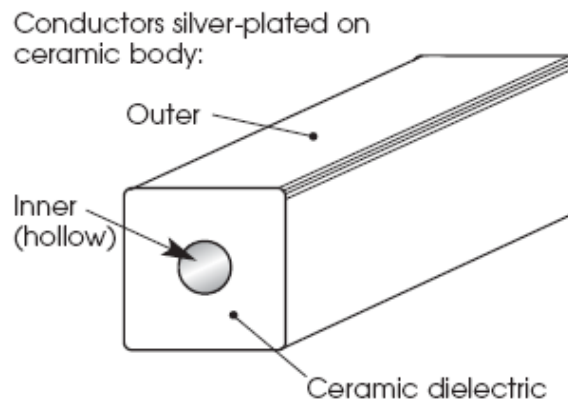


Figure 4-5 Construction of a ceramic coaxial resonator [87].

Typical resonator Q values are in the order of hundreds, but these values significantly vary with the frequency, size and the construction materials of the filter. Some ceramic filters have piezoelectric properties and the most popular ceramic material is lead Zirconate Titanate (PZT).

Ceramic coupled-resonators have been widely used in mobile transceiver duplexers. Ceramic duplexers have lower losses and are low in cost, but their bulkiness is a disadvantage. However ceramic duplexers are smaller than cavity filters but have relatively higher losses. A recently developed miniature ceramic duplexer for W-CDMA with good electrical performance is described in [88] and [89].

Traditionally, ceramic duplexers (made large to obtain a high Q) have been the only technology that can meet stringent mobile device specifications. This has changed with the development of FBAR technology.

4.2.4 SAW Duplexing Filters

SAW filters are based on the piezoelectric (pressure-electric) effect on piezoelectric materials. Examples of piezoelectric materials are Zinc Oxide (ZnO), quartz and lithium-tantalate. In piezoelectric material, the application of a force or stress results in the development of a charge in the material. This is known as

the direct piezoelectric effect. Conversely, the application of a charge to the same material will result in a change in mechanical dimensions or strain. This is known as the indirect piezoelectric effect [90]. In the direct piezoelectric effect, a surface acoustic wave generates an electric RF field and acts as the filter receiver port. In the indirect piezoelectric effect, an electric RF field generates a surface acoustic wave which acts as the filter transmitter port.

Conventionally, SAW filters use ceramic packaging and adopt the wire-bonding system of using gold wire to connect the ceramic package to the piezoelectric substrate (Figure 4-6). Recently in order to reduce the size of SAW filters, the flip-chip method of joining piezoelectric substrate with its ceramic package by using bumps to reduce the area of the pads, was adopted by Murata Mfg. Co. Ltd. [91].

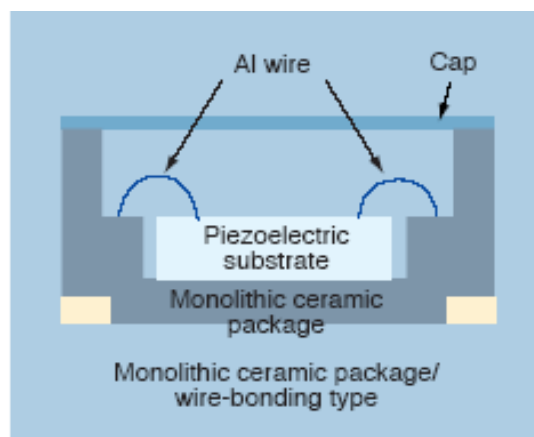


Figure 4-6 Structure of a conventional SAW filter (wire bonding type) [91].

Generally SAW duplexers are implemented using ladder filters. One such implementation is shown in Figure 4-7.

SAW filter characteristics are similar to digital FIR filters and have linear phase and sharp roll-off. SAW Filters have sharp characteristic, high Q and low loss, but SAW duplexers cannot be integrated.

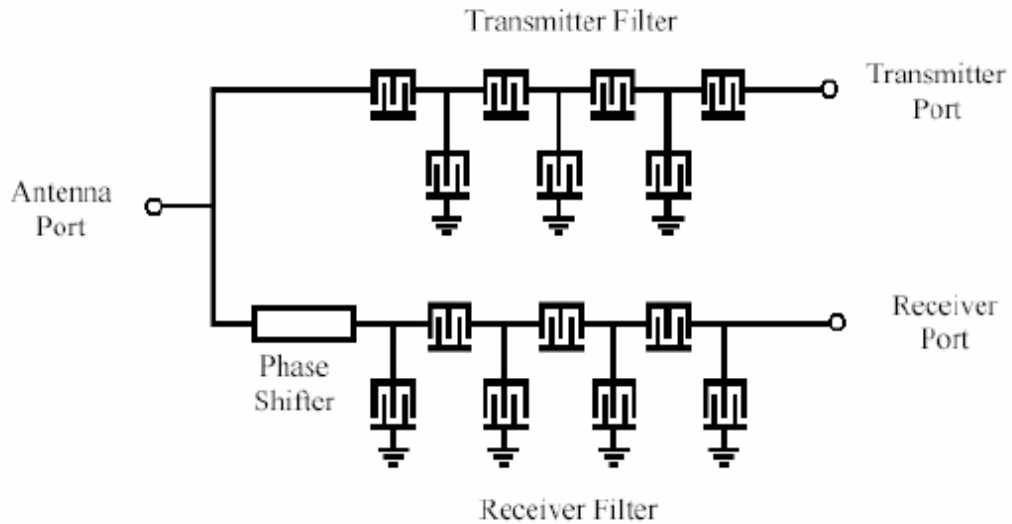


Figure 4-7 Schematic diagram of a SAW duplexer [92].

SAW filters have special packaging requirements since SAW is a surface sensitive device. The vibration travels near the surface of the medium rather than travelling throughout the medium. Any physical contact with the surface can severely damage the characteristic of a SAW filter and hence hermetically sealed packages are normally used.

With the advancements in SAW technology, ceramic duplexers have been progressively replaced with smaller, lighter and less expensive SAW duplexers [92], [93], [94].

4.2.5 MEMS Devices

Micro electro-mechanical systems provide a new approach to implement RF/microwave systems that are lower in size, weight, power requirements and cost. A MEMS system is one that is micro-scale and is a system composed of both micromechanical components, which move to perform certain tasks, and microelectronic components to convert that motion into electrical signal and vice versa. MEMS is a miniature device or an array of devices combining electrical

and mechanical components and fabricated with integrated circuit (IC) batch-processing techniques [95], [96].

There are many MEMS based devices such as inductors, varactors, switches, and resonators etc. MEMS switches can be used for tuning the values of lumped components within filters. MEMS based resonators are used to develop RF filters and duplexer applications. MEMS based tuneable front end filters/duplexers have been targeted to improve integratability in transceivers. Bulk acoustic wave filters, (which is one such MEMS based technology) are well suited for integration with ICs.

The duplexer circuit has moved from large dielectric filters to SAWs and more recently, to BAWs. Major advances in SAW filters have allowed this technology to remain competitive [97].

4.2.5.1 MEMS Resonators

There are two main design approaches to implement MEMS resonators in planar IC context, namely the vertical displacement resonator and the lateral displacement resonator. These resonators are capable of achieving low resonance frequencies in the order of hundreds of MHz. For higher resonance frequencies (GHz range), film bulk acoustic wave resonator techniques are used. FBAR filter technology is based on thin films of piezoelectrically active materials, such as aluminium nitride (AlN) or ZnO, and of suitable electrode materials, such as aluminium or molybdenum [98].

Based on the fabricated structure, Thin FBARs (TFBAR) can be classified as solidly mounted resonators and membrane type resonators. FBAR resonators are created using a thin film semiconductor process to build a Metal-Aluminium Nitride-Metal sandwich in air [99] and forming a mechanically resonant structure. A cross-section of a membrane supported FBAR resonator is shown in Figure 4-8. In FBAR devices electrical energy is converted to mechanical energy in a way similar to SAW devices, but the energy is directed into the bulk. FBARs

demonstrate high Q factors in a broad spectral range from 0.1GHz to 10GHz [100], [101]. A cross-section of a solidly mounted resonator (SMR) is shown in Figure 4-9. The SMR is fabricated on top of multiple reflectors or an array of reflectors. The number of layers depends on the reflection coefficient required and the mechanical impedance ratio between the successive layers [102]. The fabrication of the SMR is more complex than in the membrane FBAR case because of the multiple layer deposition and material parameter controls required [103].

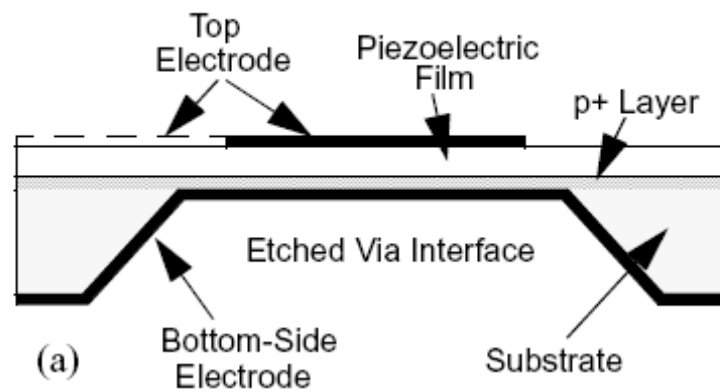


Figure 4-8 Film bulk acoustic wave resonator – fabricated on a layer of piezoelectric material placed between top and bottom metal electrodes [104].

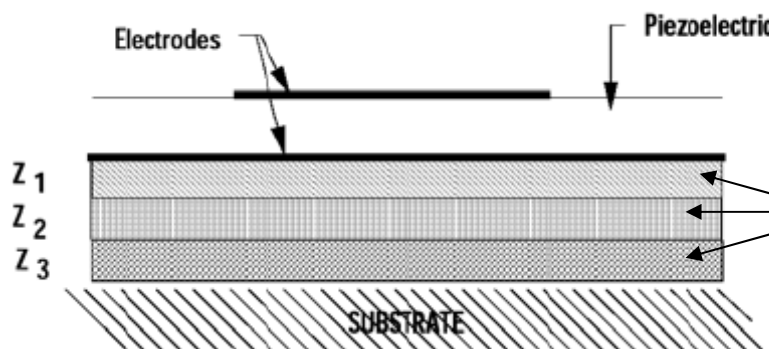


Figure 4-9 Solidly mounted resonator – fabricated on top of multiple reflectors [97].

A duplexer for PCS 1900 band designed by Agilent [97] is shown in Figure 4-10 along with its schematic diagram. This design consists of ladder type Tx and Rx filters. This is the first commercially available FBAR product.

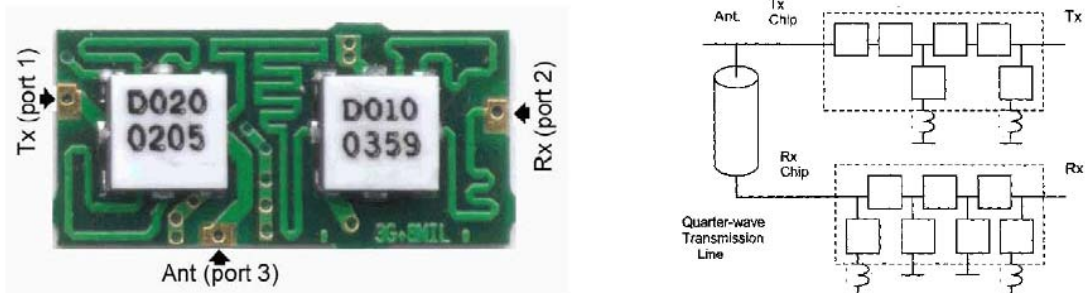


Figure 4-10 Photography of the Agilent Technologies produced FBAR duplexer and simplified schematic (designed for CDMA PCS 1900 MHz) [97].

For wireless duplexer applications Tx and Rx filters are required to have extremely sharp roll-offs. While ceramic filters can meet this requirement significantly better than SAW filters, their size, and cost make them a less desirable option. FBAR duplexer is able to address these problems [105], [106], [107], [108], [109] and is suitable for fabrication and integration with other electronics [110].

RF MEMS advantages are low power consumption, high isolation, high density and integration. Many micromechanical filters can be fabricated onto a smaller area because of their tiny size. A possible RF front end architecture [111], in which band selection is achieved by arranging a switchable matching network and a parallel bank of tuneable/switchable MEMs filters, proposed by Nguyen is shown in Figure B-1 in Appendix B. Two receiver architectures [112], proposed by Larson is shown in Figure B-2 and Figure B-3 in Appendix B. Figure B-2 shows a MEMS based receiver employing tuneable band-pass filter, which could serve partial channel selection as well as “roofing” functions for a typical receiver. Figure B-3 shows a MEMS based receiver with acoustic resonant IF filter banks. It eliminates the need for a tuneable first local oscillator by replacing it with a

fixed LO, but requires very fast switching speed and low phase-noise at very high oscillator frequencies. All of these filters can be very expensive and would have high space requirements. FBAR technology still needs further development before low cost integrated products become available.

4.2.6 Stripline or Microstrip Line Duplexing Filters

A microstrip line is, by definition, a transmission line consisting of a strip conductor and a ground plane separated by a dielectric medium [113]. Microstrip and stripline filters are based either on soft substrates or ceramic substrates with multi-layer thick film technologies. Microstrip transmission lines are broadband in frequency, compact and light in weight. Also they are of low cost since they can be easily adapted to hybrid and monolithic integrated circuit technologies.

Basic, microstrip line has a single conductor trace on one side of the substrate and a single ground plane on the other side, while the basic stripline has a single conductor embedded in dielectric substrate surrounded by two ground planes or reference planes on either side of the substrate.

The general structures of a microstrip line and a stripline are illustrated in Figure 4-11 and Figure 4-12 respectively. Here the conducting strip is shown with a width W and a thickness t . Microstrip line has a distinct fabrication advantage over stripline due to its open structure.

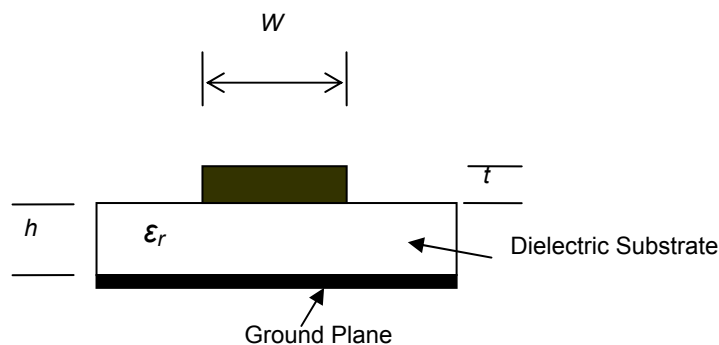


Figure 4-11 General microstrip line structure.

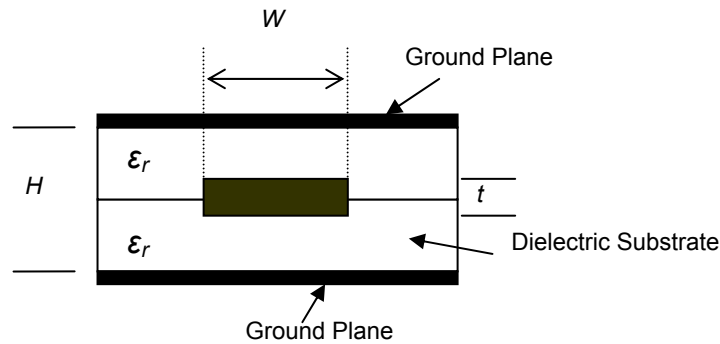


Figure 4-12 General stripline structure.

Conventional microstrip low-pass and band-pass filters (such as stepped-impedance filters, open-stub filters, semi-lumped element filters, end-coupled and parallel-coupled half-wavelength resonator filters, hairpin-line filters, interdigital and combline filters, pseudocombine filters, and stub-line filters) and conventional microstrip high-pass and band-stop filters (such as quasi-lumped element and optimum distributed high-pass filters, narrow-band and wide-band band-stop filters) are presented in detail in [72].

New design methodologies for microstrip filters are focussed on resonator geometry to produce miniaturized planar open-loop resonator filters [57], coupled-loop resonator filters [58], slow-wave-open-loop resonator filters [59], [114] and loop filters [115] in order to improve the out-of-band rejection. These filters are used to design compact duplexers in a specific band. This size however scales with wavelength, which reduces their applicability for handheld devices below 2GHz.

Stripline circuits are often used in conjunction with SAW devices. It is shown [116] that the length of the stripline influences the band-stop phase characteristics of a SAW duplexer.

Miniaturisation techniques for SAW duplexers with microstrip and stripline matching circuits are discussed in [117] and [118]. Schematics of those duplexers are shown in Figure 4-13.

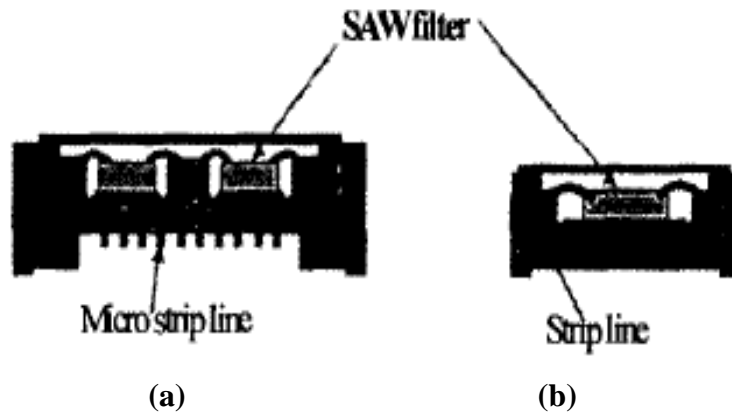


Figure 4-13 Schematics of duplexer structures (a) Two SAW filters (one Tx and one Rx) with microstrip line for matching impedance (b) One chip SAW filters (combined Tx and Rx) with stripline for matching impedance [118].

All the duplexers described in this section have the disadvantage of being fixed frequency devices. The only way to handle multi-band operation would be to switch in the appropriate duplexing filter for each band. Only MEMS/FBAR devices which can be integrated on to the RF silicon itself have the potential to solve the multi-band problem. Unfortunately the technology is not yet mature, and even if it was, it would not enable ‘future proof’ solutions, since it would not be possible to add a new band to an existing device.

The next section describes the state of the art in active duplexing where cancelling techniques are employed to reduce the need for high quality filtering solutions.

4.3 Review of Literature Related to Active/Multi-Band Duplexing Structures

Due to the novelty of the software radio concept, the current related work in the area of duplexers which cover the entire RF range and channel bandwidth requirements, is very limited or non-existent. However, the most relevant published work on general RF duplex design techniques which use active cancellation relevant to this thesis, are discussed in this section.

Recent advancements of materials and fabrication technologies, such as MEMS, monolithic microwave integrated circuit (MMIC), micromachining, high-temperature superconductor (HTS) and LTCC, have contributed to the rapid development of duplexing filters. Some recently designed duplexing devices/methods that do not use active cancellation techniques are found in [57]-[62]. The paper [119] described the main issues of the design of LTCC based front end modules and duplexers. The tuneable duplexer in [61] is designed for dual-mode AMPS/CDMA cellular system and tunes the response of the Tx filter using voltage variable capacitors. A fixed band-pass filter is used as the Rx filter. Although this Rx filter is not tuned externally its response is affected by the tuning state of the Tx filter. This duplexer is fabricated using multi-layer LTCC technology. The tuneable duplexer in [62] also uses LTCC technology with multi-layer structure and uses varactor diodes to tune both pass-band and stop-band to the desired frequency independently. It is designed for GSM 1800/1900. But they have only achieved 20dB Tx band isolation and 10dB Rx band isolation.

Very recently, in June 2005, a mechanically tuneable lumped element filter that has variable centre frequency, and variable bandwidth which can be adapted to software defined radio, was discussed [120]. This system separately controls the capacitance of each lumped element to tune the centre frequency and bandwidth.

None of these devices meet the full RF range requirements and therefore a set of duplexing filters are required for the implementation of multi-band systems.

Work of Kenworthy [121] and S. Chen [122] provides full duplexing structures using the following three techniques (Figure 4-14); (i) A dual antenna scheme, (ii) An analogue RF canceller and (iii) adaptive digital baseband filter. They use the same channel for both Tx and Rx transmission and attempt to cancel co-channel interference. Therefore only cancellation at one frequency is needed.

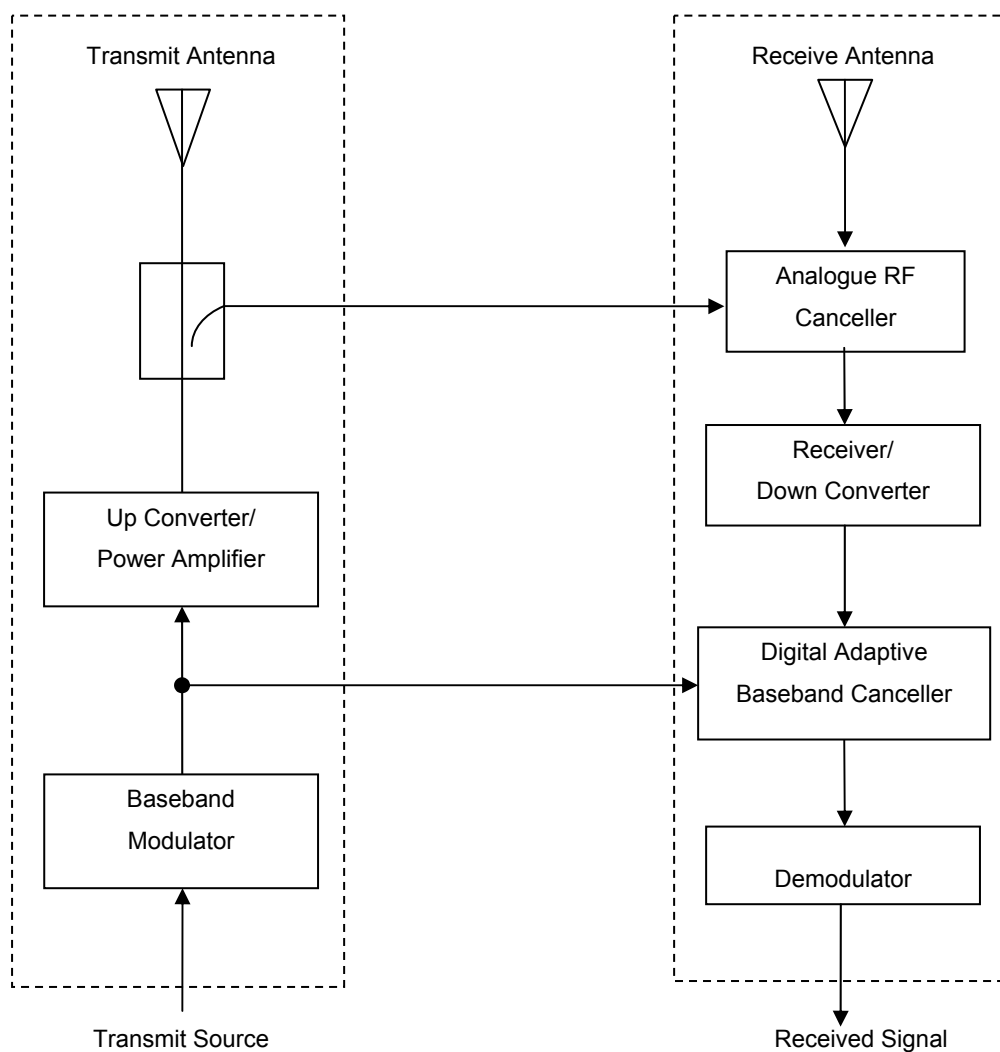


Figure 4-14 Simplified diagram of self-cancelling RF communication system (uses the same spectrum at the same time) [121].

However from those three techniques Kenworthy's patent has allocated a total of 60dB isolation; with 20dB from antenna placement, 15dB from analogue cancellation and 25dB from digital adaptive cancellation. Chen has implemented a prototype with the first two techniques and has achieved 72dB isolation. Of the duplex isolation obtained, 29dB was provided by the dual antenna, 37dB was provided by the RF echo canceller and 6dB by the insertion loss of the subtracter and the directional coupler. However this technique does not employ delay elements and only narrowband cancellation is feasible.

Gerald [123] has invented a transmitter leakage cancellation system in full duplex radar systems. Here also, the same channel is used for both Tx and Rx, since the receiver in the radar system detects the same transmitting continuous wave signal which is reflected from an object. Therefore only cancellation at one frequency is needed. This work uses delay elements to minimise the AM noise sidebands and FM (frequency modulation) noise sidebands of the Tx leakage signal.

Few researches have considered Tx leakage cancellation in full duplex systems that employ different channels for Tx and Rx. Winthrop's [124] patented work proposes a Tx leakage (Tx to Rx) cancellation system using multiplier and integrators to estimate the gain and phase adjustments needed. The described cancellation is narrowband and not adaptive. Harald et al. [125] in their patent have proposed a Tx leakage cancellation circuit for a co-located GPS (global positioning system) receiver and mobile handset. This can be a problem in a mobile communication device with localization functionality. As shown in Figure 4-15 the signal transmitted via the mobile phone antenna also reaches a positioning system antenna as an interfering signal. An interference suppression unit eliminates (cancels) the interference originating from the transmitting mobile unit. A variable attenuator and phase shifter in the interference cancellation unit was used to adaptively control the cancellation. The power of the RF input signal entering the LNA of the GPS receiver is used as an error signal to control the one dimensional search algorithm. Minimisation of the RF input power will give optimum adjustment of the attenuator and phase adjuster controls.

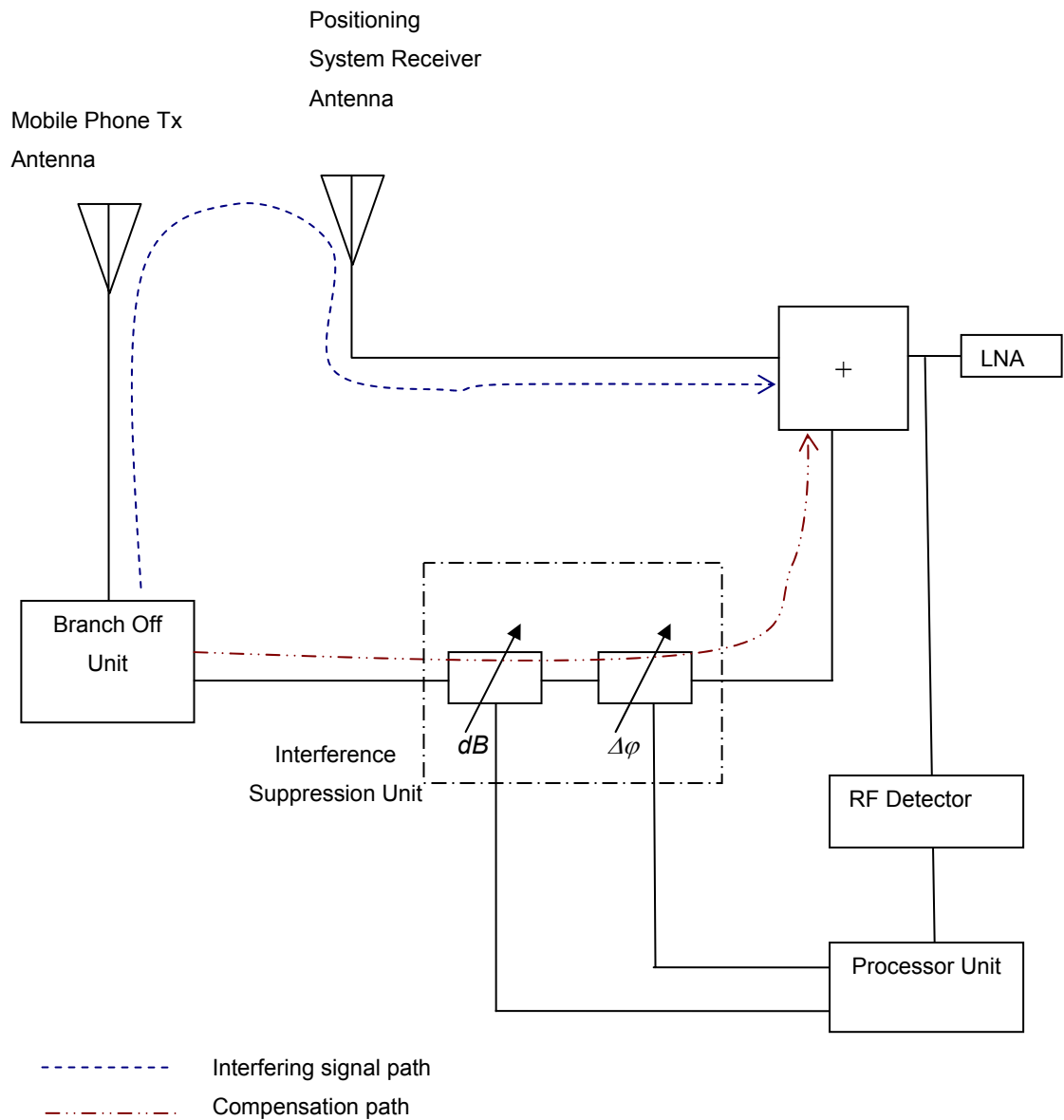


Figure 4-15 A schematic diagram of the transmitter interference cancellation arrangement for co-located GPS receiver [125].

The cancellation technique used in adaptive active duplexing structure in [126] cancels the Tx interference in the direct path and mentions the use of delay elements for longer paths which arrive from the receive antenna. However this technique does not attempt to cancel the Tx noise falling in the receiver band.

A flexible multi-band front end described in [127] involves an additional multi-band transmitter chain to cancel the transmitter interference signal, which becomes a costly exercise. Here the cancellation signal is computed over the Tx channel bandwidth in the baseband and then transformed up to RF via an auxiliary transmitter Ax as shown in Figure 4-16. Additionally this design does not cancel the transmitter noise in the receiver band because the transmitter noise and the auxiliary transmitter noise are not correlated. Instead of cancelling the transmitter noise, this design introduces additional noise components, effectively doubling the additional thermal noise flow to the receiver. This further degrades the receiver noise figure. But using this approach it is possible to obtain a wider bandwidth, because adjustments are done in the DSP domain where multiple tap structures (e.g. FIR) are easily implemented. In this thesis the proposed adaptive duplexer architecture achieves wider bandwidth by adding additional cancellation loops in the analogue domain (Section 8.3.5).

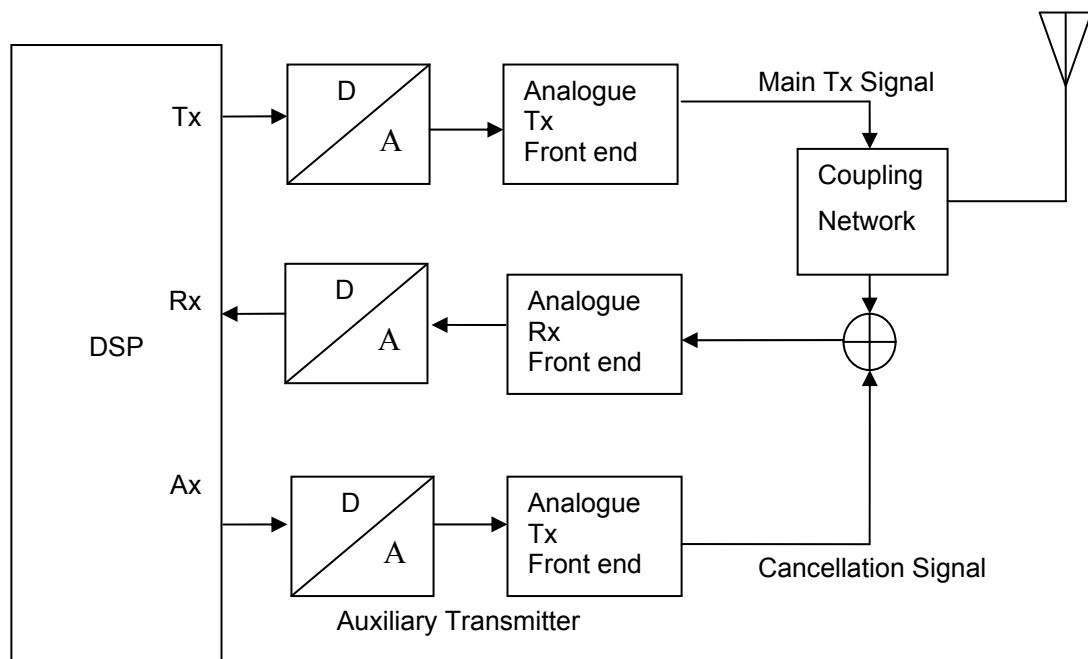


Figure 4-16 Active cancellation concept of the Tx/Rx feedthrough applying an auxiliary transmitter [127].

For transmitter noise cancellation, we can adapt the cancellation configuration proposed in [128], [129] or [130]; i.e. noise cancellation loop in the Tx path with receiver band-pass filters (Rx-BPFs) or transmitter band-reject filters (Tx-BRF) and error amplifier LNA (Figure 4-17). The drawback of this configuration for multi-band applications is that it requires switched multiple Rx-BPFs/Tx-BRFs in the cancellation loop. This results in additional costs and bulkiness due to the addition of the filters. Further, since a ‘noise only’ reference signal cannot be obtained easily, a Tx leakage signal will exist through the Rx-BPFs/Tx-BRFs in the cancellation loop reducing the main path Tx signal strength during the cancellation process. Increasing the output power of the Tx power amplifier compensates for this reduction. An increase in the power amplifier means an increase in cost of the amplifier, therefore, the above design leads to additional costs and bulkiness.

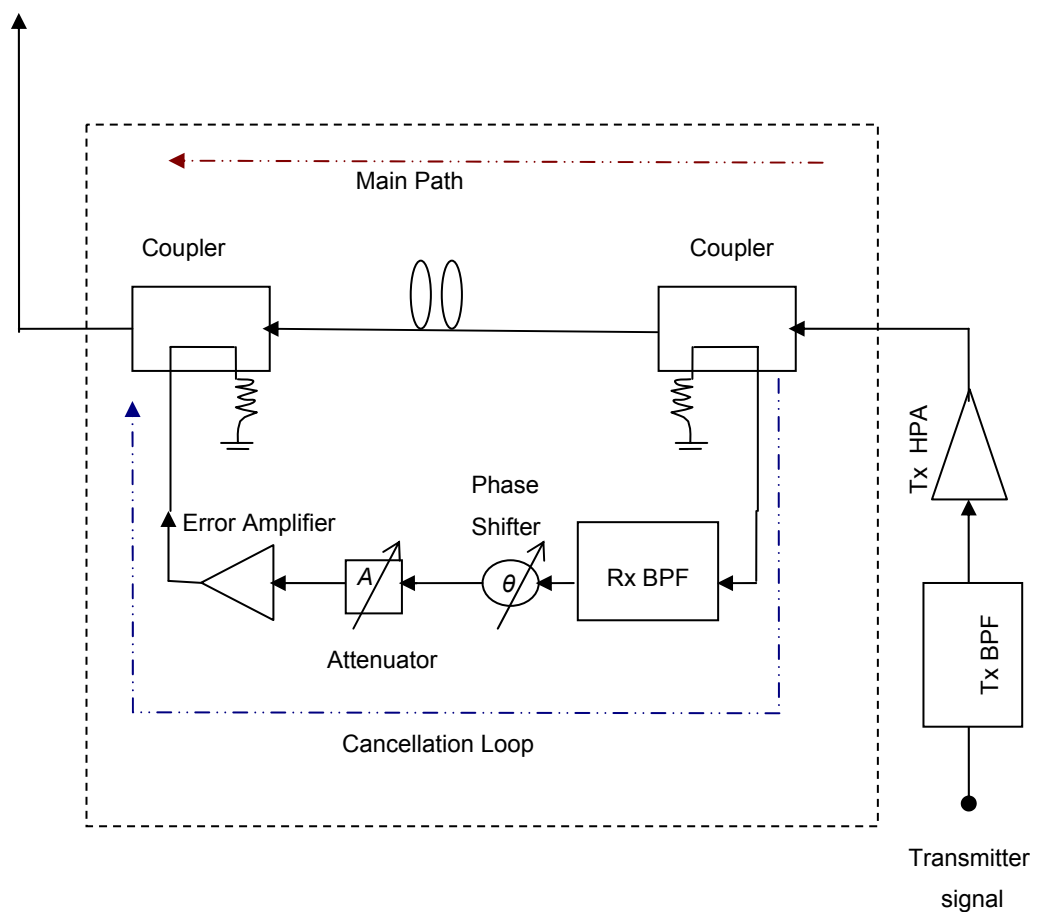


Figure 4-17 A Tx noise cancellation system configuration [128].

The noise cancellation design proposed in this thesis overcomes the above limitations with an adaptive noise cancellation technique that involves inserting a low-level pilot signal into the transmitter path.

Recently published work by O’Sullivan et al. [131] used a cancelling loop to enhance a SAW duplexer by reducing the noise levels in the receive band of the system. This system has given 20dB isolation over 2MHz bandwidth with a single cancellation path. Further improvements (Figure 4-18) by the same researchers [132] have referred to the adaptive duplexer architecture described by the author of this thesis [133], and have adopted the double loop cancellation technique to achieve a greater isolation bandwidth (20dB isolation over 4.5MHz bandwidth) for receiver noise cancellation only; i.e. two nulls in the receiver band (Figure 4-19).

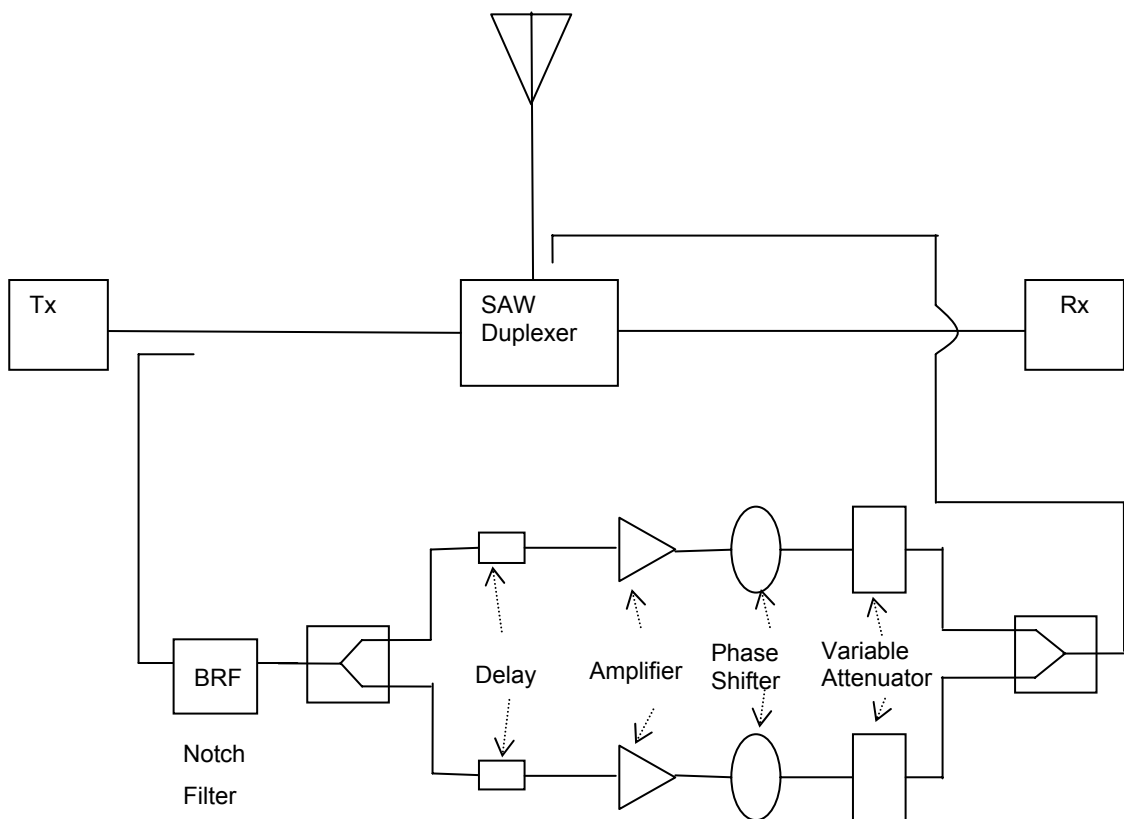


Figure 4-18 The block diagram for an adaptive duplexer with improved isolation between Tx and antenna port [132].

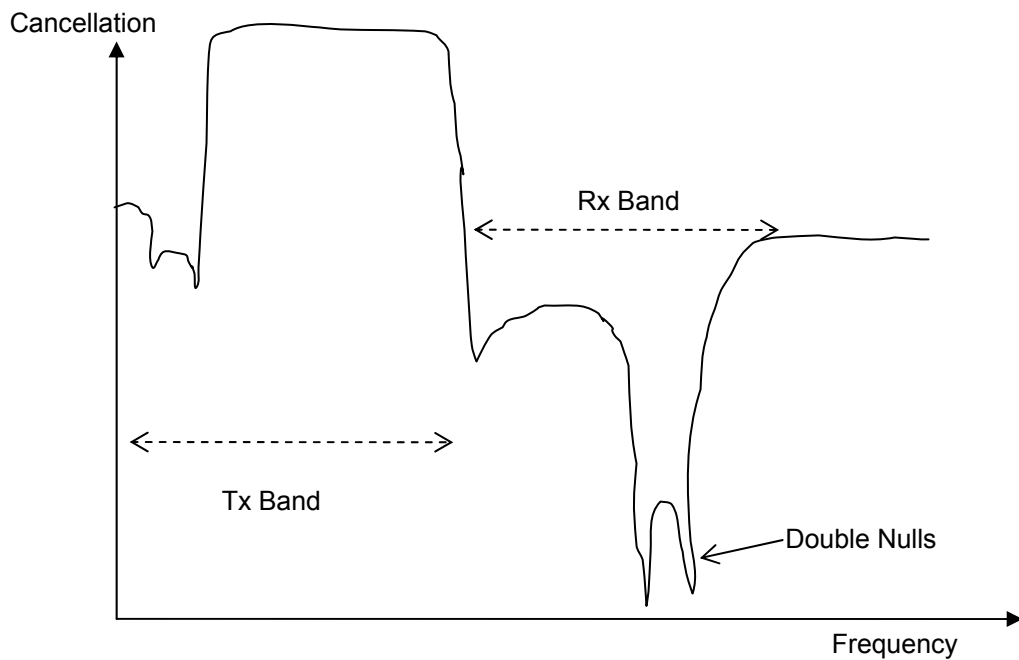


Figure 4-19 An adaptive duplexer characteristics for dual-path cancellation. Improved duplexing characteristics by achieving double nulls in the receive band of the system.

Further, they confirmed the presence of singularities in the system with dual paths, where no solution is possible. These issues were originally addressed by the author of this thesis in a paper [134] which significantly pre-dates their work (see also Sections 7.4, 7.5 & 7.6).

The work by O’Sullivan et al. [132] used poorly designed delay differences for the cancellation paths and hence the achieved added attenuation was small. Their design could be improved by minimising and choosing delay differences such that the cancellation path delays would straddle the main path delay as proved later in this thesis. Also as in [128], [129] and [130], the deficiency of multi-path configuration for multi-band applications is that, it requires switched multiple transmitter notch filters in the cancellation circuit as well as switched SAW duplexers.

Although all the above researchers have considered some form of active duplexing structure, none have considered cancellation in both Tx and Rx band simultaneously, i.e. the cancellation of Tx leakage and Tx noise in the Rx band. This is probably due to the difficulty in finding an appropriate cost function that minimises both leakage signals together.

4.4 Conclusion

Filtering is one of the major components affecting the complexity of the multi-band /multi-mode software radio. Due to the stringent requirements of multi-band transceivers including size, dynamic range, isolation and insertion loss, there has been a rapid development in passive filter technologies, mainly in miniaturisation. However, a real breakthrough in filter technology to meet the multi-band/multi-mode low cost requirements of mass produced wireless terminals has not been achieved as yet.

Active cancellation is an alternative approach to filtering. It can be used to reduce or even eliminate the need for filters.

The most relevant published work on general RF duplex design techniques which use active cancellation relevant to this thesis are discussed in this chapter. None of the published work to date considers active duplexing structures in both transmit and receive bands or provide algorithms that perform cancellation in both these bands.

The New Adaptive Duplexer Architecture

5.1 Introduction

The intention of this research is to design an adaptive duplexer architecture that is capable of handling multiple standards associated with software radio applications, i.e. it has to accommodate all FDD systems in the 2G and 3G space. This is a significant requirement in the software radio implementation process as it is nearly impossible to design tuneable RF duplexing filters that can operate over the required frequency range.

The previous chapter discussed some conventional duplexing filters followed by a review of the literature related to adaptive duplexing structures with active cancellation. This chapter begins with a system overview of the new proposed adaptive duplexer architecture. The adaptive duplexer architecture uses a low isolation device and an active/adaptive double loop cancellation method to achieve the required isolation. There is a number of issues associated with the realisation of the adaptive duplexer concept and these issues are also addressed in this chapter.

5.2 The New Adaptive Duplexer Architecture

The proposed adaptive duplexer (Figure 5-1) described in this thesis provides sufficient Tx leakage isolation between the transmitter and the associated receiver and also superior noise isolation in the receiver band. It is based on a two step isolation process. Initial isolation is firstly achieved using a passive device or scheme. This can be achieved using wideband circulators, directional couplers, low selectivity stripline/microstrip filters and separate (or cross-polar) transmit and receive antennas. The low isolation causes significant Tx signal and noise in the Rx signal path. These Tx leakage signals should be reduced by additional techniques.

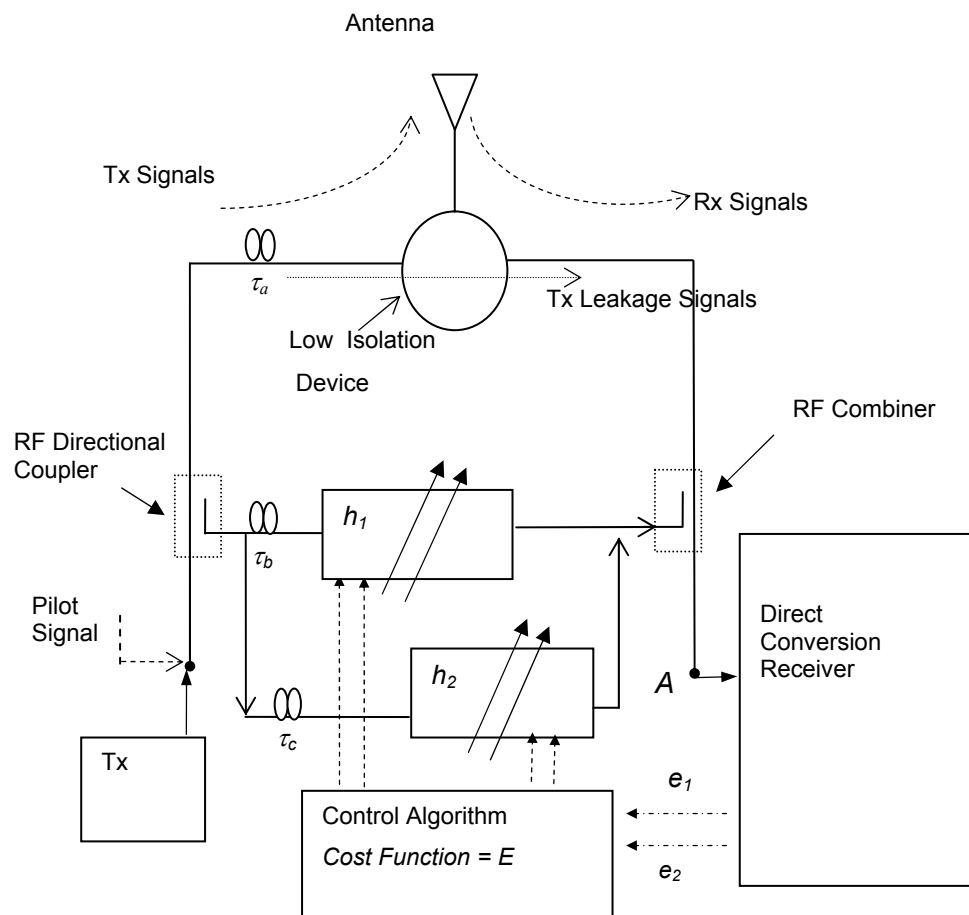


Figure 5-1 The proposed adaptive duplexer architecture.

The second step provides the remaining isolation using an adaptive double loop cancellation technique with a similar structure to a finite impulse response filter. This provides isolation in the required transmitter and receiver cancellation bands. Each cancellation path has a delay element and an adjustable vector attenuator. Directional couplers are used to couple the signal into and out of the cancellation loops. If the coupling coefficient is low, the insertion loss will also be low and performance in the transmitter and receiver paths will not be affected. However additional amplifiers in the cancellation path might be required. These use DC power and add noise which will degrade the receiver noise figure. On the other hand a high coupling coefficient causes a high insertion loss in the transmitter path, forcing the use of more power from the RF power amplifier. This significantly increases DC power consumption and reduces the power efficiency of the transmitter. High insertion loss in the receiver path increases the attenuation of the receiver signal and increases the system noise figure. Hence trade-offs between the gain/attenuation in the cancellation paths and the couplers' insertion losses are required. This work avoids the gain blocks in the cancellation paths, by selecting a reasonably good low isolation device with $>20\text{dB}$ isolation. Vector attenuators can then be used to control the gain and phase in the cancellation paths.

In this adaptive duplexer architecture, the signal components from the two cancellation paths (h_1 and h_2) are summed to generate a replica of the residual Tx leakage interference signal and a replica of the residual Tx noise signal in the receiver band. By choosing the right delay elements it is possible to obtain the Tx and Rx cancellation nulls over a wide bandwidth (Figure 1-2). It will be shown (Section 7.6) that the delays τ_b and τ_c should be chosen to straddle the expected range variation of τ_a to achieve wideband cancellation. The latter is the effective delay of the leakage path, given by the difference in phase shift at frequencies f_{Tx} and f_{Rx} . It is affected by antenna loading, external reflections and other poorly quantified factors. A robust solution should therefore cater for variations in τ_a that is as large as possible.

An alternative design would be to exclude the low isolation device (or include a device with minimal isolation) and provide the entire isolation requirements using the cancellation unit only. However this also requires an additional power amplifier in the cancellation loop or more power from the existing power amplifier to match the gain of the interference leakage signal. Then the cancellation signal will be the same as the Tx signal. This will significantly increase DC power consumption and reduce the power efficiency of the transmitter. Further, practically it is very difficult to achieve the required bandwidth and isolation, with only the cancellation unit because of the very small tolerance for gain and phase mismatch (less than 0.18 deg and 0.03dB for 50dB – Figure 6-3) between the two paths. A passive device with at least 20dB of isolation is needed to give some initial isolation.

Two feedback error signals are required for cancellation at the two frequencies f_{Rx} and f_{Tx} ($= f_{Rx} + f_d$). The error signal at f_{Tx} can be based on the Tx signal itself, while the error signal at f_{Rx} is more difficult to obtain since the transmitter noise will be masked by the desired receive signal. The solution used to solve this problem is to use a small transmitter pilot signal immediately adjacent to the desired Rx signal ($f_{Rx} + f_\delta$). This architecture is tested with a direct conversion receiver which down converts the desired receive signal ($@f_{Rx}$) to baseband and the Tx interference signal ($@f_{Tx}$) to f_d (Figure 5-2). This signal at frequency f_d can be envelope detected directly after one of the mixers in the DCR and be used as an error signal (e_1) for the Tx leakage signal cancellation. If a synchronous detector is used, a local oscillator set to f_d is needed and this only changes when a different band with different f_d is selected. The transmitter interference signal should dominate the composite baseband signal on the DCR output but some additional band-pass filtering at f_d can be used to improve the error signal quality if other large in-band jamming signals are expected.

The error signal for noise cancellation (e_2) (the amplitude of the down converted pilot ($@f_\delta$)) is obtained by filtering the pilot signal after the low-pass channel select filter in the direct conversion receiver.

A control algorithm can be used to continuously adjust the complex gain of the two cancellation loops, (h_1 and h_2) by monitoring the two error signals e_1 and e_2 as shown in Figure 5-2. Manual adjustment of h_1 and h_2 on a laboratory prototype showed the difficulties of minimising both e_1 and e_2 concurrently, invariably when one was reduced the other came up. The control algorithm must use a cost function, which when minimised, will cause the error signal e_1 and error signal e_2 also to be minimised. As described in Section 7.7, an algorithm based on a single cost function ($E = k_1|e_1|^2 + k_2|e_2|^2$) is used to optimize the cancellation by adjusting the vector attenuator control voltages. k_1 and k_2 are constants that prioritise between the two error signals

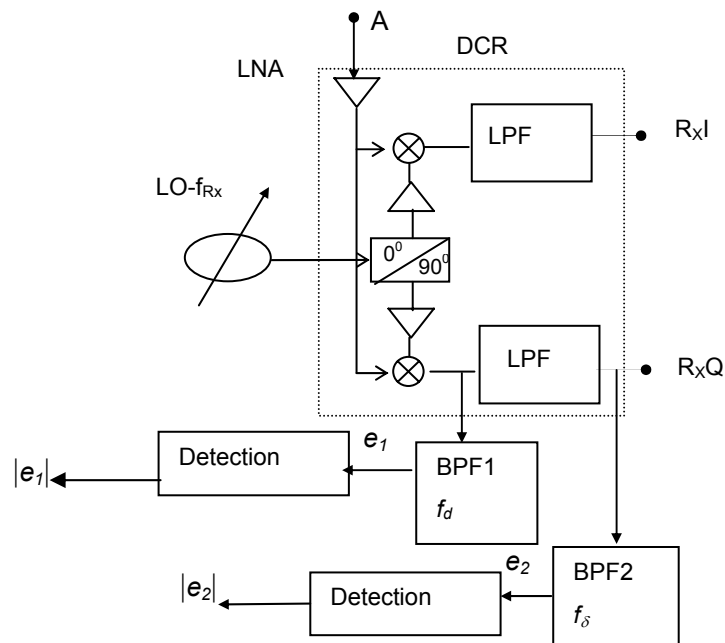


Figure 5-2 Obtaining the error signals from a direct conversion receiver.

This research is initially carried out with a single loop cancellation technique and it is described in Chapter 6. This type of cancellation can be employed if there is a Tx noise cancellation technique already present in the Tx chain (e.g. [128]). The need for double loop cancellation and the details of the technique are described in Chapters 6 and 7 respectively.

5.3 Design Considerations for the Low Isolation Device

Device

The adaptive duplexer architecture requires a low isolation device to give some initial isolation (at least 20dB). The low isolation device should cover the required RF range (800-2200MHz) for software radio. As stated earlier in the chapter some of the components that can be used for this purpose are wideband circulators, directional couplers, low selectivity stripline or microstrip line filters and separate antennas (or crossed polarised antennas).

5.3.1 Wideband Circulator

The circulator is a passive device with 3 or more ports, where power is transferred from one port to the next in a prescribed order. In a 3-port circulator (Figure 5-3 (a)) power entering port 1 leaves port 2 while port 3 is decoupled, power entering port 2 leaves port 3 while port 1 is decoupled, and power entering port 3 leaves port 1 while port 2 is decoupled [135]. It is possible to use circulators to isolate the Rx from the Tx when Tx and Rx use the same antenna (Figure 5-3 (b)).

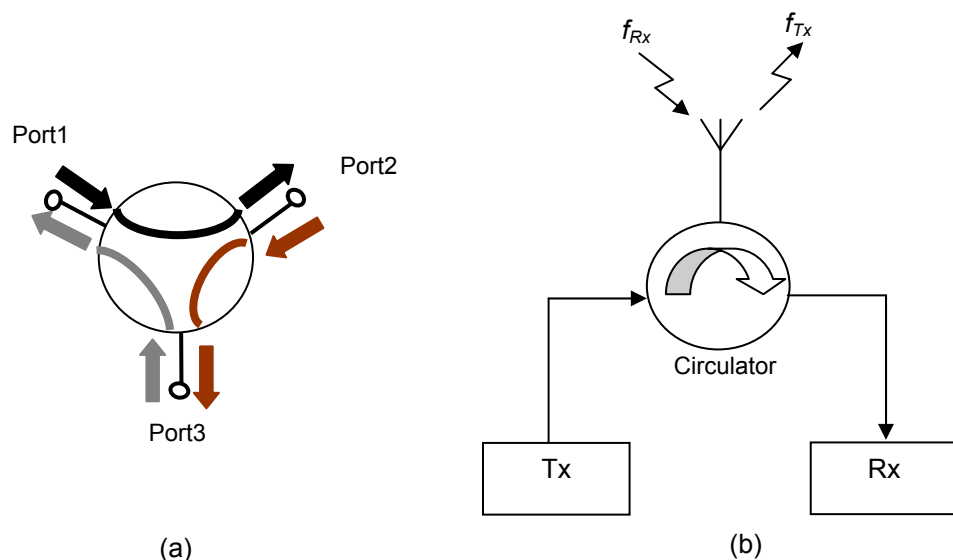


Figure 5-3 (a) A 3-port circulator (b) A circulator used as an isolation device in a transceiver.

5.3.2 Directional Coupler

A directional coupler is a 4 port device in which two transmission lines pass close enough to each other for energy propagating on one line to couple to the other line [136]. When one port is terminated internally, power coupled to the port is absorbed and not available to the user. This is called a single-directional coupler. If forward and reflected signals are allowed to be sampled simultaneously, i.e. no internal termination, it is called a bi-directional coupler. One advantage of this type of coupler is that a higher power termination can be selected to suit higher input power requirements [137]. The dual-directional coupler is constructed with two single-directional couplers. They can either be connected back-to-back in series, with the main line output of the forward coupler connected to the output of the second coupler, or integrated into one device with a single main line and two secondary lines [138]. For this project only single-directional couplers are used and hence directional couplers mean single-directional couplers.

Directional couplers are commonly used to both divide and combine signals. The basic function of a directional coupler is to operate on an input so that two output signals are available. A directional coupler separates signals based on the direction of signal propagation. These devices are used to unequally split the signal flowing in the mainline and to fully pass the signal flowing in the opposite direction [139]. Directional couplers can also be used to provide low isolation between the Tx and Rx.

5.3.3 Low Selectivity Stripline or Microstrip Filters

Stripline and microstrip duplexing filters have been discussed in Section 4.2.6. While it is difficult to achieve a high level of isolation (40dB or over) over a larger frequency band, similar isolation over a smaller frequency band is not difficult. Therefore, it is possible to implement a low isolation (20dB) duplexer using low selectivity microstrip filters for multi-band applications to give an initial isolation for this adaptive duplexer architecture. It might be possible to make these tuneable to cater for wideband operation.

5.3.4 Separate Antennas

Separate antenna schemes use two element antennas; one for transmission only and the other for reception only. The duplex isolation in this case is due to the mutual coupling loss between the two antennas. High isolation is obtained by minimising the mutual coupling effect. Increasing the separation between two antennas, or locating them in a natural transmission null, can minimise the mutual coupling effect. Two co-linear dipoles are examples of transmission null locations. The amount of separation is limited by the physical size of the mobile handset. Omni directional radiation pattern in the horizontal plane is suitable for this design and the antennas should have a wide bandwidth. The dual antenna design in [122] achieved 29dB isolation in one handset.

Dual antenna systems can be more agile in their response to different frequencies. As a result they can be used to access multi-band systems based on different standards. Future mobile handsets should be compact in size and therefore separate antennas are less likely to be an attractive solution. Dual polarised antennas might be the solution for this case.

Since it is very flexible and inexpensive to design microstrip duplexers, they are a good candidate for the low isolation device. However the implementation of this low-isolated microstrip duplexer for multi-band software radio needs theoretical and experimental investigation and is outside the scope of this Ph.D. study.

In a similar vein, LC devices directly implemented on silicon provide a low footprint low isolation device. They can also be made tuneable by varicap and switched element designs. The Q of these devices is not high, $\ll 20$, and their design is outside the scope of this thesis.

The experimental prototype described in this thesis uses a commercially available wideband circulator as the low isolation device.

5.4 Conclusion

A novel duplexer architecture is proposed and described in this chapter. Adaptive duplexing eliminates many external components in the multi-band transceivers. This solution handles the desensitisation problem and receiver sensitivity problem due to Tx leakage in multi-band software radio front end.

The proposed duplexer architecture is based on a low isolation device and an adaptive cancellation unit. Some low isolation devices have been considered and wideband circulators or dual antenna systems are good low design effort choices. In the future, tuneable filters or microstrip devices might provide a better solution since they provide some additional level of selectivity against other interfering signals.

The proposed new algorithm uses a single cost function based on the superposition of squared errors. The algorithm is simple; uses low frequency error signals (non RF) and is of low computational complexity. The scheme is suitable for low power integrated design.

Design and Implementation of the Single Loop Cancellation System

6.1 Introduction

Based on the adaptive duplexer architecture described in Chapter 5 a single loop cancellation system could be successfully employed to cancel the transmitter interference signal in the receiver path. This chapter first describes the single loop cancellation technique and its features (Section 6.2) and concludes by discussing the possibility of achieving two cancellation nulls using only a single loop cancellation technique (Section 6.8).

The cancellation process involves sampling the transmitter signal and then adjusting the phase, gain and delay to produce a replica of the transmitter leakage signal. This replica signal is then subtracted from the received signal or added to the received signal in anti-phase, so that any transmitter interference signal components in the receiver front-end are nullified. As determined in Section 3.7,

the required transmitter interference signal cancellation should be between 48 and 60dB.

The suppression of the transmitter noise, receiver noise and the noise contribution from the components of the cancellation unit were all examined using simulation techniques. Successful broadband cancellation depends on the delay, phase and gain mismatches; therefore several simulations were carried out to see the effects of these mismatches (Section 6.3 and Section 6.4). Further simulations were used to find the signal cancellation limit of the single loop process (Section 6.5). A prototype was built and the description of the experimental setup and results are shown in Section 6.6 and Section 6.7.

6.2 Single Loop Cancellation System

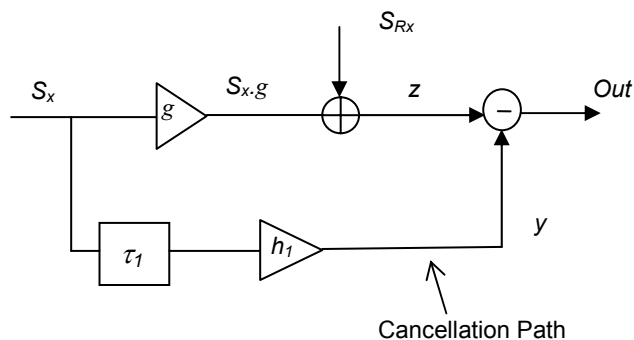


Figure 6-1 The single loop cancellation configuration.

Figure 6-1 shows the simplified single loop cancellation configuration. Here h_1 represents the complex gain/attenuation of the cancellation path and g represents the attenuation of the main path. The complex gain/attenuation h_1 includes the cancellation path loss and coupling loss due to the devices used in the sampling and cancellation points (subtraction point or summation point). The attenuation g includes the main path loss, coupler insertion loss due to the devices used in the

sampling and cancellation points as well as the attenuation of the low isolation device. The main path and the cancellation path contain a certain amount of delays and these delays should be matched to ensure that respective signals reach the cancellation point at the correct time. This is achieved by introducing a delay element in one of the two paths depending on which path has the lower delay. Here τ_l ($= \tau_b - \tau_a$ in Figure 5-1) represents the delay difference between the main path and the cancellation path. This delay can be negative. If S_x represents the transmitter interference signal, then the cancellation signal is given by

$$y = (h_1) e^{-j\omega\tau_l} S_x \quad \text{Eq. 6-1}$$

and the desired signal by

$$\text{Out} = z - y = (g) S_x + S_{Rx} - (h_1) e^{-j\omega\tau_l} S_x \quad \text{Eq. 6-2}$$

Since we are considering only the transmitter leakage signals in the receiver path the desired S_{Rx} signal can be neglected in this analysis. Therefore, the desired signal becomes

$$\begin{aligned} \text{Out} &= (g) S_x - (h_1) e^{-j\omega\tau_l} S_x \\ &= (g - h_1 e^{-j\omega\tau_l}) S_x \end{aligned} \quad \text{Eq. 6-3}$$

The duplex isolation depends on the success of the signal cancellation. Opposite phase and equal amplitude are required for signal cancellation at one frequency. For perfect cancellation, the residual signal after cancellation (error signal, resultant signal) should be zero or $-\infty$ dB. The delay should be matched for an operating band of frequencies to achieve broadband cancellation. In practice this cancellation is not perfect. Therefore the degree of cancellation depends on the degree of amplitude, phase and delay matching.

6.3 Effect of Phase and Amplitude Mismatch on Signal Cancellation

Achieving high levels of signal cancellation can be difficult due to phase and gain mismatches that occur in the practical cancellation process. Since the cancellation signals are at the same frequency, these can be represented as a summation of two sinusoids and a vector addition as shown in Figure 6-2. To see the effect of phase and gain mismatches it is assumed that there is no delay mismatch ($\tau_l = 0$) between the main signal and the cancellation signal.

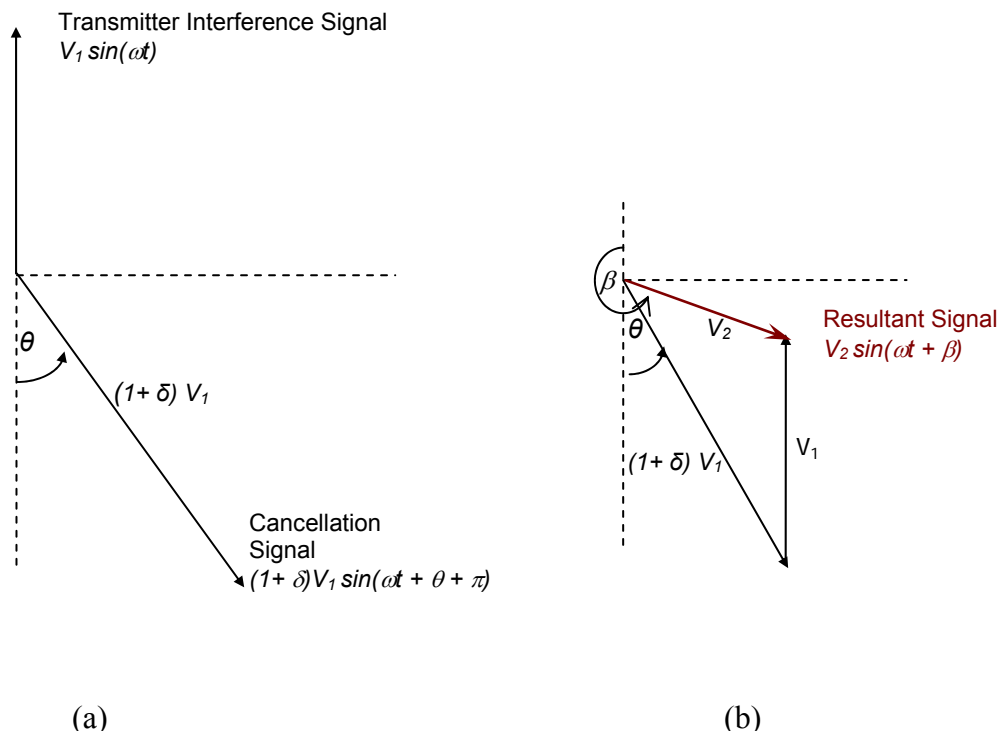


Figure 6-2 Vector representation of signal cancellation with phase and gain mismatch.

Figure 6-2(a) shows the transmitter interference signal and the cancelling signal (the signal before the cancellation) with relative phase (θ) and relative gain (δ) errors. Since the cancelling signal should be 180° out of phase, the phase of the

cancellation signal is $\omega t + \pi + \theta$. Figure 6-2(b) shows the vector addition and the resultant signal after the cancellation.

The resultant signal is

$$V_2 \sin(\omega t + \beta) = V_1 \sin(\omega t) + (1 + \delta)V_1 \sin(\omega t + \theta + \pi) \quad \text{Eq. 6-4}$$

When the transmitter interference signal is considered as the reference signal, its gain is V_1 and the gain error of the cancelling signal is δV_1 . Therefore considering vector addition and using the cosine rule, the magnitude of the resultant signal can be calculated as

$$V_2^2 = ((1 + \delta)V_1)^2 + V_1^2 - 2(1 + \delta)V_1^2 \cos \theta \quad \text{Eq. 6-5}$$

To calculate the range of amplitude error and phase error for a fixed signal cancellation level the above equation can be re-written as

$$((1 + \delta)V_1)^2 - 2V_1^2(1 + \delta)\cos \theta + V_1^2 - V_2^2 = 0 \quad \text{Eq. 6-6}$$

This is a quadratic equation and the solutions are

$$\begin{aligned} (1 + \delta) &= \frac{2V_1^2 \cos \theta \pm \left(4V_1^4 \cos^2 \theta - 4V_1^2(V_1^2 - V_2^2)\right)^{1/2}}{2V_1^2} \\ &= \cos \theta \pm \left(\frac{V_2^2}{V_1^2} - \sin^2 \theta\right)^{1/2} \end{aligned} \quad \text{Eq. 6-7}$$

Let $(1 + \delta)$ in dB be ΔV_1 and V_2^2/V_1^2 in dB be R then

$$\Delta V_1 = 20 \log \left| \cos \theta \pm \left(10^{R/10} - \sin^2 \theta\right)^{1/2} \right| \quad \text{Eq. 6-8}$$

According to Eq. 6-8 positive gain and positive phase mismatch with achievable cancellation levels can be represented graphically as shown in Figure 6-3. From this figure it can be observed that to achieve 50dB cancellation, phase and gain errors should be better than 0.18° and 0.03dB respectively. To achieve 40dB

cancellation, the phase error should be less than 0.57° and the gain error should be less than 0.085dB. As the cancellation goes higher, the range of gain and phase mismatch becomes smaller.

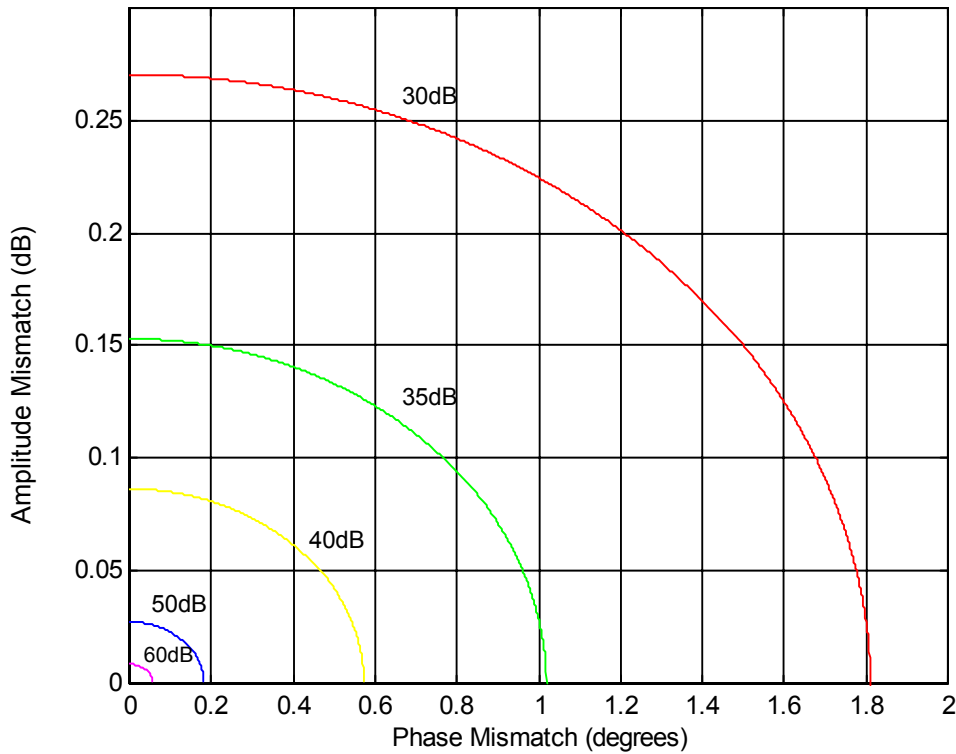


Figure 6-3 The gain phase mismatch with achievable cancellation levels for single loop cancellation.

To calculate the phase error for various signal cancellation levels, given a fixed gain mismatch, Eq. 6-7 can be re-written as

$$R = 10 \cdot \log \left(10^{0.1(\Delta V_1)} + 1 - 2 \cdot 10^{0.05(\Delta V_1)} \cdot \cos \theta \right) \quad \text{Eq. 6-9}$$

This is shown in Figure 6-4. For 40dB signal cancellation, with a gain mismatch of 0.085dB, the phase error should be less than 0.1° . A minimum of 40dB cancellation is required for the active cancelling unit in an adaptive duplexer architecture using a 20dB low isolation device, to give a total of 60dB.

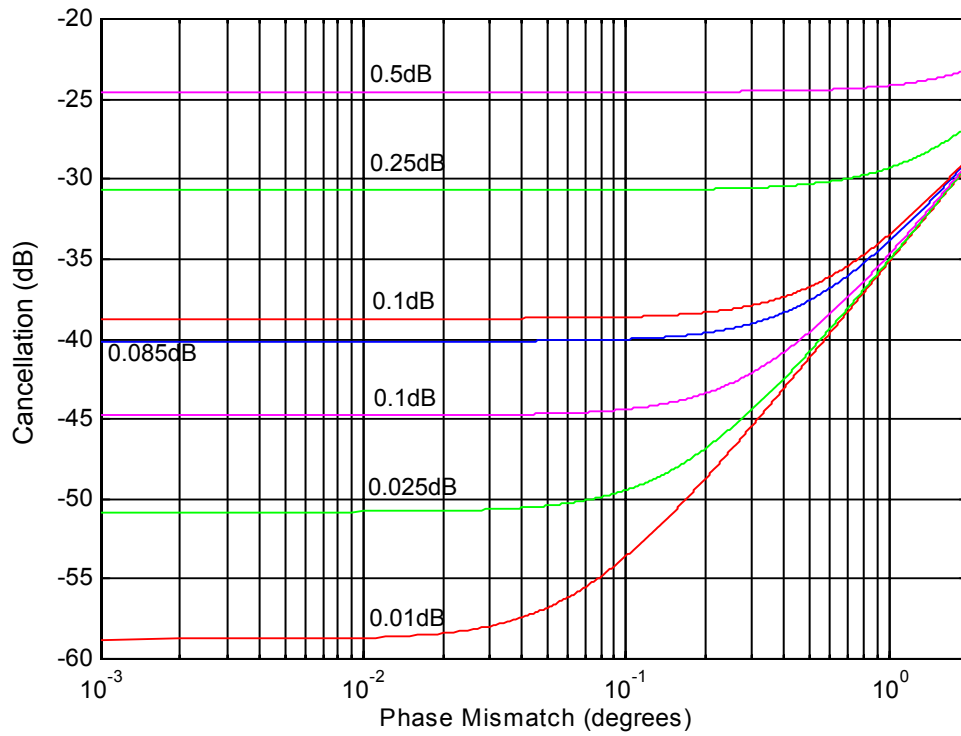


Figure 6-4 Achievable cancellation levels with phase mismatch for different values of gain mismatch.

If the cancellation is considered as a function of phase error ($\delta = 0$) then the Eq. 6-5 becomes

$$\begin{aligned} \left(\frac{V_2}{V_1}\right)^2 &= 2(1 - \cos(\theta)) \\ &= 4 \sin^2(\theta/2) \end{aligned} \quad \text{Eq. 6-10}$$

Therefore the cancellation is

$$R(dB) = 20 \log \left[2 \sin \left(\frac{\theta}{2} \right) \right] \quad \text{Eq. 6-11}$$

If the cancellation is considered as a function of gain error ($\theta = 0$) then Eq. 6-5 becomes

$$\left(\frac{V_2}{V_1}\right)^2 = \delta^2 \quad \text{Eq. 6-12}$$

Therefore the cancellation is

$$R(\text{dB}) = 20 \log \left[10^{\frac{\Delta V_1}{20}} - 1 \right] \quad \text{Eq. 6-13}$$

6.4 Effect of Delay Mismatch on Signal Cancellation

For broadband signals, the cancellation requirement should be met for each frequency in the band of interest. The delay difference between the main and cancellation paths causes a linear phase response (constant delay) over the band of interest and hence perfect broadband signal cancellation is only possible over a small frequency range. In order to eliminate the delay difference τ_1 , a delay element is introduced. If the cables are used as delay elements, they are lengthened or shortened until the delay match is achieved.

To see the effect of delay mismatch it is assumed that there is no gain or phase mismatch ($\delta = 0$, $\theta = 0$) between the main signal and the cancellation signal. The vector representation of signal cancellation with delay mismatch (τ_1) is shown in Figure 6-5. The vector triangle in Figure 6-5 (b) is an isosceles triangle and V_2 represents the magnitude of the resultant signal.

$$V_2 = 2V_1 \sin\left(\frac{\omega\tau_1}{2}\right) \quad \text{Eq. 6-14}$$

(Note: This derivation can also be obtained from Eq. 6-4 using trigonometry and comparing the amplitudes of the signals [140]).

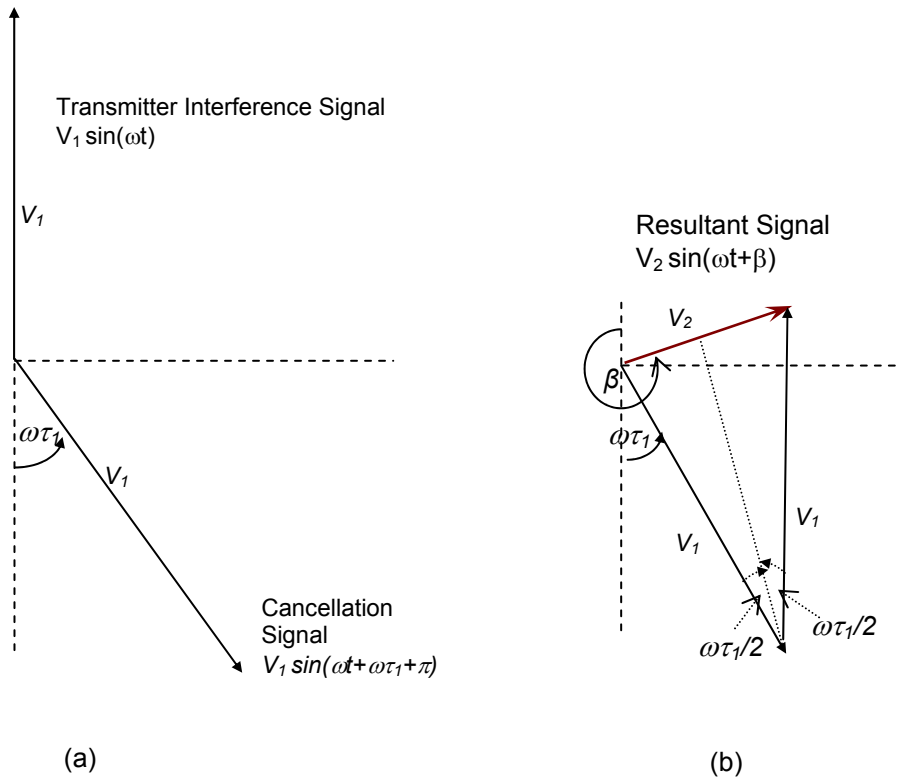


Figure 6-5 The vector representation of signal cancellation with delay mismatch.

$$\omega\tau_1 = \cos^{-1}\left(1 - \frac{V_2^2}{2V_1^2}\right) \tag{Eq. 6-15}$$

Noting firstly the delay is equal to the rate of change of phase with respect to frequency and secondly $\omega\tau_1$ in Eq. 6-15 is the deviation from the Tx interference signal, the cancellation bandwidth ($B = 2f_\Delta = \omega_\Delta / \pi$) is the range of ω for which V_2/V_1 is less than a specified level, R .

Let V_2^2/V_1^2 in dB be R then

$$B = \frac{1}{\pi\tau_1} \cos^{-1}\left(1 - \frac{10^{\frac{R}{10}}}{2}\right) \tag{Eq. 6-16}$$

Using Eq. 6-16 the delay mismatch with achievable cancellation levels can be represented graphically as shown in Figure 6-6. From this figure it can be seen that a 40dB cancellation or more can be achieved over a 10MHz band of interest with a 0.3ns delay mismatch.

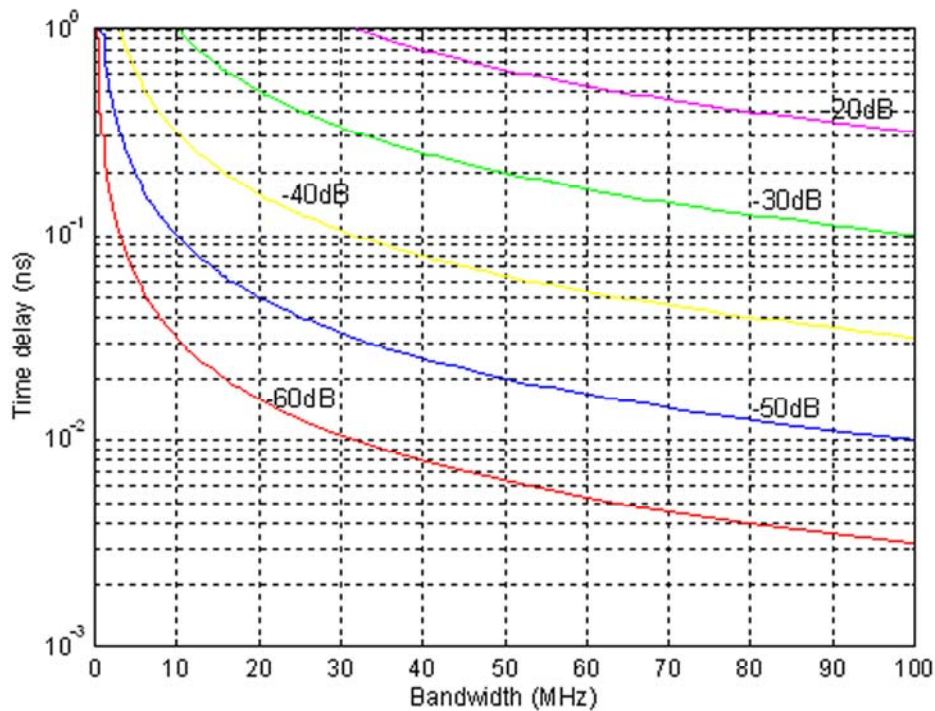


Figure 6-6 The delay mismatch with achievable cancellation levels for single loop cancellation.

The adaptive duplexer discussed in this thesis requires broadband cancellation at both the Tx frequency and the Rx frequency. If the two paths (the main path and the cancellation path) have the same delay ($\tau_l = 0$), then broadband cancellation (over Tx and Rx band) can be obtained using only a single loop. Ideally, signals should be cancelled over an unlimited bandwidth. When the delay mismatch between the two paths is τ_l ($\tau_l \neq 0$), the cancellation signal has a linear phase shift with frequency and therefore broadband cancellation over a typical 45MHz duplexing frequency band is impossible. This can be seen from Figure 6-6, i.e. to achieve about 40dB cancellation over more than 45MHz bandwidth, the delay

mismatch should not exceed 0.07ns. This is a very stringent requirement and it is not feasible because of changes in antenna loading in practical handheld environment. For this reason, we need to achieve two nulls, one at the Tx frequency and the other at the Rx frequency to achieve broadband cancellation. One way of achieving these two nulls is to use a single loop cancellation architecture with the delay difference (τ_l) between the two paths made equal to the reciprocal of the duplex frequency (f_d). This method is discussed in Section 6.8. Simulation techniques were used to find the signal cancellation limit of the process and are discussed in the next section.

6.5 Simulation of the Cancellation Unit with Single Loop

There are many different simulators provided in the Advanced Design System (ADS) package from Agilent Technologies. In this design the Harmonic Balance Simulator is used to evaluate the performance of the cancellation unit.

Harmonic Balance Simulation is a frequency-domain analysis technique for simulating distortion in nonlinear circuits and systems. It obtains frequency-domain voltages and currents, by calculating the spectral content of voltages or currents in the circuits [141].

6.5.1 Signal Cancellation

The schematic diagram of the simulated cancellation unit is shown in Figure 6-7. Two power sources were used for the transmitted signal and for the received signal. These were modelled in ADS as P-1 Tone components in the Sources-Freq domain library. The transmitter power (PORT-A) was modelled as a 10dBm, 2GHz signal and the receiver power (PORT-B) was modelled as -50 dBm, 2.045GHz signal which is 45MHz away from the transmitting signal. The receiver input was modelled in ADS as a 50-Ohm termination.

A circulator was used to partially isolate the transmitter from the receiver. In the ADS system a circulator was selected from the System-Passive library. The circulator was modelled with 20dB isolation and 1dB loss. These parameters were equivalent to that of the wideband circulator used in the practical experiment (UTE Mic CT-2008-0). Signal cancellation involves a vector addition. Therefore two directional couplers were used to divide (COUP-A) and combine (COUP-B) cancellation signals.

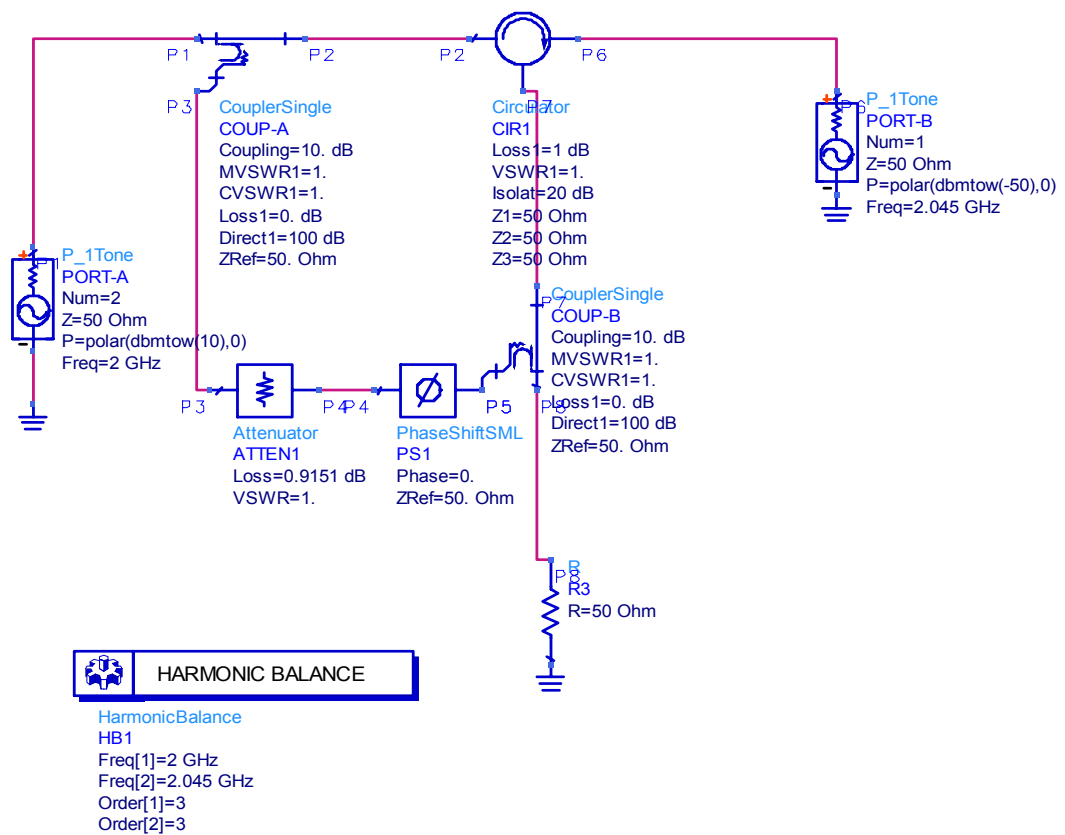


Figure 6-7 The schematic diagram of the simulated cancellation unit with single loop.

10dB directional couplers were selected based on the desire to minimise insertion loss while maintaining a large enough correction signal for the cancellation. In the ADS simulation the directional couplers were chosen from the System-Passive library. The vector attenuator is modelled by an attenuator and a phase shifter, also chosen from the System-Passive library. The attenuation was set such that the

transmitter interference signal and the cancellation signal are equal in amplitude. The phase was set at 0° degrees in the phase shifter. This was done because both directional couplers in ADS introduce a 90° phase shift and hence a total of 180° phase shift already exists in the cancellation path. In practice some degree of phase shifting is required to cancel out any phase errors between the loop's two paths caused by path differences and frequency selectivity.

The spectrum of the received signals without the cancellation loop is shown in Figure 6-8 (m1–transmitter interference signal, m2–desired received signal coming from PORT-B). Figure 6-9 shows the spectrum of the received signal with the cancellation unit.

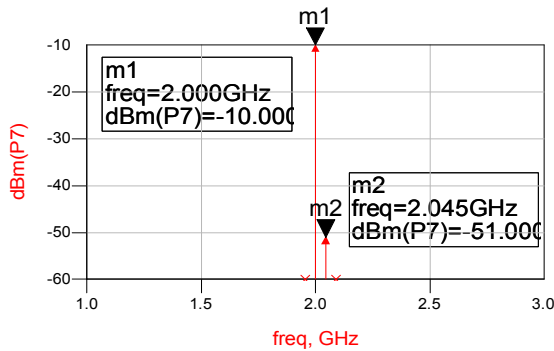


Figure 6-8 Spectrum of the received signals without the single loop cancellation unit. m1-transmitter interference signal, m2-desired receive signal.

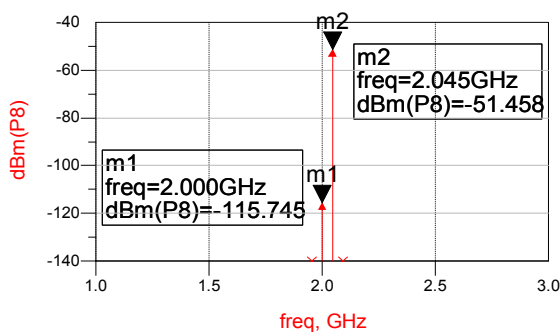


Figure 6-9 Received signal spectrum with the cancellation unit. m1-transmitter interference signal, m2-desired receive signal.

It was observed from the simulation that an additional isolation of 105.8 dB between the transmitter and the receiver (signal m1) was achieved using this adaptive cancellation technique. Therefore the overall isolation due to the cancellation unit and the circulator was about 125 dB. (Note: Many practical issues have been neglected in this simulation.)

6.5.2 Noise Cancellation

Noise can be passed into a microwave system from external sources, or it may be generated within the system itself. In a conventional duplexer, a band-pass filter in the transmitting path stops the transmitter noise leaking into the receiver. Since this adaptive duplexer architecture replaces the band-pass filters with a circulator and a cancellation unit, the transmitter noise and the noise contribution from the cancellation unit should be analysed.

It is possible to analyse the noise in the cancellation circuit by using the non-linear noise options of the ADS harmonic balance simulator. The schematic diagram of the simulated cancellation unit for noise analysis, is shown in Figure 6-10. The vector attenuator has a noise figure equal to its attenuation [142]. An amplifier was used after the power source to see the effect of increased transmitter noise.

A list of node names at which noise parameters are to be reported was specified using the Noise (2) option of the ADS simulator. The temperature was set at 16.85 degrees Celsius, which is the standard temperature for Noise Figure (NF) measurement as defined by the IEEE definition [143]. Table 6-1 shows the simulation results of noise analysis.

The COUP-A in the schematic diagram is in forward mode operation. The input noise signal is split into two output components; the main line output (P2) and coupled output (P3). These two noise signals are correlated [132] and so cancel out at the COUP-B, since the gains of the transmitter interference signal path and the cancellation signal path are equal. The noise signals due to internal resistance of the COUP-A are also cancelled out at the receiver input. The received noise

power from PORT-B and the noise power due to the internal resistance of the circulator and the attenuator are added in power at the receiver input. The noise power due to internal resistance of COUP-B is not considered because it is in reverse mode operation.

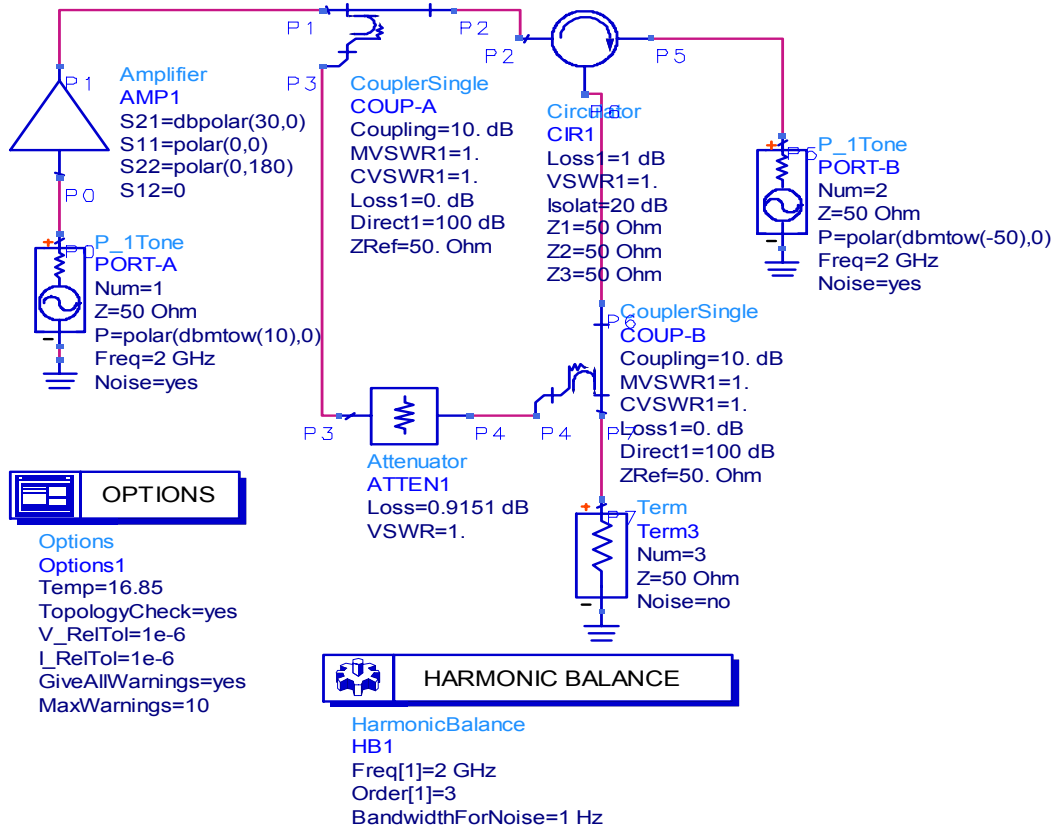


Figure 6-10 The ADS schematic diagram for the noise cancellation.

Table 6-1 Noise voltages at different nodes

Node Name	Noise Voltage $\sqrt{\text{Hz}}$
P0.noise	447.4 pV
P1.noise	44.7 nV
P2.noise	42.45 nV
P3.noise	14.16 nV
P4.noise	12.75 nV
P5.noise	37.83 nV
P6.noise	4.270 nV
P7.noise	440.1 pV

From the simulation results it can be seen that the noise voltage at the receiver input (440.1pV) is less than the minimum noise level 447.4pV. The desired receive signal is also attenuated, and the net SNR (signal to noise ratio) is still worse than the SNR at the antenna. The best case NF for this receiver is 1.32dB.

6.6 Description of the Single Loop Cancellation System

The experimental setup used to test the adaptive duplexer architecture with a single loop cancellation is shown in Figure 6-11.

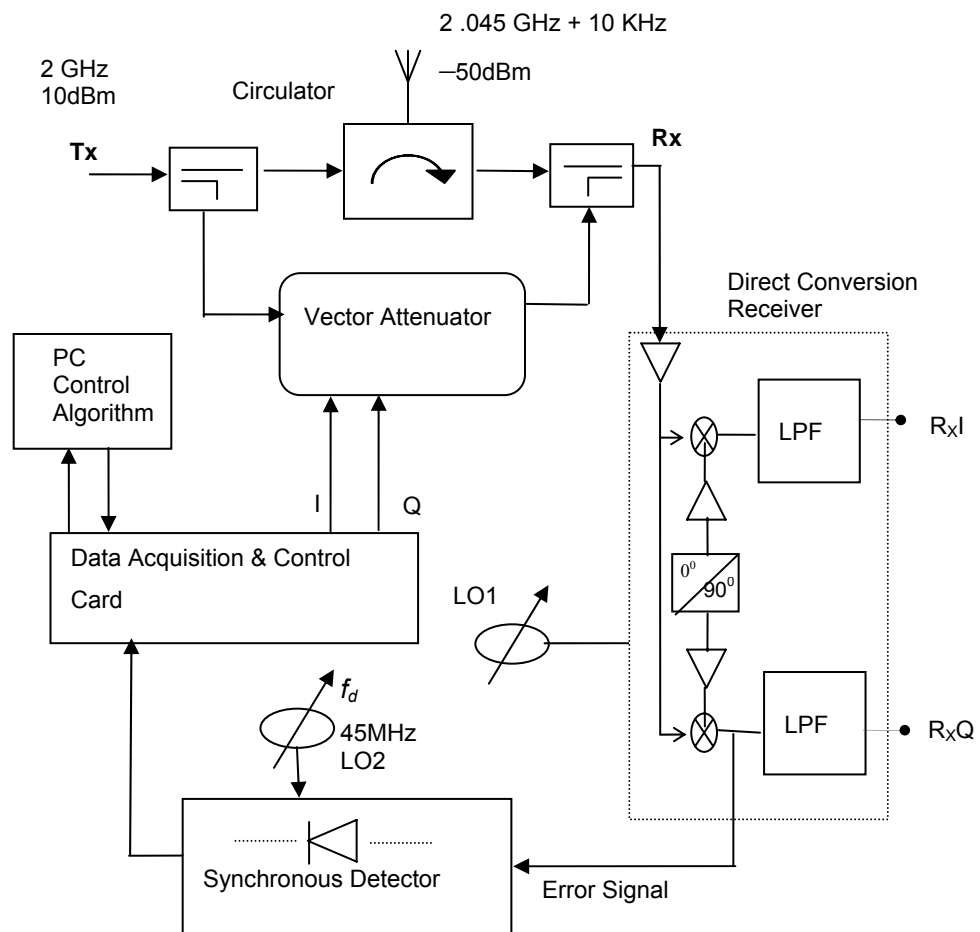


Figure 6-11 The experimental setup.

The transmitter interference signal is the part of the locally transmitted signal, which leaks back to the associated receiver via the circulator. A directional coupler (in forward mode operation) is used to obtain a sample of the transmitter signal. This sample signal is then attenuated and phase adjusted to match the out of phase transmitter interference signal using a vector attenuator. The vector attenuator is functionally equivalent to an endless phase shifter and an attenuator, but usually employs an IQ architecture. The vector attenuator also displays negligible group delay distortion and virtually no change in absolute delay with changes in control inputs [144]. To provide equal delay in the main path and the cancellation path coaxial cables are used. The use of coaxial cables as delay lines, increases insertion loss, volume, and grounding difficulties. These problems can be resolved at the expense of bandwidth restrictions by using band-pass filters as delay lines¹. After adjusting the phase and gain of the leakage signal it is then added to the received signal Rx via a directional coupler in reverse mode operation in order to cancel the transmitter signal. The received signal after the cancellation is fed to the LNA of the direct conversion receiver. The above cancellation procedure must be done before the LNA to keep the resulting input signal within the dynamic range of the LNA.

In a direct conversion receiver the desired signal is down converted to baseband and so the interfering signal will be down converted to f_d . Detection of the f_d signal occurs at the output of the mixer and this can be used as a feedback error signal to control the canceller. A synchronous detector circuit was used to detect the power (or amplitude) of this error signal and this is fed to the data acquisition card in the PC. The PC then sends two control signals (I and Q) to the vector attenuator. The LO2 in the synchronous detector is set to f_d , and only changes when a different band with different f_d is selected.

If the cancellation is not perfect then an error signal will be generated. In practice this jamming signal cannot be cancelled out completely. This could be due to the

¹ Mismatches at the end of the delay lines can limit the cancellation bandwidth. For a bandwidth of 5 MHz (WCDMA) and 45dB of cancellation, the return loss should be less than 10dB for a 1ns delay line. This is an easily achievable target.

imperfections of the electronic devices. A one dimensional search control algorithm is used to keep this error at a minimum. In this algorithm one control voltage (for example I) is incremented or decremented by a small step length while the other control voltage (Q) is held constant. The change in the output power is recorded after each step. If the output power drops then the control voltage is incremented (or decremented) further, and this continues until the output power reaches its minimum. The other direction is selected and the above procedure is repeated. This whole procedure is repeated with reducing step lengths until an optimum is reached.

6.7 Experimental Results

Experimental results for the cancellation circuit was observed as -22.38dBm before the cancellation and -71.00dBm after the cancellation. Therefore the achieved additional isolation using the cancellation unit was about 49dB . The spectrum analyser is used to monitor the transmitter interference signal and the desired receiver signal (Figure 6-12).

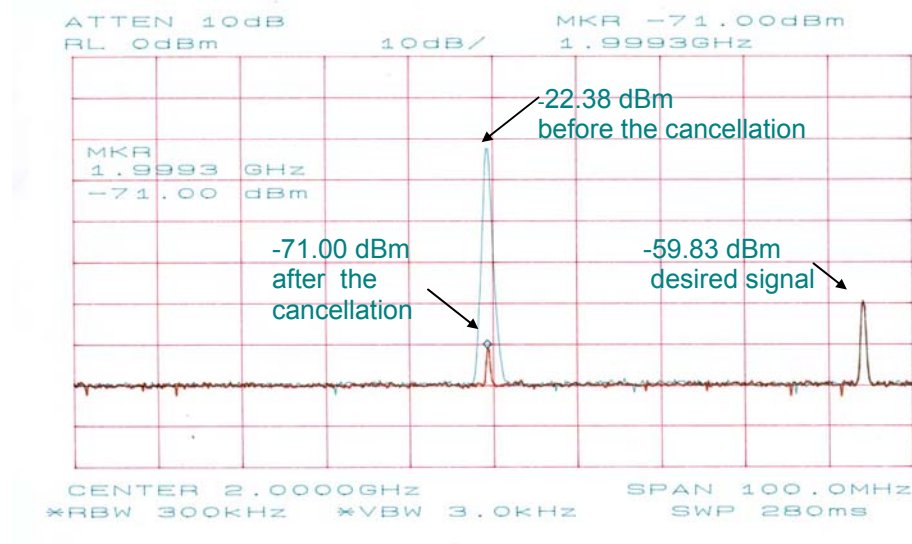


Figure 6-12 Spectrum of the received transmitter leakage signal before and after the cancellation.

Since the circulator provides an additional 20dB isolation, the achieved isolation with the circulator and the cancellation unit was about 69dB. This is more than enough to stop receiver overload or blocking.

There is a significant difference between the simulated results and the experimental results. This is due to the inability to match the phase and amplitude of the transmitter signal exactly in the experimental situations. It can be seen from Figure 6-3, that cancellation higher than 50dB leads to a very small gain phase mismatch (less than 0.18deg. & 0.03dB). It is very difficult to achieve this practically because of the DA resolution step size, noise, and non-linear behaviour of the vector attenuator characteristics.

The desired receive signal before the cancellation and after the cancellation is shown in Figure 6-13. The transmitter interference signal caused the desired signal to be distorted, and desensitised by 15dB.

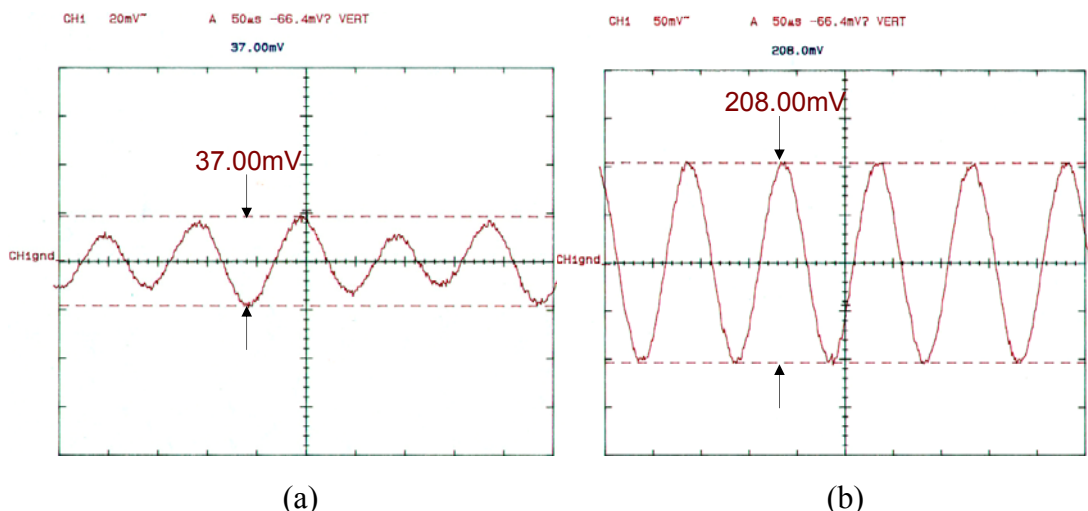


Figure 6-13 The 10kHz received signal before the cancellation (a) and after the cancellation (b). Settings: (a)-20mV/square (b)-50mV/square.

As shown in Figure 6-14 the detected error signal required 85 iterations to reduce by 35dB. The reduction is 14dB less than the achieved leakage reduction (as per Figure 6-12) and this is due to saturation in the LNA compressing the upper part of the scale.



Figure 6-14 Error learning curve.

6.8 Double Null Using Single Loop Cancellation

Cancellation in one duplex band can be achieved using a single adjustable loop as discussed in the previous sections. If the two paths in the single loop cancellation unit have the same delay ($\tau_a = \tau_b$), cancellation in both duplex bands is also possible. It is also shown (Figure 6-3) when the delay mismatch between paths is $\tau_l (= \tau_b - \tau_a \neq 0)$, broadband cancellation over the full duplexing frequency range is not feasible. As an example for 40dB isolation and a duplex frequency of $f_d = 190\text{MHz}$ (for W-CDMA), the delay mismatch ($\tau_b - \tau_a$) should be less than 0.016ns. This is an unrealistic practical requirement for given antenna loading considerations.

Further, we can achieve a double null, one at the Tx frequency and the other at the Rx frequency, using single loop cancellation. In order to achieve a double null, the delay difference between the main path and the cancellation path (τ_l) should be equal to the reciprocal of the duplexing frequency (f_d). i.e.

$$\tau_l = \frac{1}{f_d} \quad \text{Eq. 6-17}$$

Under this condition, when the gain and phase of the cancellation signal are adjusted to match the gain and anti-phase of the received interference signal at the Tx frequency, the cancellation signal at the Rx frequency will also match the gain and anti-phase of the received interference signal. This phenomenon is illustrated in the Figure 6-15.

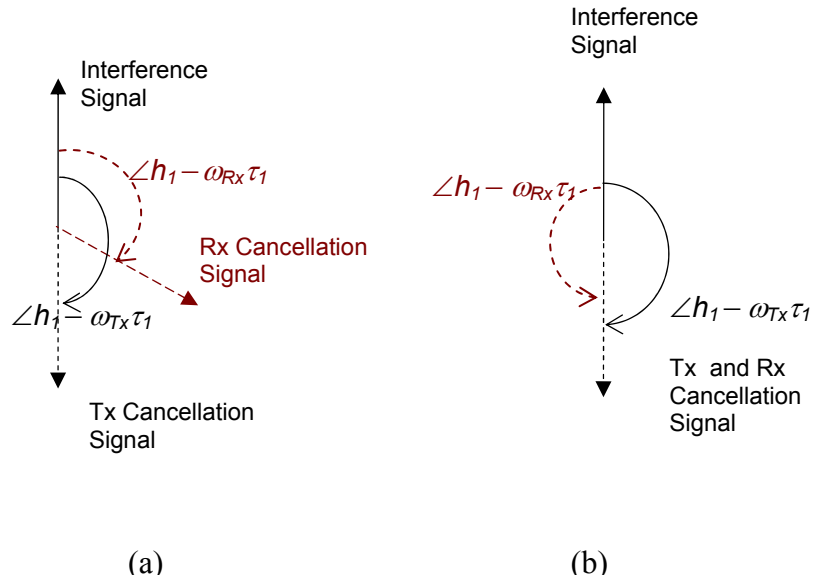


Figure 6-15 Geometric representation of cancellation signals at Tx frequency and Rx frequency using single loop cancellation (a) $\tau_1 \neq 1/f_d$, (b) $\tau_1 = 1/f_d$.

The phase difference (β_{Tx}) between the two paths (leakage and cancelling paths) at the Tx frequency (ω_{Tx}) is adjusted so that it is equal to 180° , i.e.

$$\beta_{Tx} = \angle h_1 - \omega_{Tx} \tau_1 = \pi \quad \text{Eq. 6-18}$$

where $\angle h_1$ is the required coefficient phase adjustment.

This creates one null at Tx frequency. Then the phase difference (β_{Rx}) of the two paths at the Rx frequency (ω_{Rx}) becomes

$$\begin{aligned} \beta_{Rx} &= \angle h_1 - \omega_{Rx} \tau_1 = \pi + \tau_1 \omega_{Tx} - \omega_{Rx} \tau_1 \\ &= \pi - \tau_1 (\omega_d) \end{aligned} \quad \text{Eq. 6-19}$$

where $\omega_d = \omega_{Rx} - \omega_{Tx}$

When $\tau_l = 1/f_d$, the phase difference between the two paths at the Rx frequency will be $-\pi$ and so another null will occur. Actually there will be nulls occurring at $\pm n.f_d$ regular intervals (n -integer number). The necessary phase adjustment $\angle h_l$ is given by

$$\angle h_l = \pi + 2\pi \frac{f_{Tx}}{f_d} \tag{Eq. 6-20}$$

Figure 6-16 shows the simulation outcome of the cancellation with $f_d = 190\text{MHz}$ and $f_{Tx} = 2\text{GHz}$. Here the two nulls are clearly visible at the Tx frequency (2GHz) and the Rx frequency (2.190GHz).

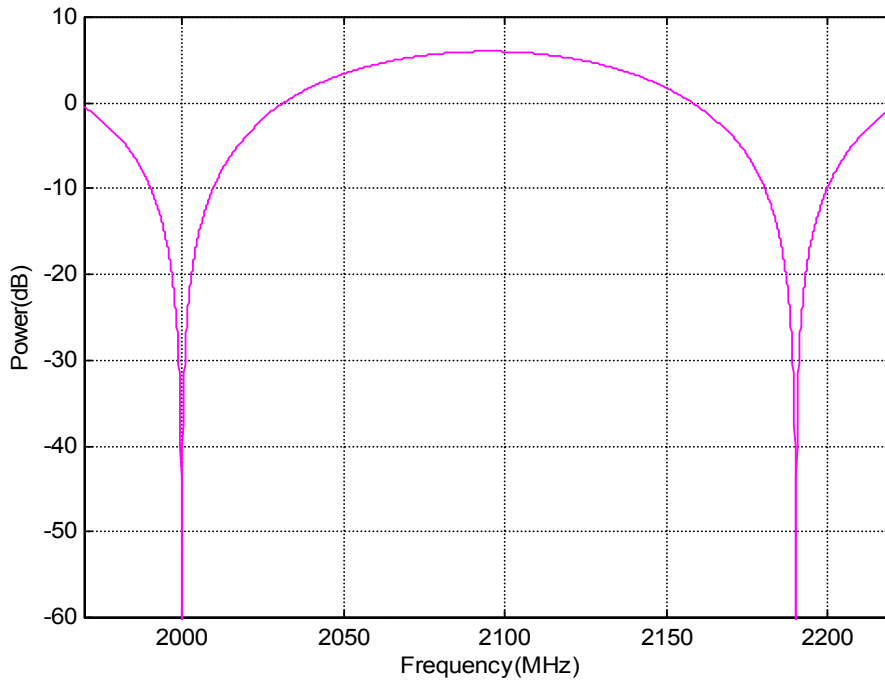


Figure 6-16 Two nulls using single loop cancellation ($f_d = 190\text{MHz}$ & $f_{Tx} = 2\text{GHz}$).

The gain-phase mismatch and delay mismatch characteristics of double nulls are the same as the single null case which is described in the Sections 6.3 and 6.4 respectively. The accuracy of the frequencies at which the double nulls occur depends on the mismatch of the delay difference $1/f_d$ and this effect can be represented as an additional phase error term $\Delta(\omega\tau)$.

$$\Delta\omega\tau = 2\pi \frac{1}{f_d + \delta f_d} \quad \text{Eq. 6-21}$$

This phase error introduces a frequency shift which could change the frequency at which the second optimum cancellation (the second null) would occur. It is clear when there is a phase error ($\delta\theta$) in the cancellation process, this would shift the frequencies of both nulls.

Even though we can achieve nulls at the Tx frequency and the Rx frequency using this method, wideband cancellation is impossible. This is because the delay mismatch ($\tau_l = 1/f_d$) between the two paths is very large. For example, the bandwidth is only 0.57MHz @ -40dB cancellation for a 190MHz duplexing frequency. Therefore it is necessary to employ a double loop cancellation technique to achieve double nulls with wider bandwidths. This gives an additional flexibility in the duplexer design.

6.9 Conclusion

Experimental results show that 69dB duplex isolation (Tx leakage signal suppression) is achievable with a circulator and a single loop cancellation unit. This is more than enough to stop the receiver overload or blocking.

ADS is a powerful simulator so that we can have a good expectation on the circuit performance before the implementation of the circuit. But here the simulated and the measured results appear to be wider apart because of the vector attenuator non-linearity and the minimum quantisation step-size of the DACs. Also, the receiver was not modelled in the schematic. In the simulation the desired signal has been attenuated by 1.5dB due to the circulator and the directional coupler attenuation. From the noise simulation it can be concluded that there is no additional noise from the simulated cancellation unit. This was a surprising result, since the couplers and splitters are noise sources. The S/N ratio at the receiver

input is about 0.38dB worse than without the cancellation unit. So the sensitivity of the receiver has not been affected much by the cancellation unit.

Cancellation in both duplex bands can be achieved using single loop cancellation but wideband cancellation is not possible.

The described scheme is simple and requires no additional pilot signals for adjustments, but it is sensitive to delay errors. The next chapter will discuss a double loop cancellation process, which is much less sensitive to delay errors.

Design and Implementation of the Double Loop Cancellation System

7.1 Introduction

The double loop cancellation technique is used in the adaptive duplexer architecture to cancel the residual Tx interference signal and Tx noise in the receiver path. The cancellation technique described in this chapter overcomes some of the limitations associated with the single loop cancellation system and allows two cancellation nulls to be achieved over a wider bandwidth. This gives an additional degree of freedom in duplexer design.

A first time analysis of the double loop cancellation system is detailed in this chapter. It uses a geometrical representation. Each loop consists of an adjustable vector attenuator and a delay element. The delay element bounds are derived for a given adjustment range of the vector attenuators (coefficients) used in the cancellation paths. The feasibility of wideband cancellation is discussed and is shown to be mainly dependent on the duplexing frequency and the operating range of delays in the main path and the cancellation paths. The limited adjustment range of the coefficients in the cancellation paths put further

constrains on these delays. The relationship between the cancellation bandwidth and the residual cancellation level is shown to be linear (6dB/octave) and related to the loop delays and the duplexing frequency. These results are verified with simulations.

A new adaptation algorithm, which uses a single cost function to control the two error signals, is also proposed in this chapter. The hardware prototype of the adaptive duplexer is described. The performance and the efficiency of the adaptive duplexer are discussed using simulated and experimental results.

7.2 Double Loop Cancellation System

The simplified double loop cancellation configuration with delay differences is shown in Figure 7-1. The delay $\tau_1 (= \tau_b - \tau_a)$ is the delay difference between the main path and the cancellation path₁. The delay $\tau_2 (= \tau_c - \tau_a)$ is the delay difference between the main path and the cancellation path₂. These delays can be negative. The coefficients, $h_1 (I_1, Q_1)$ and $h_2 (I_2, Q_2)$ represent the complex gains of cancellation path₁ and path₂ respectively.

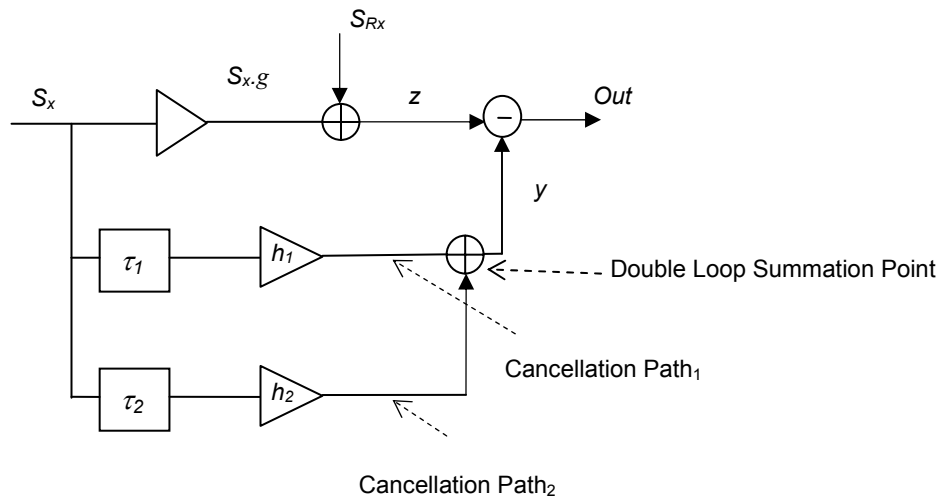


Figure 7-1 The double loop cancellation configuration.

If g represents the attenuation of the main path and S_x represents the transmitter interference signal, then the cancellation signal (at the double loop summation point) becomes

$$y = (h_1 \cdot e^{-j\omega\tau_1} + h_2 \cdot e^{-j\omega\tau_2}) S_x \quad \text{Eq. 7-1}$$

and the desired signal,

$$Out = z - y = (g) S_x + S_{Rx} - (h_1 \cdot e^{-j\omega\tau_1} + h_2 \cdot e^{-j\omega\tau_2}) S_x$$

Since we are considering only the transmitter leakage signals in the receiver path we can neglect the desired Rx signal, S_{Rx} , in this analysis. Then the desired signal is

$$Out = (g - h_1 \cdot e^{-j\omega\tau_1} - h_2 \cdot e^{-j\omega\tau_2}) S_x \quad \text{Eq. 7-2}$$

therefore, the desired signal at Tx frequency, ω_{Tx} ,

$$Out_{Tx} = (g - h_1 \cdot e^{-j\omega_{Tx}\tau_1} - h_2 \cdot e^{-j\omega_{Tx}\tau_2}) S_x \quad \text{Eq. 7-3}$$

and at Rx frequency, ω_{Rx} ,

$$Out_{Rx} = (g - h_1 \cdot e^{-j\omega_{Rx}\tau_1} - h_2 \cdot e^{-j\omega_{Rx}\tau_2}) S_x \quad \text{Eq. 7-4}$$

For simplicity this analysis assumes $S_x = 1$ and there is no amplitude difference between the main path and the cancellation paths ($g = 1$). (The latter implies that the combined directional coupling and combining coefficients of the cancelling loop is equal to the isolation provided by the circulator or other passive ‘low isolation device’ in the leakage path). The vector summation of the two cancellation signal components should be equal to 1 to achieve a perfect cancellation signal.

$$y = (h_1 \cdot e^{-j\omega\tau_1} + h_2 \cdot e^{-j\omega\tau_2}) = 1 \quad \text{Eq. 7-5}$$

If the signal vectors of cancellation path₁ and path₂ at angular frequency ω_{Tx} are P_{Tx} and Q_{Tx} then

$$P_{Tx} = h_1 e^{-j\omega_{Tx}\tau_1} \quad \text{Eq. 7-6}$$

$$Q_{Tx} = h_2 e^{-j\omega_{Tx}\tau_2} \quad \text{Eq. 7-7}$$

If the signal vectors of cancellation path₁ and path₂ at angular frequency ω_{Rx} are P_{Rx} and Q_{Rx} then

$$P_{Rx} = h_1 e^{-j \cdot \omega_{Rx} \cdot \tau_1} \tag{Eq. 7-8}$$

$$Q_{Rx} = h_2 e^{-j \cdot \omega_{Rx} \cdot \tau_2} \tag{Eq. 7-9}$$

To obtain cancellation the magnitude values of P_{Tx} , Q_{Tx} , P_{Rx} or Q_{Rx} can take in any value as shown in Figure 7-2, as long as $P_{Tx} + Q_{Tx} = 1$ and $P_{Rx} + Q_{Rx} = 1$. Four solutions are shown for four different choices of delays. Note the change in the magnitude of the cancellation vectors. The path delays cause the vectors to rotate with frequency. Figure 7-2(a) shows this position at ω_{Tx} and Figure 7-2(b) shows the position of ω_{Rx} . The complex gain coefficients h_1 and h_2 have been selected such that cancellation occurs at both frequencies.

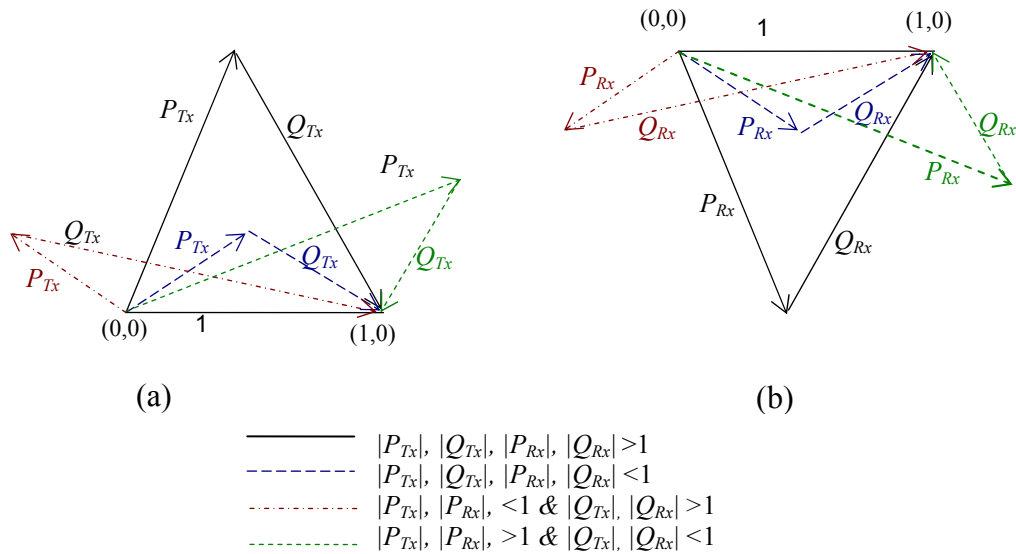


Figure 7-2 Vector representation of signal components at the double loop summation point (four different delay differences). a) at ω_{Tx} b) at ω_{Rx} . For perfect cancellation the vectors must sum to 1. Note the possible magnitude relationships.

In practical implementation the adjustment ranges of h_1 and h_2 will be limited by the device properties of the gain and phase adjusters. If vector attenuators are used, gain is not possible then the magnitude of $h_1 < 1$ and $h_2 < 1$ and hence the magnitudes of P_{Tx} , P_{Rx} , Q_{Tx} and $Q_{Rx} < 1$. The durations of the delays are limited by the above conditions. To find these limitations and to derive the operating conditions, the angles of the cancellation signal vectors are required in terms of the delay differences and the duplexing frequency. These derivations are given in Sections 7.4 & 7.5.

7.3 Delay Effects

When choosing the delays for practical implementation, the size of the delay elements, the achievable bandwidth and any limitations of the gain/phase adjusters need to be considered.

Solving Eq. 7-3 and Eq. 7-4 (with $g = 1$, $S_x = 1$) gives the coefficient values h_1 and h_2 . The frequency response can then be calculated from Eq. 7-5. This is plotted in Figure 7-3 for conditions $\tau_1 = -1\text{ns}$, $\tau_2 = 0.5\text{ns}$ with $f_d = 190\text{MHz}$ and $\tau_1 = -0.5\text{ns}$, $\tau_2 = 0.5\text{ns}$ with $f_d = 190\text{MHz}$ and also $f_d = 45\text{MHz}$. This response clearly shows two nulls, one at the Tx frequency (2GHz) and the other at the Rx frequency (2.190GHz). As the delay difference in the two paths increases, the cancellation bandwidth tends to decrease. Moreover, the cancellation bandwidth will improve as the duplexing frequency is reduced as illustrated by curve c.

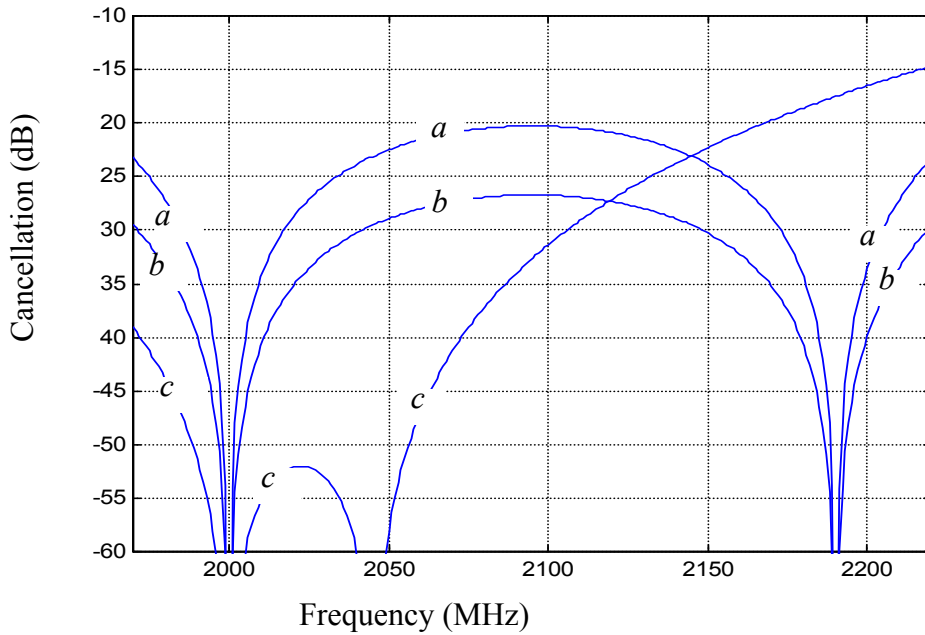


Figure 7-3 The nulls at Tx and Rx frequencies with double loop cancellation.
 (a $\Rightarrow \tau_1 = -1ns$ $\tau_2 = 0.5ns$ $f_d = 190MHz$, b $\Rightarrow \tau_1 = -0.5ns$ $\tau_2 = 0.5ns$ $f_d = 190MHz$,
 c $\Rightarrow \tau_1 = -0.5ns$ $\tau_2 = 0.5ns$ $f_d = 45MHz$)

7.4 The Relationship Between the Path Delays and the Duplexing Frequency

This section derives the constraints on τ_1 and τ_2 in terms of the duplexing frequency f_d . The constraints will be further tightened in the next section by limiting the range of the coefficient magnitudes to be less than 1 (attenuation only). Two conditions, covering all delay possibilities, are considered for the delay differences. These are ($0 < \tau_1 < \tau_2$) and ($\tau_1 < 0$ with $\tau_2 > 0$).

7.4.1 When $0 < \tau_1 < \tau_2$

For positive delay differences in cancellation path₁ and path₂ ($\tau_1 > 0$ & $\tau_2 > 0$) the complex gain coefficients (h_1, h_2) and the signal components ($P_{Tx}, Q_{Tx}, P_{Rx}, Q_{Rx}$) at the double loop summation point can be geometrically represented as shown in Figure 7-4.

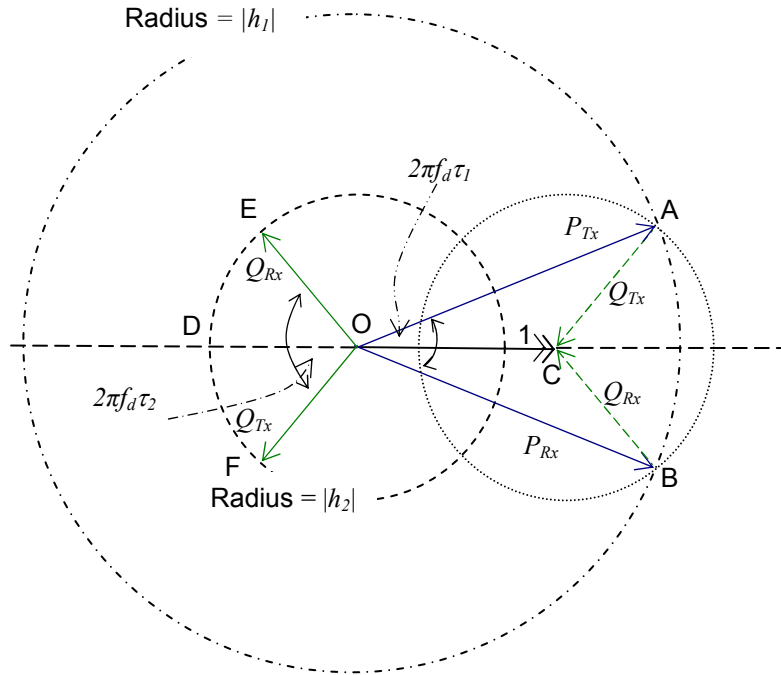


Figure 7-4 Geometric representation of signal components at the double loop summation point ($\tau_1 > 0$ and $\tau_2 > 0$). The rotation of Q (P) vector is caused by a change in frequency of f_d acting on the delay path τ_2 (τ_1). Note here in this cancellation $\tau_2 > \tau_1$ because the Q vector undergoes a greater phase shift.

The circle with radius $|h_1|$ and the circle with radius $|h_2|$ intersect at points A and B. These two points represent null conditions and this occur when $(|h_1| + |h_2|) > 1$. When $(|h_1| + |h_2|) = 1$ points A and B overlap and there will be only one null. Either of these two points can be selected to provide nulls at ω_{Tx} and ω_{Rx} . A can represent the transmit frequency cancellation point (transmit intersection point) and B can represent the receive frequency cancellation point (as shown in Figure 7-4). The other way around is also possible, with B representing the transmit

cancellation point and A the receive cancellation point. Also A can represent both as can B.

The signal vectors are

$$P_{Tx} = |h_1| \angle (\angle h_1 - \omega_{Tx} \tau_1) \quad \text{Eq. 7-10}$$

$$Q_{Tx} = |h_2| \angle (\angle h_2 - \omega_{Tx} \tau_2) \quad \text{Eq. 7-11}$$

$$P_{Rx} = |h_1| \angle (\angle h_1 - \omega_{Rx} \tau_1) \quad \text{Eq. 7-12}$$

$$Q_{Rx} = |h_2| \angle (\angle h_2 - \omega_{Rx} \tau_2) \quad \text{Eq. 7-13}$$

Since the magnitudes of P_{Tx} and P_{Rx} are equal and the magnitudes of Q_{Tx} and Q_{Rx} are equal, the AOC triangle and the BOC triangle are equal. The vectors are symmetrical about the real axis. Here $\angle P_{Tx} > \angle P_{Rx}$ and $\angle Q_{Tx} > \angle Q_{Rx}$ since $\omega_{Rx} > \omega_{Tx}$.

When $0 < \tau_1 < \tau_2$, the vector P at f_{Tx} (A) rotates clockwise to P_{Rx} (B) when its frequency is changed by f_d .

$$\begin{aligned} \angle P_{Rx} &= \angle P_{Tx} + 2n\pi - 2\pi\tau_1 f_d \\ (n &= 0, 1, 2, \dots) \end{aligned} \quad \text{Eq. 7-14}$$

Therefore due to symmetry ($\angle P_{Tx} = -\angle P_{Rx}$)

$$\angle P_{Tx} = \pi\tau_1 f_d - n\pi \quad \text{Eq. 7-15}$$

and

$$\angle P_{Rx} = -\pi\tau_1 f_d + n\pi \quad \text{Eq. 7-16}$$

Substituting Eq. 7-10 ($\angle P_{Tx}$) into Eq. 7-15

$$\angle h_1 = \pi\tau_1 (f_{Tx} + f_{Rx}) - n\pi \quad \text{Eq. 7-17}$$

Repeating the above for vector Q , the vector Q at f_{Tx} (F) rotates clockwise to Q_{Rx} (E) when its frequency is changed by f_d . Here, $\pi\tau_2 f_d = \angle DOF + m\pi$ ($m = 0, 1, 2, \dots$).

Therefore $\angle Q_{Tx} = \pi + \angle DOF$

$$\angle Q_{Tx} = \pi + \pi\tau_2 f_d - m\pi \quad \text{Eq. 7-18}$$

and

$$\angle Q_{Rx} = -\pi - \pi\tau_2 f_d + m\pi \quad \text{Eq. 7-19}$$

Also substituting Eq. 7-11 ($\angle Q_{Tx}$) into Eq. 7-18

$$\angle h_2 = \pi + \pi\tau_2 (f_{Tx} + f_{Rx}) - m\pi \quad \text{Eq. 7-20}$$

When $\tau_2 = \tau_1 \pm k/f_d$ ($k = 0, 1, 2, \dots$) the vectors P_{Tx} and Q_{Tx} are parallel and there is no joining point at A. This results in infinitely large magnitudes for h_1 and h_2 .

Eq. 7-15 and Eq. 7-18 apply when the transmit joining point of the vectors P_{Tx} and Q_{Tx} lies in the 1st or 2nd quadrant. The exact position is determined by τ_1 & τ_2 . The constraints on τ_1 and τ_2 can be obtained from the following inequalities.

$$0 < P_{Tx}$$

$$\angle P_{Tx} + (2\pi - \angle Q_{Tx}) < \pi$$

$$\pi < \angle Q_{Tx} < 2\pi$$

The middle constraint can be obtained by noting that the sum of the two angles in triangle OAC must be less than π . Substituting for $\angle P_{Tx}$ and $\angle Q_{Tx}$ gives the following delay constraints:

$$\begin{aligned} & [n\pi < \pi\tau_1 f_d < \pi\tau_2 f_d + (n-m)\pi] \& [m\pi < \pi\tau_2 f_d < (m+1)\pi] \\ \Rightarrow & \left[\frac{n}{f_d} < \tau_1 < \tau_2 + \frac{(n-m)}{f_d} \right] \& \left[\frac{m}{f_d} < \tau_2 < \frac{(m+1)}{f_d} \right] \quad \text{case (1)} \end{aligned}$$

Similarly when the transmit joining point occurs in the 3rd or 4th quadrant the general terms for the signal vector angles become

$$\angle Q_{Tx} = \pi\tau_2 f_d - m\pi \quad \text{Eq. 7-21}$$

$$\angle P_{Tx} = \pi + \pi\tau_1 f_d - n\pi \quad \text{Eq. 7-22}$$

and the delay constraints are

$$\Rightarrow \left[\tau_2 + \frac{(n-m)}{f_d} < \tau_1 < \frac{(n+1)}{f_d} \right] \& \left[\frac{m}{f_d} < \tau_2 < \frac{(m+1)}{f_d} \right] \quad \text{case (2)}$$

7.4.2 When $\tau_1 < 0$ and $\tau_2 > 0$

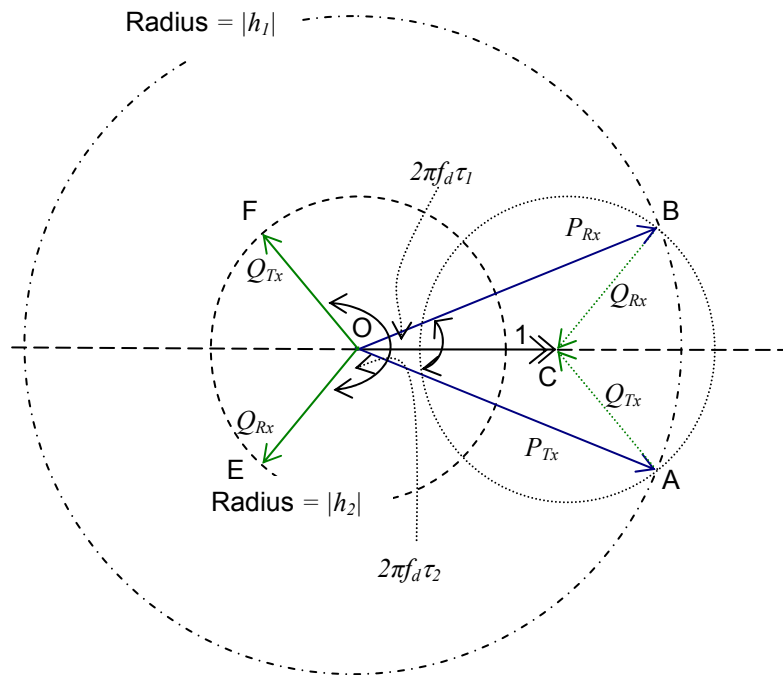


Figure 7-5 Geometric representation of signal components at the double loop summation point ($\tau_1 < 0$ and $\tau_2 > 0$). The rotation of Q (P) vector is caused by a change in frequency of f_d acting on the delay path τ_2 (τ_1).

When $\tau_1 < 0$ and $\tau_2 > 0$ the vector P_{Tx} rotates clockwise and Q_{Tx} rotates in the anticlockwise direction with increasing frequency (Figure 7-5). Here $\angle P_{Rx} > \angle P_{Tx}$

and $\angle Q_{Tx} > \angle Q_{Rx}$ since $\omega_{Rx} > \omega_{Tx}$. We follow a similar analysis to the previous sub-section. When the transmit joining point is in the 3rd or 4th quadrant;

$$\angle P_{Tx} = \pi\tau_1 f_d + n\pi \quad \text{Eq. 7-23}$$

$$\angle Q_{Tx} = \pi\tau_2 f_d - m\pi \quad \text{Eq. 7-24}$$

$$\angle h_1 = \pi\tau_1 (f_{Tx} + f_{Rx}) + n\pi \quad \text{Eq. 7-25}$$

$$\angle h_2 = \pi\tau_2 (f_{Tx} + f_{Rx}) - m\pi \quad \text{Eq. 7-26}$$

where $m, n = 0, 1, 2, \dots$

Here also, when $\tau_2 = \tau_1 \pm k/f_d$ ($k = 0, 1, 2, \dots$) the vectors P_{Tx} and Q_{Tx} are parallel and there is no joining point at A which results in infinitely large magnitudes for h_1 and h_2 .

The delay constraints are

$$\begin{aligned} & [-n\pi > \pi\tau_1 f_d > \pi\tau_2 f_d - (n+1+m)\pi] \& [m\pi < \pi\tau_2 f_d < (m+1)\pi] \\ \Rightarrow & \left[-\frac{n}{f_d} > \tau_1 > \tau_2 - \frac{(n+1+m)}{f_d} \right] \& \left[\frac{m}{f_d} < \tau_2 < \frac{(m+1)}{f_d} \right] \quad \text{case (3)} \end{aligned}$$

When the transmit joining point occurs in the 1st or 2nd quadrant the general terms for the angles of signal vectors are

$$\angle P_{Tx} = -\pi + \pi\tau_1 f_d + n\pi \quad \text{Eq. 7-27}$$

$$\angle Q_{Tx} = \pi + \pi\tau_2 f_d - m\pi \quad \text{Eq. 7-28}$$

where $m, n = 0, 1, 2, \dots$

Then the delay constraints are

$$\Rightarrow \left[\tau_2 - \frac{(n+m+1)}{f_d} > \tau_1 > -\frac{(n+1)}{f_d} \right] \& \left[\frac{m}{f_d} < \tau_2 < \frac{(m+1)}{f_d} \right] \quad \text{case (4)}$$

These four cases are listed in Table C-1 in Appendix C.

7.5 Derivation of Conditions for $|P_{Tx}| \leq 1$ and $|Q_{Tx}| \leq 1$

If vector attenuators are used, the magnitudes of h_1 and h_2 should be less than 1. Hence the magnitude values of P_{Tx} , Q_{Tx} , P_{Rx} and Q_{Rx} should be equal or less than 1. The conditions $|P_{Tx}| \leq 1$ and $|Q_{Tx}| \leq 1$ are satisfied when the transmit joining point of the vectors P_{Tx} and Q_{Tx} is on or inside the AOC triangle or the AOX portion of the circle or the ACY portion of the circle (Figure 7-6). This puts further constraints on the relationships between the delays and the duplexing frequency.

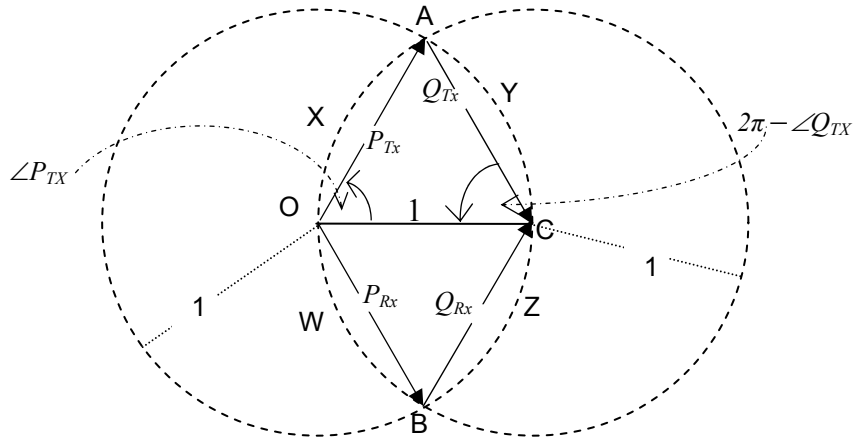


Figure 7-6 Cancellation signals when $|P_{Tx}| \leq 1$ and $|Q_{Tx}| \leq 1$ and the joining point of the vectors lies in 1st or 2nd quadrant (case (1)).

7.5.1 $\tau_1 > 0$ and $\tau_2 > 0$

When $\tau_1 > 0$, $\tau_2 > 0$ and for case (1), the transmit joining point lies in the 1st or 2nd quadrant. The angle of P_{Tx} and the angle of $(2\pi - \angle Q_{Tx})$ should be between $\pi/3$ and zero when the vectors P_{Tx} and Q_{Tx} are inside the vector triangle AOC (Figure 7-6).

Therefore, using Eq. 7-15 for $\angle P_{Tx}$ and Eq. 7-18 for $\angle Q_{Tx}$,

$$0 \leq (\angle P_{Tx}) \leq \frac{\pi}{3} \Rightarrow 0 \leq (\pi\tau_1 f_d - n\pi) \leq \frac{\pi}{3} \quad \text{and}$$

$$0 \leq \angle(2\pi - \angle Q_{Tx}) \leq \frac{\pi}{3} \Rightarrow 0 \leq 2\pi - (\pi + \pi\tau_2 f_d - m\pi) \leq \frac{\pi}{3} \quad \text{giving}$$

$$\left[\frac{n}{f_d} \leq \tau_1 \leq \frac{1}{3f_d} + \frac{n}{f_d} \right] \& \left[\frac{m}{f_d} + \frac{2}{3f_d} \leq \tau_2 \leq \frac{1}{f_d} + \frac{m}{f_d} \right] \quad \text{condition (1a)}$$

When the transmit joining point of the vectors P_{Tx} and Q_{Tx} is on the AXO arc of the circle, the vector triangle is an isosceles triangle and then

$$(2\angle P_{Tx} + 2\pi - \angle Q_{Tx}) = \pi$$

$$2(\pi\tau_1 f_d - n\pi) + 2\pi - (\pi + \pi\tau_2 f_d - m\pi) = \pi$$

Therefore when the vectors P_{Tx} and Q_{Tx} are on or inside the AOX portion of the circle, the following conditions apply

$$[(2\angle P_{Tx} + 2\pi - \angle Q_{Tx}) \leq \pi] \& \left[0 \leq (2\pi - \angle Q_{Tx}) \leq \frac{\pi}{3} \right] \& \left[\frac{\pi}{3} \leq \angle P_{Tx} \leq \frac{\pi}{2} \right] \quad \text{giving}$$

$$\left[\tau_1 \leq \frac{\tau_2}{2} + \frac{n}{2f_d} - \frac{m}{2f_d} \right] \& \left[\frac{m}{f_d} + \frac{2}{3f_d} \leq \tau_2 \leq \frac{1}{f_d} + \frac{m}{f_d} \right] \& \left[\frac{n}{f_d} + \frac{1}{3f_d} \leq \tau_1 \leq \frac{1}{2f_d} + \frac{n}{f_d} \right] \quad \text{condition (1b)}$$

Similarly when the vectors P_{Tx} and Q_{Tx} are on or inside the ACY portion of the circle we get

$$[(2(2\pi - \angle Q_{Tx}) + \angle P_{Tx}) \leq \pi] \& \left[0 \leq \angle P_{Tx} \leq \frac{\pi}{3} \right] \& \left[\frac{\pi}{3} \leq (2\pi - \angle Q_{Tx}) \leq \frac{\pi}{2} \right] \quad \text{giving}$$

$$\left[\tau_1 \leq 2\tau_2 - \frac{1}{f_d} - \frac{2m}{f_d} + \frac{n}{f_d} \right] \& \left[\frac{n}{f_d} \leq \tau_1 \leq \frac{1}{3f_d} + \frac{n}{f_d} \right] \& \left[\frac{m}{f_d} + \frac{2}{3f_d} \geq \tau_2 \geq \frac{1}{2f_d} + \frac{m}{f_d} \right] \quad \text{condition (1c)}$$

Now repeating the analysis for case (2), the transmit joining point in the 3rd or 4th quadrant, we get three more conditions. Note in this case the angles should be considered as according to Figure 7-7, Eq. 7-21 & Eq. 7-22.

If the vectors P_{Tx} and Q_{Tx} are on or inside the AOC triangle, the AOX portion or the ACY portion then conditions (2a), (2b) or (2c) should be satisfied respectively.

$$\left[\frac{n}{f_d} + \frac{2}{3f_d} \leq \tau_1 \leq \frac{1}{f_d} + \frac{n}{f_d} \right] \& \left[\frac{m}{f_d} \leq \tau_2 \leq \frac{1}{3f_d} + \frac{m}{f_d} \right] \quad \text{condition (2a)}$$

$$\left[2\tau_1 \geq \tau_2 + \frac{1}{f_d} - \frac{m}{f_d} + \frac{n}{f_d} \right] \& \left[\frac{n}{f_d} + \frac{1}{2f_d} \leq \tau_1 \leq \frac{2}{3f_d} + \frac{n}{f_d} \right] \& \left[\frac{m}{f_d} \leq \tau_2 \leq \frac{1}{3f_d} + \frac{m}{f_d} \right] \quad \text{condition (2b)}$$

$$\left[\tau_1 \geq 2\tau_2 - \frac{2m}{f_d} + \frac{n}{f_d} \right] \& \left[\frac{n}{f_d} + \frac{2}{3f_d} \leq \tau_1 \leq \frac{1}{f_d} + \frac{n}{f_d} \right] \& \left[\frac{m}{f_d} + \frac{1}{3f_d} \leq \tau_2 \leq \frac{1}{2f_d} + \frac{m}{f_d} \right] \quad \text{condition (2c)}$$

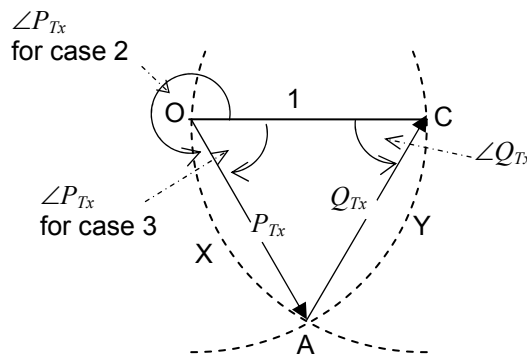


Figure 7-7 Cancellation signals when $|P_{Tx}| \leq 1$ and $|Q_{Tx}| \leq 1$ and the joining point of the vectors lies in the 3rd or 4th quadrant (case 2).

7.5.2 $\tau_1 < 0$ and $\tau_2 > 0$

When $\tau_1 < 0$ and $\tau_2 > 0$ and for case (3), the transmit joining point of the vectors lies in the 3rd or 4th quadrant. The angle of P_{Tx} should be between $-\pi/3$ and zero and the angle of Q_{Tx} should be between zero and $\pi/3$ when the vectors P_{Tx} and Q_{Tx} are inside their vector triangle AOC (Figure 7-7).

Therefore, using Eq. 7-23 and Eq. 7-24

$$0 \geq (\angle P_{Tx}) \geq -\frac{\pi}{3} \Rightarrow 0 \geq (\pi\tau_1 f_d + n\pi) \geq -\frac{\pi}{3}$$

and

$$0 \leq (\angle Q_{Tx}) \leq \frac{\pi}{3} \Rightarrow 0 \leq (\pi\tau_2 f_d - m\pi) \leq \frac{\pi}{3}$$

For negative values of τ_1 and positive values of τ_2 , with the transmit joining point on or inside the AOC triangle, the above conditions must be satisfied. i.e.

$$\Rightarrow \left[-\frac{n}{f_d} \geq \tau_1 \geq -\frac{1}{3f_d} - \frac{n}{f_d} \right] \& \left[\frac{m}{f_d} \leq \tau_2 \leq \frac{1}{3f_d} + \frac{m}{f_d} \right] \quad \text{condition (3a)}$$

Similarly for the transmit joining point on or inside the AOX portion of the circle the following condition should be satisfied.

$$\left[(2|\angle P_{Tx}| + \angle Q_{Tx}) \leq \pi \right] \& \left[0 \leq (\angle Q_{Tx}) \leq \frac{\pi}{3} \right] \& \left[-\frac{\pi}{2} \leq \angle P_{Tx} \leq -\frac{\pi}{3} \right] \quad \text{giving}$$

$$\left[\tau_1 \geq -\frac{1}{2f_d} + \frac{\tau_2}{2} - \frac{m}{2f_d} - \frac{n}{f_d} \right] \& \left[\frac{m}{f_d} \leq \tau_2 \leq \frac{1}{3f_d} + \frac{m}{f_d} \right] \& \left[-\frac{1}{2f_d} - \frac{n}{f_d} \leq \tau_1 \leq -\frac{1}{3f_d} - \frac{n}{f_d} \right] \quad \text{condition (3b)}$$

For the transmit joining point to be on or inside the ACY portion of the circle, we get

$$\left[(2\angle Q_{Tx} + |\angle P_{Tx}|) \leq \pi \right] \& \left[0 \geq (\angle P_{Tx}) \geq -\frac{\pi}{3} \right] \& \left[\frac{\pi}{3} \leq \angle Q_{Tx} \leq \frac{\pi}{2} \right] \quad \text{giving}$$

$$\left[\tau_1 \geq 2\tau_2 - \frac{1}{f_d} - \frac{2m}{f_d} - \frac{n}{f_d} \right] \& \left[-\frac{n}{f_d} \geq \tau_1 \geq -\frac{1}{3f_d} - \frac{n}{f_d} \right] \& \left[\frac{m}{f_d} + \frac{1}{3f_d} \leq \tau_2 \leq \frac{1}{2f_d} + \frac{m}{f_d} \right]$$

condition (3c)

Literally, it can be shown for case (4), the following three conditions should be satisfied. Note here the angles should be considered as according to Eq. 7-27 & Eq. 7-28.

$$\Rightarrow \left[-\frac{n}{f_d} - \frac{1}{f_d} \leq \tau_1 \leq \frac{2}{3f_d} - \frac{n}{f_d} \right] \& \left[\frac{m}{f_d} + \frac{2}{3f_d} \leq \tau_2 \leq \frac{1}{f_d} + \frac{m}{f_d} \right]$$

condition (4a)

$$\Rightarrow \left[\tau_1 \leq \frac{\tau_2}{2} - \frac{1}{f_d} - \frac{m}{2f_d} - \frac{n}{f_d} \right] \& \left[-\frac{n}{f_d} - \frac{2}{3f_d} \leq \tau_1 \leq -\frac{1}{2f_d} - \frac{n}{f_d} \right] \& \left[\frac{m}{f_d} + \frac{2}{3f_d} \leq \tau_2 \leq \frac{1}{f_d} + \frac{m}{f_d} \right]$$

condition (4b)

$$\Rightarrow \left[\tau_1 \leq 2\tau_2 - \frac{2}{f_d} - \frac{2m}{f_d} - \frac{n}{f_d} \right] \& \left[-\frac{n}{f_d} - \frac{1}{f_d} \leq \tau_1 \leq -\frac{2}{3f_d} - \frac{n}{f_d} \right] \& \left[\frac{m}{f_d} + \frac{1}{2f_d} \leq \tau_2 \leq \frac{2}{3f_d} + \frac{m}{f_d} \right]$$

condition (4c)

It is interesting to note that all the previous constraints conditions for the delay differences τ_1 and τ_2 are in terms of $1/f_d$. It is therefore possible to generalise these conditions by using the normalised delay values of $\tau_1 f_d$ and $\tau_2 f_d$ instead of the absolute values τ_1 and τ_2 . The results are then independent of the duplexing frequency.

The shaded zones in Figure 7-8 show the normalised path delay requirements for $|h_1| \leq 1$ and $|h_2| \leq 1$ when any one of the conditions (1a), (1b), (1c), (2a), (2b), (2c), (3a), (3b), (3c), (4a), (4b), (4c) for the four cases are met. This plot follows a general pattern and repeats with a period set by the reciprocal of the duplexing frequency (i.e. every 180° of angle P_{Tx} or Q_{Tx}). Negative values for path₂ delay differences are not shown because of the symmetry. Also plotted are contours of

coefficient gain, for the larger of the two coefficients ($\max(|h_1|, |h_2|)$) for different normalised delay differences ($f_d\tau_1$ and $f_d\tau_2$).

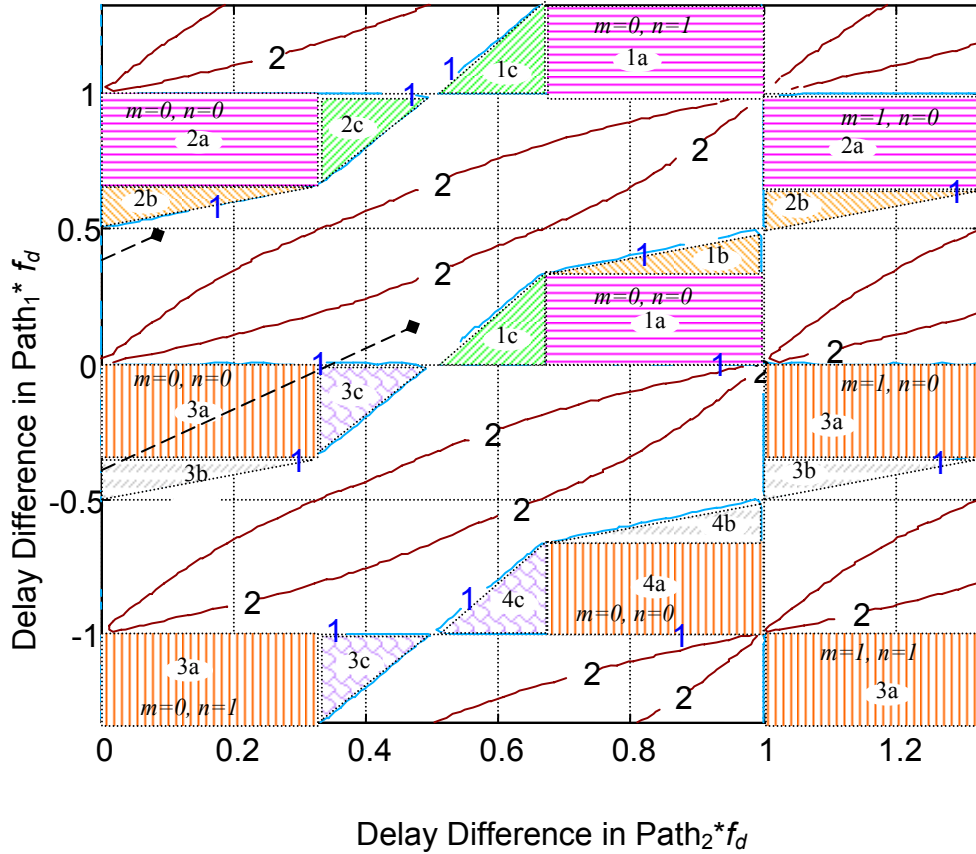


Figure 7-8 Contours of maximum ($|h_1|$ or $|h_2|$) for various delay differences, $\tau_1 f_d$ and $\tau_2 f_d$, in path₁ and path₂ (note the normalisation by f_d). The shaded areas show the conditions for coefficient gains less than unity.

The contours are numerically evaluated from the original set of equations (Eq. 7-3 and Eq. 7-4 with $g = 1$, $S_x = 1$) by solving for h_1 and h_2 over all delay combinations. The $|h| = 1$ contour follows a series of straight lines as predicted, while the contour $|h| = 2$ is curved. Increasing the allowable dynamic range of the coefficient allows the system to work over a greater range of path delays. Relaxing the gain requirement on the cancellation loops to values greater than 2 will only gain a small additional benefit in possible τ_1 , τ_2 adjustment range. The

magnitudes of h_1 and h_2 become very large when $\tau_1 = \tau_2 \pm k/f_d$ ($k = 0, 1, 2, \dots$). These delay contributions should be avoided. Dynamic range is not the only constraint determining the delays. Cancellation bandwidth also needs to be considered and this is considered in the next section.

7.6 The Relationship Between the Bandwidth and the Achievable Cancellation Level

The previous section derived the conditions for delay and coefficient gains for generating nulls at f_{Tx} and f_{Rx} ; but it did not consider the bandwidth of these nulls. The required null bandwidth and cancellation level places further constraints on the delay differences, τ_1 and τ_2 .

The residual signal after cancellation can be expressed as

$$C = 1 - (P_x + Q_x) \quad \text{Eq. 7-29}$$

and the amount of cancellation (magnitude of the residual signal) can be found from

$$\begin{aligned} |C|^2 &= \left(|h_1| \cos(\angle P_x) + |h_2| \cos(\angle Q_x) - 1 \right)^2 + \left(|h_1| \sin(\angle P_x) + |h_2| \sin(\angle Q_x) \right)^2 \\ &= |h_1|^2 + |h_2|^2 + 1 + 2|h_1||h_2| \cos(\angle P_x - \angle Q_x) - 2|h_1| \cos(\angle P_x) - 2|h_2| \cos(\angle Q_x) \end{aligned} \quad \text{Eq. 7-30}$$

Let the frequency be $f_{x1} = f_{Tx} - f\delta_1$, where $f\delta_1$ is a frequency deviation with respect to f_{Tx} (or f_{Rx}). Then the two cancellation signals at f_{x1} will be

$$P_{x1} = h_1 \cdot e^{-j2\pi\tau_1(f_{Tx} - f\delta_1)} \quad \text{Eq. 7-31}$$

$$Q_{x1} = h_1 \cdot e^{-j2\pi\tau_2(f_{Tx} - f\delta_1)} \quad \text{Eq. 7-32}$$

and the angles of P_{x1} and Q_{x1} can be expressed in terms of τ_1 , τ_2 and f_d . For example the angles of P_{x1} and Q_{x1} are expressed as $\pi\tau_1(f_d + 2f\delta_1)$ and $\pi + \pi\tau_2(f_d + 2f\delta_1)$ respectively for the condition ($\tau_2 > \tau_1 > 0$). This cancellation is geometrically shown in Figure 7-9. Point A represents the null at the Tx frequency. As the frequency f_{x1} changes, the resultant signal C moves in a symmetrical locus around the frequency $(f_{Tx} + f_{Rx})/2$. The points E and F correspond to two different frequencies ($f_{Tx} + f\delta_1$, $f_{Tx} - f\delta_2$), which straddle the Tx null frequency. Note that the angles of these cancellation signals are different with respect to the P_{Tx} angle. This results in non-symmetrical frequency response around the Tx null frequency. This behaviour is the same around the Rx null frequency and points G and H correspond to two different frequencies, which straddle the Rx null frequency. The four frequencies correspond to the points E, F, G, H (Figure 7-9), give the same cancellation level $|C_d|$ and are shown in Figure 7-10.

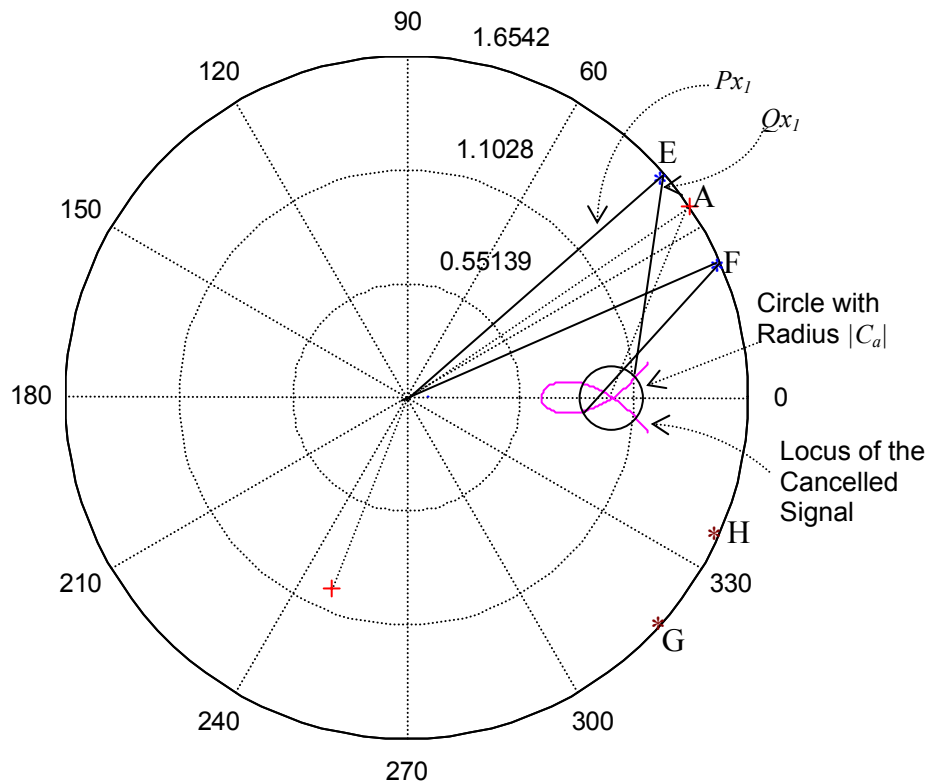


Figure 7-9 Geometrical illustration of the achievable cancellation when the frequency deviates from the null frequencies.

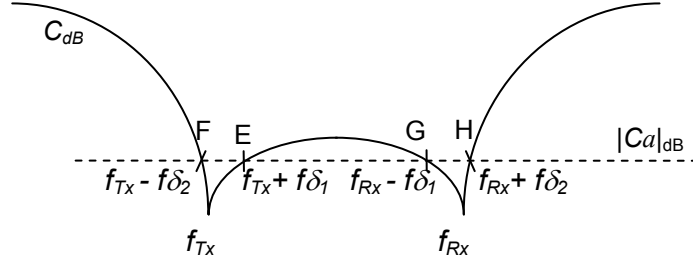


Figure 7-10 The behaviour of the frequency response. Points E, F, G, H, show the band edges for a cancellation level of $|Ca|$.

Eq. 7-30 can be expressed as a function of $f\delta$

$$|C|^2 = f(f\delta) = |h_1|^2 + |h_2|^2 + 1 + 2|h_1||h_2|(\pi(\tau_1 - \tau_2))\cos[\pi(\tau_1 - \tau_2)(f_d + 2f\delta)] \\ + 2|h_1|(\pi\tau_1)\cos[\pi\tau_1(f_d + 2f\delta)] + 2|h_2|(\pi\tau_2)\cos[\pi\tau_2(f_d + 2f\delta)]$$

Eq. 7-33

This is an expression in terms of τ_1 , τ_2 , f_d and $f\delta$ since h_1 and h_2 are a function of τ_1 , τ_2 and f_d as shown below. When perfect cancellation ($|C| = 0$) occurs at the null frequencies,

$$|h_1|\cos(\angle P_{Tx}) + |h_2|\cos(\angle Q_{Tx}) = 1 \quad \text{Eq. 7-34}$$

$$|h_1|\sin(\angle P_{Tx}) = -|h_2|\sin(\angle Q_{Tx}) \quad \text{Eq. 7-35}$$

By solving the above two equations (Eq. 7-34 & Eq. 7-35) the magnitudes of h_1 and h_2 can be expressed as a function of the signal vector angles.

$$|h_1| = 1 / \left[\cos(\angle P_{Tx}) - \frac{\sin(\angle P_{Tx})}{\tan(\angle Q_{Tx})} \right] = \frac{\sin(\angle Q_{Tx})}{\sin(\angle Q_{Tx} - \angle P_{Tx})}$$

$$|h_2| = 1 / \left[\cos(\angle Q_{Tx}) - \frac{\sin(\angle Q_{Tx})}{\tan(\angle P_{Tx})} \right] = \frac{\sin(\angle P_{Tx})}{\sin(\angle P_{Tx} - \angle Q_{Tx})}$$

A general formula for h_1 and h_2 that would cover all four delay cases can be expressed as

$$|h_1| = -n_1 \cdot \frac{\sin(\angle \pi \tau_2 f_d)}{\sin(\angle \pi (\tau_1 - \tau_2) f_d)} \quad \text{Eq. 7-36}$$

$$|h_2| = n_2 \cdot \frac{\sin(\angle \pi \tau_1 f_d)}{\sin(\angle \pi (\tau_1 - \tau_2) f_d)} \quad \text{Eq. 7-37}$$

n_1 and n_2 are sign terms and these are shown in Table 7-1 for the four delay cases.

Table 7-1 n_1 and n_2 for different cases

	Case 1	Case 2	Case 3	Case 4
n_1	1	-1	1	-1
n_2	-1	1	1	-1

The linear approximation of the residual signal power as a function of $f\delta$ can be found using the Taylor polynomial;

$$f(f\delta) = |C|^2 = f(0) + f'(0) \cdot (f\delta) + \frac{f''(0)}{2} \cdot (f\delta)^2 + \dots \quad \text{Eq. 7-38}$$

For simplicity we consider the first and second order derivative terms only. The general coefficients in the Eq. 7-38 are

$$f(0) = 0 \quad (\because \text{resultant at a null frequency is zero.})$$

$$f'(0) = -2^2 l_1 |h_1| \cdot |h_2| (\pi (\tau_1 - \tau_2)) \cdot \sin[\pi (\tau_1 - \tau_2) f_d] + 2^2 l_2 |h_1| (\pi \tau_1) \sin[\pi \tau_1 f_d] \\ + 2^2 l_3 |h_2| (\pi \tau_2) \sin[\pi \tau_2 f_d]$$

$$f''(0) = -l_1 2^3 |h_1| \cdot |h_2| (\pi (\tau_1 - \tau_2))^2 \cdot \cos[\pi (\tau_1 - \tau_2) f_d] + 2^3 l_2 |h_1| (\pi \tau_1)^2 \cdot \cos[\pi \tau_1 f_d] \\ + 2^3 l_3 |h_2| (\pi \tau_2)^2 \cdot \cos[\pi \tau_2 f_d]$$

where l_1 , l_2 and l_3 are sign terms given by Table 7-2.

Table 7-2 l_1, l_2 and l_3 for different cases

	Case 1	Case 2	Case 3	Case 4
l_1	-1	-1	1	1
l_2	1	-1	1	-1
l_3	-1	1	1	-1

By substituting for $|h_1|$ (in Eq. 7-36), $|h_2|$ (in Eq. 7-37) and using trigonometric identities $f'(0)$ can be simplified as

$$f'(0) = \frac{4 \cdot \sin(\pi\tau_1 f_d) \cdot \sin(\pi\tau_2 f_d)}{\sin(\pi(\tau_1 - \tau_2) f_d)} [l_1 \cdot n_1 \cdot n_2 \pi(\tau_1 - \tau_2) - l_2 n_1 \pi \tau_1 + l_3 n_2 \pi \tau_2] \quad \text{Eq. 7-39}$$

The $l_1 n_1 n_2$, $l_2 n_1$ and $l_3 n_2$ coefficient terms are all +1 for all four cases. Therefore the $f'(0)$ term also equals zero, leaving

$$|C|^2 = 0.5 \cdot f''(0) \cdot (f\delta)^2 \quad \text{Eq. 7-40}$$

By substituting for $|h_1|$ (in Eq. 7-36), $|h_2|$ (in Eq. 7-37) and using trigonometric identities; $f''(0)$ can be simplified to

$$f''(0) = \frac{\left[\pi^2 \tau_1 \tau_2 \left[-8 \cos^2(\pi \cdot f_d (\tau_1 - \tau_2)) + 4 \cos(2\pi\tau_1 f_d) + 4 \cos(2\pi\tau_2 f_d) \right] + 8(\pi\tau_1)^2 \sin^2(\pi\tau_2 f_d) + 8(\pi\tau_2)^2 \sin^2(\pi\tau_1 f_d) \right]}{\sin^2(\pi \cdot f_d (\tau_1 - \tau_2))} \quad \text{Eq. 7-41}$$

Here also all the coefficient terms are 1 as in $f'(0)$ and this has been included in the equation.

The approximation to the cancellation bandwidth B is considered as $2f\delta$ because the difference between $f\delta_1$ and $f\delta_2$ is small when operating under the condition of the Taylor expression. Therefore (Eq. 7-40) can be re-written as

$$|C|^2 = 0.125 f''(0) \cdot (B)^2 \quad \text{Eq. 7-42}$$

which, gives the relationship between the bandwidth and the achievable cancellation level.

$$|C|^2 = \left[\frac{\pi^2 \cdot B^2}{\sin^2(\pi \cdot f_d (\tau_1 - \tau_2))} \right] \left[\tau_1 \tau_2 \left[-\cos^2(\pi \cdot f_d (\tau_1 - \tau_2)) + 0.5 \cos(2\pi \tau_1 f_d) + 0.5 \cos(2\pi \tau_2 f_d) \right] + \tau_1^2 \sin^2(\pi \tau_2 f_d) + \tau_2^2 \sin^2(\pi \tau_1 f_d) \right] \quad \text{Eq. 7-43}$$

Contour plots illustrating effects of delays on different bandwidths using Eq. 7-43 are shown in Figure 7-11. The axes and curves are normalised by the Doppler frequency, which is justified later. When $f_d = 190\text{MHz}$, the curves correspond to bandwidths of 40MHz, 20MHz, 10MHz, 5MHz, and 2MHz (left to right). Note the numerical instability caused by the denominator when $\tau_1 = \tau_2$. This condition also results in large coefficient values (see Figure 7-8) and therefore should be avoided.

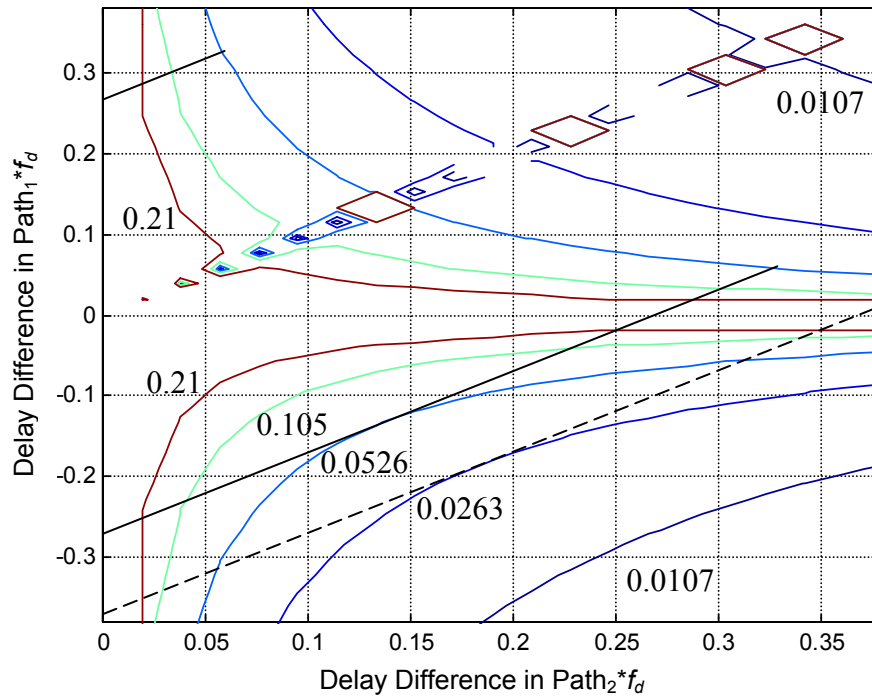


Figure 7-11 Effects of (normalised) delays, $\tau_1 f_d$ and $\tau_2 f_d$, on different (normalised) cancellation bandwidths, B/f_d , for a fixed cancellation level of $|Ca|^2 = -40\text{dB}$ (using Eq. 7-43). The curves are undefined when $\tau_1 = \tau_2$.

Figure 7-11 shows that delay differences close to zero in either of the paths results in a wide bandwidth. When $\tau_1 = 0$ or $\tau_2 = 0$, there is a possibility of infinite

bandwidth and perfect cancellation. Only one of the two loops is then required (i.e. $h_2 = 0$ when $\tau_1 = 0$ (Figure D-2 in Appendix D) and $h_1 = 0$ when $\tau_2 = 0$ (Figure D-1 in Appendix D)). The scheme then operates as per Section 6.8.

However, for maximum robustness, the fixed path delays, τ_b and τ_c , must be chosen to allow the largest possible variation in the effective delay, τ_a , of the leakage path, while still meeting the requisite bandwidth, cancellation and dynamic range requirements. This is achieved by choosing τ_b and τ_c to span the expected range variation of τ_a , or ($\tau_b < \tau_a < \tau_c$). Using T_s to represent the span,

$$T_s = \tau_c - \tau_b$$

$$f_d T_s = f_d \tau_2 - f_d \tau_1 \tag{Eq. 7-44}$$

Note, t ($\equiv f_d T_s$) is a constant and is not affected by antenna loading and other variations in the leakage path, which cause τ_a , τ_1 and τ_2 to alter. It is a design choice that determines the trade off between bandwidth and robustness.

Eq. 7-44 represents a straight line on Figure 7-11 with a slope of +1. In this example T_s is chosen to give a minimum normalised bandwidth of 0.0526 (10MHz at $f_d = 190$ MHz), resulting in $f_d \tau_1 = f_d \tau_2 - 0.27$ ($t = 0.27$) which is asymptotic to the bandwidth contour when $-\tau_1 = \tau_2$. The line meets the bandwidth requirements when $0.325 > f_d \tau_2 > -0.058$ giving a maximum possible delay variation in the leakage path of $\Delta\tau_a = 0.383/f_d$ (± 1.0 ns at $f_d = 190$ MHz). Note, the line wraps to the top left hand corner of the diagram for negative τ_2 because of the symmetry between quadrant 1 and quadrant 3 (also quadrant 2 and quadrant 4). Halving the bandwidth requirements to 0.0263 (5MHz at $f_d = 190$ MHz), gives the dotted line ($t = 0.385$), and an improved tolerance to delay variation of $0.536/f_d$ (± 1.4 ns at $f_d = 190$ MHz). (The intersection points with the 0.0263 curve are off the figure.) This is an increase of 40% and indicates an improved performance for narrow band systems.

The dotted line in Figure 7-11 representing 0.0263 normalised bandwidth (5MHz @ $f_d = 190\text{MHz}$) is plotted on Figure 7-8. The range $-0.076 < f_d \tau_2 < 0.46$ on the line represents the operating conditions to meet the bandwidth constraints. However not all the line meets the less than unity gain constraints of the vector attenuators since the line extremities are outside of the shaded areas. The range over which the unity gain and bandwidth conditions are met is now $0 < f_d \tau_2 < 0.38$ restricting the robustness to leakage path delay variations.

Allowing a small gain increase in the cancellation paths will return the full robustness since the dotted line does not penetrate far beyond the unity gain boundary.

Eq. 7-43 is still not very insightful and the operation in the $\tau_1 = \tau_2$ region must be clarified, so further simplification is considered. Removing the $\tau_1 - \tau_2$ term, halving the $2\pi f_d$ terms and normalising the bandwidth, B, gives

$$|C|^2 = \left[\frac{\pi^2 \left(\frac{B}{f_d} \right)^2 f_d^2}{\sin^2(\pi f_d (\tau_1 - \tau_2))} \right] \left[\tau_1 \tau_2 \left[1 - \sin^2(\pi \tau_1 f_d) - \sin^2(\pi \tau_2 f_d) - \left(\frac{\cos(\pi f_d \tau_1) \cos(\pi f_d \tau_2)}{+ \sin(\pi f_d \tau_1) \sin(\pi f_d \tau_2)} \right)^2 \right] + \tau_1^2 \sin^2(\pi f_d \tau_2) + \tau_2^2 \sin^2(\pi f_d \tau_1) \right]$$

Eq. 7-45

Expanding the squared term, collecting like terms and taking out the common term from the brackets gives

$$|C|^2 = \left[\frac{\pi^2 \left(\frac{B}{f_d} \right)^2 f_d^2}{\sin^2(\pi f_d (\tau_1 - \tau_2))} \right] \left[-\tau_1 \tau_2 [2 \sin(\pi f_d \tau_1) \sin(\pi f_d \tau_2) \cos(\pi f_d (\tau_1 - \tau_2))] + \tau_1^2 \sin^2(\pi f_d \tau_2) + \tau_2^2 \sin^2(\pi f_d \tau_1) \right]$$

Eq. 7-46

Completing the square produces

$$|C|^2 = \left[\frac{\pi^2 \left(\frac{B}{f_d} \right)^2 f_d^2}{\sin^2(\pi f_d (\tau_1 - \tau_2))} \left[+ \tau_1 \tau_2 [2 \sin(\pi f_d \tau_1) \sin(\pi f_d \tau_2) (1 - \cos(\pi f_d (\tau_1 - \tau_2)))] \right] \right. \\ \left. + (\tau_1 \sin(\pi f_d \tau_2) - \tau_2 \sin(\pi f_d \tau_1))^2 \right]$$

Eq. 7-47

Noting that $\cos \theta = 1 - 2 \sin^2(\theta/2)$ and dividing through gives two terms

$$|C|^2 = \left[\pi^2 \left(\frac{B}{f_d} \right)^2 f_d^2 \right. \\ \left. + \tau_1 \tau_2 \left[4 \frac{\sin(\pi f_d \tau_1) \sin(\pi f_d \tau_2)}{\sin^2(\pi f_d (\tau_1 - \tau_2))} \left(\sin^2 \left(\pi f_d \left(\frac{\tau_1 - \tau_2}{2} \right) \right) \right) \right] \right] \\ \left. + \frac{(\tau_1 \sin(\pi f_d \tau_2) - \tau_2 \sin(\pi f_d \tau_1))^2}{\sin^2(\pi f_d (\tau_1 - \tau_2))} \right]$$

Eq. 7-48

First we make the assumption that all angles are small, ie $\pi f_d \tau_1$ and $\pi f_d \tau_2$ are small. This is normally the case for most practical situations. We now consider two situations τ_1 not equal to τ_2 and τ_1 (almost) equal to τ_2 .

7.6.1 τ_1 Not Equal to τ_2

Note the second term goes to zero leaving only the first term

$$|C|^2 = \pi^4 \left(\frac{B}{f_d} \right)^2 f_d^4 \tau_1^2 \tau_2^2 \quad \text{Eq. 7-49}$$

The equation shows that cancellation improves (residual signal power, $|C|^2$, reduced) when either of the delay difference paths, τ_1 or τ_2 is reduced. Infinite cancellation ($C = 0$) is possible over infinite bandwidth when either of the delay differences go to zero. It should also be noted that the residual signal power is proportional to f_d^2 . This makes it approximately 16 times easier to achieve the required isolation with $f_d = 45\text{MHz}$ systems (e.g. IS-95) compared to $f_d = 190\text{MHz}$ (e.g. CDMA2000).

It is possible to rewrite the equation to show the normalisations of the delays with πf_d , and the normalisations of the bandwidth with $1/f_d$.

$$\pm \frac{|C|}{\left(\frac{B}{f_d}\right) \pi f_d \tau_2} = \pi f_d \tau_1 \quad \text{Eq. 7-50}$$

The inverse relationship between τ_1 and τ_2 for constant bandwidth and residual signal level is clearly shown in the graphs of Figure 7-11, with positive and negative values of τ_1 being almost the same for a given τ_2 .

The equation also shows a linear relationship between bandwidth and the residual signal level $|C|$. For example if the cancellation null is to be further reduced by 6dB (amplitude halved), then the band width of the null also halves.

7.6.2 τ_1 (Almost) Equal to τ_2

This is an interesting case. The first term is not effected and has the same value as shown above, but now the denominator of the second term goes to zero and the simple $\sin(x) = x$ approximation for the numerator cannot be used, because neglected terms now contribute. Substituting $\tau_2 = \tau_1 + \delta$, the second term of Eq. 7-48 becomes

$$\frac{(\tau_1 \sin(\pi f_d \tau_2) - \tau_2 \sin(\pi f_d \tau_1))^2}{\sin^2(\pi f_d (\tau_1 - \tau_2))} \approx \frac{(\tau_1 \sin(\pi f_d (\tau_1 + \delta)) - (\tau_1 + \delta) \sin(\pi f_d \tau_1))^2}{\sin^2(\pi f_d \delta)} \quad \text{Eq. 7-51}$$

Expanding the numerator and noting δ is very small gives

$$\approx \left[\frac{\tau_1 \cos(\pi f_d \tau_1) (\pi f_d \delta) - (\delta) \sin(\pi f_d \tau_1)}{(\pi f_d (\delta))} \right]^2 = \left[\tau_1 \cos(\pi f_d \tau_1) - \frac{\sin(\pi f_d \tau_1)}{\pi f_d} \right]^2 \quad \text{Eq. 7-52}$$

We note that this is not a large number. When combined with the first term and assuming small angles we get:

$$|C|^2 = \left(\frac{B}{f_d}\right)^2 \left[(\pi f_d \tau_1)^4 - 0.25(\pi f_d \tau_1)^6 \right] \quad \text{Eq. 7-53}$$

The last term is the extra component caused by small δ . The small angle assumption means that this term is negligible. We therefore conclude that the inverse relationship between τ_1 and τ_2 holds even as τ_1 approaches τ_2 . This is not the case as the angles get larger. Figure 7-12 shows the original Eq. 7-43 marked +, and the simplified Eq. 7-50 for $f_d = 190\text{MHz}$. The divergence is small for time delays less than 1ns (equivalent to an angle of $\pi f_d \tau_1 = 0.6$ radians). Note, the instability in Eq. 7-43 was avoided by not calculating the points where $\tau_1 = \tau_2$.

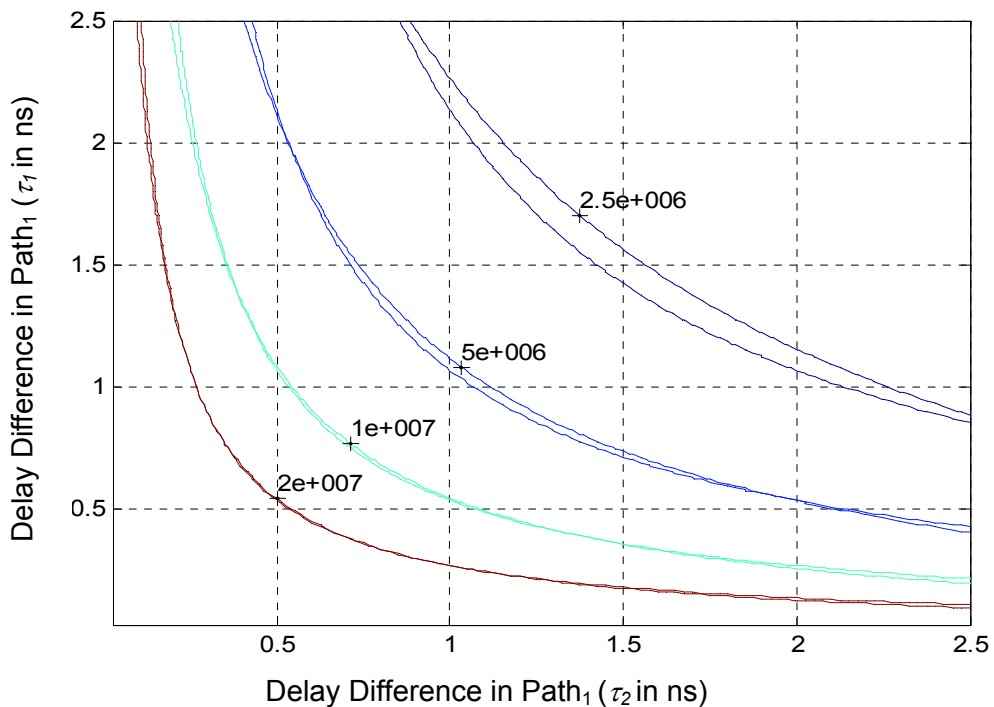


Figure 7-12 Bandwidth contours vs τ_1 and τ_2 when $f_d = 190\text{MHz}$ and the cancellation level is $< -40\text{dB}$. The simplified Eq. 7-50 and the original Eq. 7-43 (marked +). Only the first quadrant is shown.

This concludes the static analysis of the adaptive canceller. The next section will consider the practical issue of adapting the coefficients h_1 and h_2 to give the desired cancellation of the leakage transmitter signal.

7.7 The Proposed Algorithm

This section will show how two error signals can be utilised to form a cost function for the adaptive adjustment of the coefficients, h_1 and h_2 .

A pilot (refer Figure 5-1) is placed in the guard band between adjacent Rx channels (Figure 7-13). It is extracted using a BPF from the baseband output from the DCR. The magnitude of the pilot is used for the e_2 error signal. The magnitude of the Tx leakage signal is used for the e_1 error signal. A BPF at the duplex frequency extracts this signal immediately after the down conversion mixer in the DCR.

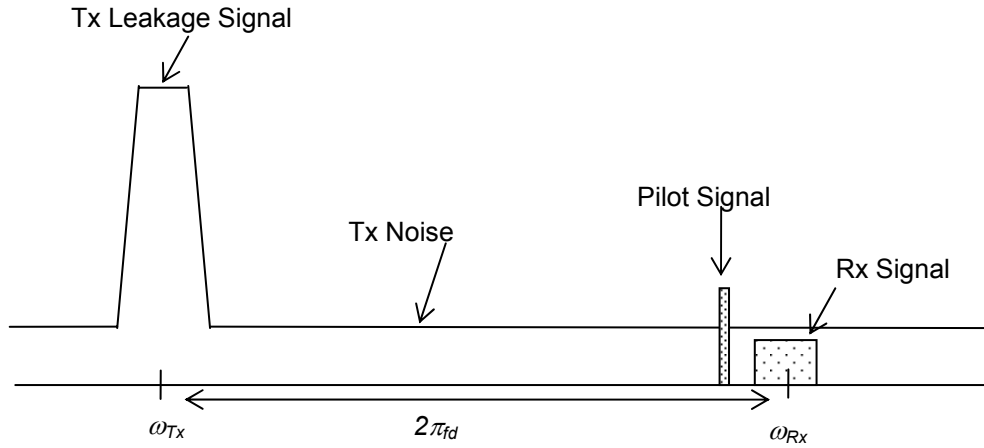


Figure 7-13 Spectrum at LNA input (with the cancellation loop inactivated).

In the double loop cancellation configuration (Figure 7-1) the residual signal is as in Eq. 7-2,

$$Out = S_x (g - h_1 e^{-j\omega_{Tx}\tau_1} - h_2 e^{-j\omega_{Tx}\tau_2})$$

This residual signal should be minimised at $f_{Tx} (\omega_{Tx})$ and $f_{Rx} (\omega_{Rx})$.

Then the two error signals, e_1 and e_2 are

$$e_1 = S_x (g - h_1 e^{-j\omega_{Tx}\tau_1} - h_2 e^{-j\omega_{Tx}\tau_2}) \quad Eq. 7-54$$

$$e_2 = S_x (g - h_1 e^{-j\omega_{Rx}\tau_1} - h_2 e^{-j\omega_{Rx}\tau_2}) \quad Eq. 7-55$$

As mentioned in Section 5.2 the algorithm uses a single cost function to control these two error signals. The proposed control algorithm as shown in Figure 7-14 is based on adding the squares of magnitudes of these errors to form a single cost function (E),

$$E = |e_1|^2 + |e_2|^2 \tag{Eq. 7-56}$$

$$\Rightarrow E(h_{1r}, h_{1i}, h_{2r}, h_{2i})$$

($h_{1r}, h_{1i}, h_{2r}, h_{2i}$: real and imaginary components of h_1 and h_2)

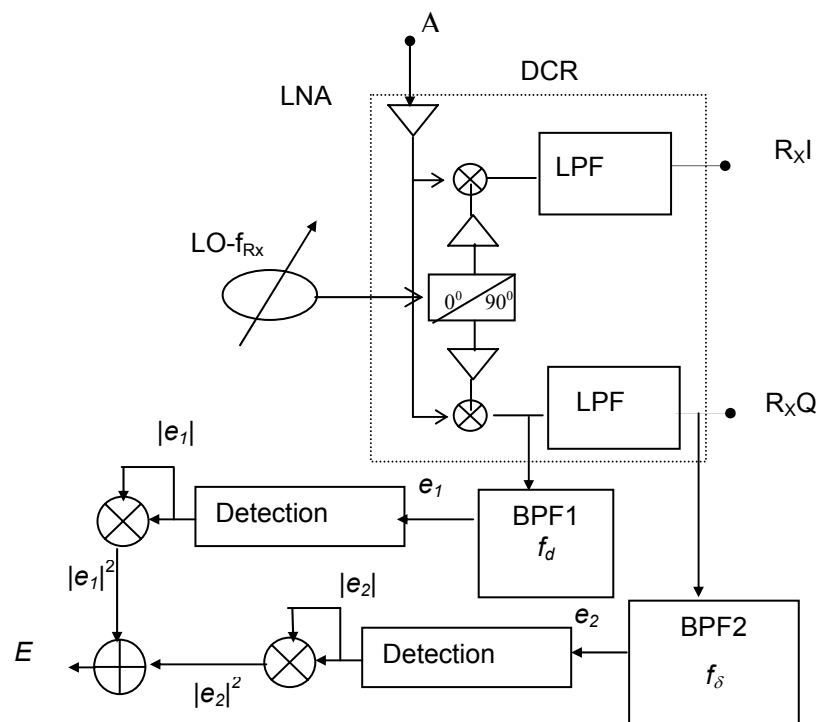


Figure 7-14 Obtaining the cost function from the direct conversion receiver. e_1 is the transmitter leakage signal and e_2 a pilot used to measure the noise leakage signal.

This is a 4 variable quadratic equation and therefore has a convex surface with a single global minimum. Many convergence algorithms are possible such as least-mean square (LMS), steepest descent and recursive least-squares (RLS) etc. However many of these algorithms require access to phase information in the error terms e_1 and e_2 . This brings the added difficulty of obtaining the correct

phase reference. In this work we operate directly on the cost function E , and reduce it using an iterative ‘one dimensional search technique’. Each adjustment h_{1r} , h_{1i} , h_{2r} , h_{2i} is taken in turn and the cost function is minimised by adjusting it with small step size increments. Convergence is slow but robust.

The learning curve of Figure 7-15 indicates slow convergence from the starting condition $h_1 = h_2 = 0$. The bumps in the curve represent the reduction of step size by 10^{-1} , which occurs whenever both coefficients stop changing.

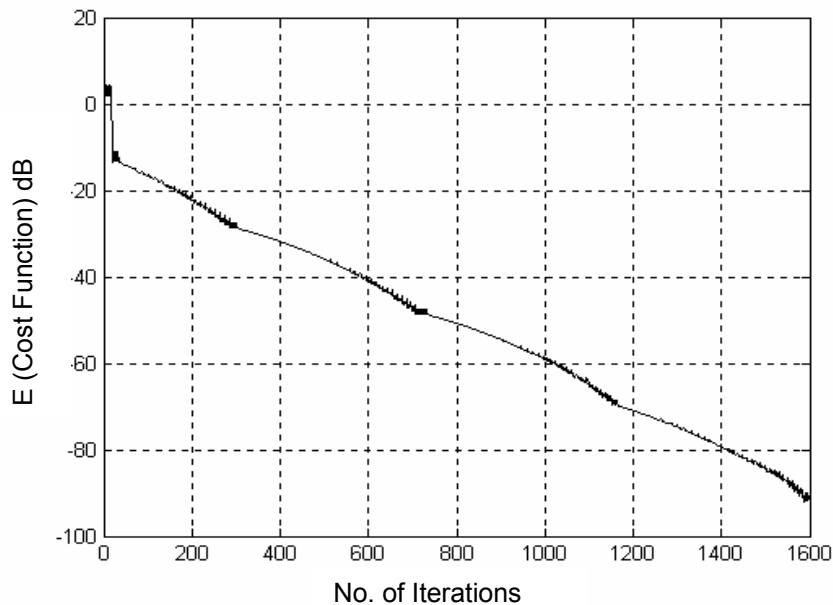


Figure 7-15 The learning curve ($\tau_2 = -\tau_1$, $\tau_1 f_d = 0.045$).

The convergence time is set by the number of iterations, and the cost function settling time required for each iteration. The former is a function of the normalised delays (the product of the reference delay period, τ_1 , and the frequency null separation, f_d). Figure 7-16 shows how $\tau_1 f_d$ effects the number of iterations required to make the cost function (E) less than -60dB. Two conditions are shown, one where the delays straddle the main path ($\tau_2 = -\tau_1$) and the other (less ideal case) where $\tau_2 = 2\tau_1$. Large $\tau_1 f_d$'s are preferred. Unfortunately the null bandwidth requirement limits the maximum value of τ_1 that can be used.

The cost function settling time is set by the bandwidth of the circuit elements in the loop. This is dominated by the narrowband filter BPF2 which must select the pilot signal situated in the guard band between two adjacent channels. The bandwidth of this filter is likely to be restricted to 100's of Hz for narrowband modulations (i.e. DAMPS) but can be 100's of kHz for wideband modulations (W-CDMA). This gives modulation dependent update times of between approximately 10ms and 10 μ s per iteration respectively. For example, W-CDMA with $f_d = 190\text{MHz}$ and $\tau_l = 1\text{ns}$ requires 110 iterations leading to a convergence time of about 1.1ms from cold. This should be fast enough to track changes in a mobile handset. On the other hand, DAMPS with $f_d = 45\text{MHz}$ and $\tau_l = 1\text{ns}$, would require 1000 iterations and over 10 seconds for convergence; too slow for handsets.

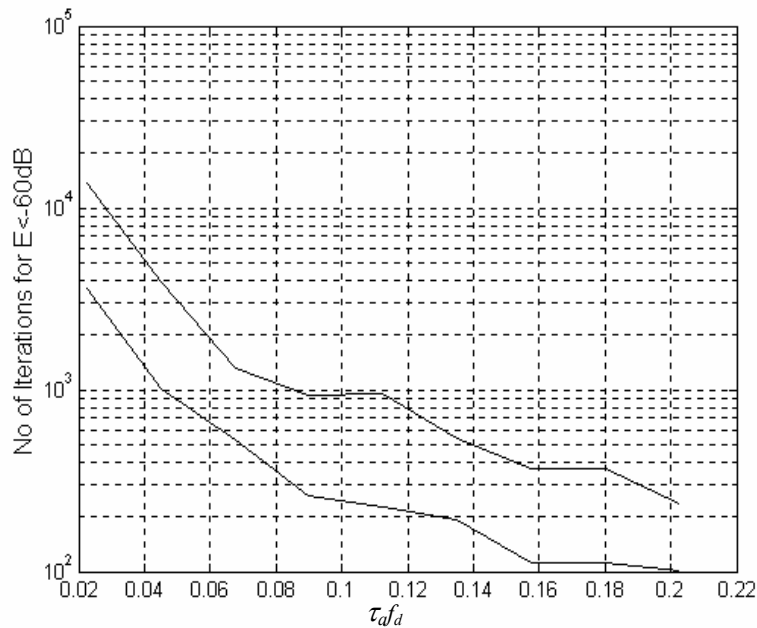


Figure 7-16 Number of iterations for $E < -60\text{dB}$ vs $\tau_l f_d$ (top: $\tau_2 = 2\tau_1$; bottom $\tau_2 = -\tau_1$).

The Figure 7-17 shows the frequency response of the canceller after 1598 iterations. The two nulls are plainly visible with bandwidth of 7MHz @50dB, when $\tau_l = 1\text{ns}$ and $\tau_2 = -1\text{ns}$. A modified cost function, $E = k_1|e_1|^2 + k_2|e_2|^2$ can be

used to emphasise the relative null depths. For example a higher isolation might be required for the transmitter leakage signal in which case ($k_1 > k_2$).

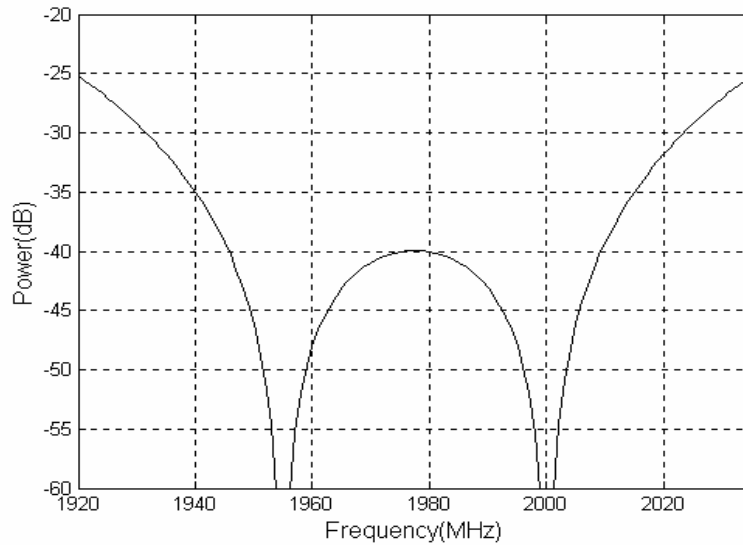


Figure 7-17 Frequency response of the canceller.

7.8 Experimental Setup and Results

The prototype is built using off the shelf components such as splitters and directional couplers. A wide band circulator gives 20dB of passive isolation. Here the transmitter signal leaks back to the receiver via the circulator. The Tx signal was set at 1.955GHz and the desired Rx signal was set at 2GHz. In order to detect the transmitter noise in the receiver band easily, a low level pilot tone signal (2.000015GHz, -30dBm) was inserted in the transmitter path. Two vector attenuators were used to control the complex gains h_1 and h_2 . The received signal after the cancellation is fed to the low noise amplifier of the direct conversion receiver (a single chip device designed for the GSM standard). The cancellation procedure must be done before the LNA to keep within the specified dynamic range. The local oscillator in the synchronous detection of e_1 is set to 45MHz, equal to the duplexing frequency. BPF1 was a simple LC network with Q of 10 (Figure 7-14). Detection of the e_2 pilot signal occurs at the output of the LPF (bandwidth = 200kHz). BPF2 ($Q = 20$) at f_δ (15KHz) is used to improve the e_2

signal. These error signals are fed to the PC data acquisition card. The PC processes the algorithm and controls the vector attenuators (MPT 1923VA).

A spectrum analyser is used to monitor the receive signal before the LNA (@A Figure 5-1 & Figure 7-14). A high-level noise signal is input to the Tx path in order to observe the double null and the cancellation with the frequency span at the receiver.

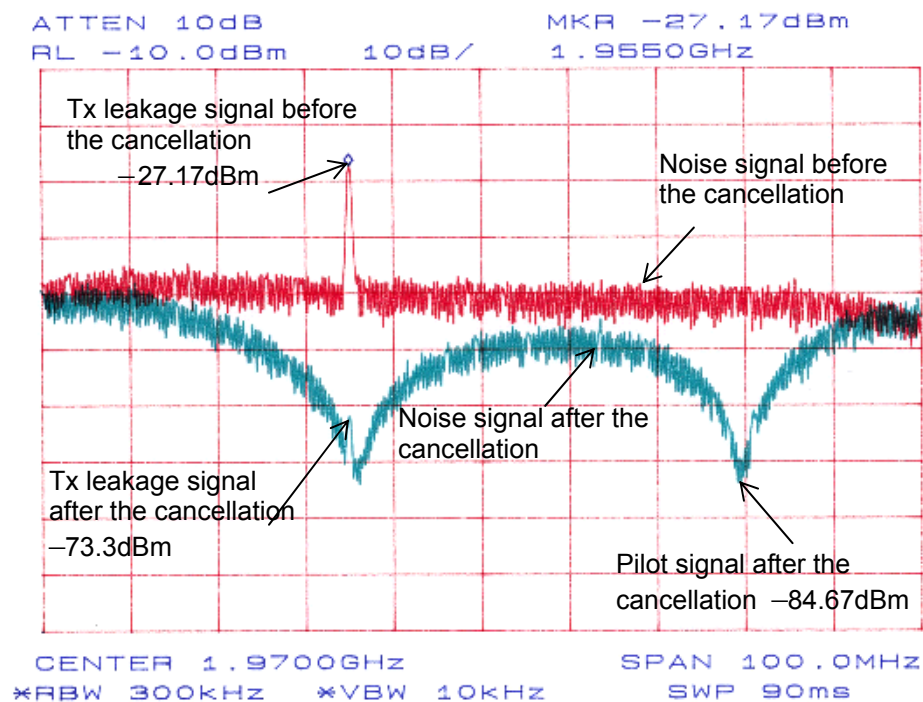


Figure 7-18 The spectrum of the received signal.

From the results (Figure 7-18) it can be seen that the obtained two nulls are at f_{Tx} (1.955GHz) and f_{Rx} (2GHz) after the convergence. The Tx interference signal before the cancellation (i.e. without the cancelling signal) was -27.17dBm . After the cancellation it was -73.3dBm : an improvement of 46dB. Therefore the achieved total isolation with the circulator (20dB) was about 66dB. This is more than enough to stop receiver overload or blocking. The pilot signal was observed

as -67.5dBm before the cancellation (this can not be seen in this figure because it is buried under the added noise floor) and about 84.67dBm after the cancellation, an improvement of 17dB. Therefore the achieved total noise suppression was about 37dB (17dB+20dB).

7.9 Performance Analysis

The simulated frequency response of the cancellation unit for conditions $\tau_1 = -1ns$, $\tau_2 = 0.2ns$ with $f_d = 190MHz$ and $\tau_1 = -1ns$, $\tau_2 = 1ns$ with $f_d = 190MHz$ and also $f_d = 45MHz$ are shown in Figure 7-19. The experiment results for the same above mentioned conditions are shown in Figure 7-20 and Figure 7-21. These results are obtained by manually controlling the inputs of the vector attenuators.

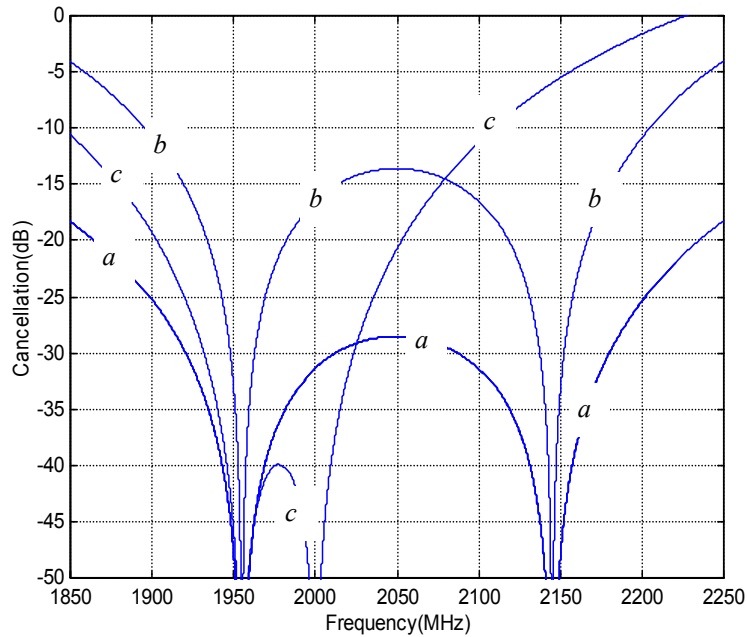


Figure 7-19 Simulated frequency response of the cancellation unit. ($a \Rightarrow \tau_1 = -1ns$, $\tau_2 = 0.2ns$, $f_d = 190MHz$; $b \Rightarrow \tau_1 = -\tau_2 = -1ns$; $f_d = 190MHz$; $c \Rightarrow \tau_1 = -\tau_2 = -1ns$, $f_d = 45MHz$)

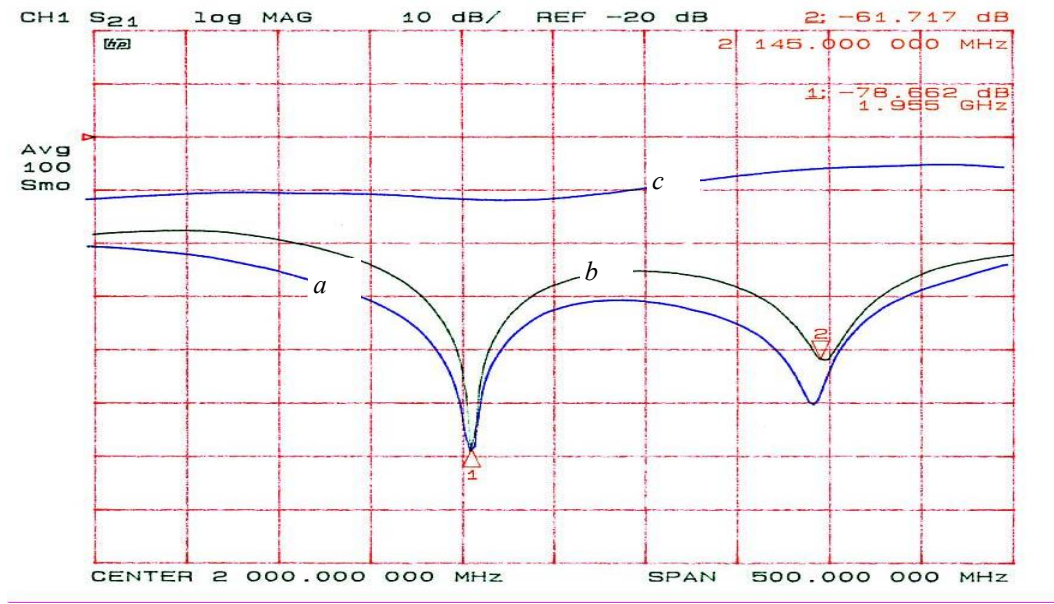


Figure 7-20 Experiment results for the cancellation unit. ($c \Rightarrow$ without the cancellation unit $a \Rightarrow \tau_1 = -1ns \ \tau_2 = 0.2ns \ f_d = 190MHz$, $b \Rightarrow \tau_1 = -1ns \ \tau_2 = 1ns \ f_d = 190MHz$)

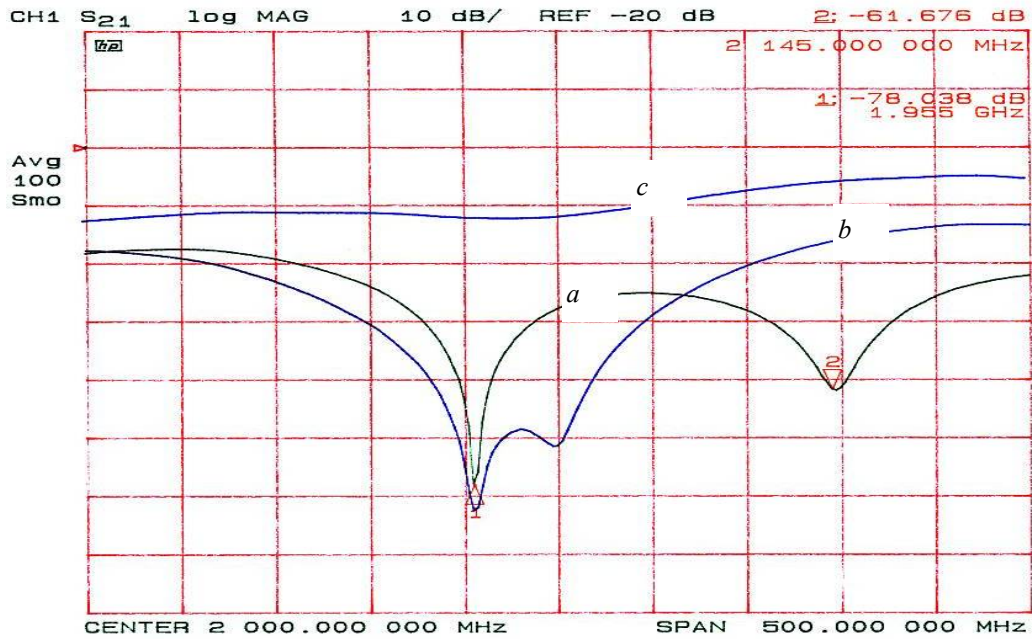


Figure 7-21 Experiment results for the cancellation unit. ($c \Rightarrow$ without the cancellation unit $a \Rightarrow \tau_1 = -\tau_2 = -1ns \ f_d = 190MHz$, $b \Rightarrow \tau_1 = -\tau_2 = -1ns \ f_d = 45MHz$)

From the experiment results and the simulation results it can be confirmed that when the delay difference or the duplexing frequency is decreased the cancellation bandwidth will improve. This agrees with *Eq. 7-49* which means the cancellation is a function of duplexing frequency and the delay differences.

The experimentally achieved Tx band cancellation and Rx band cancellation over 5MHz bandwidth for the condition $\tau_1 = -1\text{ns}$, $\tau_2 = 0.2\text{ns}$ and $f_d = 190\text{MHz}$ are 46.8dB and 38dB respectively (Figure 7-20 curve a). The simulated cancellation bandwidths at Tx frequencies and Rx frequencies for the same cancellation levels and conditions are 12.5MHz and 33.75MHz respectively (Figure 7-19 curve a). The calculated cancellation bandwidths at Tx frequencies and Rx frequencies using *Eq. 7-49* (for the same cancellation levels and conditions) are 12.19MHz and 33.58MHz respectively. This validates the derived *Eq. 7-49*. In this situation the achieved bandwidths are less than the simulation bandwidths. The experimentally achieved total isolation for the Tx interference signal is 66.8dB and total Tx noise reduction is 58dB (with the circulator).

The experimental curves have a poor optimum cancellation (null point) compared to the simulated curves but still meet the W-CDMA isolation requirements. The D/A resolutions affect the achievable optimum cancellation. By using more data bits in the D/A conversion the cancellation can be further improved. Figure 7-22 shows the frequency response of the cancellation unit using automatic control and manual control of the D/A inputs of the vector attenuators.

Manual controls give higher cancellation than the adaptive cancellation. In this prototype the achievable cancellation with automatic adjustment mainly depends on the dynamic range of the synchronous detector (40dB). The learning curve of Figure 7-23, which corresponds to the result shown in Figure 7-22 indicates that the cost function reaches its minimum value after about 450 iterations. The cancellation and the number of iterations can be improved by using or designing a synchronous detector and vector attenuators with higher dynamic ranges.

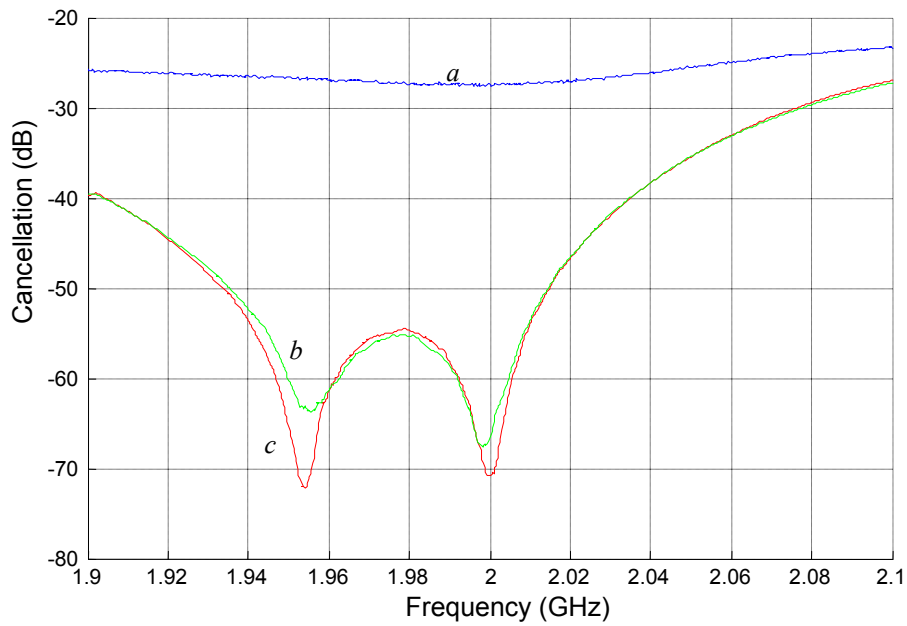


Figure 7-22 Adaptive (b) and Manual (c) frequency response for $\tau_1 = -\tau_2 = 1.1\text{ns}$ and $f_d = 45\text{MHz}$ (a) without the cancellation unit. (courtesy M. Williamson)

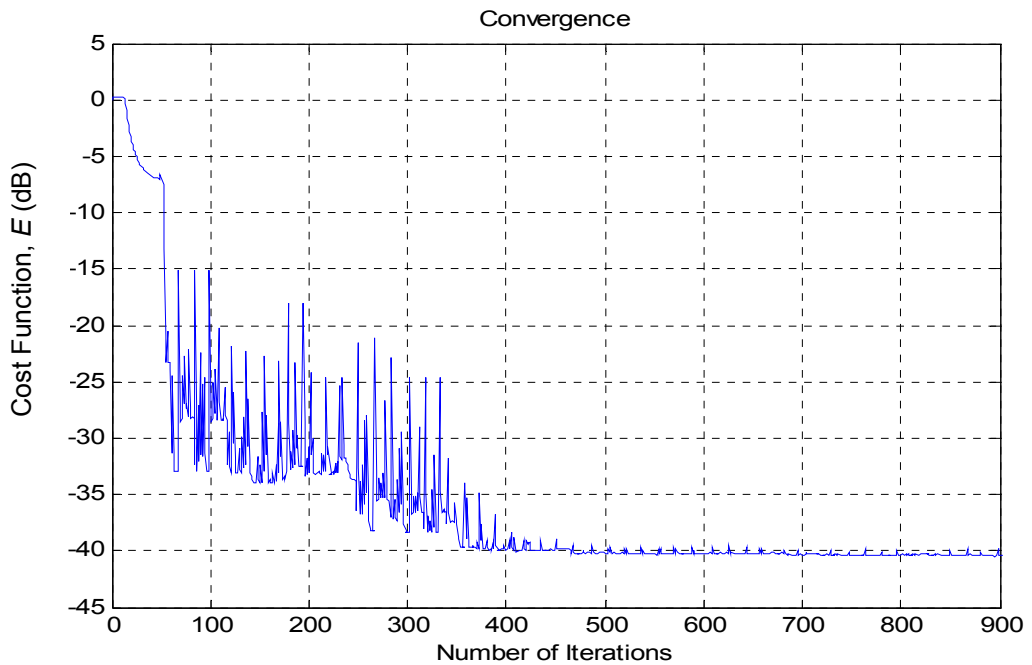


Figure 7-23 Learning curve of adaptive algorithm for $\tau_1 = -\tau_2 = 1.1\text{ns}$ and $f_d = 45\text{MHz}$. (courtesy M. Williamson)

The cancellation unit was tested for a transmitter power of 30dBm. At high power, control voltages should be set to some initial value to avoid receiver desensitisation at the beginning of the adaptation process.

In practical situations the rate of change in amplitude, phase and path delay will effect the optimum cancellation. Changes in the delay range of the main path due to antenna characteristics vary the effective operation. Further we can improve the performance using a pseudonoise (PN) signal sequence instead of a pilot tone to represent the Tx noise. Since the PN signal spreads the power over a wide frequency band (hence very low power spectral density) this will reduce transmitter interference to other terminals from the antenna. The received PN signal can be recovered using correlation techniques.

If separate antennas are used to achieve the initial low isolation, multi-band cancellation can be achieved easily although size is an issue. The vector attenuators used in the prototype operate over a limited frequency range. Further investigation is being undertaken to improve the frequency range of the vector attenuators and design for integrated circuit implementation of the system.

7.10 Conclusion

Active duplexers with double loop cancellation require variable gain and phase shifting coefficients in the cancellation paths. The behaviour of the double loop cancellation is theoretically analysed using geometrical representations. The relationship of the signal cancellation vectors to the duplexing frequency is obtained in order to derive operating conditions for suitable choices of delays. If vector attenuators are used to realise the complex coefficients in the cancellation paths, gain is not possible and this constrains the usable choices of path delay values. Some operating conditions are derived for these design constraints and verified with simulation. A good choice is $0 > f_d \tau_1 > -1/3$ and $0 < f_d \tau_2 < 1/3$. Values up to 1/2 are possible for one of the delay differences but require a

corresponding linear reduction in the other delay difference. These values are periodic in $1/f_d$. The condition $\tau_1 \approx \tau_2$ must be avoided because of the large coefficient values in each branch.

Both delay limitations and bandwidth limitations should be considered for practical implementations. The relationship between the achievable bandwidth and the given cancellation level is found and these findings are verified with simulation. The power of the residue leakage signal is proportional to the bandwidth squared, the duplexing frequency squared and the time delay differences squared. Normalising the bandwidth and delays by f_d generalises the results. Also from a bandwidth perspective the delay difference should be small. By comparing Figure 7-8 and Figure 7-11 it can be concluded that the delays τ_1 and τ_2 should be chosen to straddle the expected range variation of the delay in the main path, that is τ_1 negative and τ_2 positive. Similar constraints have been identified for the cancellation loops in wideband feed forward amplifiers [145].

From a practical perspective a large time difference between τ_1 and τ_2 would give the maximum scope for changes in phase delay in the main (antenna) path. (The latter might be caused by antenna loading variations) The bold dotted line $\tau_2 - \tau_1 = 0.385/f_d$ drawn on Figure 7-11 shows that a 5MHz bandwidth (when $f_d = 190\text{MHz}$) is always guaranteed for coefficient values < 1.0 and a variation in main path phase delay of $0.385/f_d$ ($\pm 1\text{ns}$ for W-CDMA). This value is predominantly coefficient limited, however if the coefficient gain requirement is relaxed then the possible variation can be extended, until it becomes bandwidth limited. The extended range is shown by the length of the short dotted line of Figure 7-8. The additional gain requirement is small (the line is well within the gain = 2 contour), and this allows the delay variation in the main path to be further increased by about 40%.

The cancellation in the receiver band can be improved by increasing the amplitude of the pilot signal. The pilot signal cannot be made too large as it will interfere

with other terminals. A spread spectrum pilot is a possible solution as proposed in [122].

A new algorithm which uses a single cost function is proposed. Convergence is faster for wideband signals. But, the speed of convergence using the one-dimensional search algorithm is limited by the bandwidth of the BPFs and the averaging of input signals used to remove the effect of noise on the error signals. Future work will involve investigating the use of alternative adaptation algorithms to provide faster convergence.

The cancellation is a function of duplexing frequency(f_d) and the delay differences (τ_1, τ_2). Smaller delay differences and smaller duplexing frequency give higher cancellation bandwidth. In this adaptive duplexer system a Tx band cancellation of 66.8dB and an Rx band cancellation of 58dB were achieved over 5MHz bandwidth for the delays $\tau_1 = -1ns$, $\tau_2 = 0.2ns$ and $f_d = 190MHz$.

Adaptive duplexing eliminates many external components in the multi-band transceiver front end. The described scheme and the algorithm are simple, use low frequency error signals and have low computational complexity. Therefore it is suitable for low power integrated designs for many applications.

Conclusions and Suggestions for Future work

8.1 Conclusions

The proposed new adaptive duplexer architecture eliminates the need for multiple switched duplexers in multi-band systems. A successful application of wideband cancellation for Tx interfering signals in the receiver and Tx noise signals in the receiver band, which can cover all the frequencies of interest was demonstrated. The technique is based on combining a low isolation device and an active double loop cancelling scheme. The solution was tested on a direct conversion receiver. A new algorithm, which uses a single cost function, to control an adaptive duplexer for multi-band software radio is also proposed. The speed of convergence using the algorithm is limited by the bandwidth of the BPFs and, any averaging of samples to remove the effect of noise. Convergence is faster for wideband signals because the filter bandwidths are generally wider. Future work

will involve investigating the use of alternative adaptation algorithms to provide faster convergence.

The feasibility of wideband cancellation mainly depends on the delays in the main path and the cancellation paths. These delays are limited by the attenuation coefficients in the cancellation paths. The adaptive duplexer with double loop cancellation should be designed such that the delay differences τ_1 and τ_2 straddle the expected range variation of the delay in the main path (τ_d). The achievable cancellation bandwidth also depends on the duplexing frequency. Smaller delay differences and smaller duplexing frequencies give higher cancellation bandwidths. The relationship between the cancellation bandwidth and the achievable cancellation level is linear (6dB/octave). It is concluded that the delays should be chosen such that $\tau_2 - \tau_1 = 0.385/f_d$ and $0 < \tau_2 < 0.38/f_d$ to achieve 40dB cancellation and 5MHz signal bandwidth for coefficient values < 1 .

With this approach, it has been possible to achieve 66.8dB total isolation between the transmit and receive signals and 58dB of total transmitter noise reduction at the receiver band over 5MHz bandwidth and 190MHz duplexing frequency. This is more than enough to stop the receiver from overloading or blocking and to stop the Tx noise from degrading the receiver noise figure. It also meets the W-CDMA isolation requirements.

The described scheme is simple, uses relatively low frequency error signals and has low computational complexity. Therefore it is suitable for low power integrated design.

This research was targeted at mobile handsets but it also can be used in base station applications to eliminate expensive cavity filter duplexers.

8.2 Publications Resulting from this Work

The main contributions of this work were:

- The first published simulated and experimental results from an adaptive duplexer with a single loop cancellation based on direct conversion receiver [146], [147]
- The first published measurements from a new adaptive wideband duplexer for multi-band transceiver using two loop cancellation [148], [149]
- The first analysis of the effect of delays on the coefficients values in double loop cancellation system [134]
- The first published control algorithm to cancel the Tx leakage and Tx noise in the Rx band simultaneously, based on a single cost function [150]
- The first published performance analysis of adaptive wideband duplexer using simulated and experimental results [151], [152]
- The use of a geometrical method for the analysis and the performance predictions of double loop cancellation in terms of bandwidth, cancellation level, delay and coefficient [153].

8.3 Suggestions for Future Research

The current performance of the adaptive duplexer is very promising, but the concept was proven using devices that are currently available in the market rather than designing it specifically for the purpose, due to the limited timeline for this research work. Miniaturisation can be achieved with current ASIC (Application Specific Integrated Circuits) technologies available today and there is significant potential for further advancements when future micro-electronic technologies are considered. The performance of this adaptive duplexer architecture can be further enhanced by improving the controlling method, the current algorithm cost function and the convergence time. Dramatic performance improvements are possible with the variation to the architecture which is described in Section 8.3.5

and this is a fine topic for further research. With these future improvements, higher cancellation and wide bandwidth in both duplex bands can be achieved.

8.3.1 Vector Attenuators

The vector attenuators used in this research have a limited operating frequency range. Vector attenuators that are capable of operating over the entire frequency range are needed for the software radio. This can be achieved using Gilbert cell mixers. It is possible to implement such a device since the attenuation range and phase range need not to be the same for the whole operating band. Another requirement is that the noise figure of the vector attenuator should be equal to the attenuation so that it does not degrade the receiver sensitivity. The design of a vector attenuator that meets all these requirements is currently being researched.

8.3.2 Low Isolation Device

Stripline filters are a possible solution to achieve initial isolation since its design can be integrated and miniaturised. As the required isolation is low, 20dB, it is possible to design stripline filters for the entire operating band. These filters should have a minimum insertion loss. A recently designed microstrip duplexer [58] that is capable of handling the W-CDMA 2GHz band has demonstrated 40dB isolation and less than 2.5dB insertion loss. Multi-band operation can be achieved by switching in different resonator lengths. MEMS switches can provide this function with very small footprints.

8.3.3 Adaptive Control and Algorithm

The analogue to digital interface board used in the prototype had an 8 bit A/D converter. When the span is 5V, the input resolution is 19mV. An 8 bit A/D gives a dynamic range of 48dB. If the input signal is smaller than this resolution it won't be detected accurately, and as a result, the control algorithm won't be able to further minimise the error signals. This was one of the limiting factors in the prototype described in Section 7.8. The performance can be improved by using an

ADC with a higher resolution. If 14-bit A/D converters are used the dynamic range will be 84dB and the input resolution will be 0.3mV. This will enable higher cancellation.

Future work should involve investigating the use of alternative adaptation algorithms to provide faster convergence. At the time of writing this thesis further research has already been commenced in this area. An improved adaptation method of controlling this adaptive duplexer is presented in [154]. This method uses the Singular Value Decomposition (SVD) to decouple the relationship between the system controls and the two error signals (e_1 , e_2). Here the SVD converts a multiple input multiple output (MIMO) system into two single input single output (SISO) systems. Finding the relationships among the four control signals and the two error signals can be another direction for further research.

For systems that require different isolations for the duplex bands, a modified cost function, $E = k_1|e_1|^2 + k_2|e_2|^2$ can be used to emphasise the relative null depths. There is potential opportunity for further research in this aspect, too.

8.3.4 Integration

A further development for this work is to integrate the adaptive duplexer architecture into a separate ASIC or integrate it into the direct conversion receiver. The main challenges will be the integration of the delay lines and the vector attenuators/modulators.

8.3.5 Four Loop Cancellation

Although the proposed adaptive duplexer is capable of achieving wideband cancellation, even wider bandwidth cancellation can be achieved by employing another two or more loops. Therefore this will be quite suitable for future mobile communication (e.g. 4G) devices with wider bandwidths, of 20MHz and more. This four loop cancellation can be designed so that there are two nulls close to each other in the Tx band and another two nulls close to each other in the Rx

band, as shown in Figure 8-1. The achievable cancellation in this case will be very high.

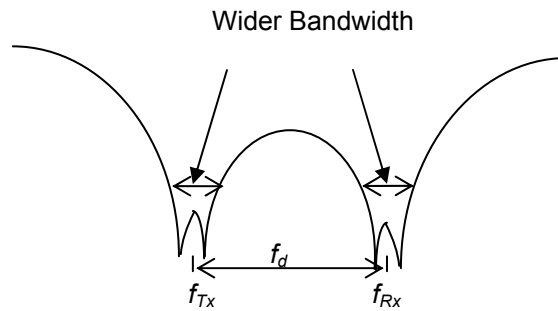


Figure 8-1 Four loop cancellation

The four loop adaptive duplexer architecture is shown in Figure 8-2. This architecture is more complex than that of the double loop cancellation architecture and may require additional devices and pilot signals requiring more integrated or miniaturised components. These issues can be further investigated in future. Further analysis of four (plus) loop cancellation, noise analysis, delay limitations and dynamic range requirements based on the same principals used for the two loop system can be performed.

This architecture could need 4 error signals and the cost function might be as shown below.

$$E = |e_1|^2 + |e_2|^2 + |e_3|^2 + |e_4|^2$$

Since it considers many error signals and many coefficients, the convergence time will be slow especially if a one dimensional control algorithm is used to minimise the cost function. A faster convergence algorithm is a likely requirement.

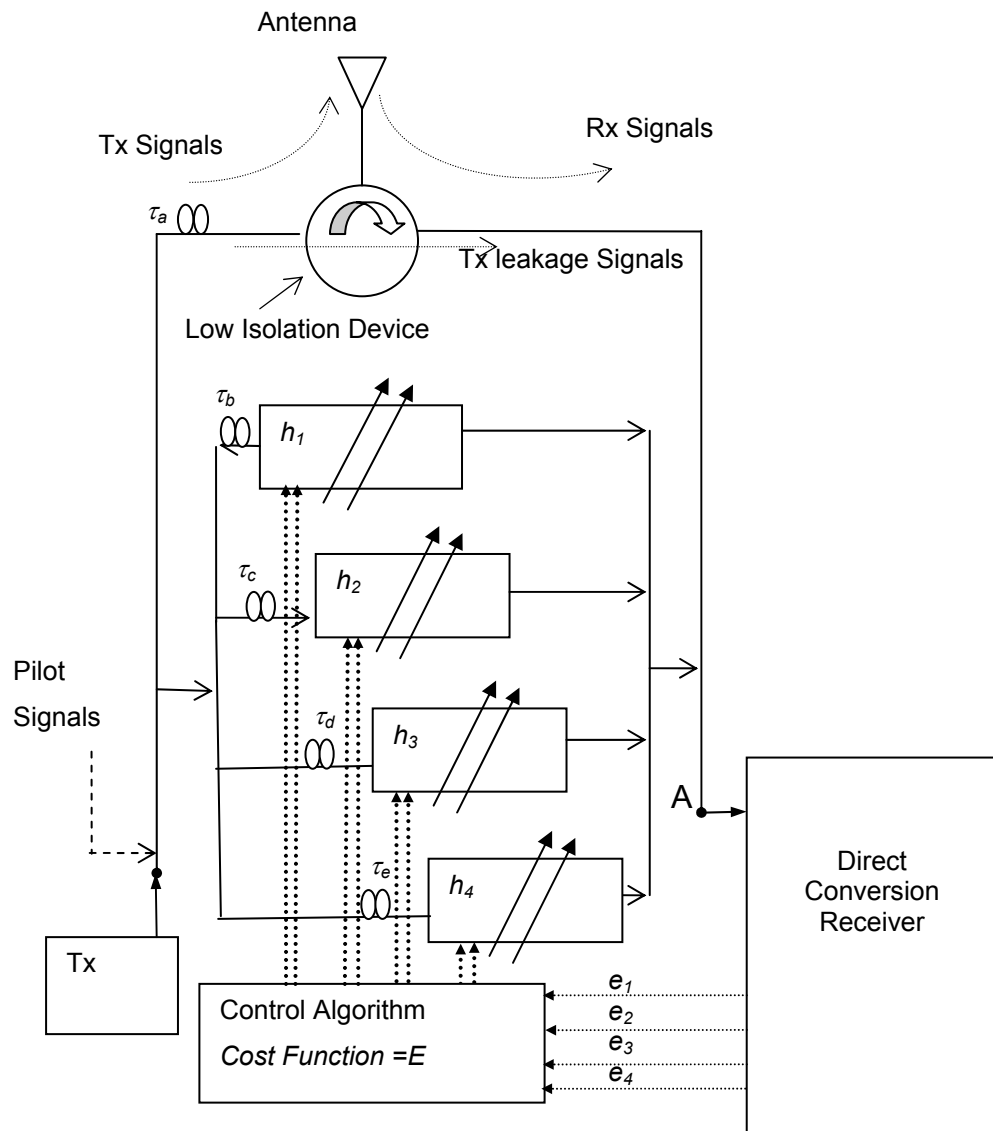


Figure 8-2 Four loop adaptive duplexer architecture

Figure 8-3 shows the frequency response for the cancellation unit with four loops. This was done by solving the four equations corresponding to the cancellation nulls at $f_{Tx} + f\delta$, $f_{Tx} - f\delta$, $f_{Rx} + f\delta$ and $f_{Rx} - f\delta$ ($f\delta = 2\text{MHz}$, $f_{Tx} = 2\text{GHz}$, $f_{Rx} = 2.045\text{GHz}$). The four delay differences used for the four cancellations paths were -0.4ns , -0.5ns , 0.3ns and 0.2ns and the duplexing frequency was 45MHz .

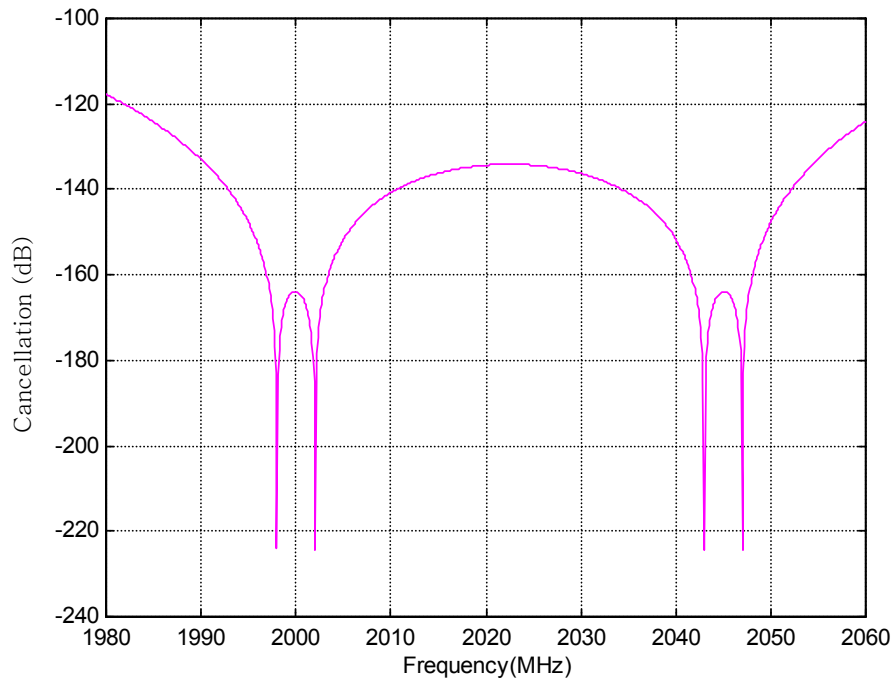


Figure 8-3 Frequency response of the four loop cancellation unit.

From this result it can be seen that the obtained cancellation is very high which is more than 100dB for the entire band. Therefore by using this four loop cancellation architecture, good broadband cancellation can be achieved.

References

- [1] IEC On-Line Education, *Evaluation of Mobile Communications*,
<http://www.iec.org/online/tutorials/umts/topic01.html>
- [2] N. J. Boucher, *Cellular Radio Handbook – A Reference for Cellular System Operation*, Quantum Publishing Inc., California, 1992.
- [3] T. S. Rappaport, *Wireless Communications Principles and Practice*, Prentice Hall PTR, New Jersey, 1996.
- [4] V. Grag, and J. E. Wilkes, *Wireless and Personal Communications Systems*, Prentice Hall, Upper Saddle River, 1996, p 445.
- [5] A. Richharia, M. Shum, M. Mamon, *Final Report- Third Generation Mobile Communications*,
<http://www.iis.ee.ic.ac.uk/~frank/surp99/report/ar497/>
- [6] L. Baldauf, M. Lovejoy, J. Karesto and L. Pajja, *Global Networking in Wireless Technology Business*, Technology Review 114/2001, Texas, 2001, pp. 33-34,
http://www.tekes.fi/julkaisut/Global_Networking.pdf
- [7] T. Nilsson, *Ericsson Review*, Issue no.2, 1998,
http://www.ericsson.com/about/publications/review/1998_02/35.shtml

- [8] M. H. Callendar, "International Mobile Telecommunications-2000 Standards Efforts of the ITU," *IEEE Personal Communications Magazine*, vol. 4, no. 4, pp. 6-7, August 1997.
- [9] M. Zeng, A. Annamali and V. K. Bhargava, "Recent Advances in Cellular Wireless Communications," *IEEE Communications Magazine*, vol. 37, no. 9, pp. 128-38, September 1999.
- [10] A. Springer and R. Weigel, "RF microelectronics for W-CDMA mobile communication systems," *Electronics & Communication Engineering Journal*, vol. 14, no. 3, pp. 92-100, June 2002.
- [11] R. E. Sheriff and Y. Fun Hu, *Mobile Satellite Communications Network*, John Wiley & Sons Ltd, Chichester, England, 2001, pp. 31-33.
- [12] Y.S. Rao, W. Yeng and A. Kripalani, "Third-Generation (3G) Radio Access Standards," *International Conference on Communication Technology Proceedings (WCC - ICCT 2000)*, vol. 2, 21-25 August 2000, pp. 1017-1023.
- [13] *UMTS World WCDMA Specification and Information Page*, <http://www.umtsworld.com/technology/wcdma.htm>
- [14] *cdma2000 Specification and Information Page*, <http://www.umtsworld.com/technology/cdma2000.htm>
- [15] *UMTS World TDCDMA Specification and Information Page*, <http://www.umtsworld.com/technology/tdcdma.htm>
- [16] *UMTS World TDSCDMA Specification and Information Page*, <http://www.umtsworld.com/technology/tdscdma.htm>
- [17] *UMTS World WCDMA Specification and Information Page*, http://www.umtsworld.com/technology/japan_wcdma.htm
- [18] W. Thomann, J. Fenk, R. Hagelauer and R. Weigel, "Fully integrated W-CDMA IF receiver and IF transmitter Including IF Synthesizer and On-

- Chip VCO for UMTS Mobiles,” *IEEE Journal of Solid-State Circuits*, vol. 36, no. 9, pp. 1407-1419, September 2001.
- [19] H. Honkasalo, K. Pehkonen, M. T. Niemi and A. T. Leino, “WCDMA and WLAN for 3G and Beyond” *IEEE Wireless Communications*, vol. 9, no. 2, pp. 14-18, April 2002.
- [20] R. D. Carsello, et al., “IMT-2000 Standards: Radio Aspects”, *IEEE Personal Communication Magazine*, pp. 30-40, August 1997.
- [21] J. Mitola, *What Is A Software Radio?*,
<http://ourworld.compuserve.com/homepages/jmitola/whatisas.htm>.
- [22] J. Mitola, “The Software Radio Architecture,” *IEEE Communication Magazine*, vol. 33, no. 5, pp. 26-38, May 1995.
- [23] J. H. Reed, *Software Radio: A Modern Approach to Radio Engineering*, Prentice Hall, 2002.
- [24] EE PRODUCT NEWS, *Floating-point DSP Accelerates to 1,5000 MFLOPS*, January 2005,
<http://www.eepn.com/Locator/Products/ArticleID/31094/31094.html>.
- [25] P. B. Kenington, “Power Consumption of A/D Converters for Software Radio Applications,” *IEEE Transactions on Vehicular Technology*, vol 49, no. 2, pp. 643-650, March 2000.
- [26] B. Le, T. W. Rondeau, J. H. Reed and C. W. Bostian, “Analog-to-Digital Convertors,” *IEEE Signal Processing Mag.*, vol. 22, no. 6, Nov. 2005, pp. 69-77.
- [27] Michael Deeney, Teltec Ireland at University College Cork, *Software Radio – the End of RF Design?*,
http://cnds.ucd.ie/teltec/old_teltec/nov96/art4.html
- [28] P. M. Athenas, I. Howitt, T. Rapport, J. Reed and B. Worner “A High Capacity Adaptive Wireless Receiver Implemented with a Reconfigurable

- Computer Architecture,” *ARPA GloMo Principle Investigators Conference*, San Diego, CA, November 1995.
- [29] M. Butterm, J. Providakes and G. Blythe, “The Layered Radio,” *MILCOM*, New York, 1998, pp. 174-179.
- [30] S. Srikanteswara, J. H. Reed, P. Athanas and R. Boyle, “A Soft Radio Architecture for Reconfigurable Platforms,” *IEEE Communications Magazine*, vol. 38, no. 2, pp. 140–147, February 2000.
- [31] S. Srikanteswara, “Design and Implementation of a Soft Radio Architecture for Reconfigurable Platforms,” *Ph.D thesis*, Faculty of Electrical and Computer Engineering, The Virginia Polytechnic Institute and State University, July 2001.
- [32] H. Tsurumi and Y. Suzuki, “Broadband RF Stage Architecture for Software Defined Radio in Hand Held Terminal Applications,” *IEEE Communications Magazine*, vol. 37, no. 2, pp. 90–95, February 1999.
- [33] Y. Kobayashi, K. Takeuchi, Y. Hirao and K. Shibata, “Antenna Duplexer,” U. S. Patent 5 534 829, 9 July 1996.
- [34] C. Tao, J. Song Junde and Wang Hai, “A New Architecture of Third Generation Mobile System Based on Software Radio,” *International Conference on Communication Technology*, Beijing, China, vol. 1, 22-24 October 1998, pp. S27-06-1 – S27-06-5.
- [35] A. Haghghat, “A Review on Essentials and Technical Challenges of Software Defined Radio,” *Proceedings of MILCOM 2002*, vol. 1, 7-10 October 2002, pp. 377–382.
- [36] B. Razavi, *RF Microelectronics*, Prentice Hall, 1998.
- [37] L. Maurer, W. Schelmbauer, H. Pretl, Z. Boos, R. Weigel and A. Springer, “Impact of IF-SAW Filtering on the Performance of a W-CDMA Receiver,” *IEEE Ultrasonic 2000 Symposium*, vol.1, 22-25 October 2000, pp. 375-378.

- [38] R. Weigel, L. Maurer, D. Pimingsdoefer and A. Springer, "RF Transceiver Architecture for W-CDMA Systems Like UMTS: State of the Art and Future Trends," *Proceedings of the International Symposiums on Acoustic Wave Devices for Future Mobile Communication Systems*, Chiba, Japan, March 5th 7th 2001, pp. 25-34.
- [39] B. Razavi, "Design Considerations for Direct-Conversion Receivers," *IEEE Transaction on Circuit and Systems-II: Analog and Digital Signal Processing*, vol. 44, no. 6, pp. 428-435, June 1997.
- [40] W. Namgoong and T. H. Meng, "Direct Conversion RF Receiver Design," *IEEE Transactions on Communications*, vol 49, No 3, pp. 518-529, March 2001.
- [41] B. Minnis and P. Moore, "A Re-Configurable Receiver Architecture for 3G Mobiles," *IEEE Radio Frequency Integrated Circuit (RFIC) Symposium*, 2-4 June 2002, pp. 187-190.
- [42] Kang-Yoong Lee, et al., "Full-CMOS 2 GHz WCDMA Direct Conversion Transmitter and Receiver," *IEEE Journal of Solid-State Circuit*, vol. 38, no. 1, pp. 43-53, January 2003.
- [43] H. Yoshida, T. Otaka and H. Tsurumi, "A Software Defined Radio Receiver Using the Direct Conversion Principle: Implementation and Evaluation," *The 11th IEEE International Symposium on Personal, Indoor and Mobile Radio communications*, vol. 2 , 18-21 September 2000, pp. 1044-1048.
- [44] T. Nakagawa, M. Kawashima, H. Hayashi and K. Araki, "A 0.9-2.5 GHz Wideband Direct Conversion Receiver for Multi-Band Applications," *Gallium Arsenide Integrated Circuit (GaAs IC) Symposium, 23rd Annual Technical Digest*, 21-24 October 2001, pp. 37-40.
- [45] S. Haruyama and R. Morelos-Zaragoza, "A Software Defined Radio Platform with Direct Conversation: SOPRANO," *IEEE 54th Vehicular*

- Technology Conference (VTC 2001 Fall)*, vol. 3, 7-11 October 2001, pp. 1558–1560.
- [46] H. Pretle, et al., “A W-CDMA Zero-IF Front End for UMTS in a 75 GHz SiGe BiCMOS Technology,” *IEEE Radio Frequently Integrated Circuits (RFIC) Symposium*, 20-22 May 2001, pp. 9-12
- [47] M. Mohajer and A. Mohammadi, “A Novel Architecture for Six-Port Direct Conversion Receiver,” *15th IEEE International Symposium on Personal, Indoor and Mobile Radio Communications*, vol. 4, 5-8 September 2004, pp. 2705–2709.
- [48] J. Crols and M. Steyaert, “A Single-chip 900 MHz CMOS Receiver Front-End with High Performance Low-IF Topology,” *IEEE Journal of Solid – State Circuits*, vol. 30, no. 12, pp. 1483-1492, December 1995.
- [49] J. Crols and M. S. J. Steyaert, “Low-IF Topologies for High-performance Analog Front Ends of Fully Integrated Receivers,” *IEEE Transactions on Circuit and systems-II: Analog and Digital Signal Processing*, vol. 45, no. 3, pp. 269-282, March 1998.
- [50] J. C. Rudell, et al., “Recent Development in High Integration Multi-Standard CMOS Transceivers for Personal Communication Systems,” *International Symposium on Low Power Electronics and Design (ISLPED 98)*, Monterey, CA USA, 10-12 August 1998, pp.149-154
- [51] Y. Urabe, H. Takai and H. Yamasaki, “Time Division Duplex Transceiver,” U. S. Patent 5 446 770, 29 August 1995.
- [52] Jack Daniel Company, *Duplexers – An Introductory Tutorial*, <http://www.rfsolutions.com/duplex.htm>.
- [53] Kiwa Electronics, *Tips for Improving Receiver Performance*, 1996, <http://www.kiwa.com/rxtips.html>.

- [54] R. C. V. Macario, *Personal & Mobile Radio Systems*, IEE Telecommunications Series 25, Peter Peregrinus Ltd., United Kingdom, 1992.
- [55] R. Dolman, R. W. Lampel and X. S. Zhou, "Method and Apparatus for Reducing Receive Band Transmitter-Chain Noise for Portable Duplex Transceiver," U. S. Patent 5 740 522, 14 April 1998.
- [56] O. K. Jensen, et al., "RF Receiver Requirements for 3G W-CDMA Mobile Equipment," *Microwave Journal*, vol. 43, no. 2, pp. 22-46, February 2000.
- [57] E. Goron, J. P. Coupez, C. Person, Y. Toutain, H. Lattard and F. Perrot, "Optimization of a Very Low-Size, Planar UMTS Duplexer, Using New Miniaturized Open-Loop Resonator Filters," *15th International Conference on Microwaves, Radar and Wireless Communications (MIKON-2004)*, vol. 1, 17-19 May 2004, pp. 355–358.
- [58] E. Goron, J. P. Coupez, C. Person, Y. Toutain, H. Lattard and F. Perrot, "Accessing to UMTS Filtering Specifications Using New Microstrip Miniaturized Loop-Filters," *IEEE MTT-S International Microwave Symposium Digest*, 8-13 June 2003, pp. 1599-1602.
- [59] Soon-Soo Oh and Young-Sik Kim, "A Compact Duplexer for IMT-2000 Handsets using Microstrip Slow-Wave Open-Loop Resonators with High-Impedance Meander Lines," *IEEE Radio and Wireless Conference*, 19-22 August 2001, pp. 177–180.
- [60] J. Zhou and W. Hong, "Design of Compact Microstrip Duplexers for 3G Mobile Communication Systems," *IEEE International Symposium Antennas and Propagation Society*, vol. 2, 16-21 July 2000, pp. 816– 819.
- [61] D. Penunuri, R. Kommrusch and N. Mellen, "A Tunable SAW Duplexer," *IEEE Ultrasonics Symposium*, vol. 1, 22-25 October 2000, pp. 361–366.

- [62] K. Saitou and K. Kageyama, "Tunable Duplexer Having Multilayer Structure Using LTCC," *IEEE MTT-S International Microwave Symposium Digest*, vol. 3, 8-13 June 2003, pp. 1763-1766.
- [63] J. Lucek and R. Damen, "Designing an LNA for a CDMA Front End," *RF Signal Processing Magazine*, pp. 20-30, February 1999, <http://images.rfdesign.com/files/4/0299Lucek20.pdf>.
- [64] N. Swanberg, J. Phelps and M. Recouly, "WCDMA Cross Modulation Effects and Implications for Receiver Linearity Requirements," *IEEE Radio and Wireless Conference*, 11-14 August 2002, pp. 13-18.
- [65] R. E. Watson, *WJ Tech-Notes, Receiver Dynamic Rang : Part 1*, vol. 14 no. 1, January/February 1987, http://www.wj.com/pdf/technotes/Rec_dyn_range1.pdf.
- [66] V. Aprain, B. Butler and P. Draxler, "Cross Modulation Distortion in CDMA Receivers," *IEEE MTT-S International Microwave Symposium Digest*, vol. 3, 11-16 June 2000, pp. 1953-1956.
- [67] B. Ko, D. Cheon, S. Kim, J. Ko, J. Kim and B. Park, "A Nightmare for CDMA RF Receiver: The Cross Modulation," *The First IEEE Asia Pacific Conference on ASICs (AP-ASIC '99)*, 23-25 August 1999, pp. 400-402.
- [68] H. Pretl, L. Maurer, W. Schelmbaue, R. Weigel, B. Adler and J. Fenk, "Linearity Considerations of W-CDMA Front-Ends for UMTS," *IEEE MTT-S International Microwave Symposium Digest*, vol. 1, 11-16 June 2000, pp. 433-436.
- [69] M. I. Adiseno and H. Olsson, "A Wide-Band RF Front-End for Multiband Multistandard High-Linearity Low-IF Wireless Receivers," *IEEE Journal of Solid-State Circuits*, vol. 37, no. 9, pp. 1162-1168, September 2002.
- [70] M. Faulkner, "IM2 Removal in Direct Conversion Receivers," *IEEE VTS 53rd Vehicular Technology Conference (VTC 2001 spring)*, vol. 3, 6-9 May 2001, pp. 1897-1901.

- [71] J. Philippe, C. Lambert, P. Krebs, S. Kadlec and S. Krassnitzer, *Wireless Future with BAW*,
www.isen.fr/martina/documents/public/papers/.
- [72] Jia-Sheng Hong and M. J. Lancaster, *Microstrip Filters for RF/Microwave Applications*, John Wiley & Sons, Inc., 2001.
- [73] Temex, *RF Filters, Duplexers & Subassemblies*,
www.temex-components.com/temex/catalog/TEM14.pdf.
- [74] R. Levy, R. V. Snyder and G. Matthaei, "Design of Microwave Filters," *IEEE Transactions on Microwave Theory and Techniques*, vol. 50, no. 3, pp. 783–793, March 2002.
- [75] A. Coon, "SAW Filters and Competitive Technologies: A Comparative Review," *IEEE Proceedings of Ultrasonics Symposium*, vol.1, 8-11 December 1991, pp. 155–160.
- [76] A.N. Mohieldin, E. Sanchez-Sinencio and J. Silva-Martinez, "A 2.7-V 1.8-GHz Fourth-Order Tunable LC Bandpass Filter Based on Emulation of Magnetically Coupled Resonators," *IEEE Journal of Solid-State Circuits*, vol. 38, no. 7, pp.1172-1181, July 2003.
- [77] F Dulger, E. Sanchez-Sinencio and J. Silva-Martinez, "A 1.3-V 5-mW Fully Integrated Tunable Bandpass Filter at 2.1 GHz in 0.35- μm CMOS," *IEEE Journal of Solid-State Circuits*, vol. 38 no. 6, pp. 918-928, June 2003.
- [78] A. Simine, et al., "Design of Quasi-Lumped-Element LTCC Filters and Duplexers for Wireless Communications," *33rd European Microwave Conference*, vol. 3, 7-9 October 2003, pp. 911–914.
- [79] K. Shoemaker, *Cavities and Duplexer*,
www.dalek.org/srg/cavity.html
- [80] RFI, *Cavity Filters*, www.rfi.com.au

- [81] Chapter 17 - Repeater Antenna Systems,
<http://www.houseofradio.gr/download/repeaters.pdf>
- [82] F. L. William, EMR Corporation, *Understanding, Maintaining & Re-Tuning Antenna Duplexers*,
[www.emrcorp.com/images/techpapers/tech_cover/antenna_duplexors\(15-6\).pdf](http://www.emrcorp.com/images/techpapers/tech_cover/antenna_duplexors(15-6).pdf).
- [83] Radio Frequency Systems (RFS), *Duplexers-GSM 1800*,
www2.rfsworld.com/RFS_Edition3/pdfs/Duplexers_755-776.pdf
- [84] I.C. Hunter, L. Billonet, B. Jarry and P. Guillon, "Microwave Filters-Applications and Technology," *IEEE Transactions on Microwave Theory and Techniques*, vol. 50, no. 3, pp. 794–805, March 2002.
- [85] J. Yohannan, A. V. P. Kumar, V. Hamsakkutty, V. Thomas and K.T. Mathew, "Synthesis of Dielectric Resonator for Microwave Filter Designing," *Progress In Electromagnetics Research Symposium*, Hangzhou, China, 22-26 August 2005.
- [86] C. Kudsia, R. Cameron and W.C. Tang, "Innovations in Microwave Filters and Multiplexing Networks for Communications Satellite Systems," *IEEE Transactions on Microwave Theory and Techniques*, vol. 40, no. 6, pp. 1133–1149, June 1992.
- [87] High Frequency Electronics, "Basic Data on High-Q Ceramic Coaxial Resonators," *High Frequency Electronics Summit Technical Media*, LLC, November 2002, p 50, www.highfrequencyelectronics.com/Archives/Nov02/HFE1102_Resonators.pdf
- [88] TOKO, *Toko's TDP is a Chip Ceramic Dielectric*,
www.toko.com/passives/filters/dielectric/pdf/tdpf1950119.pdf
- [89] Murata Manufacturing Co., Ltd., *Murata Products for Mobile Communications*,
<http://www.alkon.net/cgi-bin/pdf.pl?pdfname=murata/k09e6.pdf>

- [90] J. Phillips, “Piezoelectric Technology Primer”, *Microwave Journal*, 6 August 2001.
- [91] T. Senbo, “Advanced SAW Filters Facilitate Design of Smaller Mobile Terminals,” *Technology Focus*, Dempa Publications, December 2003, pp. 45-53, Available: www.murata.com/articles/ta0372.pdf
- [92] D. Hao, T. X. Wu, K. S. Cheema, B. P. Abbott, C. A. Finch and H. Foo, “Design of Miniaturized RF SAW Duplexer Package,” *IEEE Transactions on Ultrasonics, Ferroelectrics and Frequency Control*, vol. 51, no. 7, pp. 849–858, July 2004.
- [93] G. Kovacs, W. Ruile, M. Jakob, U. Rosler, E. Maier, U. Knauer and H. Zoul, “A SAW Duplexer with Superior Temperature Characteristics for US-PCS,” *IEEE Ultrasonics Symposium*, vol. 2, 23-27 August 2004, pp. 974–977.
- [94] M. Kadota, T. Nakao, N. Taniguchi, E. Takata, M. Mimura, K. Nishiyama, T. Hada and T. Komura, “SAW duplexer for PCS in US with Excellent Temperature Stability,” *IEEE Symposium on Ultrasonics*, vol. 2, 5-8 October 2003, pp. 2105–2109.
- [95] E. R. Brown, “RF-MEMS Switches for Reconfigurable Integrated Circuits,” *IEEE Transactions on Microwave Theory and Techniques*, vol. 46, no. 11, Part 2, pp. 1868–1880, November 1998.
- [96] J. Bryzek, K. Petersen and W. McCulley, “Micromachines on the March,” *IEEE Spectrum Magazine*, vol. 31, no. 5, pp. 20–31, May 1994.
- [97] Mumor, *Design Methodology and Technologies for Multi-Mode Radio Front-Ends*,
www.mumor.org/public/deliverables/d21_epfl_dr_pu_01_EPFL.pdf.
- [98] S. Mishin, Y. Oshmyansky, J. D. Larson and R. Ruby, *Sputtering Processes for Bulk Acoustic Wave Filters*,
www.amsincorp.com/agilent%20paper%20final%20version.pdf.

- [99] Agilent Technologies, *A Brief Overview of FBAR Technology*, www.agilent.com/about/newsroom/features/2002jul29_fbar.pdf
- [100] W. W. Lau, Y. Song and E. S. Kim, "Lateral-Field-Excitation Acoustic Resonators For Monolithic Oscillators and Filters," *Proceedings of the 50th IEEE International Frequency Control Symposium*, 5-7 June 1996, pp. 558–562.
- [101] K. M. Lakin, G. R. Kline and K. T. McCarron, "High Q Microwave Acoustic Resonators and Filters," *IEEE Transactions on Microwave Theory and Techniques*, vol. 41, no. 12, pp. 2139–2146, December 1993.
- [102] K. M. Lakin, "Thin Film Resonator Technology," *Proceedings of the 2003 IEEE International Frequency Control Symposium and PDA Exhibition Jointly with the 17th European Frequency and Time Forum*, 4-8 May 2003, pp. 765–778.
- [103] K. M. Lakin, G. R. Kline and K. T. McCarron, "Development of Miniature Filters for Wireless Applications," *IEEE Transactions on Microwave Theory and Techniques* vol. 43, no. 12, Part 2, pp. 2933–2939, December 1995
- [104] R. J. Richards and H. J. De Los Santos "MEMS for RF/Microwave Wireless Applications: The Next Wave," *Microwave Journal*, March 2001.
- [105] C. H. Tai, T. K. Shing, Y. D. Lee and C. C. Tien, "A Novel Thin Film Bulk Acoustic Resonator (FBAR) Duplexer for Wireless Applications," *Tamkang Journal of Science and Engineering*, vol. 7, no. 2, pp. 67-71, 2004.
- [106] R. Ruby, et al., "High Rejection Rx Filters for GSM Handsets with Wafer Level Packaging," *IEEE Proceedings of Ultrasonics Symposium*, vol. 1, 8-11 October 2002, pp. 925–929.
- [107] P. D. Bradley, et al., "Duplexer Incorporating Thin-Film Bulk Acoustic Resonators (FBARs)," U. S. patent 6 262 637, July 17 2001.

- [108] P. Bradley, R. Ruby, J. D. Larson, Y. Oshmyansky and D. Figueredo, “A Film Bulk Acoustic Resonator (FBAR) Duplexer for USPCS Handset Applications,” *IEEE MTT-S International Microwave Symposium Digest*, vol. 1, 2001, pp. 367-370.
- [109] R. Ruby, P. Bradley, J. D. Larson and Y. Oshmyansky, “PCS 1900 MHz Duplexer Using Thin Film Bulk Acoustic Resonators (FBARs),” *Electronics Letters*, vol. 35, no. 10, pp. 794–795, 13 May 1999.
- [110] S. Kim, J. Lee, H. Choi and Y. Lee, “The Fabrication of Thin-Film Bulk Acoustic Wave Resonators Employing a ZnO/Si Composite Diaphragm Structure Using Porous Silicon Layer Etching,” *IEEE Electron Device Letters*, vol. 20, no. 3, pp. 113–115, March 1999.
- [111] C. T. C. Nguyen, “Frequency-Selective MEMS for Miniaturized Low-Power Communication Devices,” *IEEE Transactions on Microwave Theory and Techniques*, vol. 47, no. 8, pp. 1486–1503, August 1999.
- [112] L. E. Larson, “Microwave MEMS Technology for Next-Generation Wireless Communications,” *IEEE MTT-S International Microwave Symposium Digest*, vol. 3, 13-19 June 1999, pp.1073–1076.
- [113] G. Gonzalez, Second Edition, *Microwave Transistor Amplifiers Analysis and Design*, Prentice Hall, Upper Saddle River, New Jersey, 1997.
- [114] H. Jia-Sheng, M. J. Lancaster, “Theory and Experiment of Novel Microstrip Slow-wave Open-Loop Resonator Filters,” *IEEE Transactions on Microwave Theory and Techniques*, vol. 45, no. 12 Part 2, pp. 2358-2365, December 1997.
- [115] Y. Toutain, J. P. Coupez and C. Person, “Microstrip Miniaturized Loop-Filters with High Out-Of-Band Rejection for Future 3G Mobile Terminals,” *IEEE MTT-S International Microwave Symposium Digest*, vol. 3, 20-25 May 2001, pp. 1589–1592.

- [116] H. K. Yang, H. M. Cho and J. C. Park, "The Effects of Stripline Geometries for Phase Shifting on SAW Antenna Duplexer," *IEEE Proceedings of Ultrasonics Symposium*, vol.1, 5-8 October 1998, pp. 115–118.
- [117] O. Ikata, et al., "Development of Small Antenna Duplexer using SAW Filters for Handheld Phones," *IEEE Proceedings of Ultrasonics Symposium*, vol. 1, 31 Oct.-3 Nov. 1993, pp. 111–114.
- [118] N. Hirasawa, H. Fukushima, O. Kawachi, T. Nishihara, O. Ikata and Y. Satoh, "A Study of Miniaturization Technique of SAW Antenna Duplexer for Mobile Application," *IEEE Ultrasonics Symposium*, vol. 1, 22-25 October 2000, pp. 413–416.
- [119] P. Hagn, A Przadka, V. Gebhardt and U. Baeuernschmitt, "Ceramics: the Platform for Duplexers and Front-End-Modules," *IEEE Proceedings of Ultrasonics Symposium*, vol. 1, 8-11 October 2002, pp.1–10.
- [120] S. Hontsu, K. Iguchi, K. Agemura, H. Nishikawa and M. Kusunoki, "Mechanical Tuning of Superconducting Lumped Element Filter," *IEEE Transactions on Applied Superconductivity*, vol. 15, no. 2, Part 1, pp. 972–975, June 2005.
- [121] G. R. Kenworthy, "Self-Cancelling Full-Duplex RF Communication System," U.S. Patent 5 691 978, November 1997.
- [122] S. Chen, M. A. Beach and J. P. McGeehan, "Division-free Duplex for Wireless Application," *Electronics Letters*, vol. 34, no. 2, pp. 147-148, January 1998.
- [123] S. T. Gerald, "Continuously Transmitting and Receiving Radar," E Patent 0 364 036, 18 April 1990.
- [124] S. Winthrop, "Method and Apparatuses for Cancelling In-Band Energy Leakage From Transmitter to Receiver," U. S. Patent 5 444 864, 8 August 1995.

- [125] T. Harald, K. Walter, D. Herbart and G. Roman, "Transmitter Leakage Cancellation Circuit for Co-Located GPS Receiver," E Patent 1 091 497, 11 April 2001.
- [126] J. P. McGeehan, A. Bateman, M. A. Beach, P. B. Kenington and W. T. Slingsby, "Full-Duplex Radio Transmitter/Receiver," U.S. Patent 6 229 992, 8 May 2001.
- [127] W. Schacherbauer, A. Springer, T. Ostertag, C. C. W. Ruppel and R. A. Weigel, "A Flexible Multiband Front End for Software Radios using High IF and Active Interference Cancellation," *IEEE MTT-S International Microwave Symposium Digest*, vol. 2, 20-25 May 2001, pp. 1085-1088.
- [128] J. Yong-Chae, P. Jun-Seok, A. Dal and L. Jae-Bong, "A RX cancellation Loop Configuration for Power Amplifier Module," *Asia-Pacific Microwave Conference (APMC)*, Taipei, Taiwan, vol. 3, 3-6 December 2001, pp. 1199-1202.
- [129] J. Yong-Chae, "A Feed Forward Power Amplifier with Loops to Reduce RX Band Noise and Intermodulation Distortion," *Microwave Journal Technical Feature*, pp. 80-91, January 2002.
- [130] C. Yoon and J. Park," A Study on Band Cancellation Loop of the Tx System for Frequency Hopping System," Application Note, application note-99apmc_3, http://www.telwave.co.kr/Technical/application-note_02.html.
- [131] T. O'Sullivan, R. York, B. Noren and P. Asbeck, "Adaptive Duplexer Implemented using Feedforward Technique with a BST Phase Shifter," *IEEE MTT-S International Microwave Symposium Digest*, vol. 3, 6-11 June 2004, pp. 1299-1302.
- [132] T. O'Sullivan, R. York, Noren and P. Asbeck, "Adaptive Duplexer Implemented Using Single-Path and Multipath Feedforward Technique with a BST Phase Shifter," *IEEE Transactions on Microwave Theory and Techniques*, vol. 53, no. 1, January 2005.

- [133] S. Kannanagara and M. Faulkner “Adaptive Duplexer for Multiband Transreceiver,” *IEEE Radio and Wireless Conference*, Boston, USA, 10-13 August 2003, pp 381-384.
- [134] S. Kannanagara and M. Faulkner, “Effects of Delay Differences in Double Loop Cancellation on Active Wideband Duplexer,” *7th International Symposium on Digital Signal Processing and Communication Systems*, Gold Coast, Australia, 8-11 December 2003.
- [135] Phillip’s Semiconductors, *Circulators and Isolators, Unique Passive Devices*, Application Note, 23 March 1998,
http://www.warg.waus.net/secure/component/Circulator_98035.pdf
- [136] MACOM, *RF Directional Couplers and 3dB Hybrids Overview*, Application Note, http://rfwireless.rell.com/pdfs/AN_M560.pdf
- [137] MERRIMAC, West Caldwell, NJ, *Directional Couplers Lumped Element and Stripline 100kHz to 65 GHz General Information*,
http://www.merrimacind.com/rfmw/07intro_directionalcouplers.pdf.
- [138] H. Gagne, “Directional Couplers for the Wireless Systems Designer,” *Wireless Design Magazine*, p 8, October 2000.
- [139] M. G. Ellis, Electronics System Products, *RF Directional Couplers*,
<http://members.tripod.com/michaelgellis/direct.html>.
- [140] K. J. Parsons and P. B. Kenington, “Effect of Delay Mismatch on a Feed Forward Amplifier,” *IEE Proceedings of Circuits Devices and Systems*, vol. 141, no.2, pp. 140-144, April 1994.
- [141] Agilent Technology, *Advanced Design System 1.5-Circuit Simulations*, pp. 7-1, December 2000.
- [142] Micro-Precision Technologies Inc., *MPT 1923 Vector Attenuator Preliminary Data Sheet*, <http://www.micropt.com>.

- [143] Agilent Technology, *Advanced Design System 1.5-Circuit Simulations*, pp. 1-7, December 2000.
- [144] Micro-Precision Technologies Inc., “A Vector Attenuator for Feed Forward Amplifier and RF Predistortion Use,” *Microwave Journal*, October 1997.
- [145] A. M. Smith and J.K. Cavers, “A Wideband Architecture for Adaptive Feedforward Linearization,” *48th IEEE Vehicular Technology Conference*, vol. 3, May 1998, pp. 2488-2492.
- [146] S. Kannangara and M. Faulkner, “Simulation of a Cancellation Unit in an Adaptive Duplexer for Software Radio,” *Proceedings of the 4th International Conference on Modelling & Simulation (MS’02)*, Melbourne Australia, 11-13 November 2002, pp. 148-152.
- [147] S. Kannangara and M. Faulkner, “Simulation of a Cancellation Unit in an Adaptive Duplexer for Software Radio,” *AMSE Best of book 2002*, AMSE press, pp.63-72, 2003.
- [148] S. Kannangara and M. Faulkner, “Adaptive Duplexer for Software Radio,” *2nd ATcrc Telecommunications and Networking Conference*, Fremantle, WA, Australia, November 2002.
- [149] S. Kannangara and M. Faulkner, “Adaptive Duplexer for Multiband Transreceiver,” *IEEE Proceedings of Radio and Wireless Conference*, Boston, USA, 10-13 August 2003, pp. 381-384.
- [150] S. Kannangara, and M. Faulkner, “An Algorithm to Use in Adaptive Wideband Software Radio”, *IEICE Transactions on Communications*, vol. E86-B, no. 12, pp. 3452-3455, 2003.
- [151] S. Kannangara, M. Williamson and M. Faulkner, “Performance Analysis of the Cancellation Unit in an Adaptive Wideband Duplexer for Software Radio,” *3rd ATcrc Telecommunications and Networking Conference*, Melbourne, Australia, 11-12 December 2003.

- [152] M. Williamson, S. Kannangara, and M. Faulkner, "Performance Analysis of Adaptive Wideband Duplexer," *Australian Telecommunications Networks and Applications Conference*, Melbourne, Australia, 8-10 December 2003.
- [153] S. Kannangara and M. Faulkner, "Analysis of an Adaptive Wideband Duplexer with Double Loop Cancellation," *accepted (24 July 2006) for IEEE Transactions on Vehicular Technology*.
- [154] M. Williamson and M. Faulkner, "Improved Adaptation Scheme for an Adaptive Wideband Duplexer," *The 3rd Workshop on the Internet, Telecommunications and Signal Processing*, 20-22 December 2004, Adelaide, Australia.

Appendix A – Summary of Standards

Table A-1 PCS standards overview [3]

	PACS-UB	DCS 1800	PHS
Frequencies	1920-1930 MHz	1710-1785 MHz (R) 1805-1880 MHz (F)	1895-1907 MHz
Multiple access	TDMA/FDMA/TDD	TDMA/FDMA/FDD	TDMA/FDMA/TDD
Modulation	$\pi/4$ QPSK	GMSK	$\pi/4$ QPSK
Carrier separation	300 kHz	200 kHz	300 kHz
Data rate	384 kbps	270.833 kbps	384 kbps
Voice ch./RF.ch.	4	8	4
Speech coding	ADPCM @ 32 kbps	REL P-LTP @13 kbps	ADPCM @ 32 kbps
Channel coding	CRC	Conv. R=1/2	CRC
Receiver	Coherent	Coherent	Coherent
Portable Tx. power Max./ Avg.	200 mW/20 mW	1 W/125 mW	80 mW/10 mW

Table A-2 Digital cordless air interface parameters summary [3]

	CT2	CT2+	DECT	PHS	PACS
Duplexing	TDD		TDD	TDD	FDD or TDD
Frequency band (MHz)	864-868	944-948	1880-1900	1895-1918	1850-1910/ 1930-1990 or 1920-1930
Carrier spacing (kHz)	100		1728	300	300/300
Number of carriers	40		10	77	400 or 32
Channels/carrier	1		12	4	8 or 4
Channel bit rate kbps	72		1152	384	384
Modulation	GFSK		GFSK	$\pi/4$ QPSK	$\pi/4$ QPSK
Speech coding	32 kb/s		32 kb/s	32 kb/s	32 kb/s
Average handset TX power (mW)	5		10	10	25
Peak handset TX power (MW)	10		250	80	100
Frame duration (ms)	2		10	5	2.5 or 2.0

Table A-3 TD-CDMA technical summary [15]

Frequency band	1900 MHz -1920 MHz and 2010 MHz - 2025 MHz (Time Division Duplex) Unpaired, channel spacing is 5 MHz and raster is 200 kHz. Tx and Rx are not separated in frequency, but by guard period
Minimum frequency band required	~ 5MHz, ~ 1.6MHz with 1.28Mcps
Frequency re-use	1
Voice coding	AMR (and GSM EFR) codec
Channel coding	Convolutional coding, Turbo code for high rate data TDMA frame consist of 15 timeslots Each time slot can transmit or receive Duplexer not needed Asymmetric connection supported Data by packet and circuit switch QPSK modulation
Receiver	Joint Detection, (mobile: Rake)
Chip rate	3.84Mcps or 1.28Mcps
Channel raster	200kHz
Maximum RF ch. bit rate (kbps)	~ 3.3Mbps (1/2 rate coding, spreading factor 1, 15 timeslots, ex overheads), but interference limited
Frame length	10ms
Number of slots / frame	15
Handovers	Hard
Power control period	100Hz or 200Hz UL, ~ 800Hz DL
Power control step size	1, 2, 3 dB (Variable)
Power control range	UL 65dB, DL 30dB
Mobile peak power	Power class 1: +33 dBm (+1dB/-3dB) = 2W; class 2 +27dBm, class 3 +24 dBm, class 4 +21 dBm
Number of unique base station identification codes	512/frequency
Physical layer spreading factors	1, 2, 4, 8, 16
Number of unique base station identification codes	512/frequency

Table A-4 TD-SCDMA technical summary [16]

Frequency band	2010 MHz - 2025 MHz in China (WLL 1900 MHz - 1920 MHz)
Minimum frequency band required	1.6MHz
Frequency re-use	1 (or 3)
Chip rate	1.28 Mcps
Frame length	10ms
Number of slots	7
Modulation	QPSK or 8-PSK
Voice data rate	8kbit/s
Circuit switched services	12.2 kbits/s, 64 kbits/s, 144 kbits/s, 384 kbits/s, 2048 kbits/s
Packet data	9.6kbits/s, 64kbits/s, 144kbits/s, 384kbits/s, 2048kbits/s
Receiver	Joint detection, (mobile: rake)
Power control period	200 Hz
Number of slots / frame	7
Frame length	5ms
Physical layer spreading factors	1, 2, 4, 8, 16

Table A-5 WCDMA (DoCoMo) technical summary [17]

Frequency band	1920-1980 and 2110-2170 MHz (frequency division duplex) UL and DL
Minimum frequency band required	2x5MHz
Chip rate	4.096 Mcps
Number of slots / frame	16

Appendix B – MEMS Based Front End Receiver Architectures

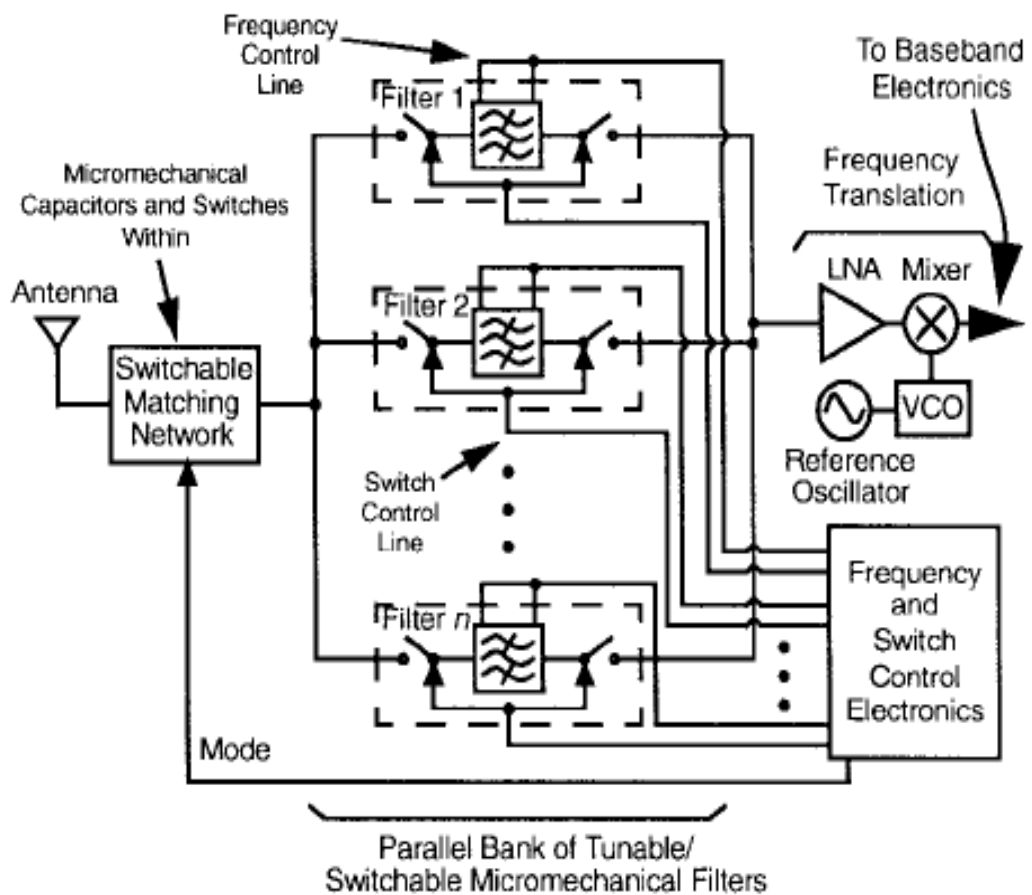


Figure B-1 Possible front end receiver architecture utilizing a parallel bank of tuneable/switchable micromechanical filters for a first stage of channel selection [111].

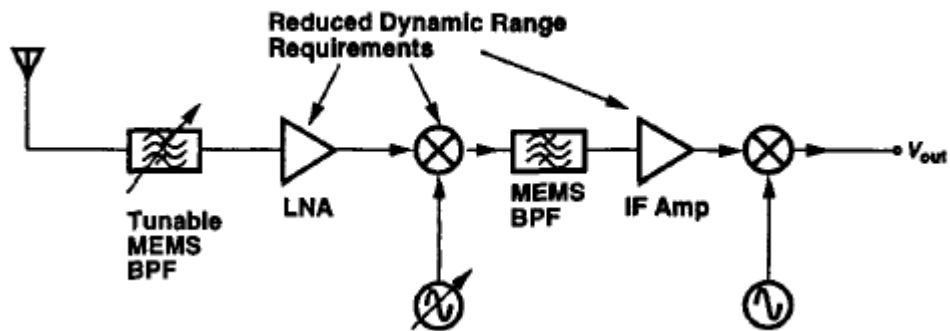


Figure B-2 MEMS based receiver employing tuneable front end filter. - Serves partial channel selection and a wide dynamic range for possible fully integrated radio receiver [112].

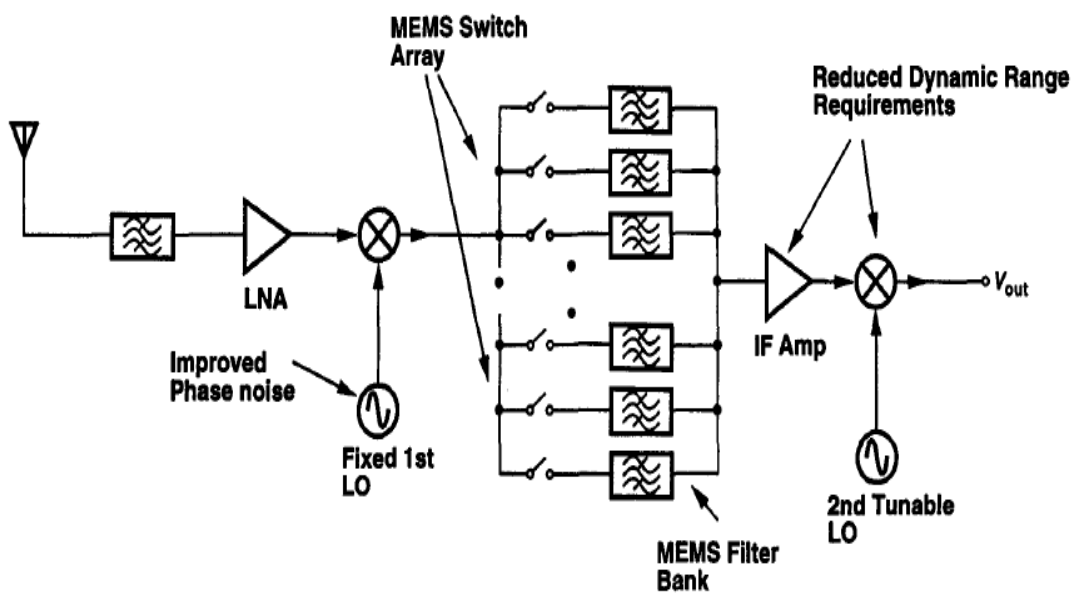


Figure B-3 Proposed MEMS based receiver with acoustic resonant IF filter banks. - Eliminates the requirement of tuning the first local oscillator, but requires very fast switching speed and low phase-noise at very high oscillator frequencies [112].

Appendix C – Four Cases of Delay Constraints

Table C-1 Four cases of delay constraints

	Delay Constraints
Case 1	$\left[\frac{n}{f_d} < \tau_1 < \tau_2 + \frac{(n-m)}{f_d} \right] \& \left[\frac{m}{f_d} < \tau_2 < \frac{(m+1)}{f_d} \right]$
Case 2	$\left[\tau_2 + \frac{(n-m)}{f_d} < \tau_1 < \frac{(n+1)}{f_d} \right] \& \left[\frac{m}{f_d} < \tau_2 < \frac{(m+1)}{f_d} \right]$
Case 3	$\left[-\frac{n}{f_d} > \tau_1 > \tau_2 - \frac{(n+1+m)}{f_d} \right] \& \left[\frac{m}{f_d} < \tau_2 < \frac{(m+1)}{f_d} \right]$
Case 4	$\left[\tau_2 - \frac{(n+m+1)}{f_d} > \tau_1 > -\frac{(n+1)}{f_d} \right] \& \left[\frac{m}{f_d} < \tau_2 < \frac{(m+1)}{f_d} \right]$

Appendix D – Delay Effects

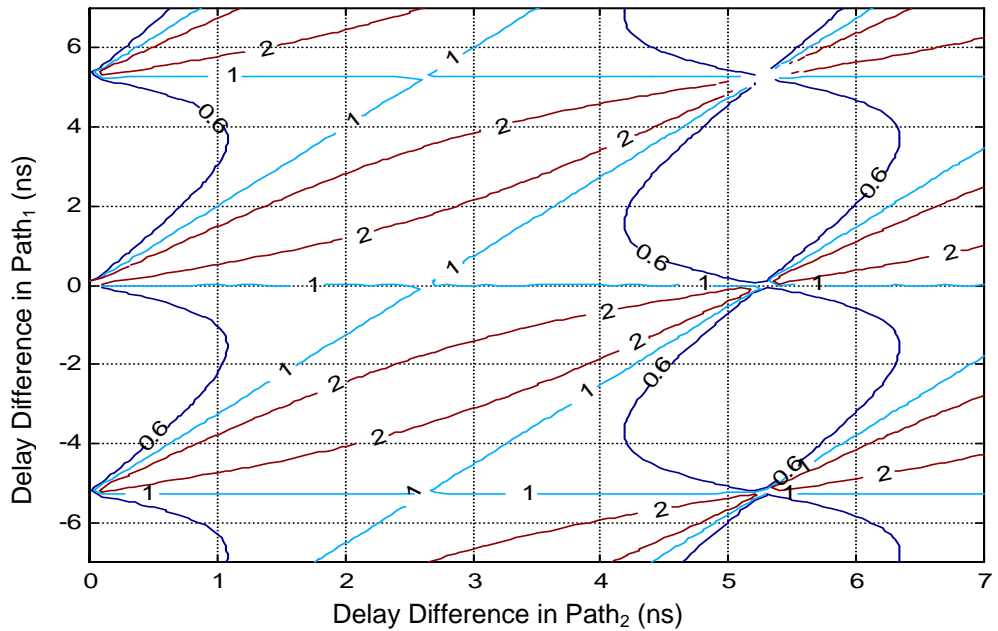


Figure D-1 Magnitude of h_1 for various delay differences in $path_1$ and $path_2$

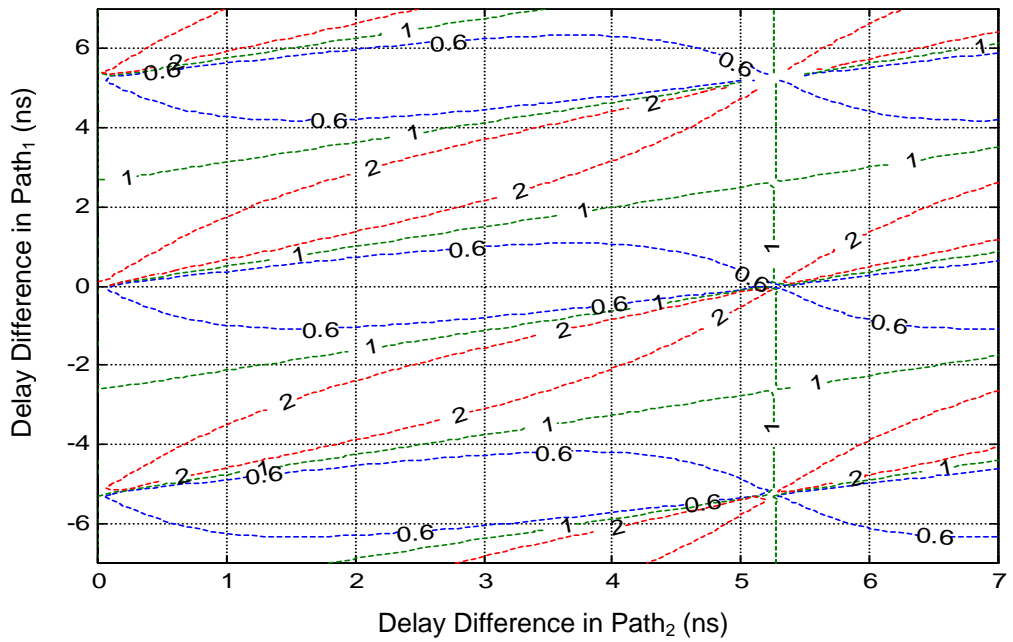


Figure D-2 Magnitude of h_2 for various delay differences in $path_1$ and $path_2$

Appendix E – Photographs of the Experimental Setup

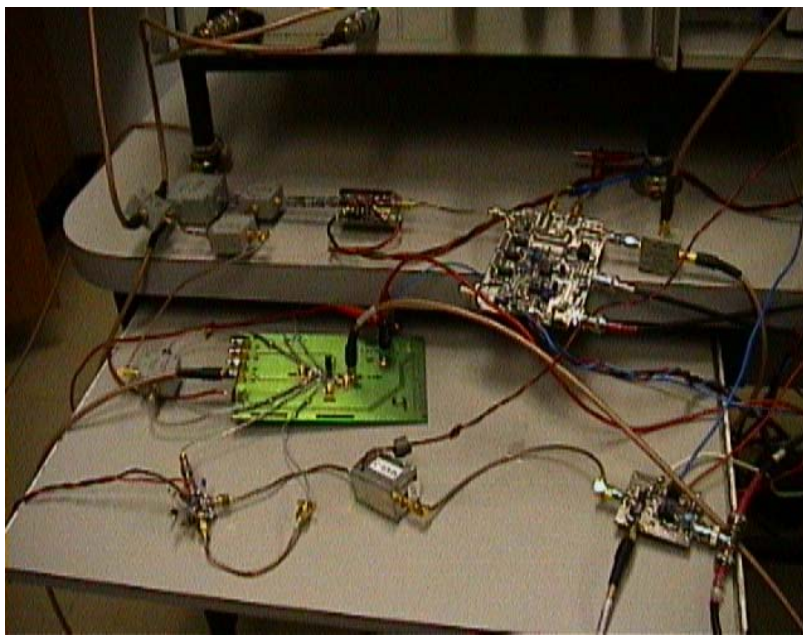
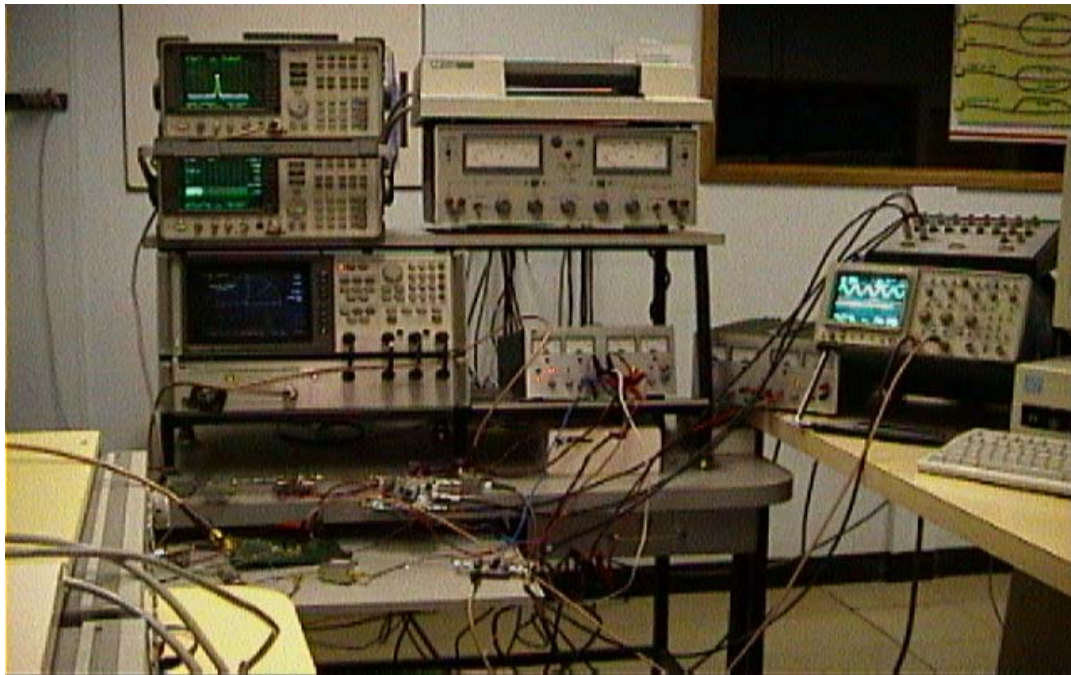


Figure E-1 Photographs of the single loop cancellation system

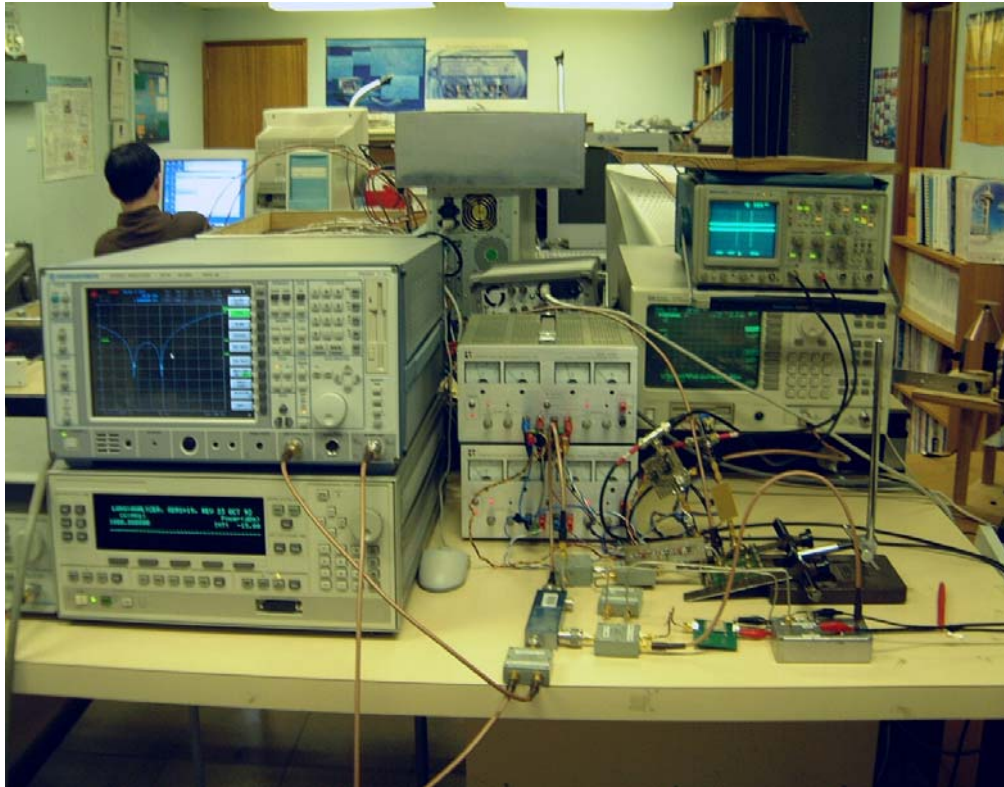


Figure E-2 Photographs of the double loop cancellation system (courtesy Matthew Williamson)